ALVEOLAR BONE: A PIVOTAL ROLE IN PERIODONTAL DISEASE PATHOBIOLOGY AND TREATMENT

EDITED BY: Frédéric Lézot, Beatriz Helena Castaneda, Petros Papagerakis and Fani Anagnostou

PUBLISHED IN: Frontiers in Physiology

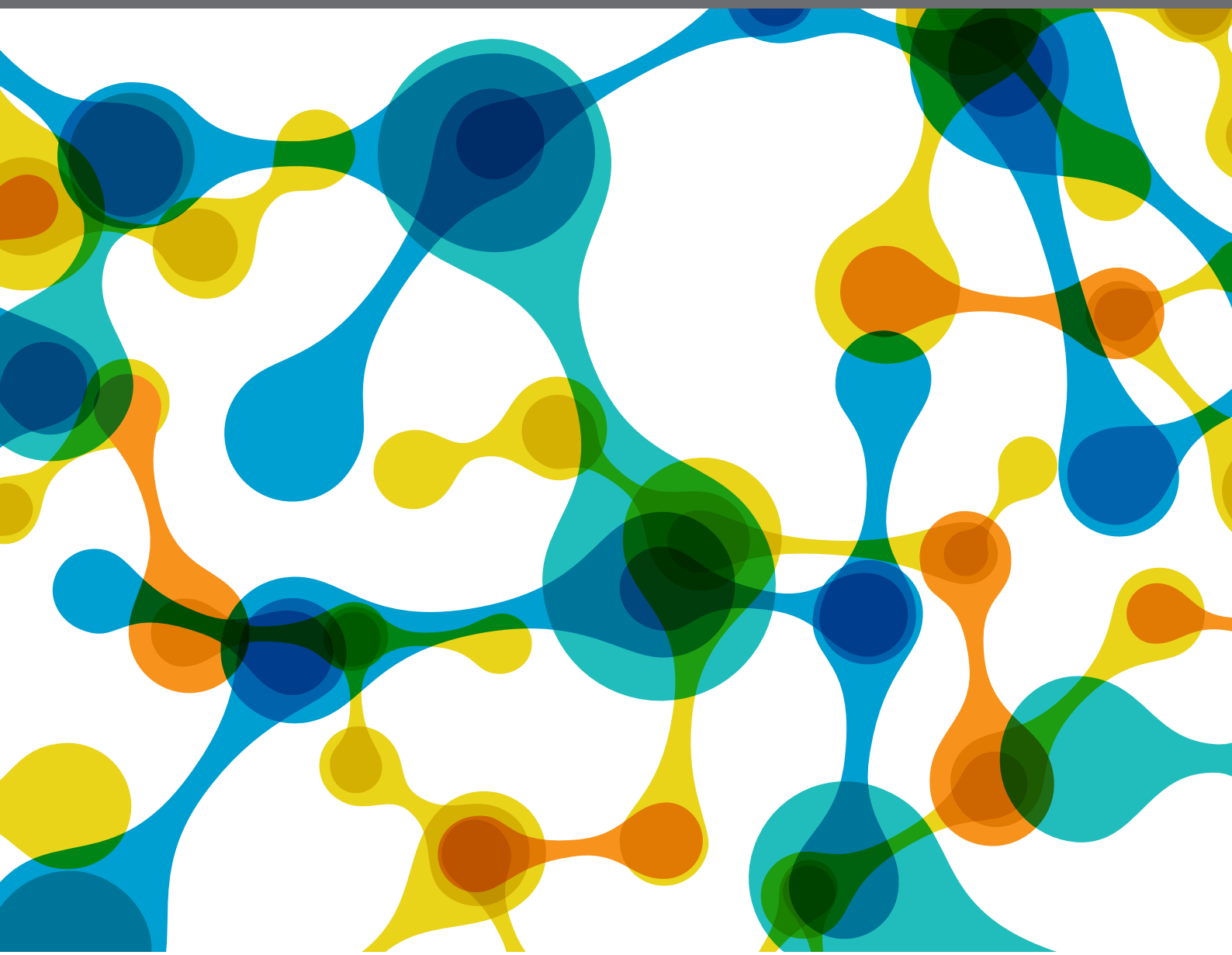

frontiers Research Topics

frontiers

ISSN 1664-8714
ISBN 978-2-88976-073-2
DOI 10.3389/978-2-88976-073-2

About Frontiers

Frontiers is more than just an open-access publisher of scholarly articles: it is a pioneering approach to the world of academia, radically improving the way scholarly research is managed. The grand vision of Frontiers is a world where all people have an equal opportunity to seek, share and generate knowledge. Frontiers provides immediate and permanent online open access to all its publications, but this alone is not enough to realize our grand goals.

Frontiers Journal Series

The Frontiers Journal Series is a multi-tier and interdisciplinary set of open-access, online journals, promising a paradigm shift from the current review, selection and dissemination processes in academic publishing. All Frontiers journals are driven by researchers for researchers; therefore, they constitute a service to the scholarly community. At the same time, the Frontiers Journal Series operates on a revolutionary invention, the tiered publishing system, initially addressing specific communities of scholars, and gradually climbing up to broader public understanding, thus serving the interests of the lay society, too.

Dedication to Quality

Each Frontiers article is a landmark of the highest quality, thanks to genuinely collaborative interactions between authors and review editors, who include some of the world's best academicians. Research must be certified by peers before entering a stream of knowledge that may eventually reach the public - and shape society; therefore, Frontiers only applies the most rigorous and unbiased reviews.
Frontiers revolutionizes research publishing by freely delivering the most outstanding research, evaluated with no bias from both the academic and social point of view. By applying the most advanced information technologies, Frontiers is catapulting scholarly publishing into a new generation.

What are Frontiers Research Topics?

Frontiers Research Topics are very popular trademarks of the Frontiers Journals Series: they are collections of at least ten articles, all centered on a particular subject. With their unique mix of varied contributions from Original Research to Review Articles, Frontiers Research Topics unify the most influential researchers, the latest key findings and historical advances in a hot research area! Find out more on how to host your own Frontiers Research Topic or contribute to one as an author by contacting the Frontiers Editorial Office: frontiersin.org/about/contact

ALVEOLAR BONE: A PIVOTAL ROLE IN PERIODONTAL DISEASE PATHOBIOLOGY AND TREATMENT

Topic Editors:
Frédéric Lézot, Institut National de la Santé et de la Recherche Médicale (INSERM), France
Beatriz Helena Castaneda, University of Antioquia, Colombia
Petros Papagerakis, University of Saskatchewan, Canada
Fani Anagnostou, Université de Paris, France

Citation: Lézot, F., Castaneda, B. H., Papagerakis, P., Anagnostou, F., eds. (2022). Alveolar Bone: A Pivotal Role in Periodontal Disease Pathobiology and Treatment. Lausanne: Frontiers Media SA. doi: 10.3389/978-2-88976-073-2

Table of Contents

frontiers | Frontiers in Physiology

EDITORIAL
published: 12 April 2022
doi: 10.3389/fphys.2022.889111

Editorial: Alveolar Bone: A Pivotal Role in Periodontal Disease Pathobiology and Treatment

Fani Anagnostou[1,2], *Beatriz Castaneda*[1], *Frédéric Lézot*[3]* *and Petros Papagerakis*[4]

[1]Service of Odontology, Hospital Pitié-Salpêtrière AP-HP, Paris, France, [2]B3OA, CNRS UMR 7052, INSERM U1271, ENVA, University of Paris, Paris, France, [3]Laboratory of Childhood Genetic Diseases, INSERM UMR933, Hospital Armand Trousseau AP-HP, Sorbonne University, Paris, France, [4]College of Dentistry, University of Saskatchewan, Saskatoon, SK, Canada

Keywords: alveolar bone, periodontal disease, Pathobiology, treatment, tooth, osseointegration

Editorial on the Research Topic

Alveolar Bone: A Pivotal Role in Periodontal Disease Pathobiology and Treatment

The periodontal disease (PD) is a complex disease of multifactorial etiology, mainly characterized by a gingival inflammation and an alveolar bone destruction (Albandar, 2005). The major etiological factor appears to be the chronic exposure to germs of the oral bacterial flora (Haffajee et al., 2008) but bacteria do not cause the destruction of periodontal tissues by themselves. Bacteria stimulate an inflammatory immune response accountable for such destruction. So, a cascade of cellular and biochemical events take their place in the pathological progression leading to PD with the final disruption of connective and bone tissues homeostasis (Hajishengallis and Sahingur, 2014). The local inflammatory response may be either attenuated or inversely amplified by several risk factors from genetic or environmental origins as well as patient lifestyle (Albandar, 2005; Nikolopoulos et al., 2008).

The aim of the present Research Topic was to assemble manuscripts addressing the questions relating to the alveolar bone physiopathology in the PD from the pathogenesis to the therapeutic approaches. In fine, this Research Topic assembles nine original research manuscripts and one mini-review manuscript.

Regarding the alveolar bone physiopathology, the manuscript by Kwack et al. and collaborators demonstrates the presence of a myeloid cell heterogeneity profile in the bone marrow of the alveolar bone that is distinct from what is observed in the bone marrow of long bones. Indeed, a reduced myeloid-derived suppressor cell population was reported that, however, evidences an increased immunosuppressive activity. In parallel, an increased B lymphocyte population was evidenced. Interestingly, to put in perspective to such B lymphocyte population increase, the manuscript by Settem et al. and collaborators, using an elegant model of conditional invalidation in mouse, demonstrated that RANKL expression by B lymphocyte contributes to the alveolar bone loss characteristic of the PD. The study presented by Yamada et al. and collaborators reports, using also a mouse model, that the Loeys-Dietz syndrome corresponding to alterations of the TGFβ signaling favors the occurrence and progression of periodontitis. This increased susceptibility associated to TGFβ signaling dysfunction may be linked to the critical part played by the TGFβ signaling in the proliferation and differentiation of osteogenic progenitor cells during the postnatal alveolar bone formation presented here by Xu et al. and collaborators. This study, with TGFβ-RII conditionally invalidated mice, at early or late stages of the osteoblast differentiation using the CRE expression driven respectively by Gli1 and Col1a1 promotors, outlines the requirement of the TGFβ signaling for a functional alveolo-periodontal-dental complex formation.

OPEN ACCESS

Edited and reviewed by:
Thimios Mitsiadis,
University of Zurich, Switzerland

***Correspondence:**
Frédéric Lézot
frederic.lezot@inserm.fr

Specialty section:
This article was submitted to Striated Muscle Physiology, a section of the journal Frontiers in Physiology

Received: *03 March 2022*
Accepted: *22 March 2022*
Published: *12 April 2022*

Citation:
Anagnostou F, Castaneda B, Lézot F and Papagerakis P (2022) Editorial: Alveolar Bone: A Pivotal Role in Periodontal Disease Pathobiology and Treatment. Front. Physiol. 13:889111. doi: 10.3389/fphys.2022.889111

Regarding the part of the periodontal ligament compartment in the PD, the manuscript by Li et al. and collaborators evidenced that epithelial cell rests of Malassez provide a favorable microenvironment to enforce the osteogenic potential of human periodontal ligament stem cells that was impaired in the periodontitis pathological or aged context. The manuscript by Mayr et al. and collaborators demonstrated that autophagy induces the expression of IL-6 by human periodontal ligament fibroblasts in response to mechanical load and overload with impact on the osteoclastogenesis and consequently the alveolar bone loss. Interestingly, Aljohani et al. and collaborators evidenced that the Methylsulfonylmethane, a naturally occurring anti-inflammatory compound, was able to increase the alveolar bone density in aged mice and so it may be of use as complementary treatment to improve bone loss-associated diseases, including PD. Finally, the mini-review presented by Syazana et al. and collaborators concerns another promising approach for PD treatment, up to now misestimated, the salivary exosomes. These exosomes provide miRNA, proteins, lipids and signaling molecules that may enable to protect the periodontal tissues and maintain the alveolar bone in the inflammatory context of PD.

The last but not least two manuscripts are relative to the osseointegration which is a key process of the restoration of a functional alveolo-periodontal-dental complex following the loss of teeth frequently due to the PD. The manuscript by Wang et al. and collaborators evidenced that high-altitude induced hypoxia has a negative effect on early osseointegration of titanium implants but such effect can be mitigated by the use of implants with rough surfaces, found to increase the expression osteogenesis-related genes in MG-63 cells under hypoxic conditions. The manuscript by Huang et al. and collaborators reported that Adipodon, an oral active synthetic small molecule with biological functions similar to adiponectin, was able to improve bone micro-architecture and to enhance the osseointegration in the diabetes mellitus-impaired bone microenvironment, which may open new perspectives for the treatment of PD and its consequences in diabetic patients.

To conclude this Research Topic underlines the dynamism of the researches on the periodontal disease with progresses in our understanding of the molecular and cellular mechanisms subjacent to the disease initiation and progression, but also in the therapeutic management of the disease whatever its stage of development. In perspective, there is no doubt that on the one hand an earlier and efficient management of the periodontal disease will be possible thanks to actual breakthrough in the molecular deciphering of this multifactorial pathology, and on the other hand that new treatments and therapeutic approaches will be available for patients in more advanced stages of the pathology.

The guest Editors want to thank all the authors for sharing their highly interesting results in this topic and all the Reviewers that kingly give their time and make this research topic possible.

AUTHOR CONTRIBUTIONS

All authors listed have contributed to the research topic and this editorial article substantially and intellectually. All agreed to the publication.

REFERENCES

Albandar, J. M. (2005). Epidemiology and Risk Factors of Periodontal Diseases. *Dental Clin. North America* 49, 517–532. v–vi. doi:10.1016/j.cden.2005.03.003

Haffajee, A. D., Socransky, S. S., Patel, M. R., and Song, X. (2008). Microbial Complexes in Supragingival Plaque. *Oral Microbiol. Immunol.* 23, 196–205. doi:10.1111/j.1399-302X.2007.00411.x

Hajishengallis, G., and Sahingur, S. E. (2014). Novel Inflammatory Pathways in Periodontitis. *Adv. Dent Res.* 26, 23–29. doi:10.1177/0022034514526240

Nikolopoulos, G. K., Dimou, N. L., Hamodrakas, S. J., and Bagos, P. G. (2008). Cytokine Gene Polymorphisms in Periodontal Disease: A Meta-Analysis of 53 Studies Including 4178 Cases and 4590 Controls. *J. Clin. Periodontol.* 35, 754–767. doi:10.1111/j.1600-051X.2008.01298.x

Conflict of Interest: The authors declare that the research was conducted in the absence of any commercial or financial relationships that could be construed as a potential conflict of interest.

frontiers in Physiology

ORIGINAL RESEARCH
published: 11 August 2021
doi: 10.3389/fphys.2021.715687

Mouse Model of Loeys–Dietz Syndrome Shows Elevated Susceptibility to Periodontitis via Alterations in Transforming Growth Factor-Beta Signaling

Satoru Yamada[1,2], Kenichiro Tsushima[1], Masaki Kinoshita[1], Hiromi Sakashita[1], Tetsuhiro Kajikawa[1†], Chiharu Fujihara[1], Hang Yuan[2], Shigeki Suzuki[2], Takayuki Morisaki[3] and Shinya Murakami[1]*

[1] Department of Periodontology, Osaka University Graduate School of Dentistry, Suita, Japan, [2] Department of Periodontology and Endodontology, Tohoku University Graduate School of Dentistry, Sendai, Japan, [3] Division of Molecular Pathology, Laboratory of Genome Technology IMSUT Hospital, Department of Internal Medicine, Human Genome Center, The Institute of Medical Science, The University of Tokyo, Bunkyo, Japan

OPEN ACCESS

Edited by:
Frédéric Lézot, Institut National de la Santé et de la Recherche Médicale (INSERM), France

Reviewed by:
Olivier Huck, Université de Strasbourg, France
Akiko Suzuki, University of Missouri–Kansas City, United States
Harald Osmundsen, University of Oslo, Norway

***Correspondence:**
Satoru Yamada
satoruy@tohoku.ac.jp

†Present address:
Tetsuhiro Kajikawa, Laboratory of Innate Immunity and Inflammation, Department of Basic and Translational Sciences, Penn Dental Medicine, University of Pennsylvania, Philadelphia, PA, United States

Specialty section:
This article was submitted to Craniofacial Biology and Dental Research, a section of the journal Frontiers in Physiology

Received: *27 May 2021*
Accepted: *23 July 2021*
Published: *11 August 2021*

Citation:
Yamada S, Tsushima K, Kinoshita M, Sakashita H, Kajikawa T, Fujihara C, Yuan H, Suzuki S, Morisaki T and Murakami S (2021) Mouse Model of Loeys–Dietz Syndrome Shows Elevated Susceptibility to Periodontitis via Alterations in Transforming Growth Factor-Beta Signaling. Front. Physiol. 12:715687. doi: 10.3389/fphys.2021.715687

Loeys–Dietz syndrome (LDS) is a syndromic connective tissue disorder caused by a heterozygous missense mutation in genes that encode transforming growth factor (TGF)-β receptor (*TGFBR*) *1* and *2*. We encountered a patient with LDS, who had severe periodontal tissue destruction indicative of aggressive periodontitis. The patient had a missense mutation in the glycine and serine-rich domain of *TGFBR1* exon 3. This G-to-T mutation at base 563 converted glycine to valine. We established an LDS model knock-in mouse that recapitulated the LDS phenotype. Homozygosity of the mutation caused embryonic lethality and heterozygous knock-in mice showed distorted and ruptured elastic fibers in the aorta at 24 weeks of age and died earlier than wildtype (WT) mice. We stimulated mouse embryonic fibroblasts (MEFs) from the knock-in mouse with TGF-β and examined their responses. The knock-in MEFs showed downregulated *Serpine 1* mRNA expression and phosphorylation of Smad2 to TGF-β compared with WT MEFs. To clarify the influence of TGF-β signaling abnormalities on the pathogenesis or progression of periodontitis, we performed pathomolecular analysis of the knock-in mouse. There were no structural differences in periodontal tissues between WT and LDS model mice at 6 or 24 weeks of age. Micro-computed tomography revealed no significant difference in alveolar bone resorption between WT and knock-in mice at 6 or 24 weeks of age. However, TGF-β-related gene expression was increased significantly in periodontal tissues of the knock-in mouse compared with WT mice. Next, we assessed a mouse periodontitis model in which periodontal bone loss was induced by oral inoculation with the bacterial strain *Porphyromonas gingivalis* W83. After inoculation, we collected alveolar bone and carried out morphometric analysis. *P. gingivalis*-induced alveolar bone loss was significantly greater in LDS model mice than in WT mice. Peritoneal macrophages isolated from *Tgfbr1*$^{G188V/+}$ mice showed upregulation of inflammatory cytokine mRNA expression induced by *P. gingivalis* lipopolysaccharide compared with WT macrophages. In this study, we established an

LDS mouse model and demonstrated that LDS model mice had elevated susceptibility to *P. gingivalis*-induced periodontitis, probably through TGF-β signal dysfunction. This suggests that TGF-β signaling abnormalities accelerate the pathogenesis or progression of periodontitis.

Keywords: TGF-beta, periodontal ligament, extracelluar matix, periodontitis, knock-in mice

INTRODUCTION

Marfan syndrome (MFS) is an autosomal dominant connective tissue disease caused by a mutation in fibrillin-1 (Dietz et al., 1991), which leads to systemic diseases with various phenotypes. It affects approximately 1 in 5,000 people and includes patients with mild disease (Dietz et al., 1991). In particular, MFS causes characteristic signs in the skeletal system (e.g., bone hyperplasia, joint relaxation, height, arachnoid finger, and spinal scoliosis), cardiovascular system (e.g., aortic aneurysm and mitral valve deviation), and ocular system (e.g., lens subluxation) (Schorr et al., 1951). Fibrillin-1 is a component of microfibrils in the extracellular matrix (Godfrey et al., 1990) and is involved in the control of transforming growth factor (TGF)-β expression and function (Neptune et al., 2003). TGF-β is a cytokine involved in the regulation of cell proliferation, differentiation, and death (Huang and Chen, 2012). In particular, it promotes collagen production and extracellular matrix remodeling (Dietz, 2007). Various MFS symptoms result from excessive TGF-β in serum caused by fibrillin-1 mutations (Matt et al., 2009). Additionally, various MFS-related diseases are caused by abnormalities in TGF-β signaling, which include Beals syndrome caused by mutations in *fibrillin-2* (Putnam et al., 1995), Loeys–Dietz syndrome (LDS) caused by mutations in *TGF-β receptor* (*TGFBR*) *1* or *TGFBR2* (Mizuguchi et al., 2004; Loeys et al., 2005, 2006), juvenile polyposis syndrome caused by mutations in *Smad4*, a TGF-β signaling factor (Howe et al., 1998), and Shprintzen–Goldberg syndrome caused by mutations in *SKI*, a gene that suppresses Smad signaling (Doyle et al., 2012).

There have been reports of patients with MFS and severe periodontitis (De Coster et al., 2002; Straub et al., 2002; Jain and Pandey, 2013; Staufenbiel et al., 2013). Patients with MFS have greater morbidity and severity of periodontitis than otherwise healthy individuals (Suzuki et al., 2015). In patients who exhibit MFS, severe chronic periodontitis has been reported with periodontitis substantial palatal and dental irregularities. To our knowledge, details of the relationships between genetic mutations and periodontitis in MFS patients and its related diseases are unclear. Thus, in this study, we first investigated the relationships between MFS, related diseases, and periodontitis. We identified a patient with LDS, who had an aggressive periodontitis-like pathology. Periodontitis progresses under a range of conditions that include environmental and genetic factors. Periodontitis is broadly divided into chronic and aggressive periodontitis, with aggressive periodontitis assumed to be more closely related to genetic factors (Meng et al., 2007). Recently, a new periodontitis classification scheme has been adopted, in which forms of the disease recognized as "chronic" or "aggressive" are now characterized by a multi-dimensional staging and grading system (Papapanou et al., 2018).

LDS is caused by mutations in *TGFBR1* or *TGFBR2* (Loeys et al., 2005). LDS and MFS share many common clinical symptoms that include aortic lesions (e.g., basal dilatation, aortic aneurysm, and aortic dissection) and skeletal system lesions (e.g., scoliosis, joint laxity, and spider finger). However, features not evident in patients with MFS (i.e., characteristic facial features such as cleft palate, dichotomy uvula, interocular dissociation, systemic blood vessel meandering, craniosynostosis, congenital heart disease, and intellectual disability) are observed at high rates in patients with LDS (Loeys et al., 2006). In vascular smooth muscle cells collected from patients with LDS, TGF-β levels are low (Gallo et al., 2014). However, a compensatory change comprises TGF-β overexpression in aortic tissues. This likely results in the onset of cardiovascular symptoms such as aortic aneurysms and aortic dissection (Loeys et al., 2005; Gallo et al., 2014). On the basis of the data collected from the LDS patient who had aggressive periodontitis, we developed genetically modified mice with the candidate genetic mutation to analyze the disease state and the effects of a mutation in a TGF-β-related gene on periodontitis.

MATERIALS AND METHODS

Patients and Mutation Analysis

All human experiments were approved by the Institutional Ethics Committee of Osaka University Graduate School of Dentistry (No. H22-E10) and the National Cerebral and Cardiovascular Center (No. M22-34). The epidemiological study included 120 patients who had visited the National Cerebral and Cardiovascular Center Hospital in Osaka, Japan, and were diagnosed with Marfan syndrome or Marfan-related syndrome by the revised Ghent nosology (Loeys et al., 2010) to survey the prevalence rate of periodontal disease in Marfan syndrome and Marfan-related syndrome patients. Informed consent was obtained from all patients involved in the study. Genomic DNA isolated from peripheral white blood cells was amplified by polymerase chain reaction (PCR) using primers in the flanking introns of *TGFBR1* and *TGFBR2*. Sequence analyses were performed using Applied Biosystems automated DNA sequencer (ABI3770, Waltham, MA, United States) in accordance with the manufacturer's protocol.

Animals

All animal experiments were approved by the Institutional Animal Care and Use Committee of Osaka University Graduate

School of Dentistry and complied with the guidelines for the care and use of laboratory animals at Osaka University. This study was carried out in compliance with the ARRIVE guidelines, where applicable. To generate *Tgfbr1*$^{G188V/+}$ mice, site-directed mutagenesis was performed to replace glycine with valine at codon 188 of *Tgfbr1* (guanine to thymine at nucleotide 563). This mutated *Tgfbr1* cDNA was cloned into pBSIISK + with a floxed neomycin resistance cassette (NeoR). Bac-based long-range PCR was used to amplify murine genomic fragments of *Tgfbr1*. The long arm (6 kb, exon 3 with G188V) and short arm (2.8 kb, exon 4) were cloned into pBS-DTA and pBS-LNL, respectively. The final targeting vector was constructed and then linearized. The targeting vector DNA was electroporated into C57BL/6 ES cells. Homologous recombination-positive ES cells were identified by Southern blot analysis. Positive clones were injected into BALB/c blastocysts and transferred into pseudopregnant female mice. Chimeric offspring were mated with C57BL/6 mice and germline transmission was confirmed by RT-PCR. The loxP-flanked NeoR was removed by mating *Tgfbr1*$^{G188V/+}$ founder mice with CAG-Cre recombinase transgenic mice (Sakai and Miyazaki, 1997). Experimental mice were backcrossed with C57BL/6 mice to remove the CAG-Cre transgene. Genotype analysis of *Tgfbr1*$^{G188V/+}$ mice was performed by genomic PCR using flanking loxP site-specific primers (5′CTAAGAGAAGTGTGCCTCCTTTACA-3′ and 5′-CCAAAGTCATAGAGCATGTGTTAGA-3′).

Cell Culture and Gene Transfection

Wildtype (WT) and *Tgfbr1*$^{G188V/+}$ mouse embryonic fibroblasts (MEFs) were isolated from embryos on day 13.5 by a previously described method (Awata et al., 2015). MEFs were cultured in Dulbecco's modified Eagle's medium (DMEM) supplemented with 10% fetal bovine serum (FBS) and 60 μg/mL kanamycin. MEFs from passages 3–5 were used in this study. Each genotype of MEFs (WT, *Tgfbr1*$^{G188V/+}$, and *Tgfbr1*$^{G188V/G188V}$) was cultured in a 12-well plate until confluency. The next day, the medium was replaced with serum-free DMEM. After serum deprivation for 24 h, the cells were stimulated with TGF-β (R&D Systems, Minneapolis, MN, United States) in serum-free DMEM for 30 min for western blot analysis and 12 h for quantitative PCR analysis.

cDNA of the mouse *Tgfbr1* gene was cloned into the p3XFLAG-CMV-14 expression vector (Sigma-Aldrich, St. Louis, MO, United States). cDNA for the *Tgfbr1* mutation (G188V: *Tgfbr1*^{G188V}) was ligated to *Tgfbr1* cDNA by the Quick Change Site-Directed Mutagenesis kit (Stratagene, LA Jolla, CA, United States) in accordance with the manufacturer's protocol. The sequence was verified by DNA sequencing. For luciferase assays, human embryonic kidney (HEK) 293 cells were seeded in a 12-well plate. After 24 h, the cells were transfected with the *Tgfbr1*^{G188V}/3XFLAG-CMV-14 expression vector or wildtype *Tgfbr1*/3XFLAG-CMV-14 expression vector mixed with Transcription Factor Reporter using a Signal SMAD Reporter Assay kit (Polyscience, Inc., Warrington, PA, United States) in accordance with the manufacturer's protocol. At 48 h after transfection, the medium was replaced with serum-free DMEM. After serum deprivation for 24 h, the cells were stimulated with 0–5 ng/ml TGF-β in serum-free DMEM for 8 h. Luciferase activity was measured by a GloMax 96 Microplate Luminometer (Promega, Madison, WI, United States).

Histological Analysis

Thoracic aortae were collected from WT and *Tgfbr1*$^{G188V/+}$ mice at 24 weeks of age and fixed overnight in 4% paraformaldehyde (PFA)/phosphate buffer (Wako Pure Chemical Industries, Osaka, Japan). Samples were embedded in paraffin and sectioned at 5 μm thicknesses using a LEICA RM2245 microtome (Leica Microsystems, Wetzlar, Germany). Sections were stained with Elastica van Gieson (EVG) for elastin staining. Maxillae from WT and *Tgfbr1*$^{G188V/+}$ mice at 6 and 24 weeks of age were fixed in 4% PFA/phosphate-buffered saline (PBS) (Wako Pure Chemical Industries) overnight at 4°C and decalcified in 0.5 M EDTA (Wako) for 1 week. After decalcification, periodontal tissues were dehydrated using 15, 20, and 25% sucrose in PBS. Then, periodontal tissues were embedded in O.C.T. Compound (Sakura Finetek, Tokyo, Japan). They were frozen and sectioned at 5 μm thicknesses in a mesiodistal orientation using the LEICA RM2245 microtome. Sections were stained with hematoxylin-eosin (HE) or using a Tartrate-Resistance Acid Phosphatase (TRAP) Staining Kit (Wako) in accordance with the manufacturer's protocol.

RNA Extraction and Quantitative PCR Analysis

Thoracic aortae, maxillae, and periodontal tissues were extracted from 6-week-old male WT and *Tgfbr1*$^{G188V/+}$ mice. Total RNA from tissues or MEFs was extracted using a PureLink RNA Mini Kit (Life Technologies, Carlsbad, CA, United States). Total RNA was reversed transcribed to cDNA using a High-Capacity RNA-to-cDNA Kit (Applied Biosystems, Foster City, CA, United States). Quantitative PCR was performed with the StepOnePlus Real-time PCR system (Applied Biosystems) using Fast SYBR Green Master Mix (Thermo Fisher Scientific, Waltham, MA, United States) and gene-specific primers (**Table 1**).

Western Blot Analysis

Cells were lysed with RIPA buffer (Millipore, Billerica, MA, United States) that contained phosphatase and proteinase inhibitors. The protein concentration of the lysates was measured by the Bradford assay (Bio-Rad, Hercules, CA, United States). Aliquots of lysates were separated by 10% sodium dodecyl sulfate-polyacrylamide gel electrophoresis and subjected to western blot analysis. Primary antibodies included a rabbit anti-TGFBR1 antibody (1:1,000; Santa Cruz Biotechnology, Santa Cruz, CA, United States), mouse anti-beta actin antibody (1:10,000, Sigma-Aldrich), rabbit anti-phospho-Smad2 antibody (1:1,000, Millipore), and rabbit anti-Smad2 antibody (1:1,000, Cell Signaling Technology, Danvers, MA, United States). Secondary antibodies were a horseradish peroxidase (HRP)-linked anti-mouse IgG antibody (1:10,000, GE Healthcare, Piscataway, NJ, United States) and HRP-linked anti-rabbit IgG antibody (1:10,000, GE Healthcare). Immunoreactive proteins were

TABLE 1 | Primer sequences.

GenBank acc.	Gene	Primer sequences
NM_009370	*Tgfb1*	5′-GATGTCAGCTCTGGGCAAAGATTAG-3′ 5′-CAGGCTGAGCTTCATGCCTTTAC-3′
NM_009371	*Tgfb2*	5′-AATGGTTGCACCACAAGCAAGA-3 5′-TTCCCAGGGCTGAGATGATAAGAG-3′
NM_009368	*Tgfb3*	5′-CAGCGCTACATAGGTGGCAAGA-3′ 5′-TGATTTCCAGACCCAAGTTGGAC-3′
NM_009370	*Tgfbr1*	5′-GATGTCAGCTCTGGGCAAAGATTAG-3′ 5′-CAGGCTGAGCTTCATGCCTTTAC-3′
NM_009371	*Tgfbr2*	5′-AGTCGGATGTGGAAATGGAA-3′ 5′-ACAGCTGTGGAAGCTTGACC- 3′
NM_007742	*Col1a1*	5′-CAGGGTATTGCTGGACAACGTG-3′ 5′-GGACCTTGTTTGCCAGGTTCA-3′
NM_008871	*Serpine1*	5′-TGCTGAACTCATCAGACAATGGAAG-3′ 5′-TCGGCCAGGGTTGCACTAA-3′
NM_025711	*Plap-1*	5′-CCATATCAGGATCGCTGAAGCA-3′ 5′-TCTGTGATTCTGTTGTTTCCAAGAC-3′
NM_021274	*Cxcl10*	5′-TGAATCCGGAATCTAAGACCATCAA-3′ 5′-AGGACTAGCCATCCACTGGGTAAAG-3
NM_031168	*Il6*	5′- CCACTTCACAAGTCGGAGGCTTA-3′ 5′-GCAAGTGCATCATCGTTGTTCATAC-3′
NM_013693	*Tnf*	5′-CAGGAGGGAGAACAGAAACTCCA-3′ 5′-CCTGGTTGGCTGCTTGCTT-3′

detected by SuperSignal West Pico Chemiluminescent Substrate (Thermo Fisher Scientific, Waltham, MA, United States) with an ImageQuant LAS4,000 (GE Healthcare).

Quantitative Analysis of Alveolar Bone Resorption

Maxillae were collected from WT and *Tgfbr1*$^{G188V/+}$ mice at 6 and 24 weeks of age and imaged by a 3D micro X-ray CT R_mCT2 (Rigaku, Tokyo, Japan). The images were analyzed using TRI/3D-BON software (RATOC System Engineering, Tokyo, Japan). The root surface area between the alveolar bone crest and cementoenamel junction was measured using WinROOF software (Mitani, Fukui, Japan). The total value of these three distances was regarded as alveolar bone resorption. Alveolar bone resorption was measured in the root surface area between the alveolar apex from the cementoenamel junction.

Porphyromonas gingivalis Bacterial Culture and Establishment of Oral Infection

Porphyromonas gingivalis strain W83 was cultured in modified Gifu anaerobic medium broth (Nissui, Tokyo, Japan) in an anaerobic jar (Becton Dickinson Microbiology System, Cockeysville, MD, United States) in the presence of an AnaeroPack (Mitsubishi Gas Chemical Co., Inc., Tokyo, Japan) for 48 h at 37°C. Bacterial suspensions were prepared in PBS without Mg^{2+}/Ca^{2+} using established growth curves and spectrophotometric analysis. The number of CFUs was standardized by measuring optical density at 600 nm. The murine experimental periodontal infection model was established in accordance with a previously described method (Aoki-Nonaka et al., 2013). The 8-week-old male mice received sulfamethoxazole and trimethoprim at final concentrations of 700 and 400 μg/mL, respectively, in water bottles administered *ad libitum* for 10 days. This treatment was followed by 3 days without antibiotics. The experimental group was then infected as follows. In total, 1×10^9 CFUs of live *P. gingivalis* were suspended in 100 μL PBS with 2% carboxymethyl cellulose (Sigma−Aldrich) and administered to each mouse through a feeding needle 10 times at 3-day intervals. The control group received the same pretreatment and was sham infected without *P. gingivalis*. At 1 day after the final treatment, the mice were sacrificed with CO_2 affixation and their maxillae were collected for micro-CT and histological analyses.

P. gingivalis Stimulation of Peritoneal Macrophages Derived From *Tgfbr1*$^{G188V/+}$ Mice

Macrophages were harvested from the peritoneal cavity of 8-week-old male WT and *Tgfbr1*$^{G188V/+}$ mice at 3 days after injection of thioglycollate (Yamaba et al., 2015) and seeded on 6-well plates. After 2 h of incubation, non-adherent cells were washed out and the remaining cells were subjected to further analysis. The peritoneal macrophages were stimulated with 1 Uμg/ml *P. gingivalis* lipopolysaccharide (LPS) (InvivoGen, Inc., San Diego, CA, United States) for the indicated times and then total RNA was isolated for quantitative PCR analysis.

Statistical Analysis

Data are represented as the mean ± SD. Statistical analyses were performed using the Student's *t*-test for paired comparisons and one-way analysis of variance for multiple comparisons using Bonferroni's *post hoc* test with Excel statistics software (Bellcurve, Tokyo, Japan). A value of $P < 0.05$ was considered statistically significant.

RESULTS

Mutation Analysis of the LDS Patient With Periodontitis

We surveyed 120 patients with Marfan syndrome or Marfan-related syndrome to determine the prevalence rate of periodontal disease in these syndromes. We found that the prevalence of chronic periodontitis in Marfan syndrome and Marfan-related syndrome patients was significantly higher compared with that in healthy controls (manuscript in preparation). In this clinical study, we encountered a 44-year-old Japanese female with LDS, who had localized vertical bone loss around molars in spite of good oral hygiene (O'Leary's plaque control record: 13.0%) as shown in **Figure 1**. She was only one patient diagnosed with aggressive periodontitis (new classification: stage III and grade B). She was diagnosed with familial thoracic aortic aneurysms and dissections. She was treated by total arch aortic and descending aorta replacement. Systemic features of the patient were a tall height (−), down slanting palpebral fissures (+), retrognathia (+), pectus carinatum deformity (−),

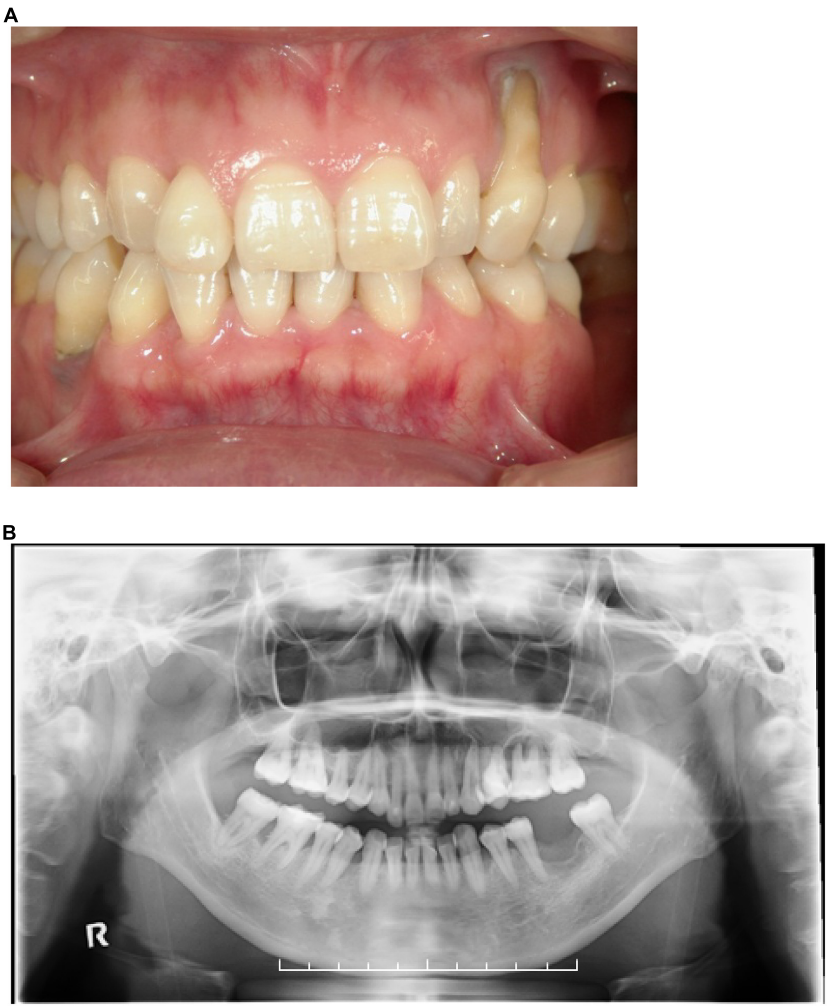

FIGURE 1 | (A) Front view of the dentition of a patient with LDS and aggressive periodontitis. **(B)** Orthopantomograph of the patient. Note the presence of localized vertical bone loss around molars.

pneumothorax (−), myopia (−), hypertelorism (+), and bifid uvula (−). Genomic sequencing of the patient revealed a mutation in the glycine and serine-rich domain of *TGFBR1* exon 3 (referred to as the GS domain). This G-to-T mutation at base 563 converted glycine to valine at residue 188 (G188V) (**Figure 2A**). To assess the effects of the G188V mutation on TGF-β signaling, we introduced mouse $Tgfbr1^{WT}$ and $Tgfbr1^{G188V}$ expression vectors into HEK293 cells. We confirmed that the TGF-β type I receptor was sufficiently expressed in both groups (**Figure 2B**). Next, we performed luciferase assays and found that TGF-β-induced luciferase activity was significantly elevated in the group with high levels of $Tgfbr1^{WT}$ and significantly suppressed in the group with $Tgfbr1^{G188V}$ (**Figure 2C**). These results suggested that the G188V mutation resulted in loss of TGF-β signaling.

Generation of $Tgfbr1^{G188V}$ Knock-In Mice

To introduce the G188V mutation into mice, we generated a knock-in construct (**Figure 3A**). $Tgfbr1^{G188V/+}$ mice were delivered spontaneously, able to breed, and were fertile with no apparent abnormalities at 6 weeks of age (**Figure 3B**). Mouse genotyping was performed using genomic DNA by PCR with a primer to identify the *Tgfbr1* allele and mutant *Tgfbr1* allele that contained the loxP sequence (**Figure 3C**). After generation of $Tgfbr1^{G188V/+}$ mice, genotyping was performed using embryos on days 13.5 and 14.5, and after birth. WT, $Tgfbr1^{G188V/+}$, and $Tgfbr1^{G188V/G188V}$ embryos were obtained at day 14.5 (**Figure 3D**). We observed no conspicuous morphological or patterning defects, although some $Tgfbr1^{G188V/G188V}$ embryos at day 14.5 showed fewer bloodstreams in craniofacial, trunk, and spinal cord regions. Among embryos on days 13.5 and 14.5, WT, $Tgfbr1^{G188V/+}$, and $Tgfbr1^{G188V/G188V}$ mice had survived. However, with respect to the number of births, only one $Tgfbr1^{G188V/G188V}$ mouse was obtained. Moreover, the $Tgfbr1^{G188V/G188V}$ mutation caused embryonic lethality after day 14.5 (**Table 2**). Therefore, the $Tgfbr1^{G188V/+}$ mouse was analyzed as an LDS model.

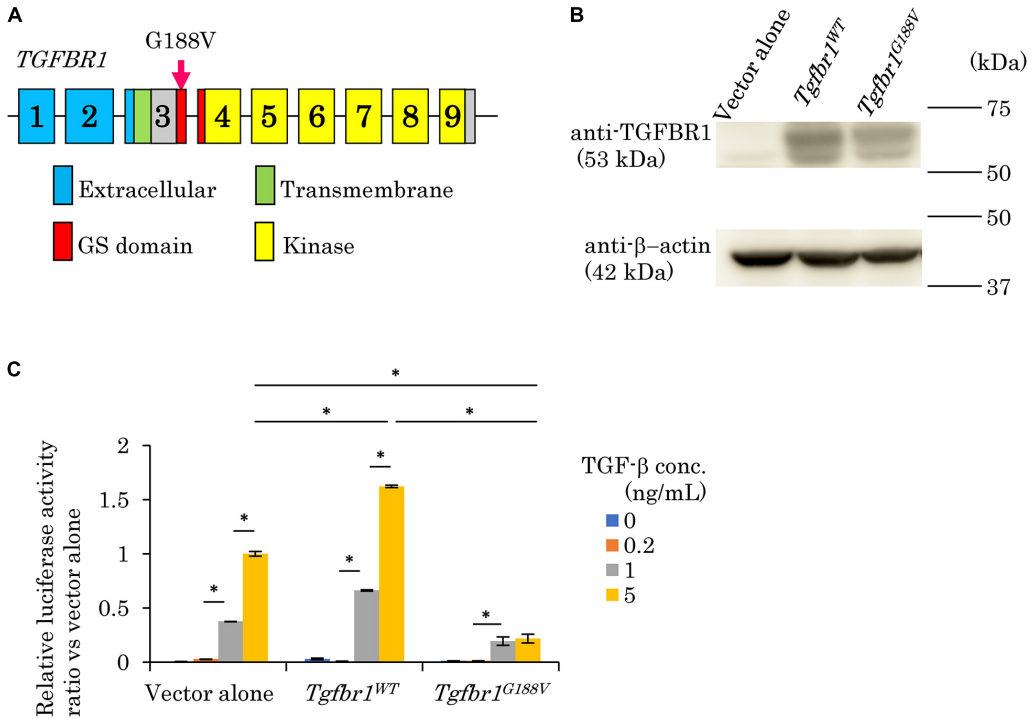

FIGURE 2 | Mutation in exon 3 of *TGFBR1* isolated from a patient with LDS and aggressive periodontitis diminishes the response to TGF-β (G188V mutation). **(A)** Location of the mutation in exon 3 of *TGFBR1*. **(B)** HEK293 cells were transfected with a vector alone, wildtype mouse *Tgfbr1* ($Tgfbr1^{WT}$), or mouse *Tgfbr1* with the G188V mutation ($Tgfbr1^{G188V}$). Lysates of transfected cells were subjected to western blot analysis using an anti-TGFBR1 antibody. **(C)** TGF-β-induced promoter activity was assessed by the dual luciferase reporter assay system. Values represent the mean ± SD in triplicate assays. *$P < 0.05$, compared with the indicated TGF-β concentration.

Pathophysiological Analysis of LDS Model Mice and Analysis of TGF-β Signaling in Response to the *Tgfbr1* G188V Mutation

The survival rate of $Tgfbr1^{G188V/+}$ mice was observed over 180 days by a Kaplan–Meier survival curve. Mutant mice had died substantially earlier than WT mice (**Figure 4A**). To analyze the cause of premature death in $Tgfbr1^{G188V/+}$ mice, tissue sections of the aorta were prepared, and elastic fibers were observed. Aortae were collected from 24-week-old male WT and $Tgfbr1^{G188V/+}$ mice. Thinly sectioned axial specimens were prepared for EVG staining. In aortic samples from $Tgfbr1^{G188V/+}$ mice, elastic fibers appeared to be distorted (**Figure 4B**, arrow) and fine rupture of elastic fibers was observed (**Figure 4B**, arrowhead). Next, TGF-β-related gene expression was analyzed in aortae from $Tgfbr1^{G188V/+}$ mice. The thoracic aortae of 24-week-old male WT and $Tgfbr1^{G188V/+}$ mice were collected. mRNA expression levels of *Tgfb1*, *Tgfb2*, and *Tgfb3*, *TGF*-β receptor genes *Tgfbr1* and *Tgfbr2*, and TGF-β targets *Col1a1* and *Serpine1* were analyzed by real-time PCR. Although the differences were not statistically significant, the mRNA levels of *Tgfb1, Tgfb3, Tgfbr1, Tgfbr2, Col1a1*, and *Serpine1* tended to be higher in $Tgfbr1^{G188V/+}$ mice than in WT mice (**Figure 4C**). Using MEFs, we analyzed changes in TGF-β activity caused by the Tgfbr1 G188V mutation. MEFs of each genotype were cultured for 24 h in the absence of FBS and then stimulated with TGF-β (0–5 ng/mL). The expression levels of TGF-β-induced *Serpine1* were evaluated after 12 h (**Figure 4D**). In WT MEFs, *Serpine1* expression was increased in a TGF-β concentration-dependent manner. In $Tgfbr1^{G188V/+}$ and $Tgfbr1^{G188V/G188V}$ MEFs, the increase in *Serpine1* expression induced by TGF-β was reduced significantly. Next, we performed intracellular signal transduction analysis of TGF-β in MEFs. MEFs were cultured for 24 h in the absence of FBS and then stimulated with TGF-β (0–10 ng/mL). Cells were recovered after 30 min and Smad2 phosphorylation was examined by western blotting. Although phosphorylation of Smad2 in WT MEFs was increased in a TGF-β concentration-dependent manner, the levels of Smad2 phosphorylation were lower in $Tgfbr1^{G188V/+}$ and $Tgfbr1^{G188V/G188V}$ MEFs than in WT MEFs (**Figure 4E**). These findings demonstrated that cellular TGF-β responses had decreased because of the *Tgfbr1* G188V mutation.

Analysis of Phenotypes in Periodontal Tissues of LDS Model Mice

Micro-CT contrast imaging was performed to evaluate maxillary alveolar bones collected from WT and $Tgfbr1^{G188V/+}$ mice. Alveolar bone resorption was measured in the area between the alveolar apex from the cementoenamel boundary (**Figure 5A**, red

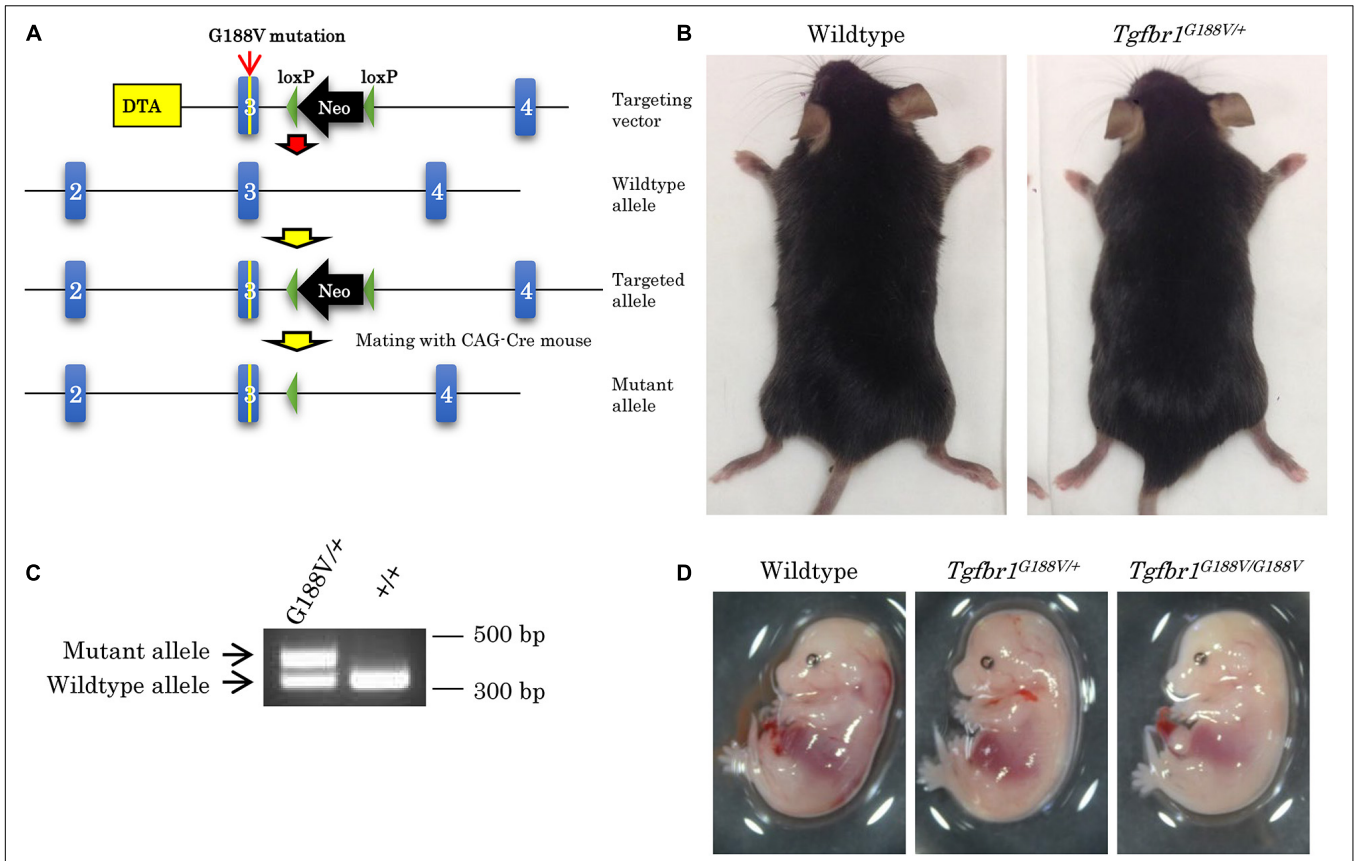

FIGURE 3 | Generation of knock-in mice with the *Tgfbr1* G188V mutation. **(A)** Structure of the *Tgfbr1* G188V mutant allele. **(B)** No clear differences in 6-week-old $Tgfbr1^{G188V/+}$ mice. **(C)** PCR genotyping of genomic DNA using tail specimens collected from $Tgfbr1^{G188V/+}$ and WT mice. **(D)** Embryos of WT, $Tgfbr1^{G188V/+}$, and $Tgfbr1^{G188V/G188V}$ at embryonic day 14.5.

line). The sums of values obtained for the first, second, and third molars were calculated. WT and $Tgfbr1^{G188V/+}$ mice showed significant increases in bone resorption with aging. However, there was no significant difference in alveolar bone resorption between WT and $Tgfbr1^{G188V/+}$ mice (**Figure 5B**). HE staining of periodontal tissues derived from WT and $Tgfbr1^{G188V/+}$ mice at 6 and 24 weeks of age revealed no structural differences between WT and $Tgfbr1^{G188V/+}$ mice (**Figure 5C**). Next, TGF-β-related gene expression was analyzed in periodontal tissues from $Tgfbr1^{G188V/+}$ mice. Periodontal tissues were collected from 6-week-old male WT and $Tgfbr1^{G188V/+}$ mice, and mRNA expression levels of TGF-β-related genes were analyzed by real-time PCR. Expression levels of *Tgfb1*, *Tgfb2*, *Tgfb3*, *Col1a1*, *Serpine*1, and *Plap-1* were significantly higher in $Tgfbr1^{G188V/+}$ mice than in WT mice (**Figure 5D**).

TABLE 2 | Number of mice with each genotype.

Genotype	Embryonic day 13.5	Embryonic day 14.5	Postnatal day 1
Wildtype	12 (24%)	15 (29%)	63 (31%)
$Tgfbr1^{G188V/+}$	25 (51%)	23 (45%)	139 (68.5%)
$Tgfbr1^{G188V/G188V}$	12 (24%)	13 (26%)	1 (0.5%)*

*$p < 0.001$ vs. embryonic days 13.5 and 14.5.

Alveolar Bone Resorption in $Tgfbr1^{G188V/+}$ Mice in Response to Oral Infection

To analyze changes in periodontal tissue caused by bacterial invasion in WT and $Tgfbr1^{G188V/+}$ mice, *P. gingivalis* was orally administered to generate an experimental periodontitis model. After *P. gingivalis* administration, the maxillary bones of the mice were recovered, micro-CT contrast imaging of periodontal tissues was performed (**Figure 6A**), and sections were prepared. Bone resorption after *P. gingivalis* administration was significantly greater in $Tgfbr1^{G188V/+}$ mice than in control mice (**Figure 6B**). Periodontal tissue sections were prepared and subjected to HE staining. Multinucleated cells near the alveolar bone were observed in WT and $Tgfbr1^{G188V/+}$ mice in the *P. gingivalis* treatment group (**Figure 6C**). To observe osteoclasts in close proximity to the alveolar bone, sections of each periodontal tissue were prepared, and TRAP staining was performed. In the *P. gingivalis* treatment group, osteoclasts were found near the alveolar bone (**Figure 6D**, arrowhead). For quantitative analysis, the numbers of osteoclasts in close

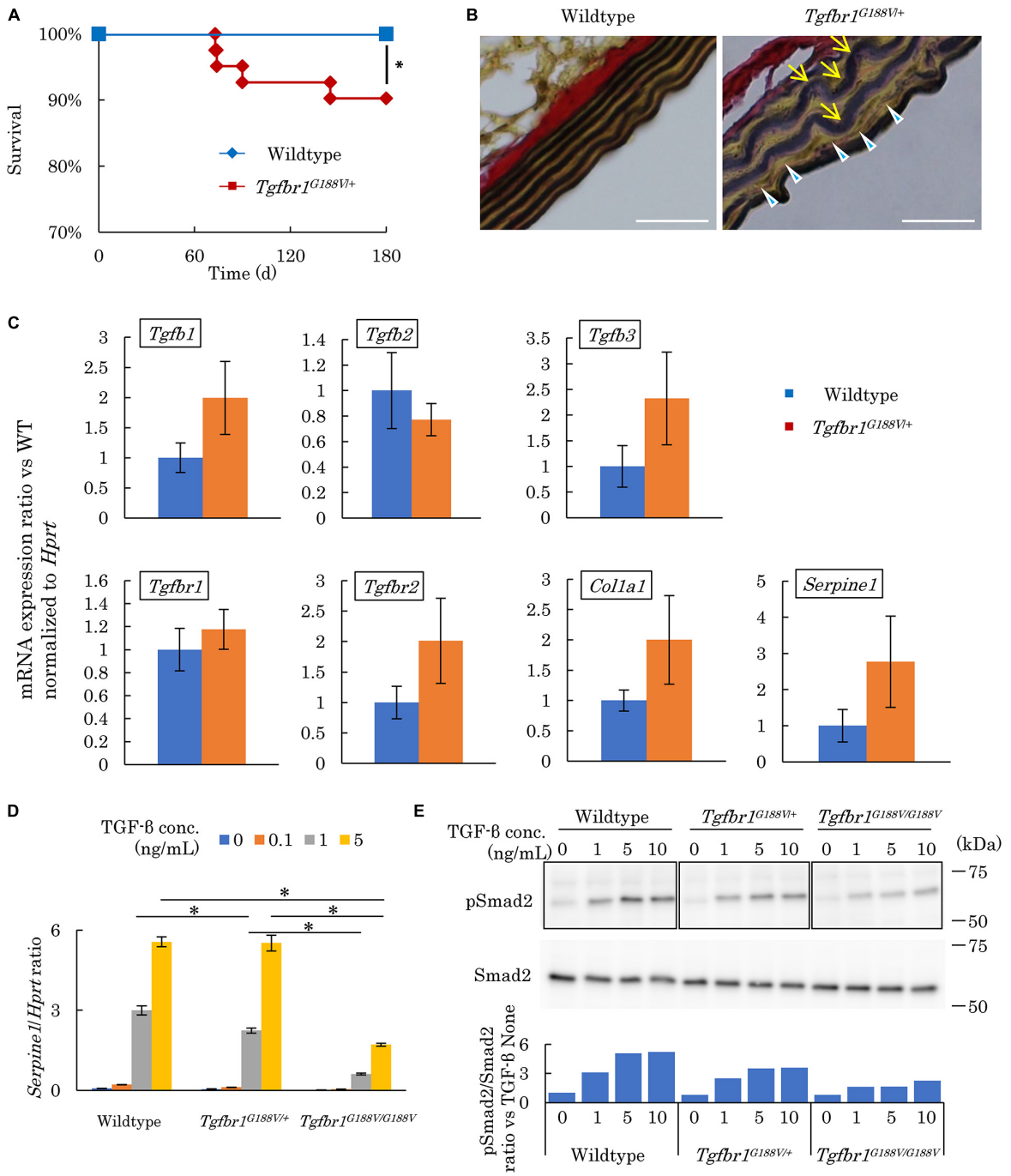

FIGURE 4 | *Tgfbr1*$^{G188V/+}$ mice recapitulate vascular LDS phenotypes. **(A)** Kaplan–Meier survival curve showing a diminishing lifespan of *Tgfbr1*$^{G188V/+}$ mice. *$P < 0.05$. **(B)** Representative aortic wall sections of *Tgfbr1*$^{G188V/+}$ mice at 24 weeks of age stained with EVG to identify elastin fibers. Scale bar: 25 μm. Arrows show elastic fiber distortion. Arrowheads show elastic fiber fragmentation. **(C)** Analysis of TGF-β-related genes in aortic tissues derived from wildtype and *Tgfbr1*$^{G188V/+}$ mice ($n = 4$). Data represent means ± SD in triplicate assays. **(D)** *Serpine1* gene expression in MEFs derived from wildtype, *Tgfbr1*$^{G188V/+}$, and *Tgfbr1*$^{G188V/G188V}$ embryos at embryonic day 13.5 stimulated with TGF-β (0–5 ng/mL). Data represent means ± SD in triplicate assays. *$P < 0.05$, compared with the indicated TGF-β concentration. **(E)** Phospho-Smad2 (pSmad2) in MEFs derived from wildtype, *Tgfbr1*$^{G188V/+}$, and *Tgfbr1*$^{G188V/G188V}$ embryos at embryonic day 13.5 stimulated with TGF-β (0–10 ng/mL). Quantitative western blot analysis is shown as the ratios of the intensities of phospho-Smad2 to Smad2.

proximity to the alveolar bone were counted between the first and second molars and between the second and third molars. These values were divided by the length of the alveolar bone surface for comparison (**Figure 6D**, red line). In *Tgfbr1*$^{G188V/+}$ mice, the number of osteoclasts was increased significantly after *P. gingivalis* administration (**Figure 6E**).

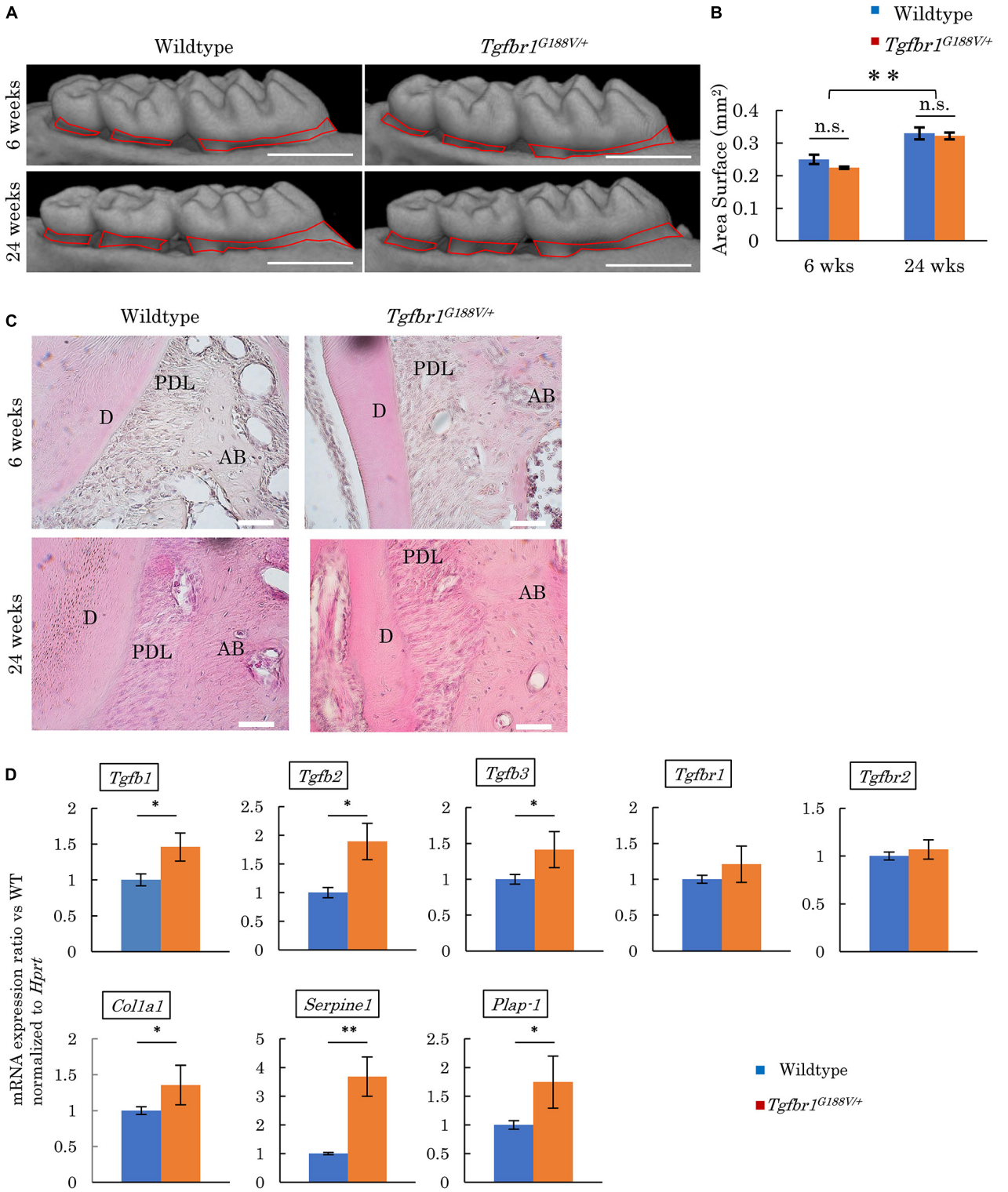

FIGURE 5 | Analysis of phenotypes in periodontal tissues of *Tgfbr1*$^{G188V/+}$ mice. **(A)** Representative images from micro-CT analysis of maxillary alveolar bones in *Tgfbr1*$^{G188V/+}$ mice. Scale bar: 1 mm. **(B)** Alveolar bone resorption was measured in the root surface area between the alveolar apex from the cementoenamel junction (red line in **Figure 4A**). Data represent means ± SD. Six-week-old wildtype: $n = 6$, 6-week-old *Tgfbr1*$^{G188V/+}$: $n = 8$, 24-week-old wildtype: $n = 20$, and 24-week-old *Tgfbr1*$^{G188V/+}$: $n = 14$. **(C)** Representative images of HE staining of the periodontium from WT and *Tgfbr1*$^{G188V/+}$ mice at 6 and 24 weeks of age. AB, alveolar bone; PDL, periodontal ligament; D, dentin. Scale bar: 50 μm. **(D)** Analysis of TGF-β-related gene expression in periodontal tissues derived from wildtype and *Tgfbr1*$^{G188V/+}$ mice ($n = 4$). Data represent means ± SD in triplicate assays. *$P < 0.05$, **$P < 0.01$, compared with wildtype.

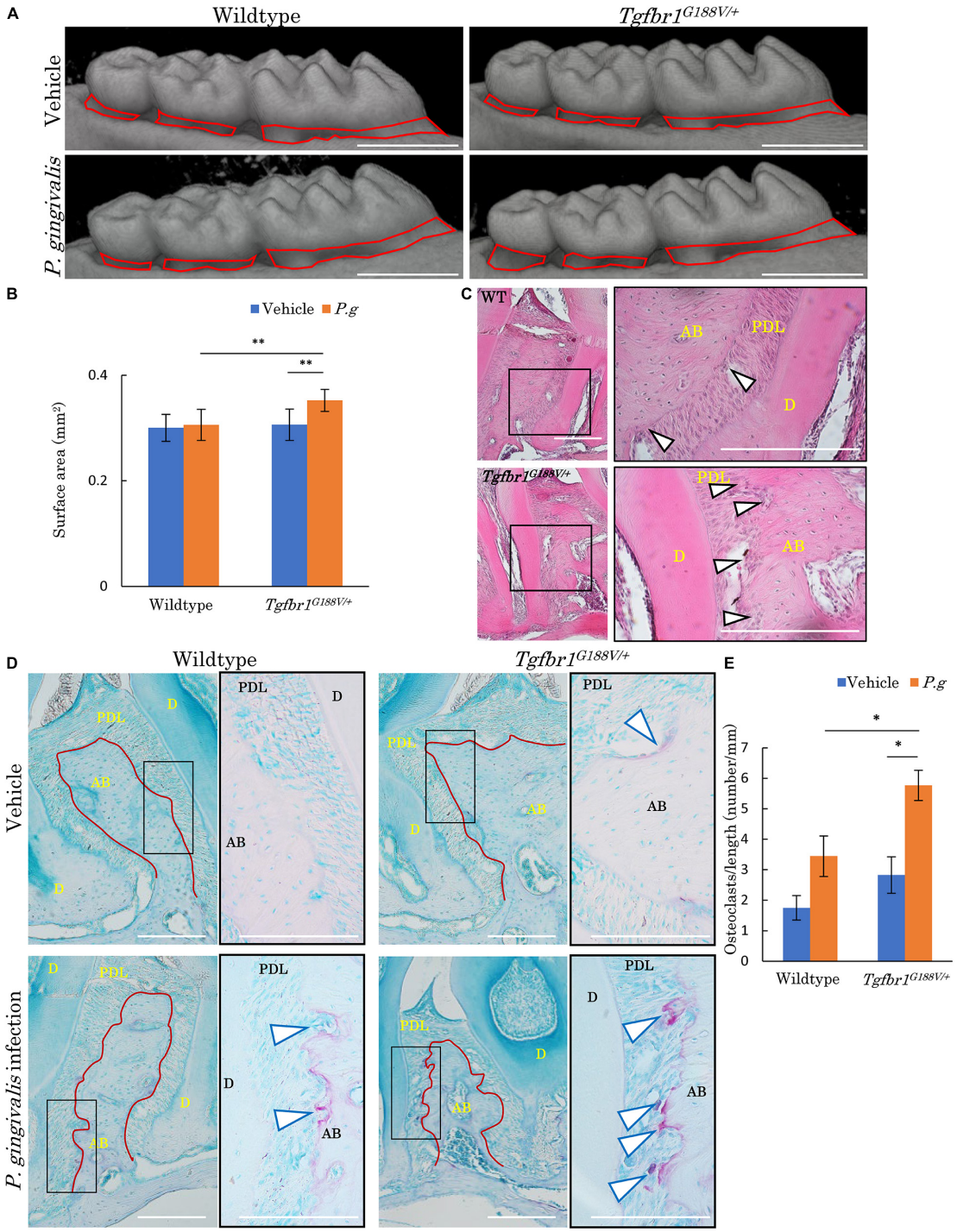

FIGURE 6 | Oral infection with *P. gingivalis* induces alveolar bone resorption in *Tgfbr1*$^{G188V/+}$ mice. **(A)** Representative images from micro-CT analysis of maxillary alveolar bones in *P. gingivalis*-infected WT and *Tgfbr1*$^{G188V/+}$ mice. Scale bar: 1 mm. **(B)** Alveolar bone resorption was measured in the root surface area between the alveolar apex from the cementoenamel junction (red line in **A**). Data represent means ± SD in triplicate assays. $^{**}P < 0.01$. Wildtype: $n = 11$ in vehicle, $n = 6$ in *P. gingivalis* infection. **(C)** Representative images of HE staining of the periodontium from *P. gingivalis*-infected wildtype and *Tgfbr1*$^{G188V/+}$ mice. Right panel shows a high magnification images of the rectangular area indicated in the left panel. Scale bar: 200 μm. Arrowheads indicate multinucleated cells. AB, alveolar bone; PDL, periodontal ligament; D, dentin. **(D)** Representative images of TRAP-stained periodontium from *P. gingivalis*-infected wildtype and *Tgfbr1*$^{G188V/+}$ mice. Right panel shows a high magnification image of the rectangular area indicated in the left panel. Scale bar: 200 μm. Arrowheads indicate TRAP-positive multinucleated cells. **(E)** Quantification of TRAP-positive cell numbers in each group. TRAP-positive cell numbers on the surface of alveolar bone were counted and divided by the length of the alveolar bone (red line in **D**). Data represent means ± SD in wildtype: $n = 3$ in vehicle, $n = 5$ in *P. gingivalis* infection. *Tgfbr1*$^{G188V/+}$: $n = 4$ in vehicle, $n = 6$ in *P. gingivalis* infection. Vehicle: sham control, *P.g*, *P. gingivalis* infection, AB, alveolar bone; D, dentin; PDL, periodontal ligament. $^{*}P < 0.05$, compared with Vehicle.

Upregulation of Inflammatory Cytokine mRNA Expression in Peritoneal Macrophages From *Tgfbr1*$^{G188V/+}$ Mice

To assess the innate immunological response of *Tgfbr1*$^{G188V/+}$ mice to *P. gingivalis*, we isolated peritoneal macrophages from WT and *Tgfbr1*$^{G188V/+}$ mice, stimulated these cells with *P. gingivalis* LPS, and then analyzed inflammatory cytokine expression by quantitative PCR (**Figure 7**). We found that mRNA expression of *Cxcl10*, *Il6* and *Tnf* was significantly upregulated in *Tgfbr1*$^{G188V/+}$ macrophages compared with WT macrophages.

DISCUSSION

In this study, we generated a knock-in mouse that reproduced the *TGFBR1* gene mutation in an LDS patient who exhibited localized and remarkable vertical bone resorption, despite generally good plaque control. We then analyzed the phenotypes of this mouse model. Aggressive periodontitis is strongly affected by genetic factors and the morbidity rate in Japan is 0.05–1% (Takahashi et al., 2011). More than 40 genetic variants associated with LDS have been reported thus far (Loeys et al., 2006). However, the patient in this study had a previously unreported mutation, namely a novel G188V mutation in the GS domain of *TGFBR1*. TGF-β binds to type 2 receptors on cell membranes, thereby forming a complex with type 1 receptors. Type 2 receptors have serine–threonine kinase activity in the intracellular region and phosphorylate the GS domain of bound type 1 receptors. The GS domain of type 1 receptors is phosphorylated and kinase activation results in signal transmission to cells via R-Smad, an intracellular signal transduction molecule (Doyle et al., 2012). The genetic mutation identified in the LDS patient in this study attenuated Smad signaling. Structural changes in the GS domain of TGFBR1 may prevent phosphorylation of the GS domain and inhibit signal transduction. However, distinct point mutations in *TGFBR1*, which spontaneously activate TGF-β signaling, have been reported as the cause of multiple self-healing squamous epithelioma, also known as Ferguson–Smith disease (Goudie et al., 2011). The detailed changes in receptor locality and the three-dimensional structure are unclear and should be examined in future studies.

In the mouse model established in this study, the *Tgfbr1* G188V/G188V mutation was lethal in embryos. Similarly, this mutation has not been identified in human homozygous patients with LDS. Therefore, Tgfbr1 is considered to be essential for survival. Some *Tgfbr1*$^{G188V/G188V}$ embryos collected at day 14.5 showed fewer bloodstreams in craniofacial, trunk, and spinal cord regions. It is important to investigate the effects of the *Tgfbr1* G188V/G188V mutation on cardiovascular development during embryogenesis to reveal the mechanisms of embryonic lethality. In *Tgfbr1*$^{G188V/+}$ mice, distortion and fine tearing of elastic fibers in aortic tissue were confirmed and a tendency toward premature death was observed. Structural abnormalities

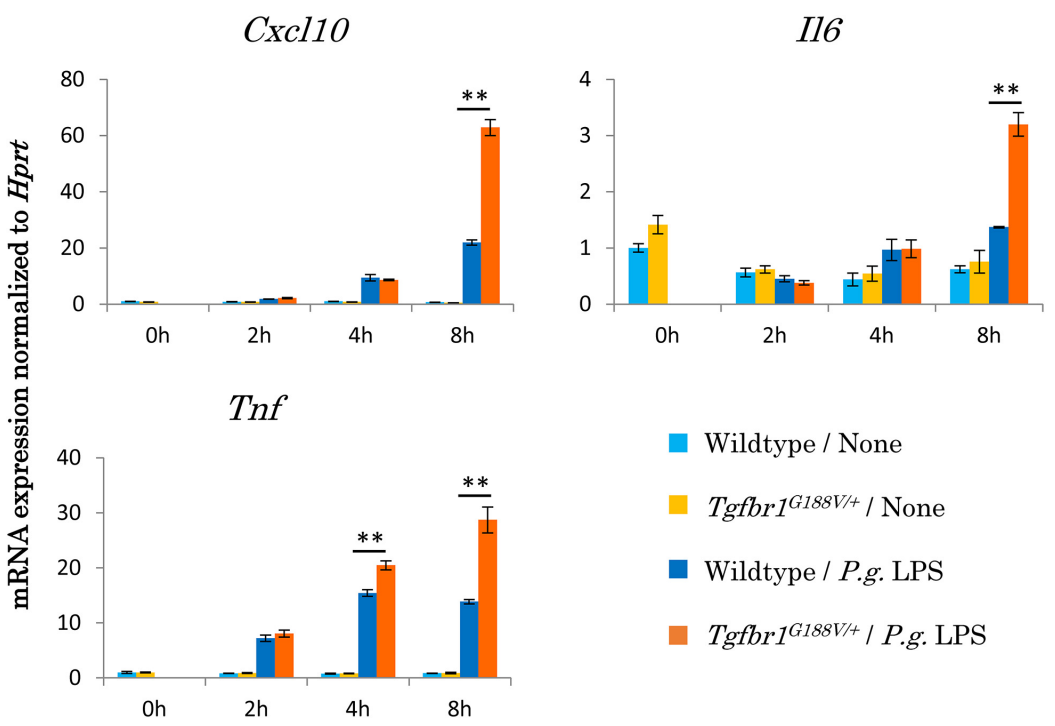

FIGURE 7 | Upregulation of inflammatory cytokine mRNA expression in peritoneal macrophages from *Tgfbr1*$^{G188V/+}$ mice. Macrophages were harvested from the peritoneal cavity of 8-week-old male WT and *Tgfbr1*$^{G188V/+}$ mice at 3 days after injection of thioglycolate. The peritoneal macrophages were stimulated with 1 μg/ml *P. gingivalis* LPS for the indicated times and then total RNA was isolated for quantitative PCR analysis. Data represent means ± SD in triplicate assays. $^{**}P < 0.01$, compared with wildtype.

of the elastic fibers of the aorta trigger pathological diseases (e.g., aortic aneurysm, aortic dissection, hemorrhage, and fibrosis) and premature death. However, because the relationship between aortic structural abnormalities and aortic aneurysm was not examined, additional studies are necessary.

In this study, *Tgfbr1*$^{G188V/+}$ MEFs showed attenuation of TGF-β signaling, but had elevated TGF-β-related gene expression in aortic tissues. In studies of aortic tissues, overexpression of TGF-β has been reported in patients with LDS and an LDS mouse model (Loeys et al., 2005, 2006; Gallo et al., 2014). TGF-β signaling involves canonical pathways via Smad and non-canonical pathways via ERK, JNK, and other molecules. Their expression patterns are regulated by a feedback mechanism that involves Smad (Lindsay and Dietz, 2011). In LDS, mutations in TGF-β receptors selectively attenuate the canonical pathway, thereby inhibiting the negative feedback mechanism that underlies TGF-β expression. Accordingly, increased levels of TGF-β in tissues contribute to excessive canonical pathway signaling. Non-canonical pathways are also presumed to cause aortic lesions by excessive activation (Lindsay and Dietz, 2011). In *Tgfbr1*$^{G188V/+}$ mice, aortic elastic fiber abnormalities likely occurred through the same mechanism.

Periodontal tissues showed significantly higher expression levels of TGF-β-related genes in *Tgfbr1*$^{G188V/+}$ mice than in WT mice, with no obvious differences in alveolar bone resorption or periodontal tissue status. TGF-β overexpression in tissues was presumed to compensate for the decrease in TGF-β signaling at the cellular level similar to the findings in aortic tissues. However, no apparent periodontal tissue-specific structural abnormalities were observed by HE staining. Therefore, abnormalities related to excessive TGF-β signaling were not triggered in periodontal tissues without pathological stimulation. In the future, detailed analyses at cellular and molecular levels are needed to evaluate structural abnormalities in periodontal tissues.

In the *P. gingivalis*-induced periodontitis model, significantly more osteoclasts were present in *Tgfbr1*$^{G188V/+}$ mice than in WT mice. Moreover, alveolar bone resorption was significantly increased in *Tgfbr1*$^{G188V/+}$ mice. *P. gingivalis* is commonly used to induce periodontitis (Baker et al., 1994; Suda et al., 2013; Arimatsu et al., 2014; Papathanasiou et al., 2016). In this experimental periodontitis model, the oral administration of *P. gingivalis* causes changes in the intestinal flora, which leads to systemic inflammation and subsequent bone resorption through immune cell responses in the oral cavity (Baker et al., 1994; Arimatsu et al., 2014). Notably, the oral administration of *P. gingivalis* may have triggered systemic inflammation in *Tgfbr1*$^{G188V/+}$ mice. A previous report has demonstrated that TGF-β signaling in macrophages suppresses Toll-like receptor (TLR) signaling through myeloid differentiation factor 88 (Naiki et al., 2005). In *Tgfbr1*$^{G188V/+}$ mouse macrophages, the mutation in *Tgfbr1* may promote TLR signaling by attenuation of TGF-β signaling, thereby increasing the macrophage response to *P. gingivalis* LPS intrinsically. In the future, more details of the mechanisms that underlie osteoclastogenesis induced by *P. gingivalis* in *Tgfbr1*$^{G188V/+}$ mice should be analyzed to understand the pathophysiology of periodontal disease caused by the *Tgfbr1*$^{G188V/+}$ mutation.

Smad-mediated TGF-β signaling inhibits osteoblast differentiation (Borton et al., 2001). In periodontal tissues of *Tgfbr1*$^{G188V/+}$ mice, excessive TGF-β signaling may suppress osteoblast differentiation. In LDS model mice with mutations in TGF-β II receptors, the femur is thinner and bone mass decreases, thereby increasing fragility (Dewan et al., 2015). In *Tgfbr1*$^{G188V/+}$ mice, cell differentiation into osteoblasts and osteocytes may be suppressed, which suggests that the alveolar bone tends to be susceptible to resorption.

CONCLUSION

In conclusion we established an LDS mouse model that showed elevated susceptibility to *P. gingivalis*-induced periodontitis, probably through TGF-β signal dysfunction. This suggests that TGF-β signaling abnormalities accelerate the pathogenesis or progression of periodontitis.

DATA AVAILABILITY STATEMENT

The original contributions presented in the study are included in the article/supplementary material, further inquiries can be directed to the corresponding author/s.

ETHICS STATEMENT

The studies involving human participants were reviewed and approved by the Institutional Ethics Committee of Osaka University Graduate School of Dentistry, and National Cerebral and Cardiovascular Center. The patients/participants provided their written informed consent to participate in this study. The animal study was reviewed and approved by Institutional Animal Care and Use Committee of Osaka University Graduate School of Dentistry.

AUTHOR CONTRIBUTIONS

SY, KT, TM, and SM conceived, designed the experiments, and wrote the manuscript. SY, KT, MK, HS, and TK performed the experiments. SY, KT, CF, TM, HY, SS, and SM analyzed the data. All authors contributed to the article and approved the submitted version.

FUNDING

This study was supported by the Japan Society for the Promotion of Science (JSPS) KAKENHI (Grant Nos. 15H02579, 17H04417, 19H01069, and 20H03862).

ACKNOWLEDGMENTS

We thank Ryan Chastain-Gross, Ph.D., and Mitchell Arico from Edanz Group (https://jp.edanz.com/ac) for editing a draft of this manuscript.

REFERENCES

Aoki-Nonaka, Y., Nakajima, T., Miyauchi, S., Miyazawa, H., Yamada, H., Domon, H., et al. (2013). Natural killer T cells mediate alveolar bone resorption and a systemic inflammatory response in response to oral infection of mice with *Porphyromonas gingivalis*. *J. Periodontal. Res.* 49, 69–76. doi: 10.1111/jre.12080

Arimatsu, K., Yamada, H., Miyazawa, H., Minagawa, T., Nakajima, M., Ryder, M. I., et al. (2014). Oral pathobiont induces systemic inflammation and metabolic changes associated with alteration of gut microbiota. *Sci. Rep.* 4:4828. doi: 10.1038/srep04828

Awata, T., Yamada, S., Tsushima, K., Sakashita, H., Yamaba, S., Kajikawa, T., et al. (2015). PLAP-1/Asporin positively regulates FGF-2 activity. *J. Dent. Res.* 94, 1417–1424. doi: 10.1177/0022034515598507

Baker, P. J., Evans, R. T., and Roopenian, D. C. (1994). Oral infection with *Porphyromonas gingivalis* and induced alveolar bone loss in immunocompetent and severe combined immunodeficient mice. *Arch. Oral Biol.* 39, 1035–1040. doi: 10.1016/0003-9969(94)90055-8

Borton, A. J., Frederick, J. P., Datto, M. B., Wang, X. F., and Weinstein, R. S. (2001). The loss of Smad3 results in a lower rate of bone formation and osteopenia through dysregulation of osteoblast differentiation and apoptosis. *J. Bone Miner. Res.* 16, 1754–1764. doi: 10.1359/jbmr.2001.16.10.1754

De Coster, P. J., Martens, L. C., and De Paepe, A. (2002). Oral manifestations of patients with Marfan syndrome: a case-control study. *Oral Surg. Oral Med. Oral Pathol. Oral Radiol. Endod.* 93, 564–572. doi: 10.1067/moe.2002.121430

Dewan, A. K., Tomlinson, R. E., Mitchell, S., Goh, B. C., Yung, R. M., Kumar, S., et al. (2015). Dysregulated TGF-beta signaling alters bone microstructure in a mouse model of Loeys-Dietz syndrome. *J. Orthop. Res.* 33, 1447–1454. doi: 10.1002/jor.22920

Dietz, H. C., Cutting, G. R., Pyeritz, R. E., Maslen, C. L., Sakai, L. Y., Corson, G. M., et al. (1991). Marfan syndrome caused by a recurrent de novo missense mutation in the fibrillin gene. *Nature* 352, 337–346. doi: 10.1038/352337a0

Dietz, H. (2007). Marfan syndrome: from molecules to medicines. *Am. J. Hum. Genet.* 81, 662–667. doi: 10.1086/521409

Doyle, A. J., Doyle, J. J., Bessling, S. L., Maragh, S., Lindsay, M. E., Schepers, D., et al. (2012). Mutations in the TGF-beta repressor SKI cause Shprintzen-Goldberg syndrome with aortic aneurysm. *Nat. Genet.* 44, 1249–1254. doi: 10.1038/ng.2421

Gallo, E. M., Loch, D. C., Habashi, J. P., Calderon, J. F., Chen, Y., Bedja, D., et al. (2014). Angiotensin II-dependent TGF-beta signaling contributes to Loeys-Dietz syndrome vascular pathogenesis. *J. Clin. Invest.* 124, 448–460. doi: 10.1172/JCI69666

Godfrey, M., Menashe, V., Weleber, R. G., Koler, R. D., Bigley, R. H., Lovrien, E., et al. (1990). Cosegregation of elastin-associated microfibrillar abnormalities with the Marfan phenotype in families. *Am. J. Hum. Genet.* 46, 652–660.

Goudie, D. R., D'Alessandro, M., Merriman, B., Lee, H., Szeverényi, I., Avery, S., et al. (2011). Multiple self-healing squamous epithelioma is caused by a disease-specific spectrum of mutations in TGFBR1. *Nat. Genet.* 43, 365–371. doi: 10.1038/ng.780

Howe, J. R., Roth, S., Ringold, J. C., Summers, R. W., Jarvinen, H. J., Sistonen, P., et al. (1998). Mutations in the SMAD4/DPC4 gene in juvenile polyposis. *Science* 280, 1086–1088. doi: 10.1126/science.280.5366.1086

Huang, F., and Chen, Y. G. (2012). Regulation of TGF-beta receptor activity. *Cell Biosci.* 2:9.

Jain, E., and Pandey, R. K. (2013). Marfan syndrome. *BMJ Case Rep.* 2013:bcr2013201632. doi: 10.1136/bcr-2013-201632

Lindsay, M. E., and Dietz, H. C. (2011). Lessons on the pathogenesis of aneurysm from heritable conditions. *Nature* 473, 308–316. doi: 10.1038/nature10145

Loeys, B. L., Chen, J., Neptune, E. R., Judge, D. P., Podowski, M., Holm, T., et al. (2005). A syndrome of altered cardiovascular, craniofacial, neurocognitive and skeletal development caused by mutations in *TGFBR1* or *TGFBR2*. *Nat. Genet.* 37, 275–281. doi: 10.1038/ng1511

Loeys, B. L., Schwarze, U., Holm, T., Callewaert, B. L., Thomas, G. H., Pannu, H., et al. (2006). Aneurysm syndromes caused by mutations in the TGF-beta receptor. *N. Engl. J. Med.* 355, 788–798. doi: 10.1056/NEJMoa055695

Loeys, B. L., Dietz, H. C., Braverman, A. C., Callewaert, B. L., Backer, J. D., Devereux, R. B., et al. (2010). The revised Ghent nosology for the Marfan syndrome. *J. Med. Genet.* 47, 476–485. doi: 10.1136/jmg.2009.072785

Matt, P., Schoenhoff, F., Habashi, J., Holm, T., Van Erp, C., Loch, D., et al. (2009). Circulating transforming growth factor-beta in Marfan syndrome. *Circulation* 120, 526–532. doi: 10.1161/CIRCULATIONAHA.108.841981

Meng, H., Xu, L., Li, Q., Han, J., and Zhao, Y. (2007). Determinants of host susceptibility in aggressive periodontitis. *Periodontol. 2000* 43, 133–159. doi: 10.1111/j.1600-0757.2006.00204.x

Mizuguchi, T., Collod-Beroud, G., Akiyama, T., Abifadel, M., Harada, N., Morisaki, T., et al. (2004). Heterozygous *TGFBR2* mutations in Marfan syndrome. *Nat. Genet.* 36, 855–860. doi: 10.1038/ng1392

Naiki, Y., Michelsen, K. S., Zhang, W., Chen, S., Doherty, T. M., and Arditi, M. (2005). Transforming growth factor-beta differentially inhibits MyD88-dependent, but not TRAM- and TRIF-dependent, lipopolysaccharide-induced TLR4 signaling. *J. Biol. Chem.* 280, 5491–5495. doi: 10.1074/jbc.C400503200

Neptune, E. R., Frischmeyer, P. A., Arking, D. E., Myers, L., Bunton, T. E., Gayraud, B., et al. (2003). Dysregulation of TGF-beta activation contributes to pathogenesis in Marfan syndrome. *Nat. Genet.* 33, 407–411. doi: 10.1038/ng1116

Papapanou, P. N., Sanz, M., Buduneli, N., Dietrich, T., Feres, M., Fine, D. H., et al. (2018). Periodontitis: consensus report of workgroup 2 of the 2017 World Workshop on the Classification of Periodontal and Peri-Implant Diseases and Conditions. *J. Clin. Periodontol.* 45, S162–S170. doi: 10.1111/jcpe.12946

Papathanasiou, E., Kantarci, A., Konstantinidis, A., Gao, H., and Van Dyke, T. E. (2016). SOCS-3 Regulates Alveolar Bone Loss in Experimental Periodontitis. *J. Dent. Res.* 95, 1018–1025. doi: 10.1177/0022034516645332

Putnam, E. A., Zhang, H., Ramirez, F., and Milewicz, D. M. (1995). Fibrillin-2 (FBN2) mutations result in the Marfan-like disorder, congenital contractural arachnodactyly. *Nat. Genet.* 11, 456–464. doi: 10.1038/ng1295-456

Sakai, K., and Miyazaki, J. (1997). A transgenic mouse line that retains Cre recombinase activity in mature oocytes irrespective of the cre transgene transmission. *Biochem. Biophys. Res. Commun.* 237, 318–324. doi: 10.1006/bbrc.1997.7111

Schorr, S., Braun, K., and Wildman, J. (1951). Congenital aneurysmal dilatation of the ascending aorta associated with arachnodactyly. *Am. Heart J.* 42, 610–616. doi: 10.1016/0002-8703(51)90157-3

Straub, A. M., Grahame, R., Scully, C., and Tonetti, M. S. (2002). Severe periodontitis in Marfan's syndrome: a case report. *J. Periodontol.* 73, 823–826. doi: 10.1902/jop.2002.73.7.823

Staufenbiel, I., Hauschild, C., Kahl-Nieke, B., Vahle-Hinz, E., von Kodolitsch, Y., Berner, M., et al. (2013). Periodontal conditions in patients with Marfan syndrome - a multicenter case control study. *BMC Oral Health* 13:59. doi: 10.1186/1472-6831-13-59

Suda, N., Moriyama, K., and Ganburged, G. (2013). Effect of angiotensin II receptor blocker on experimental periodontitis in a mouse model of Marfan syndrome. *Infect. Immun.* 81, 182–188. doi: 10.1128/IAI.00886-12

Suzuki, J., Imai, Y., Aoki, M., Fujita, D., Aoyama, N., Tada, Y., et al. (2015). High incidence and severity of periodontitis in patients with Marfan syndrome in Japan. *Heart Vessels* 30, 692–695. doi: 10.1007/s00380-013-0434-y

Takahashi, M., Chen, Z., Watanabe, K., Kobayashi, H., Nakajima, T., Kimura, A., et al. (2011). Toll-like receptor 2 gene polymorphisms associated with aggressive periodontitis in Japanese. *Open Dent. J.* 5, 190–194. doi: 10.2174/1874210601105010190

Yamaba, S., Yamada, S., Kajikawa, T., Awata, T., Sakashita, H., Tsushima, K., et al. (2015). PLAP-1/Asporin regulates TLR2- and TLR4-induced inflammatory responses. *J. Dent. Res.* 94, 1706–1714.

Conflict of Interest: The authors declare that the research was conducted in the absence of any commercial or financial relationships that could be construed as a potential conflict of interest.

frontiers in Physiology

ORIGINAL RESEARCH
published: 27 August 2021
doi: 10.3389/fphys.2021.716441

Autophagy Induces Expression of IL-6 in Human Periodontal Ligament Fibroblasts Under Mechanical Load and Overload and Effects Osteoclastogenesis *in vitro*

Alexandra Mayr[1], Jana Marciniak[1], Benedikt Eggers[2], Kim Blawat[1], Jan Wildenhof[3], Rogerio Bastos Craveiro[4], Michael Wolf[4], James Deschner[5], Andreas Jäger[1] and Svenja Beisel-Memmert[1]*

[1] Department of Orthodontics, Center of Dento-Maxillo-Facial Medicine, University of Bonn Medical Center, Bonn, Germany, [2] Department of Oral, Maxillofacial and Plastic Surgery, Center of Dento-Maxillo-Facial Medicine, University of Bonn Medical Center, Bonn, Germany, [3] Private Clinic Schloss Schellenstein, Olsberg, Germany, [4] Department of Orthodontics, Faculty of Medicine, University Hospital Aachen, Aachen, Germany, [5] Department of Periodontology and Operative Dentistry, University Medical Center of the Johannes Gutenberg University, Mainz, Germany

OPEN ACCESS

Edited by:
Frédéric Lézot, Institut National de la Santé et de la Recherche Médicale (INSERM), France

Reviewed by:
Nicholas Ktistakis, Babraham Institute (BBSRC), United Kingdom
Fuhua Yan, Nanjing Stomatological Hospital (NSH), China

***Correspondence:**
Alexandra Mayr
alexandra.mayr@ukbonn.de

Specialty section:
This article was submitted to Craniofacial Biology and Dental Research, a section of the journal Frontiers in Physiology

Received: *28 May 2021*
Accepted: *04 August 2021*
Published: *27 August 2021*

Citation:
Mayr A, Marciniak J, Eggers B, Blawat K, Wildenhof J, Bastos Craveiro R, Wolf M, Deschner J, Jäger A and Beisel-Memmert S (2021) Autophagy Induces Expression of IL-6 in Human Periodontal Ligament Fibroblasts Under Mechanical Load and Overload and Effects Osteoclastogenesis in vitro. Front. Physiol. 12:716441. doi: 10.3389/fphys.2021.716441

Objective: Autophagy is an important cellular adaptation mechanism to mechanical stress. In animal experiments, inhibition of autophagy during orthodontic tooth movement triggered increased expression of inflammation-related genes and decreased bone density. The aim of this study was to investigate how autophagy affects cytokine levels of interleukin 6 (IL-6) in human periodontal ligament (hPDL) fibroblasts under mechanical pressure and the resulting influence on osteoblast communication.

Methods: hPDL fibroblasts were subjected to physiologic mechanical load, constant overload, or rapamycin treatment for 16 to 24 h ± autophagy inhibitor 3-MA. Autophagosomes were quantified by flow cytometry. Gene expression of *il-6* as well as IL-6 levels in the supernatant were determined with rtPCR and ELISA. To investigate the influence of mechanically-induced autophagy on cell-cell communication, an osteoblast-culture was subjected to supernatant from stimulated hPDL fibroblasts ± soluble IL-6 receptor (sIL-6R). After 24 h, *osteoprotegerin* (*opg*) and *receptor activator of nuclear factor κB ligand* (*rankl*) gene expressions were detected with rtPCR. Gene expression of *a disintegrin and metalloproteinases* (*adam*) *10* and *17* in stimulated hPDL fibroblasts was examined via rtPCR.

Results: Autophagy was induced by biomechanical stress in hPDL fibroblasts in a dose-dependent manner. Mechanical load and overload increased IL-6 expression at gene and protein level. Autophagy inhibition further enhanced the effects of mechanical stimulation on IL-6 expression. Mechanical stimulation of hPDL fibroblasts downregulated *adam10* and *adam17* expressions. Inhibition of autophagy had stimulus-intensity depending effects: autophagy inhibition alone or additional application of physiological stress enhanced *adam10* and *adam17* expressions, whereas mechanical overload had adverse effects. Osteoblasts showed significantly reduced

opg expression in the presence of supernatant derived of hPDL fibroblasts treated with autophagy inhibitor and sIL-6R.

Conclusion: IL-6 levels were increased in response to pressure in hPDL fibroblasts, which was further enhanced by autophagy inhibition. This caused a decrease in *opg* expression in osteoblasts. This may serve as an explanatory model for accelerated tooth movement observed under autophagy inhibition, but may also represent a risk factor for uncontrolled bone loss.

Keywords: autophagy, cell-cell communication, IL-6, ADAM10, ADAM17, mechanical load, mechanical overload, human periodontal ligament fibroblasts

1. INTRODUCTION

Orthodontic tooth movement (OTM) is based on the principle that teeth are moved through bone. To assess processes involved in OTM at molecular level the interplay of two key tissues, periodontal ligament (PDL) and alveolar bone, needs to be examined.

The PDL, a connective tissue in which PDL fibroblasts account for approximately 50–60% of the total cell number, has two main functions: first, the transmission and absorption of mechanical load, and second, providing vascular and nutrient supply to the cementum, the alveolar bone and the PDL itself (Storey, 1973; McCulloch and Bordin, 1991). According to the "pressure-tension theory" the PDL responds to changes in mechanical loading within the bony socket. The theory proposes that PDL fibroblasts play an important role in osteoclastic resorption and/or osteoblastic apposition in accordance with the mechanical stimulus (Sandstedt, 1904; Oppenheim, 1911; Schwarz, 1932). Thus, OTM is induced by application of mechanical forces to the periodontium, resulting in a biomechanical load on cells and tissues, which is subsequently followed by a sterile inflammation involving the release of multiple inflammatory cytokines including interleukin-6 (IL-6) (Li et al., 2018).

IL-6 is a cytokine with important functions in the body's systemic defense response to injury. However, its functions also include influencing bone metabolism. It is produced by various cell types (Garman et al., 1987; Lotz et al., 1988; Gauldie et al., 1992; Ogawa, 1992). For interaction of IL-6 with its target cell, there is a classical signaling pathway and a trans-signaling pathway. The classical pathway is only important in specific cell types, such as macrophages, neutrophils, hepatocytes and some type of T-cells, whereas the trans pathway has a widespread occurrence (Scheller et al., 2011). However, activation of the trans pathway is dependent on the presence of sIL-6R, which is, among others, cleaved from cell surfaces by specific A Disintegrin And Metalloproteinases 10 and 17 (ADAM10 and ADAM17) (Müllberg et al., 1994; Matthews et al., 2003; Chalaris et al., 2007, 2010). However, the tissue reaction is dependent on the amount of biomechanical load – whereas moderate pressure is an integral part of periodontal tissue homeostasis, mechanical overload leads to cell damage associated with an increased PDL fibroblasts death rate and dysregulated bone remodeling (Tang et al., 2006; Marchesan et al., 2011; Blawat et al., 2020).

Remodeling of the alveolar bone is performed by two different types of cells – osteoblasts and osteoclasts. Osteoblasts constitute bone apposition but also control osteoclast differentiation (Karsenty, 2003). Osteoclasts are responsible for degradation of the organic matrix through dissolution of minerals in an acidic environment as well as enzymatic resorption. These multinucleated cells are formed by the union of multiple monocytic precursors (Teitelbaum, 2000; Boyle et al., 2003). Osteoblasts promote osteoclast differentiation by expression of receptor activator of nuclear factor κB ligand (RANKL) on the surface, which interacts with receptor activator of nuclear factor κB (RANK) expressed on osteoclast progenitor cells (Udagawa et al., 1995; Palmqvist et al., 2002). However, they also express osteoprotegerin (OPG), a decoy receptor for nuclear factor κB ligand (RANKL). By binding RANKL, OPG inhibits the activation of NF-κB, a central and fast-acting transcription factor for immune activation and differentiation of precursor cells into osteoclasts (Theoleyre et al., 2004). Cytokines, especially IL-6, have been reported to influence the RANK-RANKL-OPG system in favor of osteoclast differentiation (Udagawa et al., 1995).

Autophagy, the process of self-consumption, has already been proven to be an important process during OTM. In rodents, inhibition of autophagy during mechanically induced tooth movement increased the gene expression of inflammatory markers and decreased alveolar bone density thereby accelerating tooth movement (Chen and Hua, 2021). Autophagy is essential for adaption to cellular stress, including nutrient, hypoxic, inflammatory and mechanical stress signals (King, 2012; Antonioli et al., 2017). In dependence of the stress threshold, autophagy controls cell fate; it can ensure cell survival, but also induce cell death (Mariño et al., 2014). In previous studies we emphasized the importance of autophagy for periodontal stress regulation. Autophagy was induced by tensile strain as well as by pressure in PDL fibroblasts in a dose-dependent manner (Memmert et al., 2019, 2020; Blawat et al., 2020). The modulation of autophagy by cytokines is known and widely studied. Th1 cytokines are suspected to function as inducers of autophagy, whereas Th2 cytokines act as autophagy inhibitors. The downstream influence of autophagy on cytokine expression on the other hand has been much less studied so far. However, how exactly autophagy interferes with periodontal stress regulation and the subsequent effects on cell-cell communication are still unknown, although we know from different cell types

that autophagy affects cytokine expression and therefore cell communication (Harris, 2011; Lapaquette et al., 2015).

Therefore, this study aimed to investigate how autophagy affects cytokine expression of PDL fibroblasts under biomechanical load and overload, with a special focus on IL-6 expression. Furthermore, the impact of autophagy on PDL fibroblast communication with osteoblasts was studied with emphasis on osteoclastogenesis.

2. MATERIALS AND METHODS

2.1. Culture and Treatment of Cells

Human PDL (hPDL) fibroblasts were purchased in second passage (Lonza, Basel, Switzerland) and cultured in 75 cm^2 cell culture flasks (Cellstar®, Greiner Bio-One, Frickenhausen, Germany) in Dulbecco's minimal essential medium, supplemented with 10% fetal bovine serum (FBS), 100 units/ml penicillin and 100 µg/ml streptomycin (all purchased from Invitrogen, Karlsruhe, Germany) at 37°C in a humidified atmosphere of 5% CO_2. Medium was changed every 3–4 days. For experiments, hPDL fibroblasts were used between passages three and five. 100,000 cells per well were seeded on ultra-thin gas-permeable cell-culture dishes (lumox® dish 35, Sarstedt, Nümbrecht, Germany), which were previously coated with attachment factor (Biologics Attachment Factor 1x, Gibco, Thermo Fisher Scientific, Waltham, Massachusetts, MA, USA), and grown to 80% confluence. One day prior to stimulation, FBS concentration was reduced to 1%.

After approval of the Ethics Committee of the University of Bonn and written informed consent by the patients or legal guardians (#117/15 Memmert), primary human alveolar osteoblasts (phAOBs) were explanted from alveolar bone fragments, which would have been discarded otherwise. These alveolar bone fragments were obtained of donors ($n = 3$), who underwent extractions of third molars.

For cell characterization, cells were cultured on cover slips in osteogenic medium (DMEM supplemented with 1% FBS, 1% penicillin/streptomycin, 10 nM dexamethasone, 280 µM ascorbic acid and 5 mM β-glycerophosphate (Sigma-Aldrich, Munich, Germany). The medium was replaced every 3 days. After 28 d, cells were incubated with 4% paraformaldehyde (Merck, Darmstadt, Germany) for 20 min and 0.05% Triton® X-100 (Merck) for 5 min to fix the cells for subsequent staining. Cell morphology and cell viability was confirmed by a double DAPI/Phalloidin staining: cell monolayers were incubated with fluorescent conjugates of Phalloidin (Sigma-Aldrich, 100 µM) for 40 min, followed by DAPI working solution (Sigma-Aldrich, 1 µg/ml) for 5 min. Stained cells were analyzed with the ZOE^{TM} Fluorescent Cell Imager (Bio-Rad, Hertfordshire, Great Britain) (**Figure 1A**).

For immunocytochemistry, cells were blocked with 5% bovine serum albumin fraction V (Roche Diagnostics, Indianapolis, USA) in 1x PBS for 40 min followed by overnight incubation with primary antibodies: monoclonal anti-collagen I antibody ab21286 (rabbit, Abcam, Cambride, UK) and monoclonal anti-bovine osteocalcin antibody M041 (mouse, TaKaRa Bio Europe, Saint-Germain-en-Laye, France). After rinsing with 1x PBS, secondary antibodies Goat pAb to Rb igG (CY3) ab6939 (Abcam) or Texas Red-X goat anti-mouse #T6390 (Invitrogen), respectively, were incubated for 1 h. Stained cells were analyzed with the ZOE^{TM} Fluorescent Cell Imager (Bio-Rad) as described above (**Figures 1B,C**).

For analysis of mineralization, 2% alizarin solution was added for 20 min, followed by 5 washing cycles with ddH_2O. Cells were analyzed by light microscopy (Axioskop 2, Axiocam MRc, Axiovision 4.7/ AutMess, Zeiss) (**Figure 1D**).

For experiments phAOBs were used between passages three and five, seeded on 6-well cell culture plates (Cellstar®, Greiner Bio-One) and grown to 80% confluence.

hPDL fibroblasts were subjected to physiologic sustained mechanical load (2 g/cm^2) or constant overload (8 g/cm^2) for 16 or 24 h using glass weights with or without the autophagy inhibitor 3-Methyladenine (3-MA, 5 mM, Sigma-Aldrich). Pharmacological induction of autophagy by addition of rapamycin (50 nM, Enzo Life Sciences, Farmingdale, NY, USA) served as positive control. Rapamycin and 3-MA were added 1 h prior to mechanical stimulation.

phAOBs were cultured 24 h with supernatant from stimulated hPDL fibroblasts with or without additional soluble IL-6-receptor (sIL-6R, 100 ng/ml, Abcam, Cambridge, United Kingdom).

2.2. Autophagosome Quantification

Autophagosomes were quantified in hPDL fibroblasts using the Cyto-ID® Autophagy Detection Kit (#ENZ-51031, Enzo Life Sciences, Farmingdale, NY, USA) as described earlier (Memmert et al., 2019; Blawat et al., 2020). In short, cells were stimulated with load, overload or rapamycin and with or without 3-MA (Sigma-Aldrich). After 16 h of stimulation, cells were carefully detached from the bottom of the well with trypsin-EDTA (Biochrom GmbH, Berlin, Germany). Detached cells were stained according to the manufacturer's instructions with Cyto-ID® Green Detection Reagent (Enzo Life Sciences) for 30 min in the dark at room temperature. Stained autophagosomes were measured by flow cytometry (BD FACSCalibur, BD Biosciences, Franklin Lakes, NJ, USA) and analyzed using Flowing Software (http://flowingsoftware.btk.fi/).

2.3. Analysis of Protein Expression

In order to obtain information about the influence of autophagy on cytokine expression under mechanical stimulation, a simultaneous analysis of several proinflammatory cytokines in stimulated hPDL fibroblast culture supernatants at 16 h was performed by a commercially available enzyme-linked immunoassay (ELISA) kit. The Human Common Cytokines Multi-Analyte ELISArray^{TM} Kit (MEH-004A, Qiagen, Hilden, Germany) was used according to the manufacturer's instructions. Absorbance was measured with a microplate reader (PowerWave x, BioTek Instruments, Winooski, VT, USA) at 450 nm with a 570 nm correction wavelength. For validation of regulated IL-6 protein expression, protein-concentration of IL-6 in hPDL fibroblast culture supernatants after 16 and 24 h stimulation was analyzed by a commercially available enzyme-linked immunoassay (ELISA) kit (IL6 Single Analyte ELISA Kit, SEH00560A, Qiagen). The protocol provided by

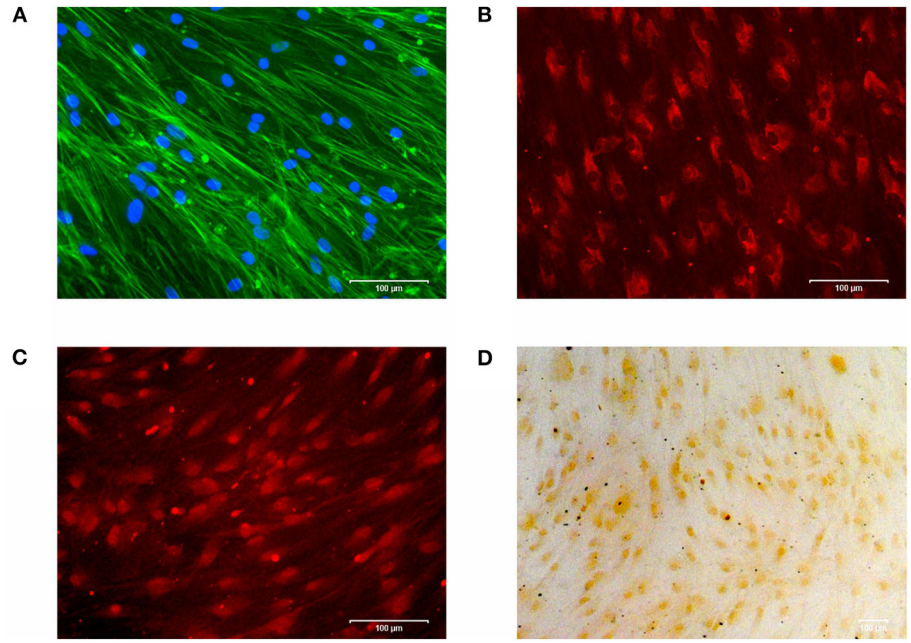

FIGURE 1 | (A) Cytoskeleton and cell viability of phAOBs were confirmed by DAPI/Phalloidin staining. **(B)** Expression of type I collagen visualized by immunofluorescence. **(C)** Immunofluorescence staining of osteocalcin. **(D)** Positive mineralization was confirmed by alizarin red staining. Scale bars indicate 100 µm. Experiments were performed in triplicates and representative images of cells from one donor are shown.

TABLE 1 | List of primers used for rtPCR.

Gene	Primer sequences	Annealing temperature (°C)
Adam10	(Primer was purchased from Qiagen)	60
Adam17	(Primer was purchased from Qiagen)	60
Gapdh	5′-CAC TCC TCC ACC TTT GAC GC-3′ 3′-CCA CCA CCC TGT TGC TGT A-5′	60
Il-6	5′-CAG GAG CCC AGC TAT GAA CT-3′ 3′-AGC AGG CAA CAC CAG GAG-5′	60
Opg	5′-TGC AGT ACG TCA AGC AGG AGT G-3′ 3′-TCC AGC TTG CAC CAC TCC AAA TC-5′	66
Rankl	5′-GCC AGT GGG AGA TGT TAG-3′ 3′-TTA GCT GCA AGT TTT CCC-5′	55
Rpl22	5′-TGA TTG CAC CCA CCC TGT AG-3′ 3′-GGT TCC CAG CTT TTC CGT TC-5′	60

the manufacturer was performed as followes: absorbance was assessed with the same microplate reader (PowerWave x) at the same conditions as mentioned above (450 nm with a 570 nm correction wavelength). Cell number was counted, using an automatic cell counter (Moelab, Hilden, Germany), and used for data normalization.

2.4. Analysis of Gene Expression

Gene expressions of *il-6* and membrane-bound proteases *adam10* and *adam17* (both purchased from Qiagen) in hPDL fibroblasts as well as expressions of *opg* and *rankl* in phAOBs were analyzed by real-time polymerase chain reaction (rtPCR). RNA was isolated using the commercially available RNeasy Protect Mini Kit (Qiagen) according to the manufacturer's instructions. RNA concentration was measured using a NanoDrop®ND-1000 spectrophotometer at 260 nm wavelength (NanoDrop Technologies, Wilmington, DE, USA) and consecutively transcribed to cDNA using the iScript™ Select cDNA Synthesis Kit (Bio-Rad Laboratories, Munich, Germany). Afterwards, 1 µl of cDNA, 2.5 µl of the specific primer (Metabion, Martinsried, Germany or Qiagen according to **Table 1**), 12.5 µl of QuantiTect SYBR Green Master Mix (Qiagen) and 9 µl of nuclease free water were mixed and gene expression was detected in the iCycler iQ™ real-time PCR detection system (Bio-Rad Laboratories). Protocol for rtPCR was as follows: an initial denaturation step at 95°C for 5 min was followed by 40 cycles of 10 s at 95°C, 30 s at annealing temperatures specific for the primers, and 30 s at 72°C for elongation. *Glycerinaldehyd-3-phosphate dehydrogenase* (*gapdh*) in phAOBs and *ribosomal protein L22* (*rpl22*) in hPDL fibroblasts served as housekeeping genes for data normalization.

2.5. Statistical Analysis

Experiments were repeated at least three times. Descriptive analyses of data were presented as means ± standard errors of the mean (SEM). Statistical analyses were performed with GraphPad Prism (Version 7.00 for Windows, GraphPad Software, San Diego, California USA, www.graphpad.com). Multiple comparisons were conducted using Kruskal-Wallis test followed by Dunnett's *T*-tests. Significance between two groups

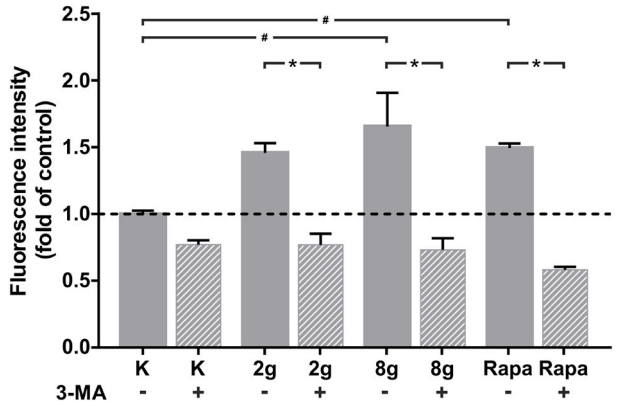

FIGURE 2 | Autophagosome accumulation, indicated by fluorescence, after 16 h of treatment with 2 g/cm^2, 8 g/cm^2 or Rapamycin (Rapa; 50 nM) with or without autophagy inhibitor 3-MA. Untreated cells served as control. Unstained cells served as negative control (not shown). Fluorescence intensity is shown as fold of control. Mean ± SEM ($n = 8$ replicates); # significant ($p < 0.05$) difference between groups as determined by Dunnett's *T*-test. * significant ($p < 0.05$) difference between two groups (uninhibited and inhibited) as determined by the Mann-Whitney-Test.

was calculated by the Mann-Whitney-Test. $P < 0.05$ were considered statistically significant.

3. RESULTS

3.1. Effects of 3-MA on Mechanical Stimulation of Autophagy

Induction of autophagy was measured by the accumulation of stained autophagosomes in hPDL fibroblasts after stimulation with sustained mechanical stress. Pharmacological induction of autophagy via rapamycin served as positive control, whereas unstained hPDL fibroblasts served as negative control. Mechanical overload of 8 g/cm^2, as well as the addition of rapamycin, for 16 h led to a significant increase in autophagosome accumulation, whereas stimulation with physiological pressure of 2 g/cm^2 did not lead to significant changes in fluorescence intensity. Addition of 3-MA to stimulated cells reliably inhibited autophagosome formation and led to a significant decrease in fluorescence intensity in all groups assessed (**Figure 2**).

3.2. Effects of Autophagy on Mechanical Induced IL-6 Expression in hPDL Fibroblasts

We were able to obtain initial indications of how cytokine expression was affected by mechanically induced autophagy using the Human Common Cytokines Multi-Analyte ELISArray^{TM} Kit (**Figure 3A** and **Table 2**). On the basis of these preliminary experiments, focus was set on targeting IL-6, the protein regulated most strongly, with a commercially available ELISA-Assay. IL-6 was significantly upregulated in hPDL fibroblasts subjected to both magnitudes of mechanical stress for 16 (**Figure 3B**) and 24 h (**Figure 3C**). Induction of autophagy via rapamycin showed no effect on IL-6-levels. Autophagy inhibition, however, led to significant increases in IL-6 protein levels in nearly all tested groups. One exception was the stimulation of physiologic sustained mechanical load over 24 h, where 3-MA addition did not enhance IL-6 levels any further. IL-6 showed a similar pattern of expression in the supernatant at both time points, although the overall amount measured at 24 h appeared to be lower. Gene expression of *il-6* was also significantly upregulated by sustained mechanical stress after 16 h in hPDL fibroblasts (**Figure 4A**). Similar to results obtained on protein level, induction of autophagy via rapamycin had no significant effect on *il-6* gene expression. But again, autophagy inhibition resulted in a significant increase of *il-6* levels in all groups. After 24 h, a significant increase in *il-6* gene expression was detected in the overload group (**Figure 4B**). Again, chemical induction of autophagy had no effect on *il-6* gene expression, whereas inhibition of autophagy again elicited an increase in *il-6* gene expression in the mechanically simulated groups.

3.3. Effects of Autophagy and Mechanical Stimulation on Cell-Cell Communication

In order to analyze the effect that autophagy exerts on cell-cell communication via the regulation of IL-6 expression, phAOBs were cultured with supernatant of stimulated hPDL fibroblasts with and without the addition of sIL-6R. Gene expression of *rankl* and *opg* was analyzed in phAOBs cultured without additional sIL-6R (**Figures 5A,B**). Without the receptor, *opg* expression did not change significantly (**Figure 5A**). Interestingly, even in the absence of the receptor, autophagy inhibition in hPDL fibroblasts under control and physiological conditions significantly reduced *rankl* gene expression (**Figure 5B**). The addition of sIL-6R to hPDL fibroblast supernatant led to a marked effect on *opg* gene expression in phAOBs (**Figure 5C**). Inhibition of autophagy resulted in a significant decrease of *opg* gene expression in all groups assessed. However, application of mechanical pressure to hPDL fibroblasts as well as autophagy induction resulted in no significant changes in *opg* expression levels. *Opg* antagonist *rankl* showed almost no response to the addition of soluble IL-6 receptor (**Figure 5D**). A significant decrease in *rankl* expression in phOABs was observed when autophagy was pharmacologically induced in hPDL fibroblasts by rapamycin.

3.4. Effects of Autophagy and Mechanical Stimulation on the Expression of ADAM Proteases

The effects of mechanical stimulation as well as autophagy on the expression of ADAM proteases, responsible for cleavage of the IL-6 receptor from cell surfaces, were also investigated in hPDL fibroblasts. The expression of both ADAM protases, *adam10* (**Figure 6A**) and *adam17* (**Figure 6B**), were significantly inhibited by both magnitudes of mechanical pressure as well as by autophagy induction. Interestingly, autophagy inhibition under control and physiological conditions resulted in a significant increase in gene expression of both ADAM proteases. Autophagy inhibition under overload, on the other hand, led to a significant

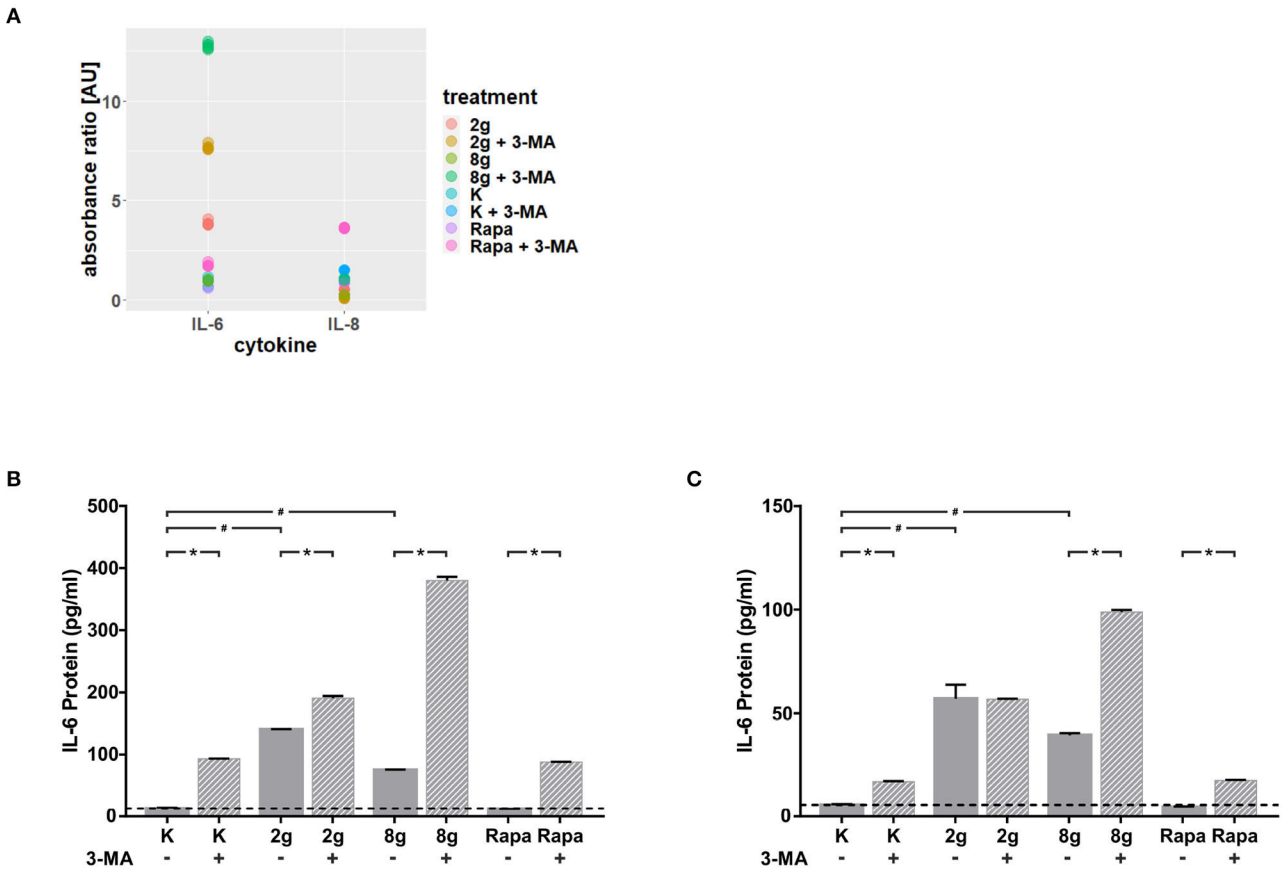

FIGURE 3 | (A) Absorbance ratios of examined cytokines with control groups above detection limit. Effects of mechanical stimulation (2 or 8 g/cm^2) or Rapamycin (Rapa; 50 nM) on cytokine levels in supernatants with or without autophagy inhibitor 3-MA at 16 h as determined by the Human Common Cytokines Multi-Analyte ELISArray^{TM} Kit (Qiagen). Untreated cells served as control. **(B)** Effects of mechanical stimulation (2 or 8 g/cm^2) or Rapamycin (Rapa; 50 nM) on IL-6 protein level in supernatants with or without autophagy inhibitor 3-MA at 16 h as determined by ELISA. Untreated cells served as control. Mean ± SEM ($n = 12$); # significant ($p < 0.05$) difference between groups as determined by Dunnett's *T*-test. * significant ($p < 0.05$) difference between two groups (uninhibited and inhibited) as determined by the Mann-Whitney-Test. **(C)** Effects of mechanical stimulation (2 or 8 g/cm^2) or Rapamycin (Rapa; 50 nM) on IL-6 protein level in supernatants with or without autophagy inhibitor 3-MA at 24 h as determined by ELISA. Untreated cells served as control. Mean ± SEM ($n = 12$); # significant ($p < 0.05$) difference between groups as determined by Dunnett's *T*-test. * significant ($p < 0.05$) difference between two groups (uninhibited and inhibited) as determined by the Mann-Whitney-Test.

decrease in gene expression of both ADAM proteases. Autophagy inhibition following chemical autophagy induction also reduced *adam10* expression levels significantly (**Figure 6A**), whereas *adam17* levels showed no significant changes (**Figure 6B**).

4. DISCUSSION

The present study adressed the influence of autophagy on IL-6 production in hPDL fibroblasts during mechanical load and overload and addresses the consequences of this regulation with respect to osteoclastogenesis *in vitro*.

The autophagic response was dose-dependent in respect to mechanical pressure stimulation and was shown to be reliably inhibited by 3-MA. Our results suggest that mechanical pressure stimulation leads to a significant upregulation of IL-6 expression on gene and protein level. Autophagy inhibition further enhanced the effects of mechanical stimulation on IL-6 expression. These regulations also had consequences on cell-cell communication. Inhibition of autophagy in hPDL fibroblasts restrained *opg* gene expression in phAOBs via IL-6 secretion. Although being interrelated, we could not demonstrate an IL-6 related effect on the expression of *rankl*. We further found that the expression of proteases *adam10* and *adam17* were significantly downregulated in hPDL fibroblasts in response to mechanical stimulation. The response to autophagy inhibition seemed to be dependent on stimulus intensity. Inhibition of autophagy in combination without additional stress or physiological load led to upregulation in *adam* expressions. Enhanced stress stimulation due to overload and chemical induction of autophagy in combination with autophagy inhibition led to reduced *adam* expressions.

We demonstrated in the current as well as in earlier studies that autophagy in hPDL fibroblasts is regulated by pressure in a dose-dependent manner (Blawat et al., 2020). Autophagy is an important adaptive mechanism to mechanical forces in

TABLE 2 | Absorbance values of tested cytokines.

Cytokine	Group	Absorbance (mean)	Cytokine	Group	Absorbance (mean)
GM-CSF	K	NA	IL-1β	K	NA
GM-CSF	K+3-MA	NA	IL-1β	K+3-MA	NA
GM-CSF	Rapa	NA	IL-1β	Rapa	NA
GM-CSF	Rapa+3-MA	NA	IL-1β	Rapa+3-MA	NA
GM-CSF	LD	0,171	IL-1β	LD	0,087
GM-CSF	LD+3-MA	NA	IL-1β	LD+3-MA	NA
GM-CSF	8g	NA	IL-1β	8g	NA
GM-CSF	8g+3-MA	NA	IL-1β	8g+3-MA	NA
IFN-γ	K	NA	IL-2	K	NA
IFN-γ	K+3-MA	NA	IL-2	K+3-MA	NA
IFN-γ	Rapa	NA	IL-2	Rapa	NA
IFN-γ	Rapa+3-MA	NA	IL-2	Rapa+3-MA	NA
IFN-γ	LD	0,069	IL-2	LD	0,123
IFN-γ	LD+3-MA	NA	IL-2	LD+3-MA	NA
IFN-γ	8g	NA	IL-2	8g	NA
IFN-γ	8g+3-MA	NA	IL-2	8g+3-MA	NA
IL-10	K	NA	IL-4	K	NA
IL-10	K+3-MA	NA	IL-4	K+3-MA	NA
IL-10	Rapa	NA	IL-4	Rapa	NA
IL-10	Rapa+3-MA	NA	IL-4	Rapa+3-MA	NA
IL-10	LD	0,050	IL-4	LD	0,072
IL-10	LD+3-MA	NA	IL-4	LD+3-MA	0,079
IL-10	8g	NA	IL-4	8g	NA
IL-10	8g+3-MA	NA	IL-4	8g+3-MA	NA
IL-12	K	NA	**IL-6**	**K**	**0,041**
IL-12	K+3-MA	NA	**IL-6**	**K+3-MA**	**NA**
IL-12	Rapa	NA	**IL-6**	**Rapa**	**NA**
IL-12	Rapa+3-MA	0,113	**IL-6**	**Rapa+3-MA**	**0,072**
IL-12	LD	0,254	**IL-6**	**LD**	**0,157**
IL-12	LD+3-MA	NA	**IL-6**	**LD+3-MA**	**0,312**
IL-12	8g	NA	**IL-6**	**8g**	**0,040**
IL-12	8g+3-MA	NA	**IL-6**	**8g+3-MA**	**0,520**
IL-17A	K	NA	**IL-8**	**K**	**0,478**
IL-17A	K+3-MA	NA	**IL-8**	**K+3-MA**	**0,722**
IL-17A	Rapa	NA	**IL-8**	**Rapa**	**0,416**
IL-17A	Rapa+3-MA	NA	**IL-8**	**Rapa+3-MA**	**1,732**
IL-17A	LD	0,085	**IL-8**	**LD**	**0,251**
IL-17A	LD+3-MA	NA	**IL-8**	**LD+3-MA**	**0,040**
IL-17A	8g	NA	**IL-8**	**8g**	**0,129**
IL-17A	8g+3-MA	NA	**IL-8**	**8g+3-MA**	**0,500**
IL-1α	K	NA	TNF-α	K	NA
IL-1α	K+3-MA	NA	TNF-α	K+3-MA	NA
IL-1α	Rapa	NA	TNF-α	Rapa	NA
IL-1α	Rapa+3-MA	NA	TNF-α	Rapa+3-MA	NA
IL-1α	LD	NA	TNF-α	LD	NA
IL-1α	LD+3-MA	NA	TNF-α	LD+3-MA	NA
IL-1α	8g	NA	TNF-α	8g	NA
IL-1α	8g+3-MA	NA	TNF-α	8g+3-MA	NA

Effects of mechanical stimulation (2 g/cm^2 or 8 g/cm^2) or Rapamycin (Rapa; 50 nM) on cytokine levels in supernatants with or without autophagy inhibitor 3-MA at 16 h as determined by the Human Common Cytokines Multi-Analyte ELISArray^{TM} Kit (Qiagen). Untreated cells served as control. If the values were below the detection limit specified by the manufacturer, the value is indicated in the table with NA. Cytokines whose control groups were above the detection limit are highlighted in bold font.

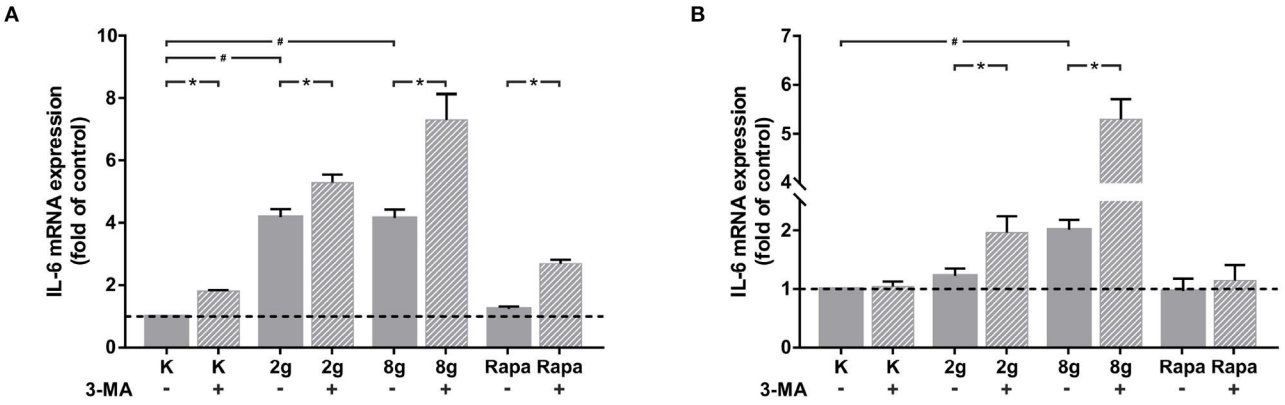

FIGURE 4 | (A) Effects of mechanical stimulation (2 or 8 g/cm^2) or Rapamycin (Rapa; 50 nM) with or without autophagy inhibitor 3-MA on *il-6* gene expression at 16 h as determined by rtPCR. Untreated cells served as control. Mean ± SEM ($n = 6$); # significant ($p < 0.05$) difference between groups as determined by Dunnett's *T*-test. * significant ($p < 0.05$) difference between two groups (uninhibited and inhibited) as determined by the Mann-Whitney-Test. **(B)** Effects of mechanical stimulation (2 or 8 g/cm^2) or Rapamycin (Rapa; 50 nM) with or without autophagy inhibitor 3-MA on *il-6* gene expression at 24 h as determined by rtPCR. Untreated cells served as control. Mean ± SEM ($n = 6$); # significant ($p < 0.05$) difference between groups as determined by Dunnett's *T*-test. * significant ($p < 0.05$) difference between two groups (uninhibited and inhibited) as determined by the Mann-Whitney-Test.

periodontal cells and tissues, this has already been shown by our group and others (Memmert et al., 2019, 2020; Blawat et al., 2020; Chen and Hua, 2021). In a previous study by our group, we focused on how autophagy is activated by stimulation with mechanical load and overload. For qualitative protein phosphorylation profiling of the mTOR signaling pathway, a human mTOR Signaling Phospho Specific Antibody Array was used. The influence of mechanical stimulation on the PI3K/AKT pathway was shown to be dose dependent. We were able to identify phosphorylation sites Thr308 and Thr474 of AKT pathway to be influenced by mechanical loading. Our results suggest at least a partial influence of mTOR on autophagy regulation via the PI3K/AKT signal pathway (Blawat et al., 2020). In this study, we focused on the effects that autophagy excites under mechanical stimulation in hPDL fibroblasts. Therefore, it was important to show in advance that with our pharmacological inhibitors and inducers, autophagy is reliably affected in hPDL fibroblasts.

The consequences of autophagy regulation and dysregulation under mechanical stimulation, especially with respect to cell-cell communication, are still unclear. Cytokines are important cell messengers and play a decisive role in cellular interactions. IL-6 is a central mediator of the body's systemic defense response to injury. It is produced in vast amounts by various cell types and reaches high circulatory levels. Its main roles include regulation of immune and inflammatory responses, hematopoiesis, control of acute phase protein synthesis and influence on bone metabolism (Garman et al., 1987; Lotz et al., 1988; Gauldie et al., 1992; Ogawa, 1992). Bone metabolism relies on the interplay of bone formation by osteoblasts and resorption by osteoclasts. IL-6 appears to stimulate resorption of bone and also regulate the activity of both cell types (Tamura et al., 1993; Xiong et al., 2011, 2015). IL-6 has been suggested to be involved in the pathogenesis of osteoporosis after estrogen loss via stimulation of osteoclast differentiation. Estrogens have been shown to inhibit IL-6 production (Jilka et al., 1992; Poli et al., 1994). We demonstrated that the production of IL-6 by hPDL fibroblasts is affected by mechanical pressure *in vitro* at both the gene and protein levels. Our research group has previously shown that inducing OTM using a 25 gram nickel-titanium coil, over a period of 3 days, resulted in an increased expression of IL-6 in rats. However, this upregulation was not found to be statistically significant (Rath-Deschner et al., 2021). A significant increase in IL-6 expression was shown in OTM experiments with mice using higher force intensities (Mo and Hua, 2018). Using our *in vivo* experimental setup to simulate physiological pressure and overload on hPDL fibroblasts during OTM, we were able to demonstrate that after both 16 and 24 h of cell stimulation, a significant increase in IL-6 expression occurred at both magnitudes of mechanical stimulation. Tension on the other hand had no significant effect on IL-6 levels, as demonstrated earlier (Rath-Deschner et al., 2021). Thus, our results suggest that the mode of mechanical stimulation rather than stimulation intensity influences the expression of this cytokine in hPDL fibroblasts.

In our *in vitro* setup, we were able to demonstrate that inhibition of autophagy using 3-MA during application of mechanical pressure causes a sharp increase of IL-6 expression in hPDL fibroblasts on gene and protein level. This observation is consistent with mouse experiments, where gene expression of inflammatory factors *il-1*, *il-6*, and *TNF-α* increased in periodontal tissues after concomitant administration of OTM and 3-MA (Mo and Hua, 2018; Chen and Hua, 2021). This response to inhibition suggests that autophagic processes may play a major role in controlling cell-cell communication, which was the focus of our study. Our findings expand and deepen the conclusions of the animal experiment. We were able to demonstrate that hPDL fibroblasts are, at least in part,

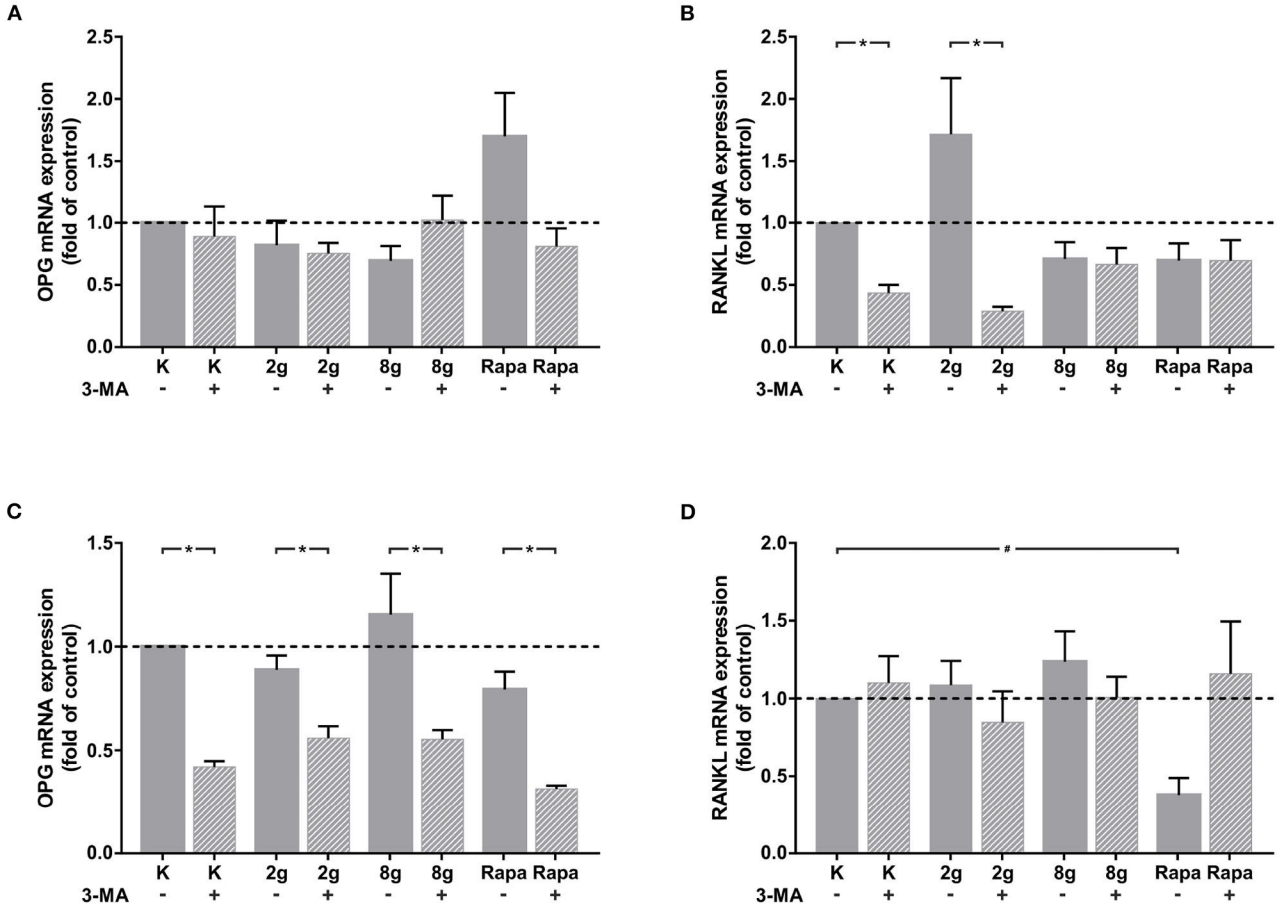

FIGURE 5 | (A) Effects on *opg* gene expression in phAOBs after 24 h cultivation without sIL-6R and with supernatant from hPDL fibroblasts with or without autophagy inhibitor 3-MA, treated with mechanical stimulation (2 or 8 g/cm^2) or Rapamycin (Rapa; 50 nM) for 16 h. Mean ± SEM ($n = 6$); # significant ($p < 0.05$) difference between groups as determined by Dunnett's *T*-test. * significant ($p < 0.05$) difference between two groups (uninhibited and inhibited) as determined by the Mann-Whitney-Test. **(B)** Effects on *rankl* gene expression in phAOBs after 24 h cultivation without sIL-6R and with supernatant from hPDL fibroblasts with or without autophagy inhibitor 3-MA, treated with mechanical stimulation (2 or 8 g/cm^2) or Rapamycin (Rapa; 50 nM) for 16 h. Mean ± SEM ($n = 6$); # significant ($p < 0.05$) difference between groups as determined by Dunnett's *T*-test. * significant ($p < 0.05$) difference between two groups (uninhibited and inhibited) as determined by the Mann-Whitney-Test. **(C,D)** Panels show the graphs respective to **(A,B)** with addition of sIL-6R.

responsible for the increase of IL-6 in periodontal tissues. One explanation for this observation could be that inhibition of autophagy deprives the cell of a key adaptive mechanism.

Since IL-6 plays an important role in cell-cell communication, we wanted to determine how sustained mechanical stress on hPDL fibroblasts affects osteoblast-osteoclast communication. IL-6 is thought to play a positive regulatory role in osteoclast differentiation (Palmqvist et al., 2002). However, for IL-6 interaction with its target cell, the so-called trans-signaling pathway is particularly important in addition to the classical signaling pathway. The latter is executed via a membrane-bound IL-6R on a few specific cells, like macrophages, neutrophils, hepatocytes and some type of T-cells. This trans-signaling pathway depends on cleaved sIL-6R, which enables signal transduction between IL-6 and the ubiquitous membrane protein gp130 (Rose-John and Heinrich, 1994; Rose-John et al., 2007; Scheller et al., 2011). In our experiments, supernatant of stimulated hPDL fibroblasts was initially added to phAOBs without sIL-6R. Subsequently, gene expression of *rankl* and *opg* were evaluated. As IL-6 signaling with osteoclasts requires interaction of IL-6 with its receptor, as expected, we did not see any effect on gene expression of *opg* in phAOBs. Therefore, all observed changes after addition of the receptor can be attributed to IL-6 secreted by hPDL fibroblasts. External addition of soluble IL-6 receptor resulted in significant decreases in *opg* expression by phAOBs in all of the groups studied. OPG functions as a decoy receptor for RANKL. By binding RANKL, OPG inhibits the activation of NF-κB, a central and fast-acting transcription factor for immune activation and differentiation of precursor cells into osteoclasts (Theoleyre et al., 2004). Our work sheds light on the background and underlying mechanisms at cellular level and highlights the cross-talk between fibroblasts and osteoblasts. Therefore, our results can be used as an explanatory model for findings of *in vivo* studies performed on mice, where

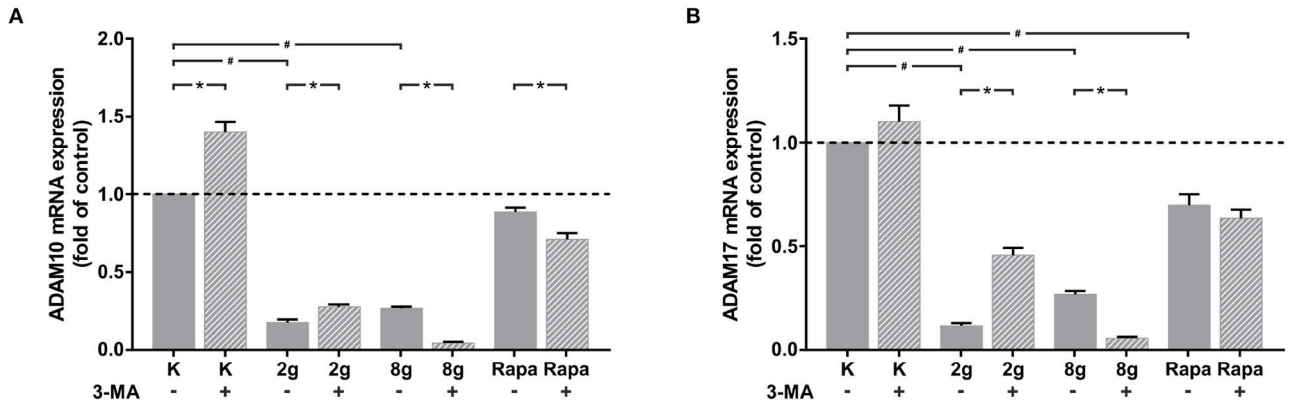

FIGURE 6 | (A) Effects of mechanical stimulation (2 g/cm^2 or 8 g/cm^2) or Rapamycin (Rapa; 50 nM) with or without autophagy inhibitor 3-MA on *adam10* gene expression at 16 h as determined by rtPCR. Untreated cells served as control. Mean ± SEM ($n = 6$); # significant ($p < 0.05$) difference between groups as determined by Dunnett's *T*-test. * significant ($p < 0.05$) difference between two groups (uninhibited and inhibited) as determined by the Mann-Whitney-Test. **(B)** Effects of mechanical stimulation (2 or 8 g/cm^2) or Rapamycin (Rapa; 50 nM) with or without autophagy inhibitor 3-MA on *adam17* gene expression at 16 h as determined by rtPCR. Untreated cells served as control. Mean ± SEM ($n = 6$); # significant ($p < 0.05$) difference between groups as determined by Dunnett's *T*-test. * significant ($p < 0.05$) difference between two groups (uninhibited and inhibited) as determined by the Mann-Whitney-Test.

micro-CT scanning demonstrated that inhibition of autophagy with simultaneous performance of OTM, resulted in a significant reduction in bone density (Chen and Hua, 2021).

When *rankl* expression was examined in stimulated phAOBs, it was found that autophagy inhibition in combination with no stress stimulus or physiological load to hPDL fibroblasts resulted in significant downregulation of *rankl* in phAOBs. However, because of the absence of soluble IL-6 receptor this effect does not appear to be dependent on IL-6-signaling. Further experimental studies are needed to investigate this observation in more detail. The only effect on *rankl* expression in phAOBs when sIL-6R was added was observed after pharmacologically induced autophagy in hPDL fibroblasts. As IL-6 was not upregulated by rapamycin stimulation in hPDL fibroblasts and a similar trend was observed without sIL-6R, we do not attribute this effect to IL-6 but to other processes triggered by autophagy induction, which will be investigated in further experiments. Interestingly in other *in vitro* studies IL-6/sIL-6R complex induced the expression of RANKL by mouse osteoblasts (Udagawa et al., 1995; Palmqvist et al., 2002). In these studies, osteoclast activity was controlled by osteoblasts through RANKL expression rather than OPG expression. However, our results suggest that in hPDL fibroblasts, osteoclast activity is more likely to be controlled via the reduction of OPG expression upon autophagy inhibition.

Next we investigated whether the expression of ADAM10 and ADAM17 is modulated by both pressure and autophagy. ADAMs play a crucial role in the trans-signaling pathway. They are able to cleave the membrane-bound IL-6 receptor, making its soluble form available, which enables signal transduction between IL-6 and the ubiquitous membrane protein gp130 (Müllberg et al., 1994; Matthews et al., 2003; Chalaris et al., 2007, 2010). ADAM10 is responsible for a slow and steady release of sIL-6R, whereas ADAM17 is responsible for rapid, short-term shedding of sIL-6R (Matthews et al., 2003). Interestingly, especially *adam10* was shown to be regulated by mechanical stimulation in a human chondrocytic cell line (Kobayakawa et al., 2016). Mechanical regulation of *adam17* has already been described in mechanically stretched rat cardiomyocytes (Niu et al., 2015). Since ADAMs influence the amount of soluble IL-6 receptor available, and ADAM17 has been shown to be strongly expressed in other periodontal cells – namely in the epithelium of gingival tissues – we investigated whether autophagy has an effect on mRNA expression of *adam10* or *adam17* in stimulated hPDL fibroblasts (Hirayama et al., 2017). We noted a significant decrease in mRNA expression for both *adam10* and *adam17* upon induction of autophagy by load, overload, and rapamycin. This was particularly evident in the pressure groups. Our results suggest that compression has a downregulatory effect on ADAM proteases while the existing literature contains evidence of upregulation of ADAM proteases during tensile strain (Niu et al., 2015; Kobayakawa et al., 2016). However, that ADAM17 plays a central role in the transduction of compressive stress has already been shown in murine tracheal epithelial cells (Shiomi et al., 2011). Autophagy inhibition in the control group and under physiological mechanical stress resulted in a significant increase in mRNA expression of both proteases. A significant inhibition, on the other hand, was observed under mechanical overload as well as induction of autophagy via rapamycin. This suggests that here again autophagy, depending on the size of the stress stimulus, has different regulatory effects on expression at different stress intensities through its bifurcated role as a cell protector and cell death inducer. To our knowledge, regulation of mRNA expression of *adam10* and *adam17* by mechanical load, overload and especially by autophagy have not been described in hPDL fibroblasts, yet. In the context of our study, our results suggest that the sIL-6R required for IL-6-induced osteoclast activation during OTM probably does not originate from hPDL fibroblasts. This suggests the involvement of other cell types

in cell-cell communication of hPDL fibroblasts, phAOBs and osteoclasts. This interesting question will be investigated in further studies.

PDL fibroblasts, due to their position in the periodontium, are of particular importance for OTM and thus for the transmission of mechanical stimulation (de Araujo et al., 2014; Li et al., 2018; Memmert et al., 2019, 2020). Their central role makes it necessary to take a close look at them at cellular level in order to uncover their functions and the influence of important processes on their role in OTM. Therefore, we used established models for *in vitro* application of mechanical stress (Ullrich et al., 2019; Blawat et al., 2020). The approach of breaking down OTM to individual *in vitro* models offers the possibility of a differentiated view on different stress stimulations. This is particular relevant for autophagy analysis, as autophagy can be induced by different types of cellular stress, which are also involved in OTM (King, 2012; Li et al., 2018; Memmert et al., 2019, 2020). Especially hypoxia is a known autophagy inducer. To eliminate the risk of limited oxygen supply to hPDL fibroblasts in our study, pressure experiments were performed exclusively on dedicated cell culture wells with gas-permeable bottoms. This ensured proper oxygen supply to the cells at all times (Ullrich et al., 2019). Autophagy usually happens rapidly. We based the selection of our time points on an earlier study by our group, which focusses on autophagy regulation by mechanical load and overload. In this study we also included earlier time points, i.e. 4 h, but our results show that autophagy regulation was most pronounced after 16 h under mechanical stimulation in PDL fibroblasts (Blawat et al., 2020). Mechanical stimulation was performed by means of physiological load on the one hand as well as by overload on the other hand. In previous experiments we have used various load magnitudes for the mechanical stimulation of hPDL fibroblasts (Blawat et al., 2020). It has been reported that cells treated with a pressure of 4 g/cm^2 suffer cell damage due to the applied excessive pressure (Kanzaki et al., 2002). In our experiments, however, increased cell death could only be reliably induced with the application of 8 g/cm^2 (Blawat et al., 2020). Therefore, our previous results suggest, that stimulation with 8 g/cm^2 exceeds a critical threshold and is rightfully termed overload. However, a load of 2 g/cm^2 was established as physiological pressure in different studies and was also used in our experimental setup (Kanzaki et al., 2002; Schröder et al., 2018; Kirschneck et al., 2019; Blawat et al., 2020). In earlier experiments by our group a mechanical load of 2 g/cm^2 appeared to have cell-protective effects (Blawat et al., 2020).

Pharmacologically, autophagy can be affected in terms of induction with the mTOR inhibitor rapamycin and inhibited by inhibitors of autophagosome formation such as 3-MA (Klionsky et al., 2016). To assess the influence of autophagy on cytokine expression and therefore on cell-cell communication a Cytokine Multi-Analyte ELISArray Kit, i.e. an unbiased approach was used. Since IL-6 was detected as the most strongly regulated cytokine, we further focused on the influence of autophagy on mechanically induced IL-6 expression. The upregulation of IL-6 protein expression due to autophagy inhibition under mechanical stimulation could be confirmed by ELISA and also on gene expression level by rtPCR. Consideration of other cytokines regulated by autophagy is beyond the scope of the manuscript and will therefore be addressed in separate studies. It should be further noted that we only analyzed the gene expression of ADAM proteases in our experiments. This is not to be equated with enzyme activity. However, other studies have also investigated ADAM10 and ADAM17 only on gene expression level, as evidence suggests that their gene expression correlates with their activity (Kinoshita et al., 2013; Cheng et al., 2021; Couselo-Seijas et al., 2021).

5. CONCLUSION

In summary, our results provide novel insights into the effects induced by autophagy regulation and deregulation in hPDL fibroblasts during mechanical load and overload. In response to pressure, IL-6 expression was induced in hPDL fibroblasts, which was further enhanced by autophagy inhibition. This led to a reduction in *opg* expression in phAOBs, which in turn could be responsible for the observed shift in the balance of bone formation and resorption during OTM under autophagy inhibition. While this could serve as an explanatory model for the accelerated tooth movement observed under autophagy inhibition, it could also represent a risk factor for unregulated bone loss.

DATA AVAILABILITY STATEMENT

The raw data supporting the conclusions of this article will be made available by the authors, without undue reservation.

ETHICS STATEMENT

The studies involving human participants were reviewed and approved by Ethics Committee of the University of Bonn (#117/15 Memmert); primary human osteoblasts were explanted from alveolar bone fragments, which would have been discarded otherwise. Written informed consent to participate in this study was provided by the participants' legal guardian/next of kin.

AUTHOR CONTRIBUTIONS

AM, MW, JD, AJ, and SB-M: conceptualization. AM, JM, RBC, KB, BE, and SB-M: methodology. AM, BE, and SB-M: validation and formal analysis. AM, JW, and SB-M: investigation. AJ and SB-M: resources. AM, JM, BE, RBC, and SB-M: data curation. AM and SB-M: writing—original draft preparation. JW, JD, MW, and AJ: writing—review and editing. JD, MW, AJ, and SB-M: supervision. AJ, JD, and SB-M: project administration. All authors contributed to the article and approved the submitted version.

FUNDING

This study was supported by the Medical Faculty of the University of Bonn, SB-M by the Deutsche Forschungsgemeinschaft (DFG, German Research Foundation)–Project-ID ME 4798/1-2.

ACKNOWLEDGMENTS

We would like to thank the Flow Cytometry Core Facility Bonn, especially Andreas Dolf, Peter Wurst and Maximilian Germer. Additionally, we would like to express our gratitude toward Ernst W. Mayr and Inka Bay-Müller for their valuable technical support.

REFERENCES

Antonioli, M., Di Rienzo, M., Piacentini, M., and Fimia, G. M. (2017). Emerging mechanisms in initiating and terminating autophagy. *Trends Biochem. Sci*. 42, 28–41. doi: 10.1016/j.tibs.2016.09.008

Blawat, K., Mayr, A., Hardt, M., Kirschneck, C., Nokhbehsaim, M., Behl, C., et al. (2020). Regulation of autophagic signaling by mechanical loading and inflammation in human pdl fibroblasts. *Int. J. Mol. Sci*. 21:9446. doi: 10.3390/ijms21249446

Boyle, W. J., Simonet, W. S., and Lacey, D. L. (2003). Osteoclast differentiation and activation. *Nature* 423, 337–342. doi: 10.1038/nature01658

Chalaris, A., Gewiese, J., Paliga, K., Fleig, L., Schneede, A., Krieger, K., et al. (2010). Adam17-mediated shedding of the il6r induces cleavage of the membrane stub by gamma-secretase. *Biochim. Biophys. Acta* 1803, 234–245. doi: 10.1016/j.bbamcr.2009.12.001

Chalaris, A., Rabe, B., Paliga, K., Lange, H., Laskay, T., Fielding, C. A., et al. (2007). Apoptosis is a natural stimulus of il6r shedding and contributes to the proinflammatory trans-signaling function of neutrophils. *Blood* 110, 1748–1755. doi: 10.1182/blood-2007-01-067918

Chen, L., and Hua, Y. (2021). Autophagy of periodontal ligament inhibits inflammation and reduces the decline of bone density during orthodontic tooth movement of mice. *Arch. Oral Biol*. 121:104960. doi: 10.1016/j.archoralbio.2020.104960

Cheng, Y., Lin, L., Li, X., Lu, A., Hou, C., Wu, Q., et al. (2021). Adam10 is involved in the oncogenic process and chemo-resistance of triple-negative breast cancer via regulating notch1 signaling pathway, cd44 and prpc. *Cancer Cel.l Int*. 21, 32. doi: 10.1186/s12935-020-01727-5

Couselo-Seijas, M., Almengló, C., R, M. A.-B., Luis Fernandez, A., Alvarez, E., J, R. G.-J., et al. (2021). Higher ace2 expression levels in epicardial cells than subcutaneous stromal cells from patients with cardiovascular disease: diabetes and obesity as possible enhancer. *Eur. J. Clin. Invest*. 51:e13463. doi: 10.1111/eci.13463

de Araujo, R. M., Oba, Y., Kuroda, S., Tanaka, E., and Moriyama, K. (2014). Rhoe regulates actin cytoskeleton organization in human periodontal ligament cells under mechanical stress. *Arch. Oral. Biol*. 59, 187–192. doi: 10.1016/j.archoralbio.2013.11.010

Garman, R. D., Jacobs, K. A., Clark, S. C., and Raulet, D. H. (1987). B-cell-stimulatory factor 2 (beta 2 interferon) functions as a second signal for interleukin 2 production by mature murine t cells. *Proc. Natl. Acad. Sci. U.S.A*. 84, 7629–7633. doi: 10.1073/pnas.84.21.7629

Gauldie, J., Richards, C., and Baumann, H. (1992). Il6 and the acute phase reaction. *Res. Immunol*. 143, 755–759. doi: 10.1016/0923-2494(92)80018-G

Harris, J. (2011). Autophagy and cytokines. *Cytokine* 56, 140–144. doi: 10.1016/j.cyto.2011.08.022

Hirayama, A., Awano, S., Seta, Y., and Ansai, T. (2017). Adam17 regulates tnf-α expression upon lipopolysaccharide stimulation in oral keratinocytes. *Biomed. Res*. 38, 157–165. doi: 10.2220/biomedres.38.157

Jilka, R. L., Hangoc, G., Girasole, G., Passeri, G., Williams, D. C., Abrams, J. S., et al. (1992). Increased osteoclast development after estrogen loss: mediation by interleukin-6. *Science* 257, 88–91. doi: 10.1126/science.1621100

Kanzaki, H., Chiba, M., Shimizu, Y., and Mitani, H. (2002). Periodontal ligament cells under mechanical stress induce osteoclastogenesis by receptor activator of nuclear factor kappab ligand up-regulation via prostaglandin e2 synthesis. *J. Bone Miner. Res*. 17, 210–220. doi: 10.1359/jbmr.2002.17.2.210

Karsenty, G. (2003). The complexities of skeletal biology. *Nature* 423, 316–318. doi: 10.1038/nature01654

King, J. S. (2012). Mechanical stress meets autophagy: potential implications for physiology and pathology. *Trends Mol. Med*. 18, 583–588. doi: 10.1016/j.molmed.2012.08.002

Kinoshita, N., Awano, S., Yoshida, A., Soh, I., and Ansai, T. (2013). Periodontal disease and gene-expression levels of metalloendopeptidases in human buccal mucosal epithelium. *J. Periodontal. Res*. 48, 606–614. doi: 10.1111/jre.12045

Kirschneck, C., Küchler, E. C., Wolf, M., Spanier, G., Proff, P., and Schröder, A. (2019). Effects of the highly COX-2-selective analgesic nsaid etoricoxib on human periodontal ligament fibroblasts during compressive orthodontic mechanical strain. *Mediators Inflamm*. 2019:2514956. doi: 10.1155/2019/2514956

Klionsky, D. J., Abdelmohsen, K., Abe, A., Abedin, M. J., Abeliovich, H., Acevedo Arozena, A., et al. (2016). Guidelines for the use and interpretation of assays for monitoring autophagy (3rd edition). *Autophagy* 12, 1–222. doi: 10.1080/15548627.2015.1100356

Kobayakawa, T., Takahashi, N., Sobue, Y., Terabe, K., Ishiguro, N., and Kojima, T. (2016). Mechanical stress loading induces cd44 cleavage in human chondrocytic hcs-2/8 cells. *Biochem. Biophys. Res. Commun*. 478, 1230–1235. doi: 10.1016/j.bbrc.2016.08.099

Lapaquette, P., Guzzo, J., Bretillon, L., and Bringer, M. A. (2015). Cellular and molecular connections between autophagy and inflammation. *Mediators Inflamm*. 2015:398483. doi: 10.1155/2015/398483

Li, Y., Jacox, L. A., Little, S. H., and Ko, C. C. (2018). Orthodontic tooth movement: The biology and clinical implications. *Kaohsiung J. Med. Sci*. 34, 207–214. doi: 10.1016/j.kjms.2018.01.007

Lotz, M., Jirik, F., Kabouridis, P., Tsoukas, C., Hirano, T., Kishimoto, T., et al. (1988). B cell stimulating factor 2/interleukin 6 is a costimulant for human thymocytes and t lymphocytes. *J. Exp. Med*. 167, 1253–1258. doi: 10.1084/jem.167.3.1253

Marchesan, J. T., Scanlon, C. S., Soehren, S., Matsuo, M., and Kapila, Y. L. (2011). Implications of cultured periodontal ligament cells for the clinical and experimental setting: a review. *Arch. Oral. Biol*. 56, 933–943. doi: 10.1016/j.archoralbio.2011.03.003

Mariño, G., Niso-Santano, M., Baehrecke, E. H., and Kroemer, G. (2014). Self-consumption: the interplay of autophagy and apoptosis. *Nat. Rev. Mol. Cell Biol*. 15, 81–94. doi: 10.1038/nrm3735

Matthews, V., Schuster, B., Schütze, S., Bussmeyer, I., Ludwig, A., Hundhausen, C., et al. (2003). Cellular cholesterol depletion triggers shedding of the human interleukin-6 receptor by adam10 and adam17 (tace). *J. Biol. Chem*. 278, 38829–38839. doi: 10.1074/jbc.M210584200

McCulloch, C. A., and Bordin, S. (1991). Role of fibroblast subpopulations in periodontal physiology and pathology. *J. Periodontal. Res*. 26(3 Pt 1):144–154. doi: 10.1111/j.1600-0765.1991.tb01638.x

Memmert, S., Damanaki, A., Weykopf, B., Rath-Deschner, B., Nokhbehsaim, M., Götz, W., et al. (2019). Autophagy in periodontal ligament fibroblasts under biomechanical loading. *Cell Tissue Res*. 378, 499–511. doi: 10.1007/s00441-019-03063-1

Memmert, S., Nogueira, A. V. B., Damanaki, A., Nokhbehsaim, M., Rath-Deschner, B., Götz, W., et al. (2020). Regulation of the autophagy-marker sequestosome 1 in periodontal cells and tissues by biomechanical loading. *J. Orofac. Orthop* 81, 10–21. doi: 10.1007/s00056-019-00197-3

Mo, S., and Hua, Y. (2018). Cystathionine gamma lyase-h(2)s contributes to osteoclastogenesis during bone remodeling induced by mechanical loading. *Biochem. Biophys. Res. Commun*. 501, 471–477. doi: 10.1016/j.bbrc.2018.05.015

Müllberg, J., Oberthür, W., Lottspeich, F., Mehl, E., Dittrich, E., Graeve, L., et al. (1994). The soluble human il-6 receptor. mutational characterization of the proteolytic cleavage site. *J. Immunol*. 152, 4958–4968.

Niu, A., Wang, B., and Li, Y. P. (2015). Tnfα shedding in mechanically stressed cardiomyocytes is mediated by src activation of tace. *J. Cell Biochem*. 116, 559–565. doi: 10.1002/jcb.25006

Ogawa, M. (1992). Il6 and haematopoietic stem cells. *Res. Immunol*. 143, 749–751. doi: 10.1016/0923-2494(92)80016-E

Oppenheim, A. (1911). Tissue changes, particularly in the bone incident to tooth movement. *Am. J. Orthod* 3, 113–132.

Palmqvist, P., Persson, E., Conaway, H. H., and Lerner, U. H. (2002). Il-6, leukemia inhibitory factor, and oncostatin m stimulate bone resorption and regulate the expression of receptor activator of nf-kappa b ligand, osteoprotegerin, and receptor activator of nf-kappa b in mouse calvariae. *J. Immunol.* 169, 3353–3362. doi: 10.4049/jimmunol.169.6.3353

Poli, V., Balena, R., Fattori, E., Markatos, A., Yamamoto, M., Tanaka, H., et al. (1994). Interleukin-6 deficient mice are protected from bone loss caused by estrogen depletion. *Embo J.* 13, 1189–1196. doi: 10.1002/j.1460-2075.1994.tb06368.x

Rath-Deschner, B., Nogueira, A. V. B., Beisel-Memmert, S., Nokhbehsaim, M., Eick, S., Cirelli, J. A., et al. (2021). Interaction of periodontitis and orthodontic tooth movement-an *in vitro* and *in vivo* study. *Clin Oral Investig.* doi: 10.1007/s00784-021-03988-4

Rose-John, S., and Heinrich, P. C. (1994). Soluble receptors for cytokines and growth factors: generation and biological function. *Biochem. J.* 300 (Pt 2):281–290. doi: 10.1042/bj3000281

Rose-John, S., Waetzig, G. H., Scheller, J., Grötzinger, J., and Seegert, D. (2007). The il-6/sil-6r complex as a novel target for therapeutic approaches. *Expert. Opin. Ther. Targets* 11, 613–624. doi: 10.1517/14728222.11.5.613

Sandstedt, C. (1904). Einige beitrage zur theorie der zahnregulierung. *Nordisk Tandläkare Tidskrift* 5, 236–256.

Scheller, J., Chalaris, A., Schmidt-Arras, D., and Rose-John, S. (2011). The pro- and anti-inflammatory properties of the cytokine interleukin-6. *Biochim. Biophys. Acta* 1813, 878–888. doi: 10.1016/j.bbamcr.2011.01.034

Schröder, A., Bauer, K., Spanier, G., Proff, P., Wolf, M., and Kirschneck, C. (2018). Expression kinetics of human periodontal ligament fibroblasts in the early phases of orthodontic tooth movement. *J. Orofac. Orthop* 79, 337–351. doi: 10.1007/s00056-018-0145-1

Schwarz, A. M. (1932). Tissue changes incidental to orthodontic tooth movement. *International Journal of Orthodontia, Oral Surgery and Radiography* 18, 331–352. doi: 10.1016/S0099-6963(32)80074-8

Shiomi, T., Tschumperlin, D. J., Park, J. A., Sunnarborg, S. W., Horiuchi, K., Blobel, C. P., et al. (2011). Tnf-α-converting enzyme/a disintegrin and metalloprotease-17 mediates mechanotransduction in murine tracheal epithelial cells. *Am. J. Respir. Cell Mol. Biol.* 45, 376–385. doi: 10.1165/rcmb.2010-0234OC

Storey, E. (1973). The nature of tooth movement. *Am. J. Orthod* 63, 292–314. doi: 10.1016/0002-9416(73)90353-9

Tamura, T., Udagawa, N., Takahashi, N., Miyaura, C., Tanaka, S., Yamada, Y., et al. (1993). Soluble interleukin-6 receptor triggers osteoclast formation by interleukin 6. *Proc. Natl. Acad. Sci. U.S.A.* 90, 11924–11928. doi: 10.1073/pnas.90.24.11924

Tang, L. L., Xian, C. Y., and Wang, Y. L. (2006). The mgf expression of osteoblasts in response to mechanical overload. *Arch. Oral. Biol.* 51, 1080–1085. doi: 10.1016/j.archoralbio.2006.06.009

Teitelbaum, S. L. (2000). Bone resorption by osteoclasts. *Science* 289, 1504–1508. doi: 10.1126/science.289.5484.1504

Theoleyre, S., Wittrant, Y., Tat, S. K., Fortun, Y., Redini, F., and Heymann, D. (2004). The molecular triad opg/rank/rankl: involvement in the orchestration of pathophysiological bone remodeling. *Cytokine Growth Factor Rev.* 15, 457–475. doi: 10.1016/j.cytogfr.2004.06.004

Udagawa, N., Takahashi, N., Katagiri, T., Tamura, T., Wada, S., Findlay, D. M., et al. (1995). Interleukin (il)-6 induction of osteoclast differentiation depends on il-6 receptors expressed on osteoblastic cells but not on osteoclast progenitors. *J. Exp. Med.*182, 1461–1468. doi: 10.1084/jem.182.5.1461

Ullrich, N., Schröder, A., Jantsch, J., Spanier, G., Proff, P., and Kirschneck, C. (2019). The role of mechanotransduction versus hypoxia during simulated orthodontic compressive strain-an *in vitro* study of human periodontal ligament fibroblasts. *Int. J. Oral. Sci.* 11, 33. doi: 10.1038/s41368-019-0066-x

Xiong, J., Onal, M., Jilka, R. L., Weinstein, R. S., Manolagas, S. C., and O'Brien, C. A. (2011). Matrix-embedded cells control osteoclast formation. *Nat. Med.* 17, 1235–1241. doi: 10.1038/nm.2448

Xiong, J., Piemontese, M., Onal, M., Campbell, J., Goellner, J. J., Dusevich, V., et al. (2015). Osteocytes, not osteoblasts or lining cells, are the main source of the rankl required for osteoclast formation in remodeling bone. *PLoS ONE* 10:0138189. doi: 10.1371/journal.pone.0138189

Conflict of Interest: The authors declare that the research was conducted in the absence of any commercial or financial relationships that could be construed as a potential conflict of interest.

Publisher's Note: All claims expressed in this article are solely those of the authors and do not necessarily represent those of their affiliated organizations, or those of the publisher, the editors and the reviewers. Any product that may be evaluated in this article, or claim that may be made by its manufacturer, is not guaranteed or endorsed by the publisher.

frontiers in Physiology

ORIGINAL RESEARCH
published: 09 September 2021
doi: 10.3389/fphys.2021.697738

AdipoRon Promotes the Osseointegration of Dental Implants in Mice With Type 2 Diabetes Mellitus

BoRui Huang†, Wei Bi†, Yang Sun, Ruixue Li, Xingwen Wu and Youcheng Yu**

Department of Dentistry, Zhongshan Hospital, Fudan University, Shanghai, China

AdipoRon is an oral active synthetic small molecule with biological functions similar to adiponectin (APN). It is an APN receptor agonist that can improve insulin resistance and glucose intolerance. However, the role of AdipoRon in bone metabolism and related molecular mechanisms remains to be investigated. To explore the effect of AdipoRon on bone absorption and bone integration of type 2 diabetes mellitus (T2DM) mice with implants, we established surgery-induced model of osseointegration of dental implantation in T2DM mice of C57BL/6 db/db and normal mice homologous to diabetic mice. Micro-CT was used to analyze the femurs with the implant in the mice to detect the bone mass, H&E, and tartrate-resistant acid phosphatase (TRAP), and Safranin O-fast green staining was performed to analyze the bone formation and bone resorption. Bone integration-related markers as Rankl, bone morphogenetic protein 2 (BMP2), osteoprotegerin (OPG), osteopontin (OPN), and runt-related transcription factor 2 (Runx2) were also measured using immunohistochemistry. Our results indicated that diabetic mice showed a lower bone mass and decreased the osteoblast differentiation. AdipoRon attenuated diabetes-impaired bone volume (BV)/total volume (TV), trabecular thickness (Tb.Th), trabecular number (Tb.N), trabecular separation (Tb.Sp), and bone integration-related markers variation and promoted bone hyperplasia as well as repressed the osteoclast formation, especially in diabetic mice. AdipoRon may improve the osseointegration of dental implants in mice with T2DM by promoting osteogenesis and inhibiting bone resorption, and AdipoRon may serve as a promising oral strategy to improve the osseointegration ability of patients with diabetes.

Keywords: AdipoRon, osseointegration, dental implants, type 2 diabetes mellitus, micro-CT

OPEN ACCESS

Edited by:
Petros Papagerakis, University of Saskatchewan, Canada

Reviewed by:
Joo Cheol Park, Seoul National University, South Korea
Patrizia Ferretti, University College London, United Kingdom

****Correspondence:***
Youcheng Yu
yu.youcheng@zs-hospital.sh.cn
Xingwen Wu
dentistwxw@foxmail.com

† These authors have contributed equally to this work

Specialty section:
This article was submitted to Craniofacial Biology and Dental Research, a section of the journal Frontiers in Physiology

Received: *20 April 2021*
Accepted: *30 July 2021*
Published: *09 September 2021*

Citation:
Huang B, Bi W, Sun Y, Li R, Wu X and Yu Y (2021) AdipoRon Promotes the Osseointegration of Dental Implants in Mice With Type 2 Diabetes Mellitus. Front. Physiol. 12:697738. doi: 10.3389/fphys.2021.697738

INTRODUCTION

Dental implants are applied for the rehabilitation of partially edentulous patients. Poor oral hygiene along with smoking and a history of periodontitis correlated with peri-implant disease strongly. Moreover, periodontitis with diabetes has been considered as the sixth major complication of diabetes, and it will lead to loosening and falling out of the teeth of patients and seriously affect their physiological functions such as chewing, swallowing, nutritional intake, speech, and facial expression (Chee et al., 2013). For tooth loss caused by periodontitis, implant treatment is the most comfortable and convenient way to repair it. As previously reported, the implant-supported restorations survival rates are related to complicated factors (Tatarakis et al., 2014). The implants may be affected by many biological complications after the initial integration phase, among which the progressive implant bone loss is generally caused by peri-implant diseases,

especially by peri-implantitis with increasing high prevalence as implant therapy is implemented widespread (Lindhe et al., 2008). Moreover, there are studies concerning that type 2 diabetes mellitus (T2DM) patients with dental implants showed very similar psychosocial profiles, clinical as well as microbiological, and salivary biomarkers to those of non-diabetic individuals (Tatarakis et al., 2014), and previous researchers have confirmed that diabetic patients with poor blood glucose control have a higher failure rate of implant repair (Mellado-Valero et al., 2007).

Type 2 diabetes mellitus is a metabolic disorder characterized by hyperglycemia and lipid metabolism changes along with many complications. At present, a lot of patients with T2DM arose with an aging population and the increasing prevalence of obesity (Zheng et al., 2018; Ortega et al., 2020). Numerous previous studies indicate that macrophages in the adipose tissue interstitium of T2DM might produce a large number of pro-inflammatory factors (Chawla et al., 2011; Esser et al., 2014), which may affect bone integration. Moreover, hyperglycemia may change the biological function of bone cells to affect bone formation, bone mineralization, and bone reconstruction (Javed and Romanos, 2009), increasing the osteoclast activity and promoting the bone resorption (Catalfamo et al., 2013) to weaken the osseointegration ability of implants in patients with T2DM (Mellado-Valero et al., 2007). Therefore, poor blood glucose control is a high-risk factor for oral implant treatment, and the development of an intervention strategy that can not only effectively control blood sugar but also improve the function of damaged bone cells, so as to improve the osseointegration ability of implants, is particularly important for improving the probability of implantation success in patients with diabetes.

AdipoRon is an oral synthetic small molecular compound that was reported to bind to adiponectin (APN) receptors, specifically, AdipoR1 and AdipoR2. APN was considered to improve insulin resistance and antagonize diabetes, and it acted as an anti-inflammatory factor. APN is reported to play an important role in bone and associated with whole-body energy homeostasis, and it acts as a regulator of bone metabolism to negatively correlate with bone mineral density (Naot et al., 2017). AdipoRon can act as a potent APN receptor agonist and a potential alternative to replace APN. It was reported as an anticancer molecule to affect cell cycle progression and promote cell death in osteosarcoma cells (Sapio et al., 2020). In another report, AdipoRon can promote apoptosis while suppressing cell proliferation in myeloma cell lines (Wang S.J. et al., 2020). According to the study by Wang Z. et al. (2020), AdipoRon promoted new bone formation in diabetes mediated by impaired endochondral ossification (ECO)-induced delayed bone repair. In our previous study, we also found that AdipoRon could activate the endogenous receptors of APN to affect bone anabolism in mice with T2DM-related periodontitis and may serve as an effective multipronged approach to target periodontitis correlated with T2DM (Wu Y.C. et al., 2019). The role of AdipoRon in the osseointegration of T2DM individuals with dental implants has not been reported so far.

In the present study, the effect of AdipoRon on bone absorption and bone integration in diabetic mice along with normal control animals implanted with dental implants in the femur was explored, which may provide a new idea for enhancing the oral osseointegration ability of patients with diabetes.

MATERIALS AND METHODS

Model of Osseointegration of Dental Implantation Induced by Surgery in Mice and Group

All the animal experiments were conducted and approved by the Animal Ethics Committees of Fudan University. Surgery-induced osseointegration of dental implantation model using male C57BL/6 db/db mice (diabetes), 6–8 weeks old, 28 $\pm$ 2 g, with fasting blood glucose (FBG) (16 h) higher than 7.0 mmol/L (FBG: 7.7 $\pm$ 1.8), and wild-type born within the same brood as control (FBG: 4.9 $\pm$ 1.3). The mice were intraperitoneally injected ketamine (100 mg/kg)/xylazine (10 mg/kg) for anesthesia and then surgical procedures were performed under sterile conditions. According to the previous study (Liu et al., 2017) with some modifications, the mice were fixed on the operating table in the supine position with skin on the lower one-third of the femur and the upper one-third of the tibia on both sides of the mouse being prepared, and the operation area was disinfected. Then a longitudinal incision of about 10 mm was made from the distal end of the femur on the medial side of the knee joint, and the incision reached the bone surface (BS). The skin and subcutaneous tissue were bluntly separated to expose the articular surface of the epiphysis, whereas the femoral periosteum was fully protected. The joint of mice was bent and the intercondylar fossa was selected as the implantation site. The implant socket with a parallel direction to the long axis of the femur and toward the proximal medullary cavity was prepared using a 25G needle under the cold condition of physiological saline. Later, the implant titanium rod with 0.5 mm in diameter and 10 mm in length from Straumann A.G. Co. (Basel, Switzerland) was tapped until its end entered slightly below the joint surface 1 mm with initial stability as well as without loosening. The peeled structure around the knee joint was reset, layered, and tightly sutured, and the window was closed. Mice were given intramuscular injections of antibiotics for three consecutive days after the operation to prevent infection.

Three days after implantation, 14 diabetic mice were divided into 2 groups with 7 mice in each group, i.e., diabetes control (D-control) with the equal volume of vehicle and diabetic mice were given 75 mg/kg/day AdipoRon (Life Sciences, United States) by intravenous administration for 2 weeks (D-AdipoRon) (Wu X. et al., 2019), and 14 wild-type mice (normal mice) were divided into 2 groups with 7 mice in each group, i.e., wild control (W-control) with the equal volume of vehicle and wild-type mice were intragastrically administrated with 75 mg/kg/day AdipoRon for 2 weeks (W-AdipoRon).

After the treatment of 2 weeks, the femurs of mice were fixed in 4% paraformaldehyde and then maintained in 75% ethanol according to the previous study (Du et al., 2020). Bone mass of femurs with the plant in the mice was analyzed using micro-CT (SkyScan 1172, Bruker) and then the femurs were

harvested, fixed, decalcified, paraffin-embedded, and sectioned for pathological examination. The sections in the region surrounding the explant were selected for analysis.

Micro-CT

Micro-CT (SkyScan 1172, Bruker) was used to analyze the femurs with the plant in the mice among all the groups to detect the volume and structure of trabecular bone. The micro-CT parameters were as follows: diameter, 21.5 mm; pixel size, 10 μm per pixel; high resolution; 212 tier; temporal integration, 250 ms; and continuous beam rotation. Set thresholds to distinguish between different organizations are as follows: gray scale values between 215 and 700 indicate trabeculae, values between 700 and 1,000 is the implant, and values less than 215 indicate non-mineralized tissue. After scanning, CT-analyzer (version: 1.15.4.0)[1] was used for 3D reconstruction. The 0.5 mm tubular area around the implant was selected as the area of interest, the rebuild threshold to 1,000 was set. The CT-analyzer was used to perform bone histometric analysis, including trabecular thickness (Tb.Th), trabecular number (Tb.N), trabecular separation (Tb.Sp), BS/bone volume (BV), and BV/total volume (BV/TV).

H&E Staining

After micro-CT scan, femurs were decalcified in ethylenediaminetetraacetic acid (EDTA) (10%) for 3 weeks with implant, the implant was removed and embedded in paraffin, and 5 μm sections were obtained. H&E staining was performed according to the previous study (Yang et al., 2011). In brief, the sections of femurs were dewaxed and hydrated, and then hematoxylin staining was performed. Finally, images were obtained under a microscope (Eclipse Ci-L; Nikon, Tokyo, Japan).

Tartrate-Resistant Acid Phosphatase Staining

Based on the previous study (Du et al., 2020), sections of femur samples from mice were stained using a commercial kit of tartrate-resistant acid phosphatase (TRAP) (Sigma) according to the instruction of the manufacturer. Preosteoclasts and osteoclasts were identified by TRAP-positive cells and then counted and photographs were taken using a microscope (Nikon, Eclipse Ci-L, Japan). TRAP-positive cells in the peri-implant were detected by the presence of dark-purple staining granules in the cytoplasm. Image-Pro Plus 6.0 was used for TRAP staining analysis, and five fields of vision were randomly selected in each section. The percentage of TRAP-positive cells is calculated as the TRAP-positive stained area/total area × 100%, which is used to indicate osteoclasts.

Safranin O-Fast Green Staining

Safranin O-fast green staining was performed to observe osteogenesis as reported in a previous study (Pritzker et al., 2006). In brief, the sections of femur samples from mice were stained in fast green dye solution for 5–10 min and then washed followed by staining in safflower dye solution for 15–30 s. After being sealed, the sections were observed under a microscope along with images acquisition and analysis. The cartilage is red or salmon-red with a green background. CaseViewer2.2 Scanning Browser software was used to select the target area of the tissue for imaging. The Safranin O-positive cartilage was analyzed by ImagePro Plus 6.0 (Media Cybernetics, Bethesda, MD, United States).

Immunohistochemistry

Immunohistochemistry was used to detect the expressions of Rankl, bone morphogenetic protein 2 (BMP2), osteoprotegerin (OPG), osteopontin (OPN), and runt-related transcription factor 2 (Runx2) in femoral bone with dental implants in mice. The sections of femur samples from mice were incubated in hyaluronidase and skimmed milk for blocking. And then the sections were incubated with primary rabbit polyclonal antibodies to Rankl (Abcam, CN. ab216484, 1:100), BMP2 (ZEN BIO, CN. 500231, 1:100), OPG (Abcam, CN. ab183910,1:100), OPN (SANTA CRUZ, CN. sc-21742, 1:100), or Runx2 (Abcam, CN. ab192256, 1:100) at 4°C overnight. After washing in phosphate-buffered saline, sections were incubated with the corresponding horseradish peroxidase (HRP) conjugated secondary antibody (1:3,000) at room temperature for 30 min followed by visualization using diaminobenzidine (DAB) and counterstaining with hematoxylin. Images were obtained using an Eclipse Ci-L microscope. Image-Pro Plus 6.0 software was used to analyze images. All proteins were categorized based on a histochemical score (H-score), and positive comprehensive scores were obtained from five visual fields in each section according to the same criteria. A numerical value from a weighted summation of percentage staining accounts for both the staining intensity and the percentage of cells at that intensity.

Data Statistics

GraphPad Prism (8.0, United States) was used to analyze the data that were obtained from at least three independent samples and presented as the mean ± standard deviation (SD). Two-way repeated-measures analysis of variance (ANOVA) was used to analyze the data from three or more groups and an unpaired *t*-test was used to analyze the data from two groups. When *p*-value is ≤0.05, differences were considered statistically.

RESULTS

AdipoRon Promotes Bone Formation Around Dental Implants in Mice

Bone morphology and formation of mice were observed using micro-CT. Results of micro-CT detection are shown in **Figure 1**. Diabetic mice (Diabetes-control, D-control) showed lower bone mass around dental implants compared with the normal mice (Wild-control, W-control). The 3D reconstruction images from micro-CT are shown in **Figure 1A**, BV/TV in **Figure 1B**, and Tb.Th in **Figure 1D**. Also, Tb.N (**Figure 1F**) was significantly decreased, whereas Tb.Sp (**Figure 1E**) was increased in diabetic

[1] www.Skyscan.be

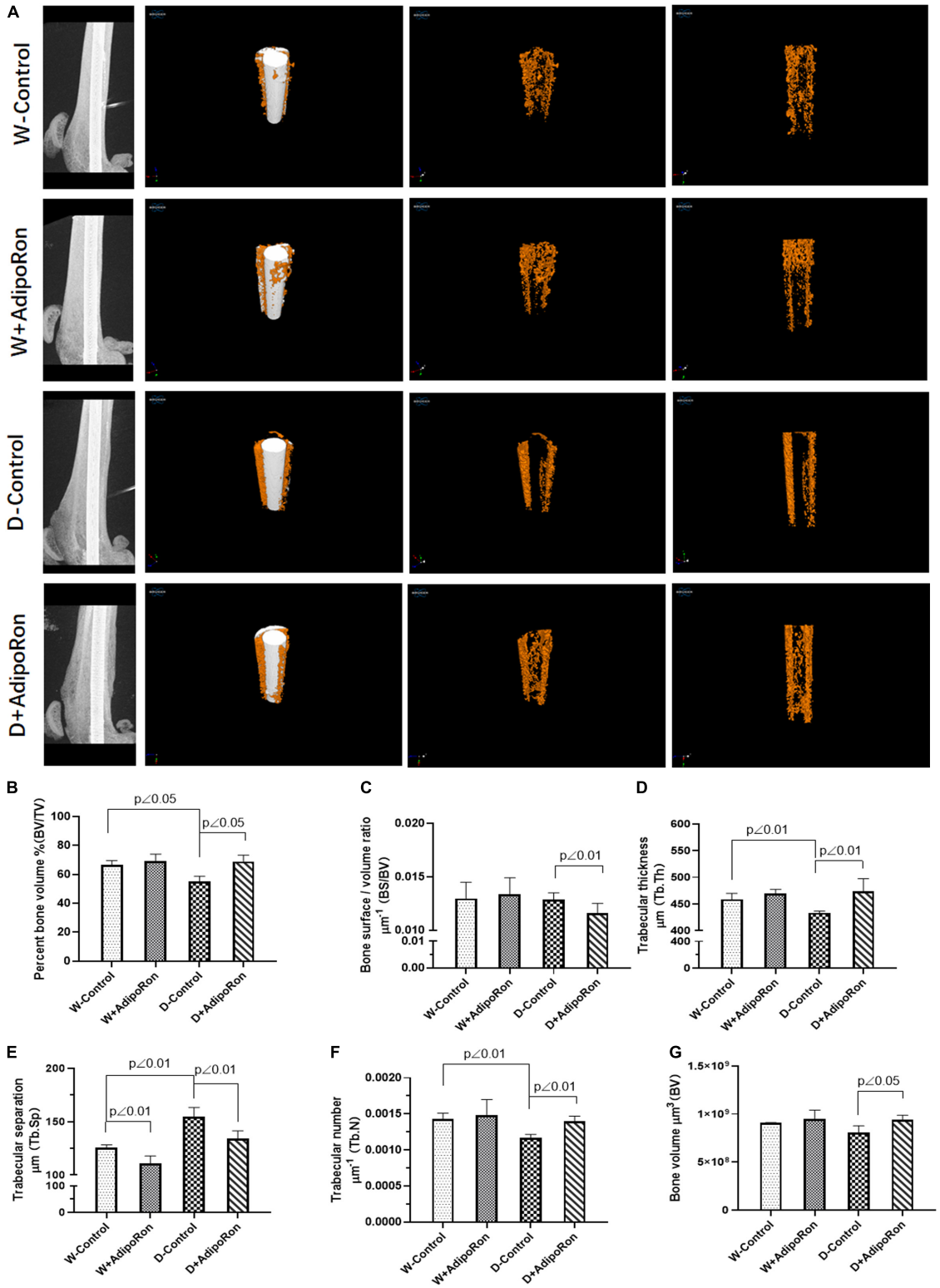

FIGURE 1 | Evaluation of femoral bone structure with dental implants in mice. Femoral bone structure with dental implants in mice was assessed using micro-CT (n = 7). Normal mice (Wild-control, W-control), normal mice treated with AdipoRon (Wild + AdipoRon, W + AdipoRon), diabetic mice (Diabetes-control, D-control), and diabetic mice treated with (Diabetes + AdipoRon, D + AdipoRon) were involved. **(A)** 3D reconstruction images of femoral bone structure with dental implants in mice are shown. Values of bone volume/tissue volume (BV/TV) **(B)**, bone surface/bone volume (BS/BV) **(C)**, trabecular thickness (Tb.Th) **(D)**, trabecular separation (Tb.Sp) **(E)**, trabecular number (Tb.N) **(F)**, and bone volume (BV) **(G)** were analyzed.

mice compared with normal mice. AdipoRon could attenuate the induction of diabetes in BV/TV, Tb.Th, Tb.N, and Tb.Sp. Although there was almost no difference between diabetic mice and the normal mice, AdipoRon treatment decreased BS/BV (**Figure 1C**) along with increased BV (**Figure 1G**) of diabetic mice. Diabetic mice showed lower bone mass around dental implants compared with normal mice, which may be attenuated by AdipoRon.

AdipoRon Promotes the Osteoblast Differentiation and Inhibits Osteoclast

Pathological exploration of femoral bone after dental implantation and AdipoRon treatment in mice was performed. As shown in **Figure 2A**, bone hyperplasia mediated by the osteoblast differentiation was significantly decreased in diabetic mice (Diabetes-control, D-control) compared with normal mice (Wild-control, W-control). AdipoRon promoted bone hyperplasia both in normal and diabetic mice, especially in the latter. The osteoclast formation indicated by TRAP-positive staining was significantly increased in D-control compared with W-control, whereas the osteoclast formation decreased significantly ($p < 0.05$) in both the AdipoRon-treated diabetic mice (Diabetes + AdipoRon, D + AdipoRon) and the normal mice (Wild + AdipoRon, W + AdipoRon) (**Figures 2B,C**).

AdipoRon Represses the Osteoclast Formation of Safranin O-Fast Green Staining

The osteoclast formation in femoral bone with dental implants in mice was further investigated using Safranin O-fast green staining. Results were shown in **Figure 3** that Tb.N was decreased in diabetic mice (Diabetes-control, D-control) compared with normal mice (Wild-control, W-control) (**Figures 3A,D**) although there was no difference in the percentage of the trabecular area (Tb.Ar) (**Figure 3B**), Tb.Th (**Figure 3C**), and Tb.Sp (**Figure 3E**) among all the mice involved in W-control and D-control which was slightly different from the results from micro-CT. AdipoRon increased the values of Tb.Ar, Tb.Th, and Tb.N, but decreased

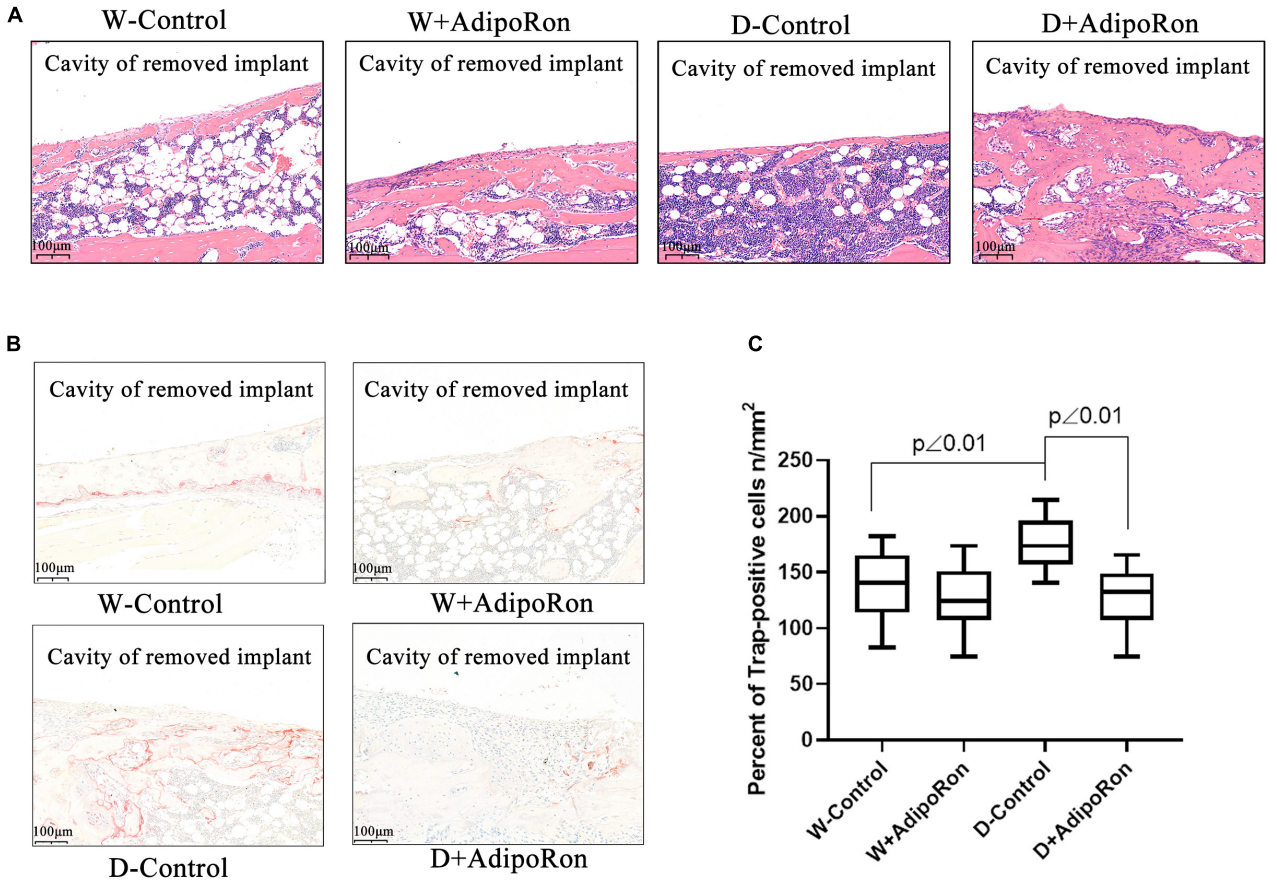

FIGURE 2 | Pathological examinations of femoral bone with dental implants in mice. Femoral bone pathology was observed. Normal mice (Wild-control, W-control), normal mice treated with AdipoRon (Wild + AdipoRon, W + AdipoRon), diabetic mice (Diabetes-control, D-control), and diabetic mice treated with (Diabetes + AdipoRon, D + AdipoRon) were involved. $n = 7$. **(A)** H&E staining of femoral bone with dental implants in mice was shown. One section in the region surrounding the explant of each sample was selected for analysis and five fields of vision were randomly selected in each section. The green arrow indicates bone hyperplasia mediated by the osteoblast differentiation. **(B)** TRAP staining of femoral bone with dental implants in mice is shown. The blue arrow indicates the osteoclast formation. **(C)** TRAP-positive cells of osteoclast were analyzed.

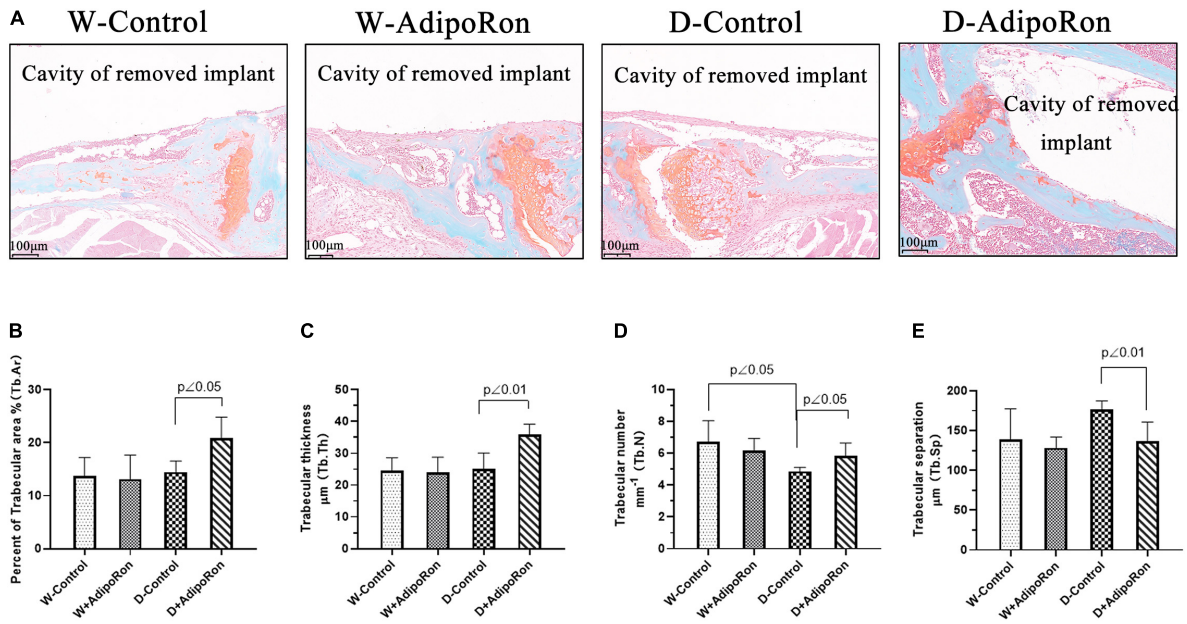

FIGURE 3 | The osteoclast formation was measured using Safranin O-fast green staining. Normal mice (Wild-control, W-control), normal mice treated with AdipoRon (Wild + AdipoRon, W + AdipoRon), diabetic mice (Diabetes-control, D-control), and diabetic mice treated with (Diabetes + AdipoRon, D + AdipoRon) were involved (n = 7). **(A)** Femoral bone with dental implants in mice was stained using Safranin O-fast green. One section in the region surrounding the explant of each sample was selected for analysis and five fields of vision were randomly selected in each section. Percentage of trabecular area (Tb.Ar) **(B)**, trabecular thickness (Tb.Th) **(C)**, trabecular number (Tb.N) **(D)**, and trabecular separation (Tb.Sp) **(E)** were analyzed.

Tb.Sp in diabetic mice. Safranin O-fast green staining results confirmed that AdipoRon may suppress the osteoclast formation.

AdipoRon Suppresses Proteins of Rankl as Well as Promotes the Expressions of BMP2, OPG, OPN, and Runx2 in Diabetic Mice

The expressions of proteins, such as Rankl, BMP2, OPG, OPN, and Runx2, in femoral bone with dental implants in mice were measured using immunohistochemical staining. As shown in **Figure 4**, the expression of protein Rankl (**Figures 4A,B**) was significantly increased and the expressions of proteins BMP2 (**Figures 4A,C**), OPG (**Figures 4A,D**), OPN (**Figures 4A,E**), and Runx2 (**Figures 4A,F**) were significantly decreased in diabetic mice (Diabetes-control, D-control) compared with normal mice (Wild-control, W-control) ($p < 0.05$). However, AdipoRon inhibited the expression of protein Rankl along with the promoted expressions of BMP2, OPG, OPN, and Runx2 significantly in diabetic mice ($p < 0.05$). Results of examination of protein expression suggested that AdipoRon suppressed the osteoclast formation and promoted the osteoblast differentiation in diabetic mice.

DISCUSSION

Type 2 diabetes mellitus with a lot of complications affects human life and health expenditures along with rapid economic development and urbanization (Onyango and Onyango, 2018). Periodontitis is one of the major complications of diabetes including teeth loosening and falling, which affects the physiological functions of teeth of patients seriously (Chee et al., 2013). Although implant treatment is the most important way to repair the lost tooth, hyperglycemia induced a higher failure rate of implant repair (Mellado-Valero et al., 2007). Macrophages in the adipose tissue of T2DM patients correlated with bone integration including bone formation, bone mineralization, and bone reconstruction (Javed and Romanos, 2009) as well as osteoclast activity and promote bone resorption (Catalfamo et al., 2013) and hyperglycemia may impair bone integration of T2DM patients with implants. Along with imposing restrictions on hyperglycemia, improving the function of damaged bone cells and the osseointegration ability of implants is particularly important for implantation success in patients with diabetes. We established the surgery-induced model of osseointegration of dental implantation in mice to investigate the difference in bone formation and bone resorption between diabetic mice (C57BL/6 db/db, T2DM mice) and the normal mice homologous to diabetic mice and tend to found an effective intervention strategy to implant repair loss tooth under hyperglycemia.

As one of the insulin-sensitizing fatty factors, APN is secreted by fat cells to improve insulin resistance and attenuate hyperglycemia as well as impair RANKL-stimulated RAW264.7 cells through its receptors as AdipoR1, AdipoR2 (Okada-Iwabu et al., 2013), and T-Cadherin (Denzel et al., 2010; Parker-Duffen et al., 2013) and its downstream factors of cohesive protein APPL1 (Mao et al., 2006). APN can also promote osteogenic differentiation (Chen et al., 2015; Pu et al., 2016).

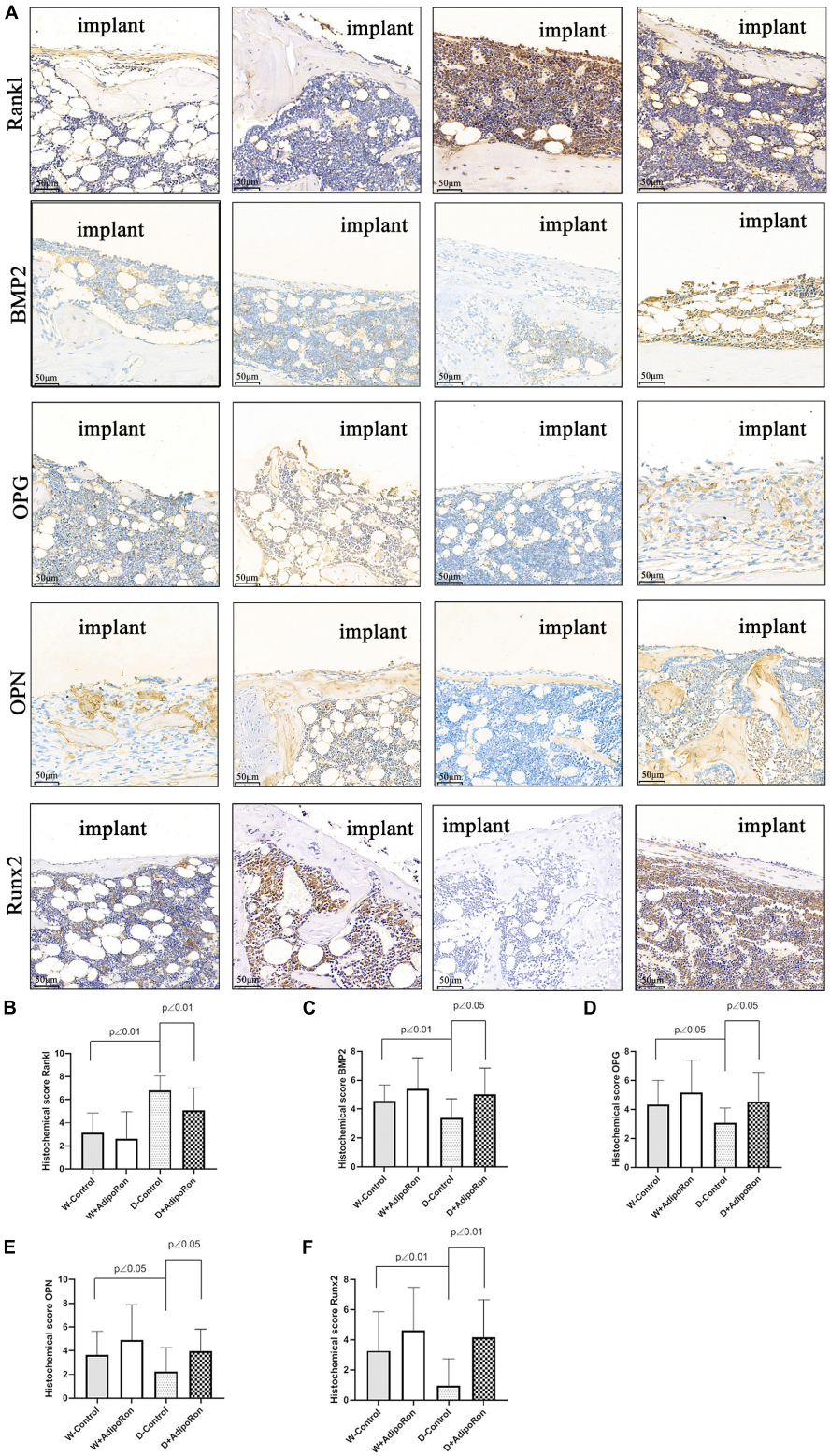

FIGURE 4 | Proteins of Rankl, BMP2, OPG, OPN, and Runx2 in femoral bone with dental implants in mice were quantized using immunohistochemical staining. Normal mice (Wild-control, W-control), normal mice treated with AdipoRon (Wild + AdipoRon, W + AdipoRon), diabetic mice (Diabetes-control, D-control), and diabetic mice treated with (Diabetes + AdipoRon, D + AdipoRon) were involved (n = 7). **(A)** Femoral bone with dental implants in mice was immunohistochemically stained. One section in the region surrounding the explant of each sample was selected for analysis and five fields of vision were randomly selected in each section. Quantitation of Rankl **(B)**, BMP2 **(C)**, OPG **(D)**, OPN **(E)**, and Runx2 **(F)** are indicated using histochemical scores.

However, the clinical application of APN was limited as potential adverse immune reactions, deserving high-dose intravenous administration and complex protein structures are not conducive to industrial production. AdipoRon is an oral synthetic small molecular compound as it has a feasible effect on reducing insulin resistance and blood glucose tolerance in high-fat diet mice by specifically binding to APN receptors AdipoR1 and AdipoR2. AdipoRon might exert similar antidiabetic effects to APN through AMPK and PPAR-α pathway. Some studies also indicated that AdipoRon could promote diabetic fracture repair, enhance alveolar bone regeneration, and increase the survival and migration of BMSCs. According to a recent study, AdipoRon appears to have a pro-osteogenic, anti-adipogenic, and anti-osteoclastogenic effect in young mice (Liu et al., 2021).

We explored the effect of AdipoRon on bone formation and bone resorption in diabetic mice. Micro-CT and pathological examination using H&E, TRAP, and Safranin O-fast green staining were performed to evaluate bone integration. Our results indicated that diabetic mice showed lower bone mass around dental implants compared with the normal mice as BV/TV, Tb.Th, and Tb.N was significantly decreased compared with normal mice. Results of pathological exploration by H&E staining of femoral bone showed that bone hyperplasia mediated by the osteoblast differentiation was significantly decreased in diabetic mice compared with normal mice. As shown in Safranin O-fast green staining results, the osteoclast formation in femoral bone with dental implants in diabetic mice was improved as Tb.N was decreased compared with normal mice. AdipoRon attenuated diabetes-impaired BV/TV, Tb.Th, Tb.N, and Tb.Sp variation and promoted bone hyperplasia as well as repressed the osteoclast formation, especially in diabetic mice.

Rankl is positively related to osteoclast differentiation in periodontitis (Li et al., 2020). Down expression of BMP2 and RUNX2 is involved in reducing osteogenic differentiation (Kang et al., 2020). OPG is a physiological inhibitor of RANKL, both of which regulated the delicate bone balance involving the interplay of soluble mediators. As a decoy receptor, OPG could prevent RANKL from binding to RANK exerting an osteoprotective effect (Dereka et al., 2010). OPG was also reported as one of the factors in predicting the severity of gestational diabetes mellitus, and it is considered as OPG presents a high precision potential in the identification of periodontal disease destruction (Hernandez et al., 2020). OPN accompanied with RUNX2 showed an increased expression as high glucose-inhibited osteogenesis of periodontal ligament stem cells was reversed (Yan et al., 2020). Therefore, bone formation and osteogenic differentiation-related markers of the expressions of Rankl, BMP2, OPG, OPN, and Runx2 were assayed in femoral bone with dental implants in mice. The expression of protein Rankl was significantly increased as well as the expressions of BMP2, OPG, OPN, and Runx2 were significantly decreased in diabetic mice compared with normal mice ($p < 0.05$). AdipoRon suppressed the expression of protein Rankl and promoted the expressions of BMP2, OPG, OPN, and Runx2 in diabetic mice significantly ($p < 0.05$), which suggested that AdipoRon suppressed the diabetes-induced osteoclast formation and promoted the osteoblast differentiation in diabetic mice. These results were consistent with our previous study (Wu Y.C. et al., 2019). AdipoRon may improve insulin resistance by activating AdipoR1/AMPK/PGC1α signaling pathways (Kim and Park, 2019). In addition, AMPK is an important molecular target to metabolic diseases, such as diabetes, to enhance the recovery of osteoblast function and osseointegration around implants. It is necessary for us to perform further study to expound whether AdipoRon can regulate the expression of bone-related proteins through AMPK. Taking together, our results confirmed that AdipoRon may improve the osseointegration of dental implants in mice with T2DM for 2 weeks through promoting osteogenesis and inhibiting bone resorption mediated by the regulation of bone formation-related markers such as Rankl, BMP2, OPG, OPN, and Runx2. However, the enduring effect of AdipoRon and the specific molecular mechanism remains to be explored in further long-term studies. Overall, AdipoRon may serve as a promising oral strategy to improve the osseointegration ability of patients with diabetes.

DATA AVAILABILITY STATEMENT

The original contributions presented in the study are included in the article/supplementary material, further inquiries can be directed to the corresponding authors.

ETHICS STATEMENT

The animal study was reviewed and approved by Animal Ethics Committees of the Fudan University.

AUTHOR CONTRIBUTIONS

BH and WB: project developing, data analysis, writing, and revision. YS: project developing and data collection. RL: data analysis and collection. XW and YY: manuscript writing, revision, and editing.

FUNDING

This study was supported by the National Natural Science Foundation of China to YY (No. 81870793) and Shanghai Sailing Program (No. 21YF1406600) to XW.

REFERENCES

Catalfamo, D. L., Britten, T. M., Storch, D. L., Calderon, N. L., Sorenson, H. L., and Wallet, S. M. (2013). Hyperglycemia induced and intrinsic alterations in type 2 diabetes-derived osteoclast function. *Oral Dis.* 19, 303–312. doi: 10.1111/odi.12002

Chawla, A., Nguyen, K. D., and Goh, Y. P. (2011). Macrophage-mediated inflammation in metabolic disease. *Nat. Rev. Immunol.* 11, 738–749. doi: 10.1038/nri3071

Chee, B., Park, B., and Bartold, P. M. (2013). Periodontitis and type II diabetes: a two-way relationship. *Int. J. Evid. Based Healthc.* 11, 317–329. doi: 10.1111/1744-1609.12038

Chen, T., Wu, Y. W., Lu, H., Guo, Y., and Tang, Z. H. (2015). Adiponectin enhances osteogenic differentiation in human adipose-derived stem cells by activating the APPL1-AMPK signaling pathway. *Biochem. Biophys. Res. Commun.* 461, 237–242. doi: 10.1016/j.bbrc.2015.03.168

Denzel, M. S., Scimia, M. C., Zumstein, P. M., Walsh, K., Ruiz-Lozano, P., and Ranscht, B. (2010). T-cadherin is critical for adiponectin-mediated cardioprotection in mice. *J. Clin. Invest.* 120, 4342–4352. doi: 10.1172/jci43464

Dereka, X. E., Markopoulou, C. E., Fanourakis, G., Tseleni-Balafouta, S., and Vrotsos, I. A. (2010). RANKL and OPG mRNA level after non-surgical periodontal treatment. *Inflammation* 33, 200–206. doi: 10.1007/s10753-009-9174-7

Du, J., Yang, J., He, Z., Cui, J., Yang, Y., Xu, M., et al. (2020). Osteoblast and osteoclast activity affect bone remodeling upon regulation by mechanical loading-induced leukemia inhibitory factor expression in osteocytes. *Front. Mol. Biosci.* 7:585056. doi: 10.3389/fmolb.2020.585056

Esser, N., Legrand-Poels, S., Piette, J., Scheen, A. J., and Paquot, N. (2014). Inflammation as a link between obesity, metabolic syndrome and type 2 diabetes. *Diabetes Res. Clin. Pract.* 105, 141–150. doi: 10.1016/j.diabres.2014.04.006

Hernandez, M., Baeza, M., Contreras, J., Sorsa, T., Tervahartiala, T., Valdes, M., et al. (2020). MMP-8, TRAP-5, and OPG Levels in GCF diagnostic potential to discriminate between healthy patients', mild and severe periodontitis sites. *Biomolecules* 10:1500. doi: 10.3390/biom10111500

Javed, F., and Romanos, G. E. (2009). Impact of diabetes mellitus and glycemic control on the osseointegration of dental implants: a systematic literature review. *J. Periodontol.* 80, 1719–1730. doi: 10.1902/jop.2009.090283

Kang, M., Huang, C. C., Lu, Y., Shirazi, S., Gajendrareddy, P., Ravindran, S., et al. (2020). Bone regeneration is mediated by macrophage extracellular vesicles. *Bone* 141:115627. doi: 10.1016/j.bone.2020.115627

Kim, Y., and Park, C. W. (2019). Mechanisms of adiponectin action: implication of adiponectin receptor agonism in diabetic kidney disease. *Int. J. Mol. Sci.* 20:1782. doi: 10.3390/ijms20071782

Li, J., Sun, Z., Lin, Y., Yan, Y., Yan, H., Jing, B., et al. (2020). Syndecan 4 contributes to osteoclast differentiation induced by RANKL through enhancing autophagy. *Int Immunopharmacol.* 91:107275. doi: 10.1016/j.intimp.2020.107275

Lindhe, J., Meyle, J., and Group, D.o.E.W.o.P. (2008). Peri-implant diseases: consensus report of the sixth european workshop on periodontology. *J. Clin. Periodontol.* 35, 282–285. doi: 10.1111/j.1600-051x.2008.01283.x

Liu, H., Liu, S., Ji, H., Zhao, Q., Liu, Y., Hu, P., et al. (2021). An adiponectin receptor agonist promote osteogenesis via regulating bone-fat balance. *Cell prolif.* 54:e13035.

Liu, X., Tan, N., Zhou, Y., Wei, H., Ren, S., Yu, F., et al. (2017). Delivery of antagomiR204-conjugated gold nanoparticles from PLGA sheets and its implication in promoting osseointegration of titanium implant in type 2 diabetes mellitus. *Int. J. Nanomed.* 12, 7089–7101. doi: 10.2147/ijn.s124584

Mao, X., Kikani, C. K., Riojas, R. A., Langlais, P., Wang, L., Ramos, F. J., et al. (2006). APPL1 binds to adiponectin receptors and mediates adiponectin signalling and function. *Nat. Cell Biol.* 8, 516–523. doi: 10.1038/ncb1404

Mellado-Valero, A., Ferrer Garcia, J. C., Herrera Ballester, A., and Labaig Rueda, C. (2007). Effects of diabetes on the osseointegration of dental implants. *Med. Oral Patol. Oral Cir. Bucal* 12, E38–E43.

Naot, D., Musson, D. S., and Cornish, J. (2017). The Activity of adiponectin in bone. *Calcif. Tissue Int.* 100, 486–499. doi: 10.1007/s00223-016-0216-5

Okada-Iwabu, M., Yamauchi, T., Iwabu, M., Honma, T., Hamagami, K., Matsuda, K., et al. (2013). A small-molecule AdipoR agonist for type 2 diabetes and short life in obesity. *Nature* 503, 493–499. doi: 10.1038/nature12656

Onyango, E. M., and Onyango, B. M. (2018). The rise of noncommunicable diseases in kenya: an examination of the time trends and contribution of the changes in diet and physical inactivity. *J. Epidemiol. Glob. Health* 8, 1–7. doi: 10.2991/j.jegh.2017.11.004

Ortega, M. A., Fraile-Martinez, O., Naya, I., Garcia-Honduvilla, N., Alvarez-Mon, M., Bujan, J., et al. (2020). Type 2 diabetes mellitus associated with obesity (diabesity). the central role of gut microbiota and its translational applications. *Nutrients* 12:2749. doi: 10.3390/nu12092749

Parker-Duffen, J. L., Nakamura, K., Silver, M., Kikuchi, R., Tigges, U., Yoshida, S., et al. (2013). T-cadherin is essential for adiponectin-mediated revascularization. *J. Biol. Chem.* 288, 24886–24897. doi: 10.1074/jbc.m113.454835

Pritzker, K. P., Gay, S., Jimenez, S. A., Ostergaard, K., Pelletier, J. P., Revell, P. A., et al. (2006). Osteoarthritis cartilage histopathology: grading and staging. *Osteoarthr. Cartil.* 14, 13–29. doi: 10.1016/j.joca.2005.07.014

Pu, Y., Wu, H., Lu, S., Hu, H., Li, D., Wu, Y., et al. (2016). Adiponectin promotes human jaw bone marrow stem cell osteogenesis. *J. Dent. Res.* 95, 769–775. doi: 10.1177/0022034516636853

Sapio, L., Nigro, E., Ragone, A., Salzillo, A., Illiano, M., Spina, A., et al. (2020). AdipoRon affects cell cycle progression and inhibits proliferation in human osteosarcoma cells. *J Oncol.* 2020:7262479.

Tatarakis, N., Kinney, J. S., Inglehart, M., Braun, T. M., Shelburne, C., Lang, N. P., et al. (2014). Clinical, microbiological, and salivary biomarker profiles of dental implant patients with type 2 diabetes. *Clin. Oral Implants Res.* 25, 803–812. doi: 10.1111/clr.12139

Wang, S.J., Wang, C., Wang, W. Q., Hao, Q. Q., and Liu, Y. F. (2020). [Adiponectin receptor agonist adiporon inhibits the proliferation of myeloma cells via the ampk/autophagy pathway]. *Zhongguo Shi Yan Xue Ye Xue Za Zhi* 28, 171–176.

Wang, Z., Tang, J., Li, Y., Wang, Y., Guo, Y., Tu, Q., et al. (2020). AdipoRon promotes diabetic fracture repair through endochondral ossification-based bone repair by enhancing survival and differentiation of chondrocytes. *Exp. Cell Res.* 387:111757. doi: 10.1016/j.yexcr.2019.111757

Wu, X., Qiu, W., Hu, Z., Lian, J., Liu, Y., Zhu, X., et al. (2019). An adiponectin receptor agonist reduces type 2 diabetic periodontitis. *J. Dent. Res.* 98, 313–321. doi: 10.1177/0022034518818449

Wu, Y.C., Wang, W. T., Lee, S. S., Kuo, Y. R., Wang, Y. C., Yen, S. J., et al. (2019). Glucagon-like peptide-1 receptor agonist attenuates autophagy to ameliorate pulmonary arterial hypertension through Drp1/NOX- and Atg-5/Atg-7/Beclin-1/LC3beta pathways. *Int. J. Mol. Sci.* 20:3435. doi: 10.3390/ijms20143435

Yan, Y., Zhang, H., Liu, L., Chu, Z., Ge, Y., Wu, J., et al. (2020). Periostin reverses high glucose-inhibited osteogenesis of periodontal ligament stem cells via AKT pathway. *Life Sci.* 242:117184. doi: 10.1016/j.lfs.2019.117184

Yang, R. N., Ye, F., Cheng, L. J., Wang, J. J., Lu, X. F., Shi, Y. J., et al. (2011). Osteoinduction by Ca-P biomaterials implanted into the muscles of mice. *J. Zhejiang Univ. Sci. B* 12, 582–590. doi: 10.1631/jzus.b1000204

Zheng, Y., Ley, S. H., and Hu, F. B. (2018). Global aetiology and epidemiology of type 2 diabetes mellitus and its complications. *Nat. Rev. Endocrinol.* 14, 88–98. doi: 10.1038/nrendo.2017.151

Conflict of Interest: The authors declare that the research was conducted in the absence of any commercial or financial relationships that could be construed as a potential conflict of interest.

frontiers in Physiology

ORIGINAL RESEARCH
published: 14 September 2021
doi: 10.3389/fphys.2021.722859

B-Cell RANKL Contributes to Pathogen-Induced Alveolar Bone Loss in an Experimental Periodontitis Mouse Model

*Rajendra P. Settem[1], Kiyonobu Honma[1], Sreedevi Chinthamani[1], Toshihisa Kawai[2] and Ashu Sharma[1]**

[1] Department of Oral Biology, University at Buffalo, Buffalo, NY, United States, [2] Department of Periodontology, College of Dental Medicine, Nova Southeastern University (NSU), Fort Lauderdale, FL, United States

Periodontitis is a bacterially-induced inflammatory disease that leads to tooth loss. It results from the damaging effects of a dysregulated immune response, mediated largely by neutrophils, macrophages, T cells and B cells, on the tooth-supporting tissues including the alveolar bone. Specifically, infiltrating B cells at inflamed gingival sites with an ability to secrete RANKL and inflammatory cytokines are thought to play roles in alveolar bone resorption. However, the direct contribution of B cells in alveolar bone resorption has not been fully appreciated. In this study we sought to define the contribution of RANKL expressing B cells in periodontitis by employing a mouse model of pathogen-induced periodontitis that used conditional knockout mice with B cell-targeted RANKL deletion. Briefly, alveolar bone loss was assessed in the wild-type, B-cell deficient (Jh), or B-cell-RANKL deleted ($RANKL^{\Delta B}$) mice orally infected with the periodontal pathogen *Tannerella forsythia*. The $RANKL^{\Delta B}$ mice were obtained by crossing Cd19-Cre knock-in mice with mice homozygous for conditional RANKL-flox allele ($RANKL^{flox/flox}$). The alveolar bone resorption was determined by morphometric analysis and osteoclastic activity of the jaw bone. In addition, the bone resorptive potential of the activated effector B cells was assessed *ex vivo*. The data showed that the RANKL producing B cells increased significantly in the *T. forsythia*-infected wild-type mice compared to the sham-infected mice. Moreover, *T. forsythia*-infection induced higher alveolar bone loss in the wild-type and $RANKL^{flox/flox}$ mice compared to infection either in the B cell deficient (Jh) or the B-cell specific RANKL deletion ($RANKL^{\Delta B}$) mice. These data established that the oral-pathogen activated B cells contribute significantly to alveolar bone resorption *via* RANKL production.

Keywords: periodontitis, alveolar bone loss, RANKL, B-cells, *Tannerella forsythia*

OPEN ACCESS

Edited by:
Frédéric Lézot, Institut National de la Santé et de la Recherche Médicale (INSERM), France

Reviewed by:
Charles Shuler, University of British Columbia, Canada
Siew-Ging Gong, University of Toronto, Canada

****Correspondence:***
Ashu Sharma
sharmaa@buffalo.edu

Specialty section:
This article was submitted to Craniofacial Biology and Dental Research, a section of the journal Frontiers in Physiology

Received: *09 June 2021*
Accepted: *09 August 2021*
Published: *14 September 2021*

Citation:
Settem RP, Honma K, Chinthamani S, Kawai T and Sharma A (2021) B-Cell RANKL Contributes to Pathogen-Induced Alveolar Bone Loss in an Experimental Periodontitis Mouse Model. Front. Physiol. 12:722859. doi: 10.3389/fphys.2021.722859

INTRODUCTION

Periodontitis (PD) is a chronic inflammatory disease affecting over 50% of the United States adult population that results in the loss of tooth supporting tissues including the alveolar bone (Pihlstrom et al., 2005; Darveau, 2010). PD is caused by a dysregulated immune response orchestrated by the supra- and sub-gingival microbes which collectively constitute the oral microbiome (Kumar et al., 2006). PD is also a risk factor for many systemic diseases including

diabetes, Alzheimer's, obesity, and rheumatoid arthritis (Pischon et al., 2007; Seymour et al., 2007). Multiple clinical and experimental studies have shown that both innate and adaptive immune cells (monocytes, macrophages, neutrophils, T and B-cells) play critical roles in the maintenance of periodontal health as well as progression of the disease (Dutzan et al., 2016). Particularly, specific B cell subtypes have been shown to be associated with the disease severity (Nikolajczyk, 2010). Studies have shown that the B cell stimulatory cytokines BLyS (B lymphocyte stimulator) and APRIL (a proliferation-inducing ligand) have been shown to be elevated in periodontitis and required for B cell-dependent alveolar bone loss in a murine model (Abe et al., 2015). Further support for the pathological role of B cells in periodontitis comes from the findings that show that the B cell-deficient mice are protected from *P. gingivalis*-induced alveolar bone loss (Abe et al., 2015; Oliver-Bell et al., 2015). Moreover, studies have shown that the B cells in gingival tissues of individuals with periodontitis express RANKL (the receptor activator of NF-κB ligand), a key osteoclastogenic cytokine (Kawai et al., 2006). A more direct evidence for the role of B cells and their RANKL in periodontitis comes from the studies that showed that bacterially-activated B cells expressed RANKL and adoptive transfer of these cells promoted alveolar bone resorption in a rodent model (Han et al., 2006, 2009). B cells with an anti-inflammatory role also exist in the gingival tissues. For example, a subset of B-regs (B regulatory cells), B10, has been suggested to play anti-inflammatory and anti-bone resorbing functions due its ability to secrete IL-10 (Dai et al., 2017; Hu et al., 2017; Wang et al., 2017), The adoptive transfer of B10 cells in mice has been shown to suppress the RANKL/OPG (osteoprotegerin, a soluble decoy receptor of RANKL) ratio and increase IL-10 production in gingival tissues, and thus these cells may play a regulatory role in osteoclastogenesis (Wang et al., 2017). The bone-damaging effects of B cell secreted RANKL has been shown in other bone diseases as well such as rheumatoid arthritis (Yeo et al., 2011) and osteoporosis (Onal et al., 2012). However, the evidence in favor of B cell-RANKL role in bacterially-induced periodontitis is so far indirect. In our laboratory we study the pathogenesis of the periodontal pathogen *Tannerella forsythia*. Our studies have demonstrated that the TLR2-Th2 inflammatory axis drives the alveolar bone resorption upon *T. forsythia* infection in mice (Myneni et al., 2011).

The purpose of the present study was to determine the contribution of B cell expressed RANKL in periodontitis. We utilized *T. forsythia* as a periodontal pathogen of choice in inducing periodontitis (alveolar bone loss) in a murine model using the wild-type and the conditional knockout mice having B cell specific RANKL deficiency ($RANKL^{\Delta B}$). Our results established that RANKL expressing effector B cells are involved in alveolar bone resorption in response to the pathogen infection.

EXPERIMENTAL PROCEDURES

Animals and Bacterial Infection

Tannerella forsythia was grown in broth or on agar plates (1.5% agar in Broth) under anaerobic conditions as described previously (Chinthamani et al., 2021). Specific-pathogen free wild-type BALB/cJ and C57BL/6J mice, and *CD19-Cre* mice were purchased from Jackson Laboratory (Bar Harbor, ME, United States). B cell deficient mice (Jh; $Igh^{-/-}$) were purchased from Taconic Biosciences. Mice harboring a conditional RANKL allele (RANKL-flox) generated previously (Onal et al., 2012) were obtained as gift from Charles O'Brien at the University of Arkansas. B cell-specific RANKL deletion mice were generated by crossing conditional RANKL-floxed mice with CD19-Cre mice by a three-step breeding strategy. Briefly, homozygous *CD19-Cre* (Cre inserted into B cell CD19 gene) transgenic mice were crossed with heterozygous RANKL-flox mice ($RANKL^{flox/+}$) to generate heterozygous RANKL-flox offspring with and without a Cre allele. These offspring were then intercrossed to generate homozygous RANKL-flox ($RANKL^{flox/flox}$) mice with and without a Cre allele. Lastly, $RANKL^{flox/flox}$ mice with or without a Cre allele were intercrossed, generating progeny (50%) with the required genotype (homozygous RANKL-flox mice with hemizygous transgenic Cre) and 50% with homozygous RANKL-flox allele serving as littermate controls. Offspring were genotyped by PCR by using the following primer sequences as described before. Cre-for, 5′-GCGGTCTGGCAGTAAAAACTATC-3′; Cre-rev, 5′-GTGAAACAGCATTGCTGTCACTT-3′, product size 102 bp; RANKLflox-for, 5′-CTGGGAGCGCAGGTTAAATA-3′; RANKLflox-rev, 5′-GCCAATAATTAAAATA CTGCAGGAAA-3′, product size 108 bp (wild-type) and 251 bp (floxed allele). The DNA fragment pattern for each genotype is shown in **Supplementary Figure 1**. Mice were maintained in HEPA-filtered cages with autoclaved food, water, and bedding. Animals (eight male mice per group; housed as 2 littermates per cage) within an experimental group were age matched (n = 8, 6–8 weeks old). All procedures were performed in accordance with protocols approved by the University at Buffalo Institutional Animal Care and Use Committee (IACUC). Mice were infected with *T. forsythia* as previously described with following modifications (Myneni et al., 2011). Briefly, mice were first treated with kanamycin (1 mg/mL) in drinking water for 7 days followed by a 3-day antibiotic-free period to suppress resident flora. This was followed by infection with live bacteria (*T. forsythia*) through oral gavage using a feeding needle. Infection was given as 100 μL bacterial suspension (10^{10} c.f.u./mL) in 2% carboxymethyl cellulose (CMC) six times at 48 h intervals. Infection was monitored and confirmed by swabbing gingival tissues around teeth followed by PCR with *T. forsythia* 16S rRNA gene primers (5′-GCGTATGTAACCTGCCCGCA-3′ and 5′-TGCTTCAGTTCAGTTATACCT-3′, amplifying a 641-bp amplicon) as described previously (Settem et al., 2012). The control sham-infected mice received antibiotic pre-treatment and 100 μL of 2% carboxymethyl cellulose only. PCR analysis of oral swabs confirmed that all mice infected with *T. forsythia* were positive for the *T. forsythia*-specific 620-bp 16S rRNA gene product and the sham-infected were negative (data not shown). After 6 weeks of the first infection mice were sacrificed to assess the alveolar bone loss morphometrically, serum

antibody response by ELISA and B cell RANKL expression by flow cytometry.

ELISA for Bacteria-Specific Serum IgG Titers

To determine whether B cell RANKL deficiency had any impact on the antibody response against *T. forsythia*, enzyme-linked immunosorbent assays (ELISAs) were performed as described previously (Settem et al., 2012). Briefly, 96-well Immuno MaxiSorp plates (Nalgene, Rochester, NY, United States) were coated with formalin-fixed *T. forsythia* (1×10^8 cells/well). Sera were added in a two-fold serial dilution, and *T. forsythia*-specific IgG was detected using horseradish peroxidase-conjugated goat anti-mouse IgG (Bethyl Laboratories, Montgomery, TX, United States). ELISA wells were color developed with TMB (3,3′,5,5′-tetramethylbenzidine) microwell enzyme substrate (KPL, Gaithersburg, MD, United States). After stopping the enzyme reaction with 0.1 N H_2SO_4, plates were read at 495 nm. The antibody titer was defined as the $\log_2$ of the highest dilution giving an absorbance 0.1 units above the background.

Assessment of Alveolar Bone Loss

Mice ($n = 8$) were sacrificed after 6 weeks of the first infection, jaws were autoclaved, de-fleshed and immersed overnight in 3% hydrogen peroxide, and stained with 1% methylene blue. Mouse jaw was then placed horizontally on a platform such that the same plane was analyzed for each mouse. The horizontal bone loss was assessed morphometrically by measuring the distance between the cementoenamel junction (CEJ) and the alveolar bone crest (ABC) at seven buccal sites on the three molars (3, 2 and 2 sites on molars 1, 2, and 3, respectively) on the left side and seven sites on the right side of the maxilla. Measurements at these 14 buccal sites per mouse were made under a stereo zoom microscope (Nikon SMZ1000) with a wide zoom range (0.8×–8×) and a 10x eyepiece, providing an overall magnification of 8×–80×. This microscope was attached to a digital camera (Brook-Anco, Rochester, NY, United States) fitted with an Aquinto imaging measurement system (a4i America). To minimize the effects of any measurement biases, the jaws were independently positioned and read in a random and blinded manner by two evaluators. Total alveolar bone loss per group was calculated by averaging total CEJ-ABC distances (14 sites per mouse) of all mice.

Flow Cytometric Analysis

RANKL Expression on B-Cells

Flow cytometry was performed to assess and compare the level of RANKL expression on B cells from different treatment groups. This analysis was performed to also confirm that conditional deletion of *Rankl* gene in B cells indeed led to the loss of RANKL expression on B cells. For this purpose, spleens and cervical lymph nodes (cLNs) were collected from each mouse at the time of sacrifice and B cells were purified by using the EasySep™ mouse CD19 Positive Selection Kit II (STEMCELL Technologies, MA, United States) as per manufacturer's instructions. Purified B lymphocytes were cultured in RPMI medium 1640 (Life Technologies, Grand Island) supplemented with 5% heat-inactivated fetal bovine serum (Sigma-Aldrich, St. Louis, MO, United States), 50 μM 2-ME (Sigma-Aldrich), 2 mM L-glutamine,100 U/mL penicillin, and 100 μg/mL streptomycin (Life Technologies) for 48 h. The cells were stained with APC-conjugated rat-anti-mouse CD19 monoclonal antibody (BD Pharmingen, Clone 1D3) and biotin-conjugated rat anti-mouse RANKL monoclonal antibody (eBioscience, Clone IK22/5) followed by streptavidin-FITC (eBioscience). Appropriate rat IgG2a k isotype controls were used as negative controls (eBiosciences). Data were acquired using a Fortessa flow cytometer (BD Biosciences) and the number of positively stained cells in the total counted cells was analyzed for each sample using FCS express (*De Novo* software).

RT-qPCR Analysis

Reverse transcription quantitative PCR (RT-qPCR) analysis was performed to assess the levels of RANKL mRNA in B cells in response to *T. forsythia* infection. For this purpose, B cells from spleens of sham—and *T. forsythia*—infected mice were purified and then stimulated with *T. forsythia* at an m.o.i. of 50 and 100 for 48 h. After stimulation, toral RNA was isolated from B cells with an RNAeasy mini kit (Qiagen) incorporating DNase treatment as per the manufacturer's protocol. Retrotranscription of RNA (500 ng) into cDNA was performed with iScript reverse transcriptase kit (Bio-Rad laboratories). Quantitative real-time PCR was performed with a Bio-Rad iCycler (Bio-Rad) using SYBR Green master mix reagent (Bio-Rad). Two step PCR was performed with 94°C for 15 s and 58°C for 30 s for 40 cycles. Gene expression values were calculated based on the $2^{-\Delta\Delta Ct}$ method using *Gapdh* expression as an internal control. The primer sequences were: GAPDH, 5′-GGATGCAGGGATGATGTTCT-3′ and 5′-AACTTTGCCATTGTGGAAGG-3′; RANKL, 5′-AGCCATTTGCACACCTCAC-3′ and 5′-CGTGGTACCAAGA GGACAGAGT-3′.

TRAP Staining

Ex vivo Osteoclastogenesis

The ability of activated B cells to induce osteoclastogenesis *via* RANKL was evaluated by an *ex vivo* assay utilizing TRAP (tartrate-resistant acid phosphatase) based staining of osteoclasts. Wild type BALB/cJ mice were treated with Kanamycin (1 mg/mL) in drinking water for 1 week to suppress the natural flora effect. After 3 days of antibiotic-free water mice were infected with 100 μL of *T. forsythia* at 1×10^{10} c.f.u./mL per dose for a total of six doses given at 48 h interval. Sham group received 100 μL of 2% CMC alone. After 2 weeks of the first infection mice were sacrificed and $CD19^+$ B cells were isolated with CD19 positive selection kit (Stemcell Technologies) as per the manufacturer instructions. The $CD19^+$ cells were primed with *T. forsythia* for 3 days at an m.o.i. of 10 and 50. The primed B cells were washed twice with PBS and co-cultured with mouse bone marrow derived macrophages (BMMs) for 3 days. In some conditions B cell and macrophage co-cultures were incubated in the presence of mouse OPG-Fc at a concentration of 10 μg/mL to confirm that the osteoclastogenesis is mediated by RANKL-RANK interaction. TRAP (tartrate-resistant acid phosphatase)

staining for detecting osteoclasts was performed as described previously (Settem et al., 2013). TRAP-positive cells with three or more nuclei were considered as matured osteoclasts and counted microscopically.

In vivo Osteoclastgenesis

For evaluation of *in vivo* osteoclastic activity, mouse jaw bone sections were TRAP stained. Mice (C57BL6, $RANKL^{\Delta B}$ and $RANKL^{flox/flox}$) maxillary and mandibular jaw bones (n = 4) were fixed in 10% phosphate-buffered formalin and decalcified in 10% EDTA. The samples were embedded in paraffin, and sections at 4 μm were prepared and TRAP stained. The stained slides were digitally scanned with a Scan Scope CS system (Aperio) immediately to minimize color fading. The scanned slides were viewed with Image Scope viewing software (Aperio). The right maxillary and mandibular inter-dental areas (average of 10 higher power fields/slide) of the crestal alveolar bone from the first molar to third molar were used to quantify osteoclasts.

Data Analysis

Prism 9 software (GraphPad Software) was used for all statistical analyses. Statistical significance was determined by two-tailed paired or unpaired Student's t test for two groups or one-way ANOVA with Tukey's *post hoc* test for multiple groups. Comparisons of two non-parametric data sets were done by the Mann–Whitney U test. A p value of less than 0.05 was considered statistically significant.

RESULTS

B Cell Deficiency Attenuates Pathogen Induced Alveolar Bone Loss

To evaluate the impact of B cell deficiency on pathogen-induced alveolar bone loss, 6 weeks after the first *T. forsythia* infection alveolar bone resorption was measured at 14 buccal sites of left and right (7 + 7) maxillary jaw bones. Because cementum is progressively exposed with increasing bone resorption, the distance between the CEJ to ABC was determined as a measure of bone resorption at each site. As shown in **Figure 1A** the wild-type mice showed a significant elevation in bone resorption at all sites measured when infected with *T. forsythia* (**Figure 1C**, top right panel) as compared to sham infection (**Figure 1C**, top left panel). On the other hand, B cell deficient Jh ($Igh^{-/-}$) mice exhibited reduced alveolar bone resorption at all molar sites in response to *T. forsythia* infection (**Figure 1C**, bottom left, sham; bottom right, Tf infection) as compared to the sham

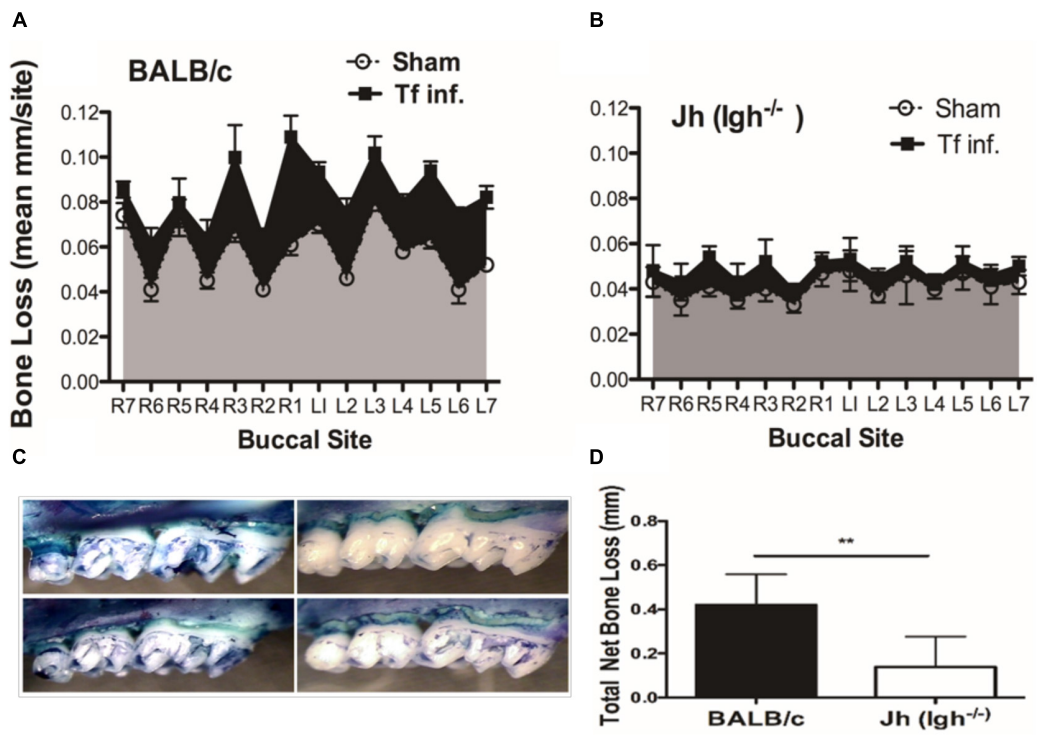

FIGURE 1 | B cell deficiency attenuates pathogen induced alveolar bone loss. Wild type and Jh ($Igh^{-/-}$) mice (n = 8) were infected by oral gavage either with *T. forsythia* cells (Tf. Inf) mixed in carboxymethyl cellulose (CMC) or CMC alone (Sham). Alveolar bone destruction was assessed after 6 weeks by measuring the distance from the ABC to the CEJ at 14 maxillary buccal sites per mouse (R1 to R7, right jaw; L1 to L7, left jaw). Average alveolar bone loss at 14 buccal sites wild-type **(A)** and Jh (mature B-cell deficient) mice **(B)**. **(C)** Representative images of maxillary jaw bones showing alveolar bone levels at each site measured as distances between ABC to CEJ. **(D)** Net bone loss calculated as average of total bone loss in *T. forsythia* infected group—total bone loss in sham group) in wild-type and Jh ($Igh^{-/-}$) group. As indicated, the net bone loss in the B cell deficient mice is significantly lower as compared to the wild-type mice. Data show means with standard deviations. Statistically significant differences are indicated with asterisks. p–values less than 0.05 were considered significant. (***P < 0.001; *P < 0.05).

infection (**Figure 1B**). As seen in **Figure 1D** the total net bone loss due to *T. forsythia* infection was significantly higher in the wild-type BALB/cJ as compared to the Jh ($Igh^{-/-}$) mice. These data showed that *T. forsythia*-induced bone loss, similar to that by the oral pathogen *P. gingivalis* shown previously, requires mediation of B cells (Abe et al., 2015; Oliver-Bell et al., 2015). These data confirmed that mature B-cells play a significant role in the pathogen induced alveolar bone resorption.

Tannerella forsythia Induces RANKL Expression on B Cells

RANKL expression in B cells was assessed by analyzing B cells from spleens and cervical draining lymph nodes (cLN) after infection. B cells were purified from the wild-type or conditional knockout (cKO) mice with B cell specific RANKL deletion ($RANKL^{\Delta B}$) 6 weeks after the first *T. forsythia*—or sham-infection dose. Purified splenic B cells ($CD19^{+}$) were activated *in vitro* for 48 h with *T. forsythia* at an m.o.i. (multiplicity of infection) of 10 and 50. The RT-qPCR data showed a significant fold-increase in RANKL mRNA expression in B cells from *T. forsythia*-infected wild-type (C57BL/6J) mice in comparison to sham mice (control) (**Figure 2A**). There was no measurable RANKL mRNA expression in B cells from $RANKL^{\Delta B}$ mice, sham- or *T. forsythia*—infected (Data not shown; C_t values were over the range set at 40 cycles). In addition, the flow cytometry data showed that *T. forsythia*-infected wild-type mice had higher percentages of $RANKL^{+}$ B cells as compared to the sham-infected mice. On the other hand, $RANKL^{\Delta B}$ mice exhibited no significant increase in $RANKL^{+}$ B cell population following infection and the percentages of $RANKL^{+}$ B cells remained low. As shown, *T. forsythia*-infected wild-type mice alone showed increased $CD19^{+}/RANKL^{+}$ cell population (**Figure 2B**).

B Cell RANKL Contributes to *T. forsythia*-Induced Osteoclastogenesis

We assessed the contribution of RANKL induction in B cells due to activation by *T. forsythia* on osteoclastogenesis. For this purpose, purified splenic B cells from the sham- or *T. forsythia*-infected wild-type mice were first activated with *T. forsythia* and then co-incubated with mouse bone marrow derived macrophages. The formation of multinucleated osteoclasts was evaluated by TRAP (tartrate-resistant acid phosphatase) staining. The data showed significantly increased numbers of TRAP positive cells in culture containing B cells from *T. forsythia*-infected animals as compared to those from the sham-infected mice (**Figures 3A,B**). In addition, the number of multinucleated TRAP positive cells diminished significantly in the presence of osteoprotegerin (OPG, a RANKL decoy receptor), thereby

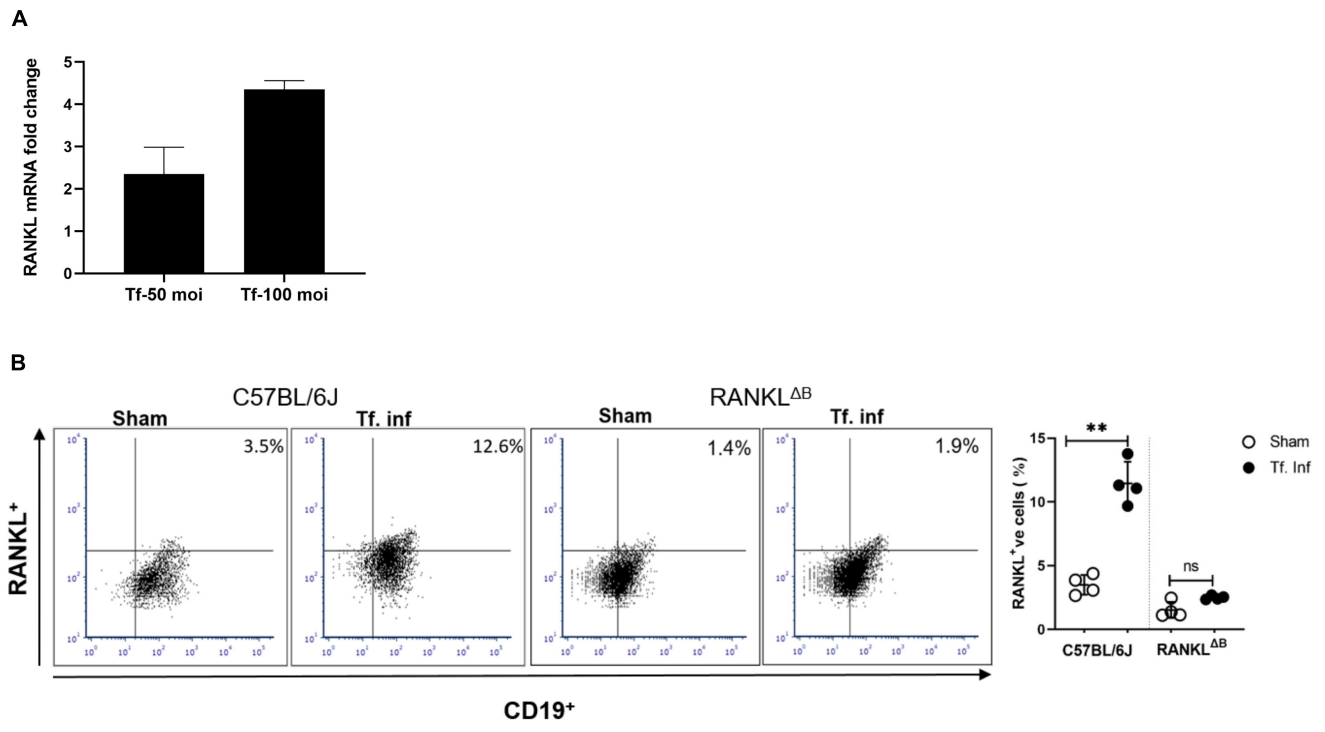

FIGURE 2 | *T. forsythia* infection induces RANKL expression on B cells. Expression levels of RANKL in mouse B cells. *T. forsythia* infected mouse spleen B cells were purified and re-stimulated with *T. forsythia* at an MOI of 50 and 100 for 48 h. After re-stimulation, RANKL mRNA and B cell surface expression levels were determined by RT-qPCR **(A)** and flow cytometry **(B)**, respectively. **(A)** Data show fold-increase in RANKL expression in B cells from *T. forsythia*-infected mice versus sham-infected mice. **(B)** Representative flow cytometry plots of draining cLN B cells showing dual RANKL/CD19 positive cells in the upper right quadrant. Bar graphs on the right show mean (±s.d) percentages of RANKL producing cells in one of two experiments with four mice in each group. Data are presented as means ± s.d. (n = 4 animals/group). $^{**}P < 0.01$.

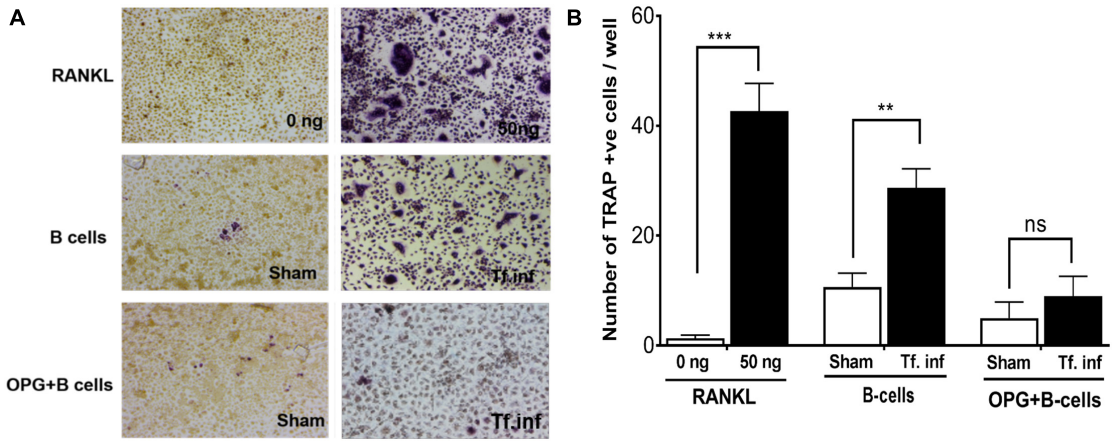

FIGURE 3 | *T. forsythia* causes osteoclastogenesis *via* induction of RANKL^{+} effector B cells. Evaluation of osteoclastogenesis *in vitro* by TRAP staining. CD19^{+}ve B cells from mice were co-cultured with bone marrow derived macrophages. In some condition's co-cultures were performed in the presence of mouse OPG-Fc at a concentration of 10 μg/mL to confirm the osteoclastogenesis is mediated by RANKL-RANK interaction. TRAP staining was performed to determine the number of multinucleated osteoclasts. **(A)** Representative histological staining showing increased multinucleated TRAP positive cells (magenta-red) in cocultures of bone marrow derived macrophages with B cells from *T. forsythia* infected (Tf. Inf) versus sham infected mice. **(B)** Data are means ± s.d. of TRAP^{+} cells per well for each treatment from a representative experiment performed with three replicates per condition. Inclusion of OPG in cocultures significantly reduced the number of TRAP positive cells. $^{**}p < 0.01$; $^{***}p < 0.001$.

validating that the ability of activated B cells to promote osteoclast formation was mediated *via* RANKL.

Deletion of RANKL on B Cell Attenuates Pathogen Induced Alveolar Bone Loss

Next, alveolar bone resorption in response to oral infection by *T forsythia* in the wild-type and B cell specific RANKL deletion mice (RANKL$^{\Delta B}$) was compared to confirm the role of B cell produced RANKL in the pathogen-induced alveolar bone resorption. Before analyzing the alveolar bone loss in mice, we assessed the antibody response to *T. forsythia* in both the wild-type and conditional KO mice to confirm that the B cells' ability to mount an antibody response was not compromised in any way due to RANKL deletion. The data showed (**Figure 4**) a significant elevation of serum antibody titers against *T. forsythia* in both the wild-type and RANKL$^{\Delta B}$ mice infected with *T. forsythia* as compared to the respective sham-infected mice. These data suggested that RANKL did not impact the antibody response of B cells. The antibody titers in sham-infected animals against *T. forsythia* represent cross-reactive anti-bacterial antibodies induced by the mouse resident flora. Next, the total and net alveolar bone loss associated with the maxillary jaw bones was calculated as described above. As shown in **Figure 5A**, total alveolar bone loss in the wild-type mice infected with *T. forsythia* was significantly higher as compared to that in the sham-infected wild-type mice. On the other hand, the *T. forsythia* infected RANKL$^{\Delta B}$ mice exhibited only a marginal but non-significant increase in bone loss. This marginal increase in bone loos could be attributed to RANKL expression in other cell types as such as the T cells and neutrophils as has been previously shown. Both the homozygous flox and the CD19 heterozygous genotype mice infected with *T. forsythia* showed a significant alveolar bone loss similar to the *T. forsythia* infected wild-type mice. The net bone loss for each group (total average alveolar bone loss of the sham-infected mice subtracted from that of the *T. forsythia*-infected mice). As is evident from the data (**Figure 5B**), *T. forsythia* induced similar levels of net alveolar bone loss in the wild-type, RANKL$^{flox/flox}$, or CD19-Cre heterozygous mice but the RANKL$^{\Delta B}$ mice were significantly resistant (**Figure 5C**, panels showing representative maxillae from each group). The alveolar bone loss observed was confirmed by evaluation of the osteoclastic activity in the jaw bones by TRAP staining. The TRAP staining results showed increased numbers of TRAP positive cells in *T. forsythia* infected wild-type, RANKL$^{flox/flox}$ and CD19-Cre mice as compared to the RANKL$^{\Delta B}$ mice (**Figure 6**). Taken together, these data demonstrated that RANKL production by B cells contributes

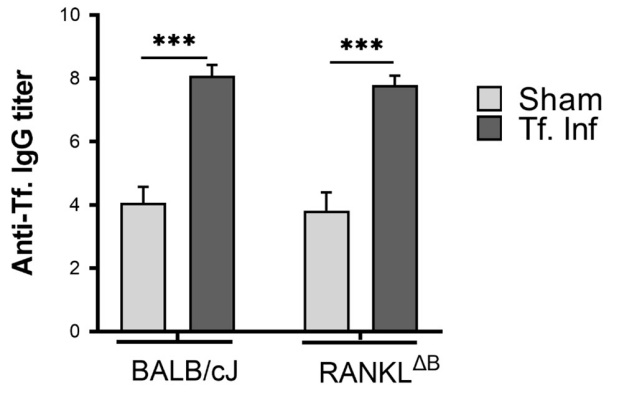

FIGURE 4 | Deletion of RANKL in B cells did not alter the IgG response. Sera was collected from sham and *T. forsythia* infected mice (BALB/cJ and RANKL$^{\Delta B}$) and analyzed for *T. forsythia*-specific IgG by ELISA. Antibody levels are presented as $\log_2$ titers. Data are the means and standard deviations for each group ($n = 8$); $^{***}P < 0.001$ vs the sham-infected group.

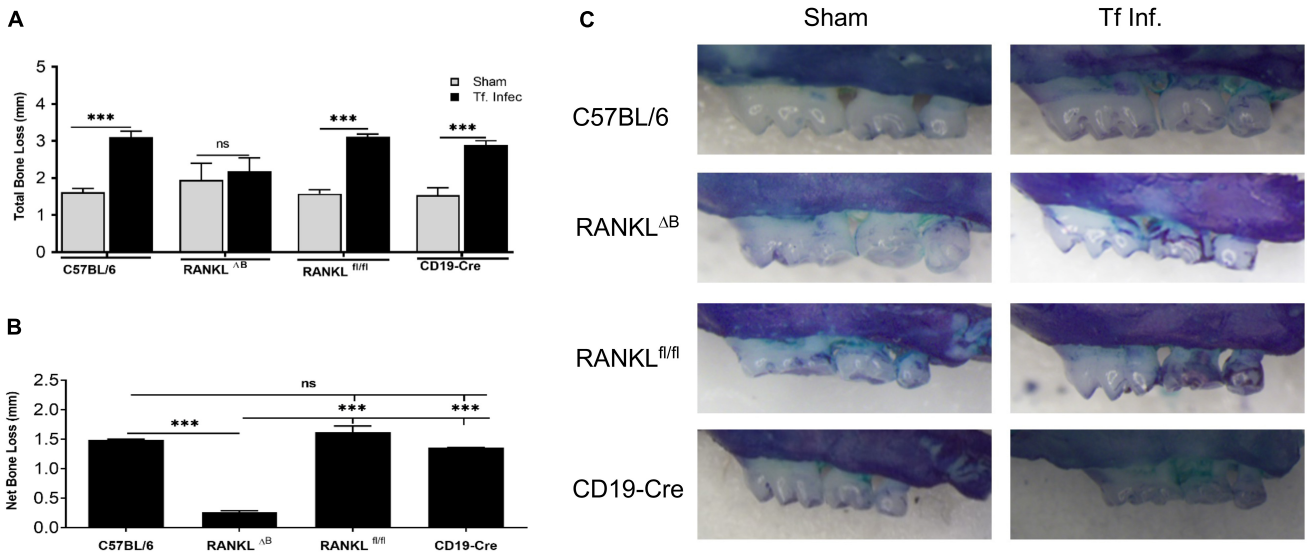

FIGURE 5 | Deletion of RANKL in B cells attenuates *T. forsythia* induced alveolar bone loss. Mice were infected by oral gavage with 6 doses (10^9 cells/dose) of either *T. forsythia* (10^9 cells/dose; Tf WT) or sham-infected and alveolar bone levels were determined. **(A)** Alveolar bone destruction was assessed by measuring the distance from the ABC to the CEJ at 14 maxillary buccal sites per mouse ($n = 8$). **(A)** Total alveolar bone loss per group was calculated by averaging total CEJ-ABC distances (14 sites per mouse) of all mice. **(B)** The net bone loss, calculated as mean total ABC-CEJ distance of *T. forsythia* infected group minus mean total ABC-CEJ distance of the sham-infected group, show that the net bone loss caused by *T. forsythia* is significantly higher in RANKL$^{fl/fl}$ mice than RANKL$^{\Delta B}$ mice. **(C)** Representative images of maxillae from each group stained with methylene blue and imaged with a Nikon SMZ 1000 microscope (original magnification X3). Bars indicate means and standard deviations. ***$p < 0.001$.

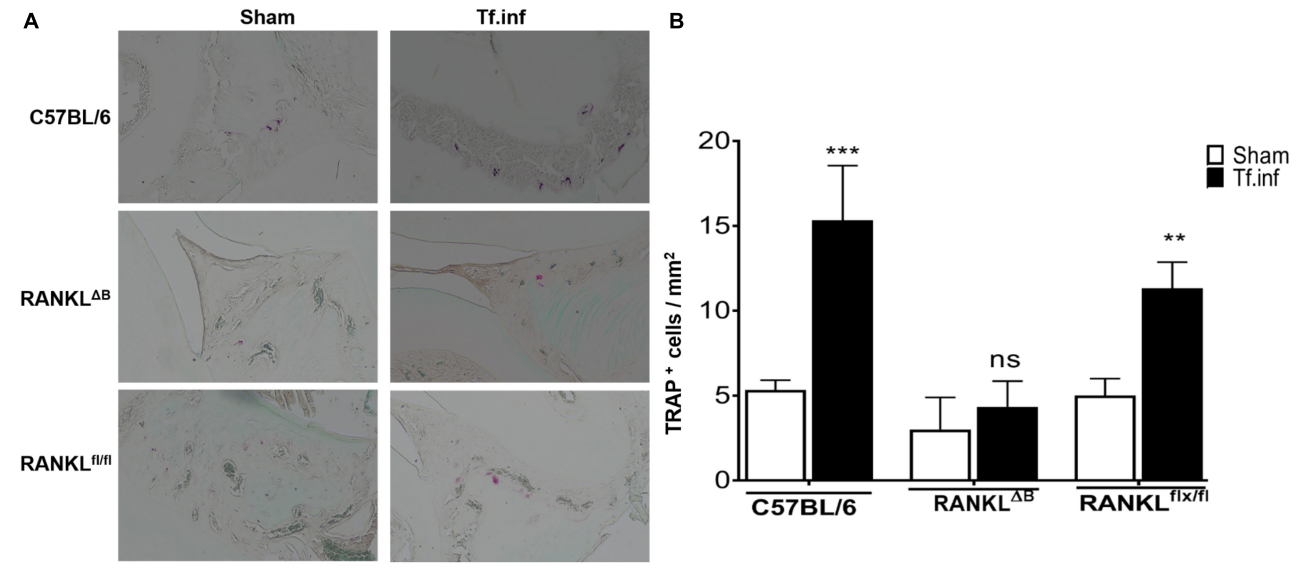

FIGURE 6 | Alveolar bone loss correlates with osteoclastic activity. **(A)** Representative histological sections showing TRAP$^+$ cells from *T. forsythia* (Tf. Inf) and sham (Sham) infected mice (×400). **(B)** Average number of TRAP$^+$ cells in 10 high-power magnification fields/slide ($n = 4$ mice/group). **$p < 0.01$, ***$p < 0.001$; Tf. Inf vs Sham.

significantly to pathogen infection induced osteoclastogenesis in the jaw bone, culminating in alveolar bone loss in mice.

DISCUSSION

In this study we demonstrated that the mature B cell deficient mice and mice deficient specifically in B cell associated RANKL (cKO RANKL$^{\Delta B}$) were resistant to pathogen-induced alveolar bone loss. These data confirm that activated B cells *via* RANKL expression contribute significantly to pathogen associated alveolar bone loss observed in periodontitis. Previous studies have shown that activated T and B cells in gingival tissues of individuals with periodontitis express RANKL (receptor activator of nuclear factor κB ligand, also known as TNFSF11) (Taubman et al., 2005; Han et al., 2006, 2009; Kawai et al., 2006).

RANKL is a tumor necrosis factor (TNF) family inflammatory cytokine which is a key positive inducer of osteoclastogenesis due its role in the differentiation, survival, and activation of osteoclasts (Boyce and Xing, 2007; Nakashima et al., 2012). In light of the fact that mice with B cell specific RANKL deficiency exhibited some pathogen-induced alveolar bone loss, albeit minimally, indicates that other RANKL expressing cells in addition to the B cells are likely also involved in driving alveolar bone loss. Nevertheless, our data establishes a significant role and contribution of RANKL expressing effector B cells in driving alveolar bone loss during periodontitis.

In periodontitis, various subtypes of T (Th1, Th2, Th17, and Tregs) and B (plasma cells, B1, B2, and B- regs) lymphocytes with inflammatory or anti-inflammatory properties play a crucial roles in modulating periodontal inflammation and bone loss (Figueredo et al., 2019). In heath and disease, the proportion of each of these subtypes in the gingival tissues has been shown to differs. For instance, with regard to B cells, lower numbers of memory B cells are present in periodontitis lesions compared to gingivitis and the numbers of antibody-secreting $CD138^{+}$ plasma cells increase in periodontitis compared to healthy or gingivitis tissues (Mahanonda et al., 2016). A recent study showed that RANKL expression increases in all subsets of activated B cell in severe periodontitis (Demoersman et al., 2018). However, the mechanisms by which RANKL expression in B lymphocytes is induced are unclear. Nevertheless, IL-33 has been implicated in the activation of RANKL expression in T and B cells during periodontitis (Malcolm et al., 2015). It was demonstrated that IL-33 treatment along with pathogen infection can significantly increase the population of RANKL-expressing T and B cells compared to pathogen infection alone. Strikingly, IL-33 is an inducer of Th2 cells (Murakami-Satsutani et al., 2014) and a regulator of B cell proliferation and differentiation (Komai-Koma et al., 2011; Stier et al., 2019). How these effects of IL-33 might impact periodontitis remains to be determined. Moreover, B cells in the gingival tissues can also produce inflammatory cytokines (IL-1β and TNF-α) in response to TLR ligands (Jagannathan et al., 2009), that in turn can induce RANKL expression and inflammation to cause alveolar bone loss. We have previously shown that TLR2-Th2 axis is involved in driving the *T. forsythia* induced alveolar bone loss in mice. However, how this axis is linked to B cell RANKL induction remains to be determined. It is tempting to speculate that in addition to the RANKL induction *via* TLR2 pathway in B cells mentioned above, Th2 cytokine IL-4 might help to promote B cell proliferation and maturation (Granato et al., 2014).

B cells with an anti-inflammatory role have also been reported in gingival tissues. A subset of B-regs (B regulatory cells), B10, has been found in gingival tissues of patients with and without periodontitis, and has been suggested to play anti-inflammatory and anti-bone resorbing functions due its ability to secrete IL-10 (Dai et al., 2017; Hu et al., 2017; Wang et al., 2017). B10 cells by virtue of IL-10 secretion can potentially regulate osteoclastogenesis by inhibiting the secretion of TNF-α and IL-1β and suppressing the ratio of RANKL/OPG in gingival tissues (Wang et al., 2017). The cKO mouse model for B cell RANKL described in our study serves as a model system for evaluation of the contribution of other B cell cytokines in periodontitis. For instance, the role of B cell secreted OPG (Tnfrsf11b) or 1L-10 can be interrogated by conditional deletion of respective alleles in B cells by employing $Tnfrsf11b^{flox/flox}$ or $IL\text{-}10^{flox/flox}$ mice, respectively, bred with CD19-Cre mice.

In summary, we have shown by utilizing B cell-specific conditional knockout mice that activated B cells are significant contributors of RANKL in the oral pathogen-induced alveolar bone loss. However, what kind of B cell subtype(s) becomes $RANKL^{+}$ effector cell in the gingival tissue in response to the pathogen could not be ascertained with the current study, Finally, our findings indicate that the B cell cKO mouse model described here for RANKL can be adapted for defining the contribution of other B cell mediators in periodontitis progression.

DATA AVAILABILITY STATEMENT

The original contributions presented in the study are included in the article/**Supplementary Material**, further inquiries can be directed to the corresponding author/s.

ETHICS STATEMENT

The animal study was reviewed and approved by IACUC, University at Buffalo.

AUTHOR CONTRIBUTIONS

AS conceived the work. AS and RS wrote the manuscript. RS, KH, and SC performed the experiments. AS, RS, and TK critically analyzed the data and all authors were critical reviewers of the manuscript.

FUNDING

This work was funded by the NIH/NIDCR award number DE014749 and DE029497 to AS.

ACKNOWLEDGMENTS

The authors would like to thank the Laboratory Animal Facility staff of the University at Buffalo for their assistance in mice handling and care.

SUPPLEMENTARY MATERIAL

The Supplementary Material for this article can be found online at: https://www.frontiersin.org/articles/10.3389/fphys.2021.722859/full#supplementary-material

Supplementary Figure 1 | Electrophoretic patterns of PCR products from different mouse genotypes.

REFERENCES

Abe, T., AlSarhan, M., Benakanakere, M. R., Maekawa, T., Kinane, D. F., Cancro, M. P., et al. (2015). The B Cell-Stimulatory Cytokines BLyS and APRIL Are Elevated in Human Periodontitis and Are Required for B Cell-Dependent Bone Loss in Experimental Murine Periodontitis. *J. Immunol.* 195, 1427–1435. doi: 10.4049/jimmunol.1500496

Boyce, B. F., and Xing, L. (2007). Biology of RANK, RANKL, and osteoprotegerin. *Arthritis. Res. Ther.* 9(Suppl. 1):S1.

Chinthamani, S., Settem, P. R., Honma, K., Nakajima, T., and Sharma, A. (2021). Purification of Tannerella forsythia Surface-Layer (S-Layer) Proteins. *Methods Mol. Biol.* 2210, 135–142. doi: 10.1007/978-1-0716-0939-2_13

Dai, J., Bi, L., Lin, J., and Qi, F. (2017). Evaluation of interleukin-10 producing CD19(+) B cells in human gingival tissue. *Arch. Oral. Biol.* 84, 112–117. doi: 10.1016/j.archoralbio.2017.09.009

Darveau, R. P. (2010). Periodontitis: a polymicrobial disruption of host homeostasis. *Nat. Rev. Microbiol.* 8, 481–490. doi: 10.1038/nrmicro2337

Demoersman, J., Pochard, P., Framery, C., Simon, Q., Boisrame, S., Soueidan, A., et al. (2018). B cell subset distribution is altered in patients with severe periodontitis. *PLoS One* 13:e0192986. doi: 10.1371/journal.pone.0192986

Dutzan, N., Konkel, J. E., Greenwell-Wild, T., and Moutsopoulos, N. M. (2016). Characterization of the human immune cell network at the gingival barrier. *Mucosal. Immunol.* 9, 1163–1172. doi: 10.1038/mi.2015.136

Figueredo, C. M., Lira-Junior, R., and Love, R. M. (2019). T and B Cells in Periodontal Disease: New Functions in A Complex Scenario. *Int. J. Mol. Sci.* 20:16.

Granato, A., Hayashi, E. A., Baptista, B. J., Bellio, M., and Nobrega, A. (2014). IL-4 regulates Bim expression and promotes B cell maturation in synergy with BAFF conferring resistance to cell death at negative selection checkpoints. *J. Immunol.* 192, 5761–5775. doi: 10.4049/jimmunol.1300749

Han, X., Kawai, T., Eastcott, J. W., and Taubman, M. A. (2006). Bacterial-responsive B lymphocytes induce periodontal bone resorption. *J. Immunol.* 176, 625–631. doi: 10.4049/jimmunol.176.1.625

Han, X., Lin, X., Seliger, A. R., Eastcott, J., Kawai, T., and Taubman, M. A. (2009). Expression of receptor activator of nuclear factor-kappaB ligand by B cells in response to oral bacteria. *Oral. Microbiol. Immunol.* 24, 190–196. doi: 10.1111/j.1399-302x.2008.00494.x

Hu, Y., Yu, P., Yu, X., Hu, X., Kawai, T., and Han, X. (2017). IL-21/anti-Tim1/CD40 ligand promotes B10 activity in vitro and alleviates bone loss in experimental periodontitis in vivo. *Biochim. Biophys. Acta Mol. Basis Dis.* 1863, 2149–2157. doi: 10.1016/j.bbadis.2017.06.001

Jagannathan, M., Hasturk, H., Liang, Y., Shin, H., Hetzel, J. T., Kantarci, A., et al. (2009). TLR cross-talk specifically regulates cytokine production by B cells from chronic inflammatory disease patients. *J. Immunol.* 183, 7461–7470. doi: 10.4049/jimmunol.0901517

Kawai, T., Matsuyama, T., Hosokawa, Y., Makihira, S., Seki, M., Karimbux, N. Y., et al. (2006). B and T lymphocytes are the primary sources of RANKL in the bone resorptive lesion of periodontal disease. *Am. J. Pathol.* 169, 987–998. doi: 10.2353/ajpath.2006.060180

Komai-Koma, M., Gilchrist, D. S., McKenzie, A. N., Goodyear, C. S., Xu, D., and Liew, F. Y. (2011). IL-33 activates B1 cells and exacerbates contact sensitivity. *J. Immunol.* 186, 2584–2591. doi: 10.4049/jimmunol.1002103

Kumar, P. S., Leys, E. J., Bryk, J. M., Martinez, F. J., Moeschberger, M. L., and Griffen, A. L. (2006). Changes in periodontal health status are associated with bacterial community shifts as assessed by quantitative 16S cloning and sequencing. *J. Clin. Microbiol.* 44, 3665–3673. doi: 10.1128/jcm.00317-06

Mahanonda, R., Champaiboon, C., Subbalekha, K., Sa-Ard-Iam, N., Rattanathammatada, W., Thawanaphong, S., et al. (2016). Human Memory B Cells in Healthy Gingiva, Gingivitis, and Periodontitis. *J. Immunol.* 197, 715–725. doi: 10.4049/jimmunol.1600540

Malcolm, J., Awang, R. A., Oliver-Bell, J., Butcher, J. P., Campbell, L., Planell, A. Adrados, et al. (2015). IL-33 Exacerbates Periodontal Disease through Induction of RANKL. *J. Dent. Res.* 94, 968–975. doi: 10.1177/0022034515577815

Murakami-Satsutani, N., Ito, T., Nakanishi, T., Inagaki, N., Tanaka, A., Vien, P. T., et al. (2014). IL-33 promotes the induction and maintenance of Th2 immune responses by enhancing the function of OX40 ligand. *Allergol. Int.* 63, 443–455. doi: 10.2332/allergolint.13-oa-0672

Myneni, S. R., Settem, R. P., Connell, T. D., Keegan, A. D., Gaffen, S. L., and Sharma, A. (2011). TLR2 signaling and Th2 responses drive Tannerella forsythia-induced periodontal bone loss. *J. Immunol.* 187, 501–509. doi: 10.4049/jimmunol.1100683

Nakashima, T., Hayashi, M., and Takayanagi, H. (2012). New insights into osteoclastogenic signaling mechanisms. *Trends Endocrinol. Metab.* 23, 582–590. doi: 10.1016/j.tem.2012.05.005

Nikolajczyk, B. S. (2010). B cells as under-appreciated mediators of non-auto-immune inflammatory disease. *Cytokine* 50, 234–242. doi: 10.1016/j.cyto.2010.02.022

Oliver-Bell, J., Butcher, J. P., Malcolm, J., MacLeod, M. K., Planell, A., Campbell, L., et al. (2015). Periodontitis in the absence of B cells and specific anti-bacterial antibody. *Mol. Oral. Microbiol.* 30, 160–169. doi: 10.1111/omi.12082

Onal, M., Xiong, J., Chen, X., Thostenson, J. D., Almeida, M., Manolagas, S. C., et al. (2012). Receptor activator of nuclear factor kappaB ligand (RANKL) protein expression by B lymphocytes contributes to ovariectomy-induced bone loss. *J. Biol. Chem.* 287, 29851–29860. doi: 10.1074/jbc.m112.377945

Pihlstrom, B. L., Michalowicz, B. S., and Johnson, N. W. (2005). Periodontal diseases. *Lancet* 366, 1809–1820.

Pischon, N., Heng, N., Bernimoulin, J. P., Kleber, B. M., Willich, S. N., and Pischon, T. (2007). Obesity, inflammation, and periodontal disease. *J. Dent Res.* 86, 400–409. doi: 10.1177/154405910708600503

Settem, R. P., El-Hassan, A. T., Honma, K., Stafford, G. P., and Sharma, A. (2012). *Fusobacterium nucleatum* and Tannerella forsythia Induce Synergistic Alveolar Bone Loss in a Mouse Periodontitis Model. *Infect. Immun.* 80, 2436–2443. doi: 10.1128/iai.06276-11

Settem, R. P., Honma, K., Stafford, G. P., and Sharma, A. (2013). Protein-linked glycans in periodontal bacteria: prevalence and role at the immune interface. *Front. Microbiol.* 4:24146665.

Seymour, G. J., Ford, P. J., Cullinan, M. P., Leishman, S., and Yamazaki, K. (2007). Relationship between periodontal infections and systemic disease. *Clin. Microbiol. Infect.* 13(Suppl. 4), 3–10.

Stier, M. T., Mitra, R., Nyhoff, L. E., Goleniewska, K., Zhang, J., Puccetti, M. V., et al. (2019). IL-33 Is a Cell-Intrinsic Regulator of Fitness during Early B Cell Development. *J. Immunol.* 203, 1457–1467.

Taubman, M. A., Valverde, P., Han, X., and Kawai, T. (2005). Immune response: the key to bone resorption in periodontal disease. *J. Periodontol.* 76(11 Suppl.), 2033–2041.

Wang, Y., Yu, X., Lin, J., Hu, Y., Zhao, Q., Kawai, T., et al. (2017). B10 cells alleviate periodontal bone loss in experimental periodontitis. *Infect. Immun.* 2017:10.

Yeo, L., Toellner, K. M., Salmon, M., Filer, A., Buckley, C. D., Raza, K., et al. (2011). Cytokine mRNA profiling identifies B cells as a major source of RANKL in rheumatoid arthritis. *Ann. Rheum. Dis.* 70, 2022–2028.

Author Disclaimer: The content is solely the responsibility of the authors and does not represent the official views of the NIDCR or the NIH.

Conflict of Interest: The authors declare that the research was conducted in the absence of any commercial or financial relationships that could be construed as a potential conflict of interest.

Publisher's Note: All claims expressed in this article are solely those of the authors and do not necessarily represent those of their affiliated organizations, or those of the publisher, the editors and the reviewers. Any product that may be evaluated in this article, or claim that may be made by its manufacturer, is not guaranteed or endorsed by the publisher.

frontiers in Physiology

ORIGINAL RESEARCH
published: 24 September 2021
doi: 10.3389/fphys.2021.721775

TGF-Beta Receptor II Is Critical for Osteogenic Progenitor Cell Proliferation and Differentiation During Postnatal Alveolar Bone Formation

Chunmei Xu[1,2], *Xudong Xie*[1,2], *Hu Zhao*[3], *Yafei Wu*[1], *Jun Wang*[1,2]* *and Jian Q. Feng*[2]*

[1] State Key Laboratory of Oral Diseases, National Clinical Research Center for Oral Diseases, Department of Periodontics, West China Hospital of Stomatology, Sichuan University, Chengdu, China, [2] Department of Biomedical Sciences, College of Dentistry, Texas A&M University, Dallas, TX, United States, [3] Department of Comprehensive Dentistry, College of Dentistry, Texas A&M University, Dallas, TX, United States

OPEN ACCESS

Edited by:
Fani Anagnostou, Université de Paris, France

Reviewed by:
Greg Holmes, Icahn School of Medicine at Mount Sinai, United States
Xiaoying Wang, Shandong University, China

***Correspondence:**
Jian Q. Feng
jfeng@tamu.edu
Jun Wang
junwang@scu.edu.cn

Specialty section:
This article was submitted to Craniofacial Biology and Dental Research, a section of the journal Frontiers in Physiology

Received: *07 June 2021*
Accepted: *27 August 2021*
Published: *24 September 2021*

Citation:
Xu C, Xie X, Zhao H, Wu Y, Wang J and Feng JQ (2021) TGF-Beta Receptor II Is Critical for Osteogenic Progenitor Cell Proliferation and Differentiation During Postnatal Alveolar Bone Formation. Front. Physiol. 12:721775. doi: 10.3389/fphys.2021.721775

Transforming growth factor beta (TGFβ) signaling plays an important role during osteogenesis. However, most research in this area focuses on cortical and trabecular bone, whereas alveolar bone is largely overlooked. To address the role of TGFβR2 (the key receptor for TGFβ signaling) during postnatal alveolar bone development, we conditionally deleted *Tgfβr2* in early mesenchymal progenitors by crossing *Gli1-Cre*^{ERT2}; *Tgfβr2*$^{flox/flox}$; *R26R*^{tdTomato} mice (named early cKO) or in osteoblasts by crossing *3.2kb Col1-Cre*^{ERT2}*; Tgfβr2* $^{flox/flox}$*; R26R*^{tdTomato} mice (named late cKO). Both cKO lines were induced at postnatal day 5 (P5) and mice were harvested at P28. Compared to the control littermates, early cKO mice exhibited significant reduction in alveolar bone mass and bone mineral density, with drastic defects in the periodontal ligament (PDL); conversely, the late cKO mice displayed very minor changes in alveolar bone. Mechanism studies showed a significant reduction in PCNA+ PDL cell numbers and OSX+ alveolar bone cell numbers, as well as disorganized PDL fibers with a great reduction in periostin (the most abundant extracellular matrix protein) on both mRNA and protein levels. We also showed a drastic reduction in β-catenin in the early cKO PDL and a great increase in SOST (a potent inhibitor of Wnt signaling). Based on these findings, we conclude that TGFβ signaling plays critical roles during early alveolar bone formation via the promotion of PDL mesenchymal progenitor proliferation and differentiation mechanisms.

Keywords: mandible, alveolar bone, GLI1, osteoprogenitor, osteoblast, TGFβR2

INTRODUCTION

The skeleton is formed by two osteogenic processes: endochondral ossification and intramembranous ossification (Long, 2011). Similarly, mandibular bone is considered to be formed by the same processes, with the mandibular body formed through intramembranous ossification and the mandibular ramus built via endochondral ossification (Hinton et al., 2015, 2017; Jing et al., 2015). On the other hand, we have recently begun to gain knowledge on a third

type of ossification process within alveolar bone, which holds teeth. Cell lineage tracing studies showed that periodontal ligament (PDL) progenitor cells contribute to alveolar bone formation and regeneration (Ren et al., 2015; Hosoya et al., 2020; Men et al., 2020). This occurrence is distinct from that of other cell sources such as periosteum for the mandible body or chondrocytes for the mandible ramus (Hinton et al., 2015, 2017; Jing et al., 2015). Importantly, alveolar bone displayed a much higher bone formation rate than other types of bones (Ren et al., 2015).

Periodontitis, the most common disorder known to mankind, particularly affects alveolar bone. The advanced form of this condition results in loss of surrounding soft tissue and bone, leading to tooth loss in adults. This severe result was found in 10–15% of adults in population studies (Fox, 1992; Douglass and Fox, 1993; Fox et al., 1994). In addition, several pieces of evidence support a two-way relationship between periodontitis and diabetes (i.e., diabetes increases the risk for periodontitis, while periodontitis negatively disturbs glycemic control) (Hallmon and Mealey, 1992; Khader et al., 2006; Mealey and Ocampo, 2007; Salvi et al., 2008; Chavarry et al., 2009; Preshaw et al., 2012). Research has also demonstrated a close link between osteoporosis and periodontitis (Wang and McCauley, 2016). Experts have long aimed to develop effective treatment methods for the bone loss in these diseases (Pihlstrom et al., 2005). Thus, understanding the mechanism by which alveolar bone formation is regulated will facilitate future drug development.

It has been known that TGFβ signaling plays critical roles in intramembranous bone formation. These roles include bone development and fracture healing processes (Oka et al., 2007; Seo and Serra, 2007, 2009; Tang and Alliston, 2013; Wu et al., 2016; Xia et al., 2020) as well as regulation for the differentiation of osteogenic cells and extracellular matrix synthesis (Tang and Alliston, 2013; Peters et al., 2017).

TGFβR2 is required for the proliferation and differentiation of osteogenic progenitors from embryonic stages (Sasaki et al., 2006; Oka et al., 2007; Seo and Serra, 2009; Chen et al., 2012; Abou-Ezzi et al., 2019). Deletion of *Tgfβr2* driven by *Prx1-Cre* in the mesenchymal cells led to severe skeletal phenotypes characterized by short limbs and absent parietal bones as well as frontal bone at E15.5 (Seo and Serra, 2007). Oka et al. also reported reduced cell proliferation activity in mandibles of $Tgf\beta r2^{flox/flox}$; *Wnt1-Cre* mice at E13.5 (Oka et al., 2007). In addition, TGFβ signaling plays a critical role in osteoblast lineage cells after birth (Meng et al., 2018). Disturbance of TGFβ signaling leads to severe defects in postnatal skeletal development (Peters et al., 2017; Corps et al., 2021). However, there is a debate regarding the exact role of TGFβ signaling in a specific population of cells. For example, Peters et al. reported disturbed differentiation of osteoblasts and reduced bone mass in long bone when *Tgfβr2* was removed in OSX+ bone cells (Peters et al., 2017). Abou-Ezzi et al. confirmed similar defects in trabecular bone and cortical bone (Abou-Ezzi et al., 2019). However, a drastic increase in trabecular bone mass was observed when *Tgfβr2* was conditionally deleted in OCN+ bone cells (Qiu et al., 2010). Few studies have focused on alveolar bone phenotypes, which require further investigation, especially during postnatal bone formation (Sasaki et al., 2006; Kim et al., 2015).

Given the limitations of non-inducible Cre transgenic mice in early studies and differing results from different studies, we intended to assess the postnatal effects of TGFβ signaling in alveolar bone development using inducible Cre mouse lines. Specifically, we included Gli1 (a marker for mesenchymal progenitor cells in various tissues including PDL and alveolar bone) to target the early progenitor cells (Kitaura et al., 2014; Feng et al., 2017; Shi et al., 2017; Hosoya et al., 2020; Liu et al., 2020; Men et al., 2020; Yi et al., 2021); 3.2 kb Col1 was used to target osteoblasts (Rossert et al., 1995; Qin et al., 2019). Our findings revealed a key role in TGFβ signaling during early postnatal alveolar bone development.

MATERIALS AND METHODS

Breeding Transgenic Mice

All experimental protocols followed ARRIVE (Animal Research Reporting of *in vivo* Experiments) guidelines and were approved by the Animal Care and Use Committees (IACUC) at Sichuan University West China School of Stomatology and Texas A&M University College of Dentistry.

All mice (background: C57BL/6J) were housed in a temperature-controlled environment with 12-h light/dark cycles. To induce disrupted TGFβ signaling among osteogenic cells at different stages, we generated conditional *Tgfβr2* knockout mice (*Tgfβr2* cKO) driven by $Gli1\text{-}Cre^{ERT2}$ (Ahn and Joyner, 2004) and the *3.2 kb* $Col1\text{-}Cre^{ERT2}$ transgene, respectively (Rossert et al., 1995). The $Gli1\text{-}Cre^{ERT2/+}$ mice were crossed with $R26R^{tdTomato/+}$ reporter mice (stock number: 007905 from Jackson Laboratory) to trace the Cre activity. Next, we crossed the $Gli1\text{-}Cre^{ERT2/+}$; $R26R^{tdTomato/+}$ mice with $Tgf\beta r2^{flox/+}$ mice (stock number: 012603 from Jackson Laboratory) to gain $Gli1\text{-}Cre^{ERT2/+}$; $R26R^{tdTomato/+}$; $Tgf\beta r2^{flox/+}$ mice. Then, the $Gli1\text{-}Cre^{ERT2/+}$; $R26R^{tdTomato/+}$; $Tgf\beta r2^{flox/flox}$ mice were obtained by crossing $Gli1\text{-}Cre^{ERT2/+}$; $R26R^{tdTomato/+}$; $Tgf\beta r2^{flox/+}$ mice with the $Tgf\beta r2^{flox/+}$ mice. The same strategy was then applied to generate *3.2 kb* $Col1\text{-}Cre^{ERT2/+}$; $R26R^{tdTomato/+}$; $Tgf\beta r2^{flox/flox}$ mice. The genotypes of the mice were determined via a PCR analysis of genomic DNA extracted from tail biopsies (primer sequences are listed in **Supplementary Table 1**). Tamoxifen (75 mg/kg body weight) was prepared as previously described (Wang et al., 2020) and a one-time injection of the drug was administered at postnatal day 5 (P5) to both control mice (CTR: $Gli1\text{-}Cre^{ERT2/+}$/*3.2 kb* $Col1\text{-}Cre^{ERT2/+}$; $R26R^{tdTomato/+}$) and cKO mice ($Gli1\text{-}Cre^{ERT2/+}$/*3.2 kb* $Col1\text{-}Cre^{ERT2/+}$; $R26R^{tdTomato/+}$; $Tgf\beta r2^{flox/flox}$). The animals were subsequently harvested at either P6 or P28. Mandibles were dissected and fixed in 4% paraformaldehyde (PFA) and decalcified in 10% ethylenediaminetetraacetic acid (EDTA), then stored at 4°C for future use.

Histological Analysis and Immunostaining

Mandibles intended for histological staining were embedded in paraffin using standard histological procedures, then sectioned

at 5-μm thickness for Masson's trichrome, Sirius red, and TRAP staining as previously reported (Wang et al., 2017). Samples for cell lineage tracing were dehydrated with 30% sucrose and embedded in OCT. Next, 10-μm-thick sections were prepared with a Leica cryostat equipped with Cryojane as previously reported (Xie et al., 2019). Immunostaining was then carried out as previously described (Wang et al., 2020) using the following primary antibodies: anti-OSX rabbit antibody (1:200, ab22552), anti-PERIOSTIN goat antibody (1:400, AF2955), anti-MEPE rabbit antibody (1:100, LF-155), anti-SOST goat antibody (1:100, AF1589), anti-PCNA rabbit antibody (1:100, Cst13110s). The secondary antibodies used for immunostaining: Goat anti-Rabbit IgG-Alexa Fluor 488 (1:200, Invitrogen); Rabbit anti-Goat IgG-Alexa Fluor 488 (1:200, Invitrogen); and Goat Anti-Rabbit IgG-unconjugated (1:100, Vector laboratories).

Micro–Computed Tomography (μ-CT) and X-Ray Radiography Analysis

Micro-CT analysis by the Scanco μ-CT35 image system and X-ray radiography were performed as previously described (Wang et al., 2017).

RNAscope Assay Procedures for RNA Detection

Mandibles were harvested and fixed in 10% formalin for 24 h at room temperature and then decalcified in 10% ethylenediaminetetraacetic acid (EDTA) for 3 weeks at 4°C. Well-decalcified samples were embedded in paraffin and cut according to previously mentioned standard histological procedures. 5-μm-thick sections were collected and an RNAscope assay was performed following the RNAscope® 2.5 BROWN (Advanced Cell Diagnostics, 322300, 322310) for FFPE manufacturer protocol (Wang et al., 2012) with use of the β-catenin RNA probe (537601) and Periostin RNA probe (418581).

Statistical Analysis

Statistical analyses were performed by an independent sample *t*-test for parametric analysis and the Mann-Whitney test was used for non-parametric analysis using SPSS 19.0 (SPSS Inc, Chicago, IL). A *P*-value < 0.05 was considered statistically significant.

RESULTS

Removing TGFβ Signaling in Gli1+ Progenitors Resulted in Disturbance of Periodontal Homeostasis and Postnatal Alveolar Bone Loss Due to a Defect in PDL Progenitor Cells

To address the postnatal effects of TGFβ signaling on osteogenic progenitors, we generated *Gli1*^{Lin} *Tgfβr2* cKO mice and performed a one-time injection of tamoxifen in both the control and cKO mice at P5. Mice were harvested at P28 (**Figure 1A**). Our representative X-ray images showed no obvious differences in hindlimbs between the control and cKO mice (**Supplementary Figure 1**). However, the sagittal section

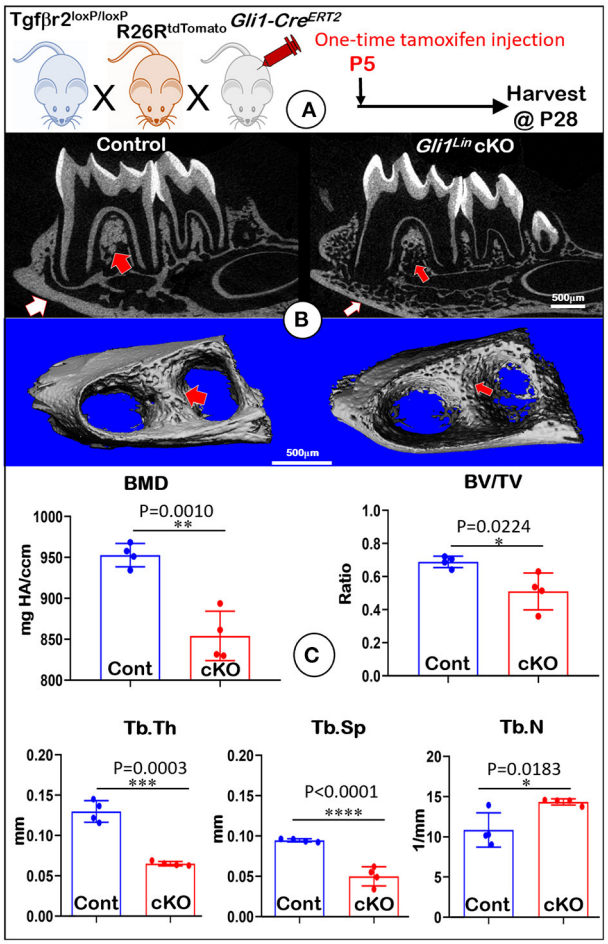

FIGURE 1 | Micro-computed tomography (μCT) analyses showed defective mandibles from Gli1^{Lin} *Tgfβr2* conditional knockout (cKO) mice. **(A)** A schematic illustration of the generation of the *Gli1-Cre*^{ERT2} induced *Tgfβr2* cKO mice in the R26R^{tdTomato} tracing background. A one-time tamoxifen injection was administered at P5, and harvested at P28. **(B)** The cKO mice showed remarkable decrease of bone mass at both trabecular (red arrows) and cortical (white arrows) regions. **(C)** Quantitative data based on the trabecular bone showed a significant reduction in bone mineral density (BMD) (*upper left*), the bone volume fraction (BV/TV) (*upper right*), and trabecular thickness (Tb.Th) (*lower left*), and trabecular separation (Tb.Sp) (*lower middle*). Of note, there was significant increase in trabecular number (Tb. N) (*lower right*). $n = 4$, $^{*}P < 0.05$; $^{**}P < 0.01$; $^{***}P < 0.001$; $^{****}P < 0.0001$.

(**Figure 1B**, *upper panels*) and three-dimensional reconstruction (**Figure 1B**, *lower panels*) images displayed drastic bone loss in *Gli1*^{Lin} *Tgfβr2* cKO mandibles (**Figure 1B**, *right panels*). The overall cKO bone structure was porous in both alveolar bone and cortical bone (**Figure 1B**, *arrows*). The quantitative μCT data on alveolar bone (**Figure 1C**, $n = 4$) displayed a significant decrease in bone mineral density (BMD, $P = 0.0010$), bone volume fraction (BV/TV, $P = 0.0224$), trabecular bone thickness (Tb.Th, $P = 0.0003$), and trabecular bone separation (Tb.Sp, $P < 0.0001$). There was a moderate increase in trabecular bone numbers (Tb.N, $P = 0.0183$) in the cKO mice compared to

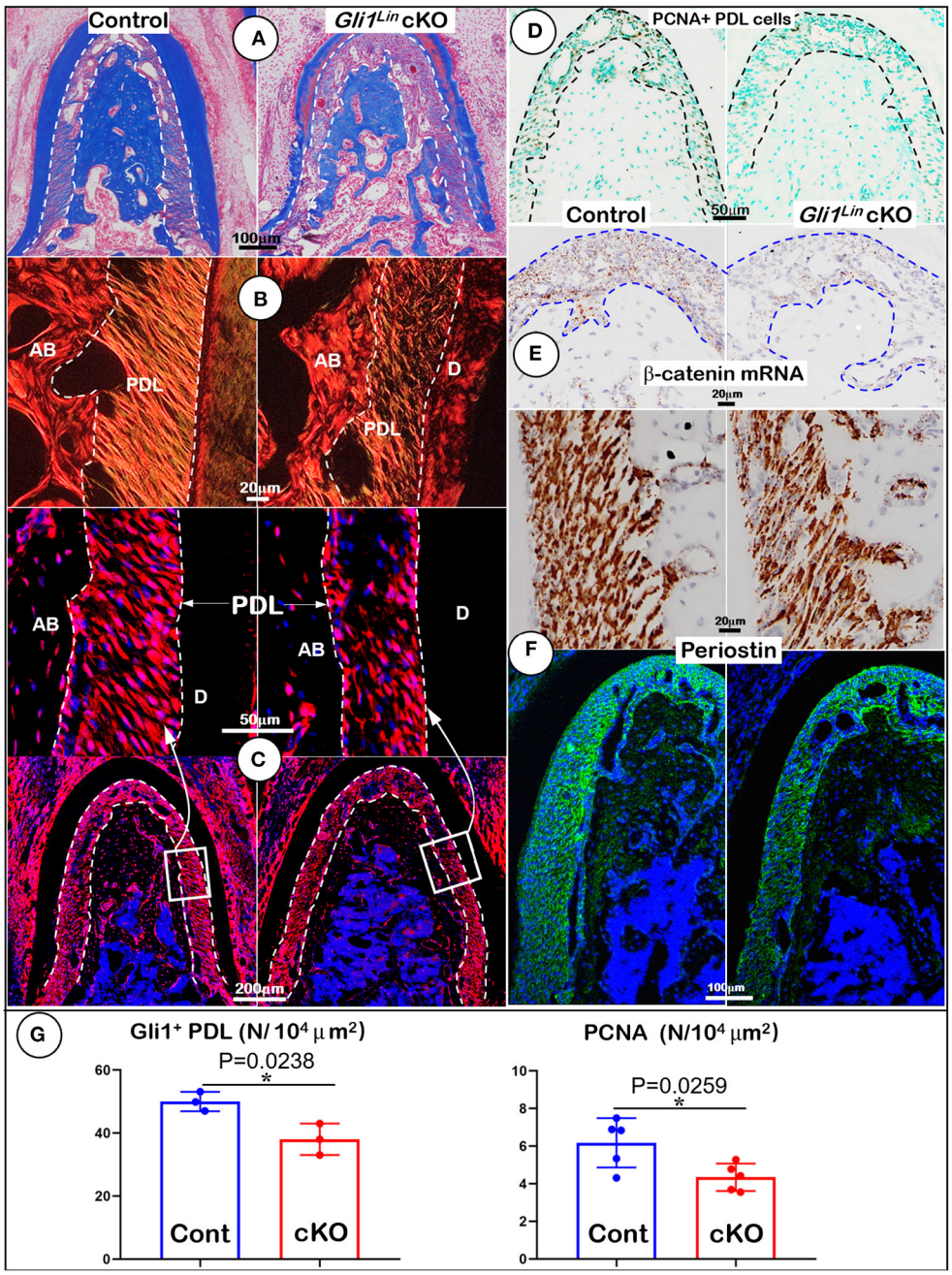

FIGURE 2 | Morphological analyses of mandibles from Gli1^{Lin} *Tgfβr2* conditional knockout (cKO) mice at cellular levels. **(A)** Masson's Trichrome staining showed drastic reduction of alveolar bone mass in cKO mice (*right*); **(B)** Polarized light images displayed a decrease in periodontal ligament (PDL) with a disorganized collagen fiber distribution in cKO mice (*right*); **(C)** Gli1^{Lin} tracing images revealed pathological changes in the cKO PDL: irregular cell shape and a significant reduction in tdTomato+ PDL cell number compared to the spindle-shape PDL cells in the control (*upper right*); **(D)** The immunostaining images of PCNA showed a significant decline in proliferating cells in the cKO PDL; **(E)** The RNAscope images showed a drastic reduction in β-catenin mRNA level in the cKO PDL (*right*); and **(F)** a decrease of Periostin expression at both mRNA level (*upper right*) and protein level (*lower right*). **(G)** Quantitative analyses of the number of tdTomato+ PDL cells (*left*) and PCNA expressing cells in PDL (*right*). $n = 3$–5, $^*P < 0.05$. AB, alveolar bone; PDL, periodontal ligament; D, dentin.

control mice. These changes support the vital role of TGFβ signaling in control of postnatal alveolar bone formation.

To further address the impact of TGFβ signaling on osteogenesis at cellular levels, we first performed Masson's trichrome staining. The test showed a reduction of the cKO alveolar bone mass and collagen fibers in the cKO PDL (**Figure 2A**). Our representative images of polarized light revealed decreased and disorganized collagen fibers in the cKO

PDL (**Figure 2B**). To elucidate the cell fate of mesenchymal progenitor cells in postnatal alveolar bone formation, we examined the biological features of Gli1^{Lin} cells in the early cKO mice using cell lineage tracing techniques (i.e., removing *Tgfβr2* and activating the tdTomato fluorescent protein in Gli1^{Lin} PDL cells at the same time). At P6, there were few tdTomato+ cells in PDL area and in adjacent bone marrow areas after 24-h induction (**Supplementary Figure 2A**). By P28, there were numerous tdTomato+ cells throughout the entire PDL and alveolar bone, indicating a great contribution of the Gli1^{Lin} PDL progenitor cells to PDL and alveolar bone development during the period from P5 to P28 (**Figure 2C**, *left panel*). On the other hand, removing *Tgfβr2* in the Gli1^{Lin} cells led to a significant reduction in the number of tdTomato+ PDL cells (**Figure 2C**, *right panels*; **Figure 2G**, *left*, $P = 0.0238$, $n = 3$).

To study the underlying molecular mechanism, we examined expression levels of key molecules essential for PDL and alveolar bone formation. The immunostaining images showed a significant reduction of PCNA+ cells in the cKO PDL in comparison with control group (**Figures 2D,G**, *right*, $P = 0.0259$, $n = 5$), supporting the key role of TGFβ signaling in maintaining the proliferation rate of mesenchymal cells in PDL. Next, we analyzed the RNA expression level of β-catenin (a critical factor for differentiating of mesenchymal cells into osteoblasts) using RNAscope technique. This expression was sharply decreased in the early cKO PDL, supporting the likely role of TGFβ signaling in regulation of Wnt signaling (**Figure 2E**, *right panel*). Finally, we studied expression profiles of Periostin (a key matrix protein essential for PDL function) (Rios et al., 2005, 2008) at both RNA and protein levels. The levels were greatly reduced in cKO PDL (**Figure 2F**, *right panels*), suggesting the positive regulation of Periostin by TGFβ signaling in maintaining PDL homeostasis (**Figure 2F**).

TGFβ Signaling Regulates Osteogenic Differentiation of PDL Progenitor Cells

To understand the molecular mechanisms by which the abnormal alveolar bone occurred in early cKO mice, we examined expression levels of various bone markers. Markers were examined in the tracing background using immunostaining confocal techniques. Our data showed a significant reduction in tdTomato+ osteocyte numbers (**Figure 3A**, $P = 0.0131$, $n = 4$) and the ratio of Gli1^{Lin} osteocytes/total osteocytes (**Supplementary Figure 2C**, *right*, $P = 0.0255$, $n = 4$) in the cKO alveolar bone. The expressions of OSX (a transcriptional molecule essential for osteogenesis) (Zhou et al., 2010) were significantly decreased, which is reflected by the ratio of OSX^{+}-Gli1^{Lin} osteocytes vs. total Gli1^{Lin} osteocytes in the cKO alveolar bone (**Figure 3B**, $P = 0.0458$, $n = 4$). We also showed a significant reduction in the MEPE levels of cKO Gli1^{Lin} osteocytes (**Figure 3C**, $P = 0.0153$, $n = 4$). On the other hand, there was a drastic increase of SOST, an osteocyte marker and potent inhibitor of Wnt signaling (Balemans et al., 2001) in the early cKO group. The ratio of SOST^{+}-Gli1^{Lin} osteocytes vs. total Gli1^{Lin} osteocytes was significantly increased in early cKO mice compared to the control (**Figure 3D**, $P = 0.0280$, $n = 4$). We then performed TRAP staining to exclude the potential impact of removing *Tgfβr2* in Gli1^{Lin} PDL cells on osteoclast lineage cells. The staining showed no significant difference between the cKO mice and control (**Supplementary Figure 3A**, $P = 0.0975$, $n = 4$).

Collectively, the above data support the essential role of TGFβ signaling in controlling alveolar bone formation via regulation of Gli1^{Lin} PDL progenitor cell proliferation and differentiation.

TGFβ Signaling Has a Moderate Effect on Osteoblasts

To investigate the effect of TGFβ signaling on osteoblasts, we generated *Tgfβr2* cKO mice under the control of *3.2 kb Col1-Cre^{ERT2}* (**Figure 4A**). Similar to the *Gli1*^{Lin} *Tgfβr2* cKO mice, removing *Tgfβr2* in the 3.2 kb Col1^{Lin} cells had no apparent effects on the overall hindlimb structure (**Supplementary Figure 4**). Unlike *Gli1*^{Lin} *Tgfbr2* cKO mice, μCT data showed mild changes in alveolar bone of *3.2 kb Col1*^{Lin} *Tgfβr2* cKO mice (**Figure 4B**, *right panels, arrows*). Our representative μCT images showed a mild decrease in BMD (**Figure 4C**, *upper left*, $P = 0.0513$, $n = 4$) and the BV/TV of trabecular bone (**Figure 4C**, *upper left*, $P = 0.0224$, $n = 4$) in the late cKO mice. There was also a reduction of Tb.Th in cKO mice (**Figure 4C**, *lower left*, $P = 0.0043$, $n = 4$) with no statistic changes in Tb.Sp (**Figure 4C**, $P = 0.5634$, *lower middle*, $n = 4$) or Tb.N (**Figure 4C**, *lower right*, $P = 0.4558$, $n = 4$). Altogether, disruption of TGFβ signaling in osteoblasts led to a mild reduction in alveolar bone mass and mineral density.

To examine the impact of TGFβ signaling in late cKO mice at the cellular level, we performed Masson's trichrome staining. Our staining results showed no apparent changes in the cKO alveolar bone mass or in the PDL collagen fibers (**Figure 5A**). The representative images of polarized light revealed a distribution profile of collagen fibers in the cKO PDL, which was similar to that of the control group (**Figure 5B**). Our cell lineage tracing analyses showed no apparent change in tdTomato+ bone cell numbers or cell distribution pattern in cKO mice (**Figure 5C**, *right panels*; **Supplementary Figure 2C**, *left*, $P = 0.8491$, $n = 4$). We also examined the expression levels of several markers essential for bone function. The immunostaining showed a moderate but significant reduction in the expression ratio of OSX^{+}-3.2 kb Col1^{Lin} osteocytes vs. total 3.2 kb Col1^{Lin} osteocytes in the cKO alveolar bone in comparison with control (**Figure 6A**; $P = 0.0076$, $n = 4$). However, removing *Tgfβr2* in the *3.2 kb Col1*^{Lin} cells had little impact on the expression ratio of osteocyte markers such as MEPE (**Figure 6B**, $P = 0.1502$, $n = 4$) or SOST (**Figure 6C**, $P = 0.2619$, $n = 4$).

DISCUSSION

TGFβ signaling plays an essential role in cell proliferation and differentiation of osteogenic cells during both intramembrane and endochondral bone formation. However, the role of TGFβ signaling during mandibular bone development remains largely unclear. In this study, we used inducible Cre mouse lines to remove *Tgfβr2* in osteogenic progenitors (*Gli1-Cre^{ERT2}/+*; *R26R^{tdTomato}/+*; *Tgfβr2$^{flox/flox}$*; Early cKO) and osteoblasts (*3.2 kb Col1-Cre^{ERT2}/+*; *R26R^{tdTomato}/+*; *Tgfβr2$^{flox/flox}$*; Late cKO),

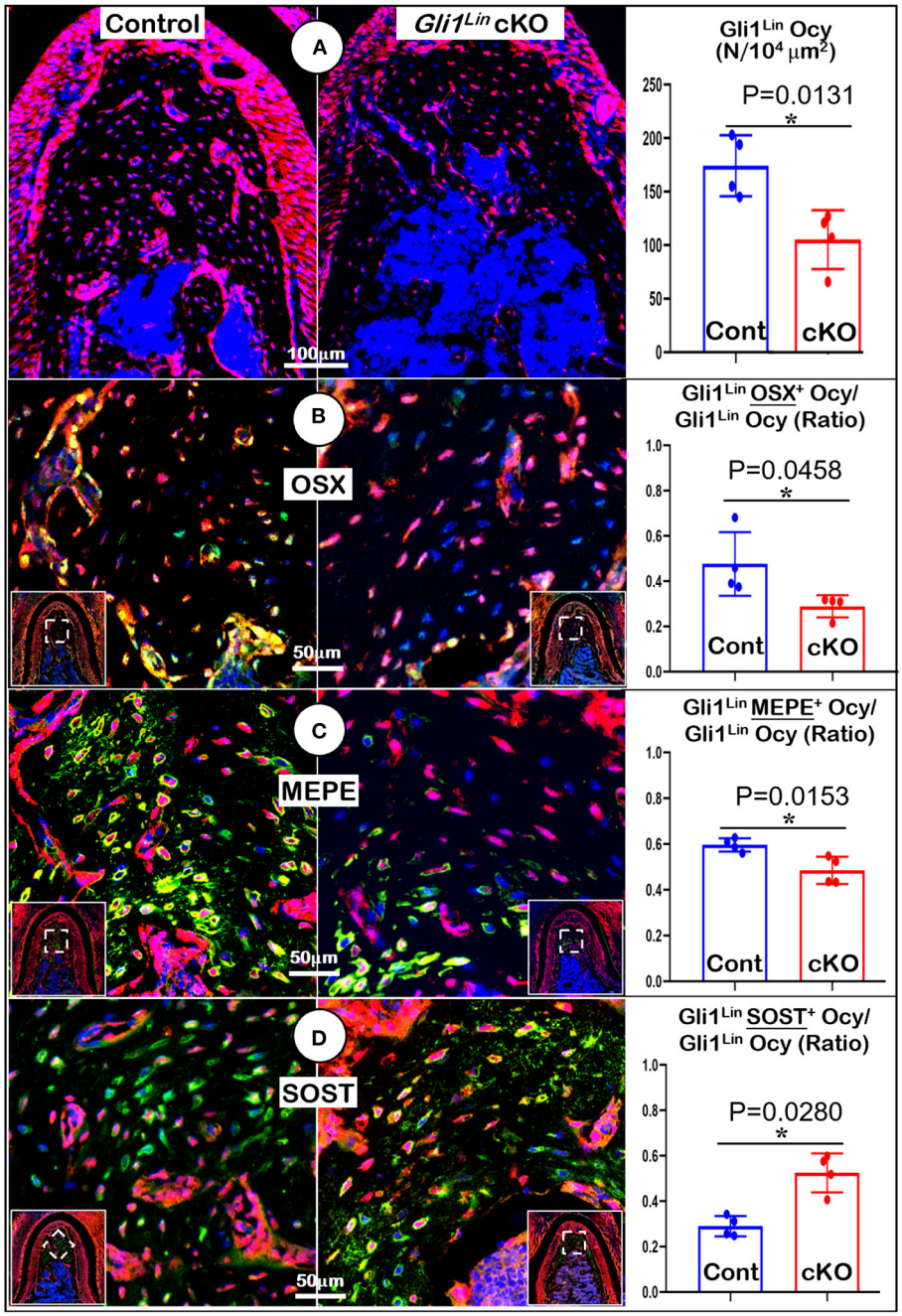

FIGURE 3 | Molecular analyses of mandibles from Gli1^{Lin} *Tgfβr2* conditional knockout (cKO) mice **(A)** The confocal images revealed a great reduction in bone volume and number of Gli1^{lin} Ocy in cKO alveolar bone, which is statistically significant from the control (*right panel*); **(B)** The OSX immunostaining images showed a significant decrease in the raito of OSX^{+}-Gli1^{Lin} Ocy to the total Gli1^{lin} Ocy; **(C)** The confocal images of MEPE immunostainings showed a significant reduction in the raito of MEPE^{+}-Gli1^{Lin} Ocy to the total Gli1^{lin} Ocy in the cKO alveolar bone (*right panel*); **(D)** The confocal images of SOST immunostainings showed an increase in the raito of SOST^{+}-Gli1^{Lin} Ocy to the total Gli1^{Lin} Ocy in the cKO alveolar bone, which was statistically significant from the control (*right panel*). $n = 4$. $^{*}P < 0.05$; Ocy, osteocytes.

respectively. We aimed to provide a better understanding of the roles played by TGFβ signaling during postnatal alveolar bone formation. We used multiple techniques such as radiography, μCT, Masson's trichrome staining, and immunostaining combined with cell lineage tracing methods. Our comprehensive analyses showed drastic defects in the PDL and alveolar bone of early cKO mice but a moderate alveolar bone phenotype in late cKO mice. Our data support the essential role of *Tgfβr2* in osteogenic PDL cells during early alveolar bone development with limited impact on later osteogenesis.

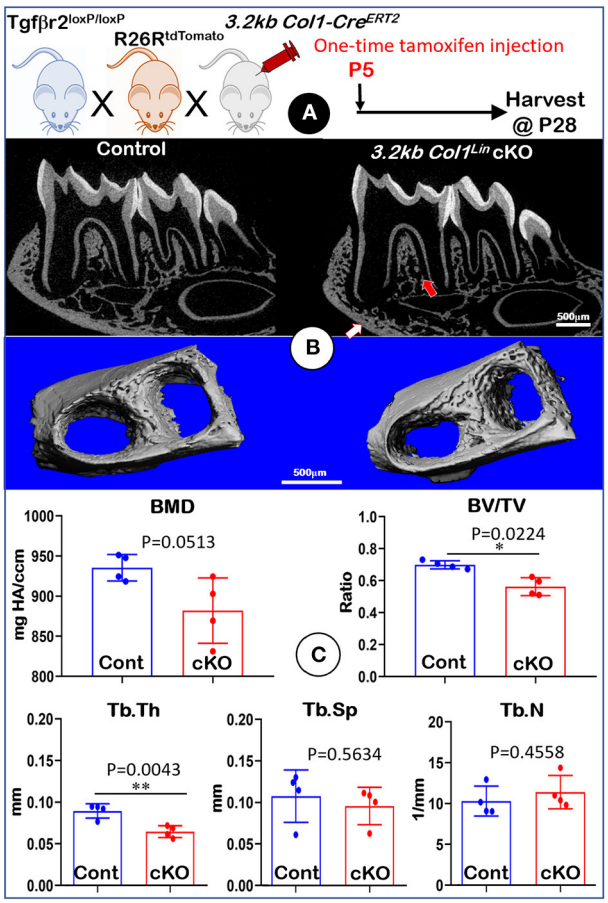

FIGURE 4 | Micro-computed tomography (μCT) analyses of mandibles from *3.2 kb Col1*^{Lin} *Tgfβr2* conditional knockout (cKO) mice. **(A)** A schematic illustration of the generation of the *3.2 kb Col1-Cre*^{ERT2} induced *Tgfβr2* mice in the R26R^{tdTomato} tracing background. A one-time tamoxifen injection was administered at P5, and harvested at P28. **(B)** The cKO mice showed a mild decrease of bone mass at both trabecular (red arrow) and cortical (white arrow) regions. **(C)** Quantitative data based on the trabecular bone showed a reduction in bone mineral density (BMD) with no statistical significance (*upper left*), although there was a significant reduction in bone volume fraction (BV/TV) (*upper right*) and trabecular thickness (Tb. Th) (*lower left*). Of note, there was no apparent change in trabecular separation (Tb.Sp) (*lower middle*) and trabecular number (Tb.N) (*lower right*). $n = 4$, $^{*}P < 0.05$; $^{**}P < 0.01$.

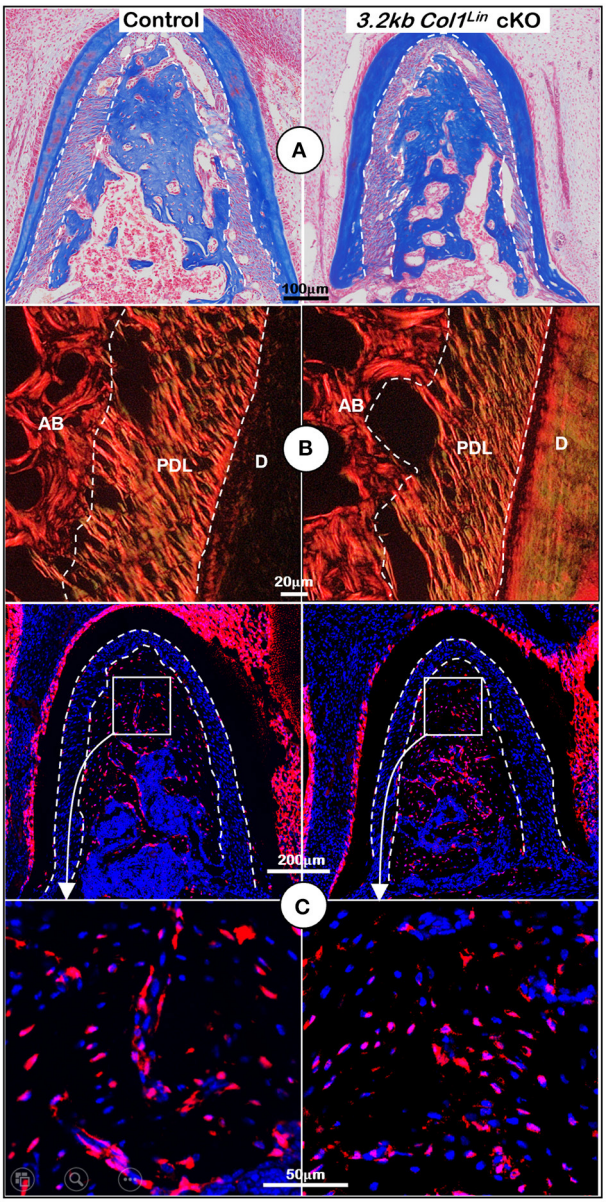

FIGURE 5 | Morphological analyses of mandibles from *3.2 kb Col1*^{Lin} *Tgfβr2* conditional knockout (cKO) mice at the cellular level. **(A)** Masson's trichrome staining showed no apparent change of alveolar bone mass in the cKO mice (*right*). **(B)** Polarized light images displayed a similar collagen fiber distribution of periodontal ligament (PDL) in the control and cKO group (*right*). **(C)** The 3.2 kb Col1^{Lin} tracing images revealed largely similar red cell numbers in both the control and the cKO alveolar bone. AB, alveolar bone; PDL, periodontal ligament; D, dentin.

The quantitative μCT analyses in our study showed that ablation of *Tgfβr2* in Gli1^{Lin} cells led to a significant reduction in alveolar bone volume and mineralization. This outcome was likely caused by a defect that occurred in PDL progenitors based on the following three pieces of information. (1) Molecular immunostaining and cell lineage tracing data revealed a significant reduction of PCNA+ and tdTomato+ PDL cells in the cKO mice; (2) The cell lineage tracing data showed a significant reduction of tdTomato+ bone cell numbers. (3) Masson's trichrome staining and polarized light images displayed defects in PDL and alveolar bone matrices along with a sharp decrease in three key molecules (Periostin in PDL, OSX, and MEPE in alveolar bone). In fact, the current findings of TGFβ signaling controlling cell proliferation and osteoblast differentiation agree with its roles in craniofacial bone and long bone (Sasaki et al., 2006; Peters et al., 2017).

Further mechanism studies using the RNAscope assay and immunostaining analyses showed that TGFβ signaling likely affected Wnt-β-catenin signaling, as shown by a sharp reduction

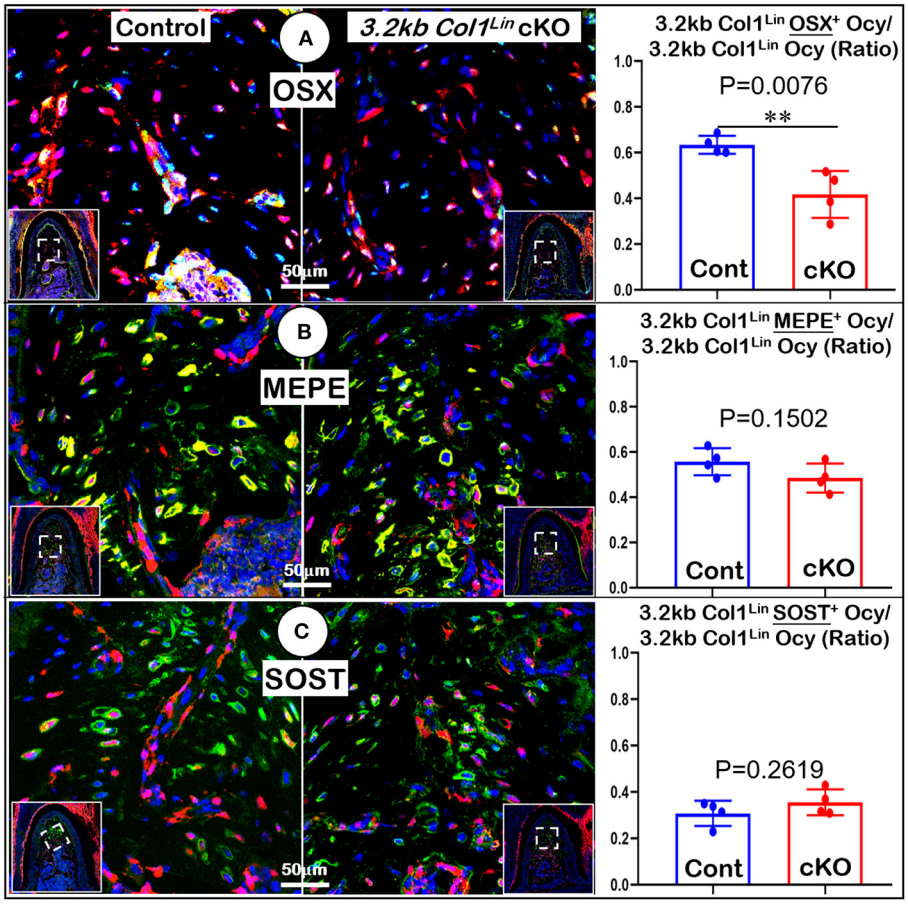

FIGURE 6 | Molecular analyses of mandibles from *3.2 kb Col1*^{Lin} *Tgfβr2* conditional knockout (cKO) mice. **(A)** The confocal images of OSX immunostainings revealed a decrease in the raito of OSX^{+}-3.2 kb Col1^{Lin} Ocy to the total 3.2 kb Col1^{Lin} Ocy in cKO alveolar bone, which was statistically significant from the control (*right panel*); **(B)** No apparent change was observed in the MEPE expression of cKO mice; and **(C)** The images of SOST immunostainings showed no apparent differences in signals between the cKO and control groups. $n = 4$. $^{**}P < 0.01$; Ocy, osteocytes.

in β-catenin mRNA within early cKO PDL and an increase in SOST (a potent inhibitor of Wnt signaling) within alveolar bone. Currently, we do not know whether there is a direct or indirect connection between the β-catenin in PDL and SOST inside alveolar bone. However, our previous studies demonstrated that removing *Periostin* in PDL led to severe defects in both PDL and alveolar bone; further deletion of sclerostin in osteocytes or applications of SOST- neutralized antibodies greatly improved both PDL and alveolar bone phenotypes via an interaction between Sharpey's fibers and osteocyte dendrites (Ren et al., 2015). TGFβ signaling may indirectly regulate Sharpey's fibers, a critical bridge between PDL and alveolar bone cells. This idea needs to be part of future studies.

Nevertheless, *Gli1-Cre*^{ERT2} was not only activated in PDL cells but also in cells from bone marrow, as shown from cell lineage tracing date in the present study and previous studies (Feng et al., 2017; Hosoya et al., 2020; Yi et al., 2021). To date, no specific markers could be used to discern differences between PDL-derived and bone-marrow-derived Gli1^{Lin} cells. However, the positive correlation between the Gli1^{Lin} PDL cell numbers and the Gli1^{Lin} alveolar bone cell numbers within the control support the contribution of Gli1^{Lin} PDL progenitor cells for alveolar bone formation. The negative correlation between the Gli1^{Lin} PDL cell numbers and the Gli1^{Lin} alveolar bone cell numbers within the early cKO further support this hypothesis.

It is previously reported that loss of TGFβ signaling in osteoblasts had an indirect effect on osteoclasts by reducing the number of osteoclasts in both long bones and mandibles (Qiu et al., 2010; Wang et al., 2013). However, our study observed no significant differences in either late or early cKO mice compared to their respective control groups. Results were based on TRAP staining, excluding the indirect role of osteoclasts on the bone loss phenotype.

Overall (**Figure 7**), removing *Tgfβr2* in the Gli1+ osteogenic progenitor cells led to significant alveolar bone loss as well as a decrease in OSX, β-catenin, PERIOSTIN, and MEPE. Conversely, there was a drastic increase in SOST (a potent inhibitor of WNT signaling). Deletion of *Tgfβr2* in 3.2 kb Col1+ osteoblasts resulted in mild changes in alveolar bone morphology and mild bone loss. Thus, we conclude that TGFβ signaling is essential

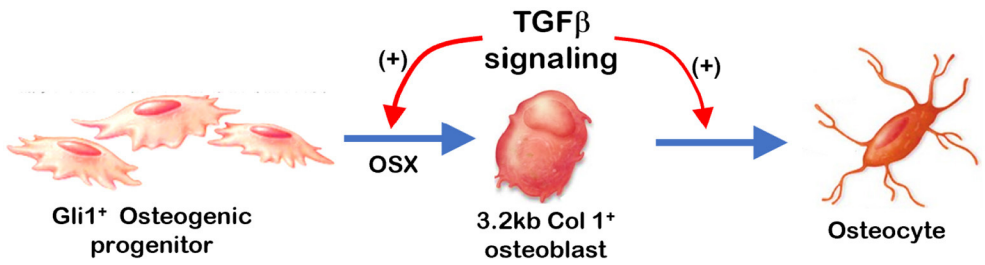

FIGURE 7 | Summary: TGFβ signaling plays a stage-dependent role during mandible bone growth based on the loss of *Tgfβr2* in Gli1+ osteogenic progenitors and 3.2 kb Col1+ osteoblasts in the R26R^{tdTomato} tracing background, respectively. Removing *Tgfβr2* in the Gli1+ progenitor cells at early postnatal stage led to a significant bone loss and a decrease in OSX. Deletion of *Tgfβr2* in the 3.2 kb Col1+ osteoblasts at early postnatal stage result in mild changes in alveolar bone morphologies and bone volume.

for regulating the proliferation and differentiation of osteogenic progenitors during early postnatal alveolar bone formation.

DATA AVAILABILITY STATEMENT

The original contributions presented in the study are included in the article/**Supplementary Material**, further inquiries can be directed to the corresponding author/s.

ETHICS STATEMENT

The animal study was reviewed and approved by Animal Care and Use Committees (IACUC) at Texas A&M University College of Dentistry and Sichuan University West China School of Stomatology.

AUTHOR CONTRIBUTIONS

CX contributed to the conception, design, data acquisition, analysis, interpretation, and also drafted and critically revised the manuscript. XX contributed to data acquisition and manuscript revision. YW and HZ contributed to data analysis and interpretation together with critically revising the manuscript. JW and JF contributed to conception, design, data analysis and interpretation for the project, and they drafted and critically revised the manuscript. All authors gave final approval and agreed to be accountable for all aspects of the work.

FUNDING

This study was supported by grants from the National Institutes of Health (Grant Nos. DE025659, DE025014, and DE028291) to JF and from the National Natural Science Foundation of China (Grant Nos. 82071127 and 81700980) to JW.

ACKNOWLEDGMENTS

We thank Vivian Shi and Meghann Holt for their assistance with the editing of this article. We also acknowledge technical assistance on the RNAscope assay from Changchun Dong and Xiaofang Wang.

SUPPLEMENTARY MATERIAL

The Supplementary Material for this article can be found online at: https://www.frontiersin.org/articles/10.3389/fphys.2021.721775/full#supplementary-material

REFERENCES

Abou-Ezzi, G., Supakorndej, T., Zhang, J., Anthony, B., Krambs, J., Celik, H., et al. (2019). TGF-beta signaling plays an essential role in the lineage specification of mesenchymal stem/progenitor cells in fetal bone marrow. *Stem Cell Reports* 13, 48–60. doi: 10.1016/j.stemcr.2019.05.017

Ahn, S., and Joyner, A. L. (2004). Dynamic changes in the response of cells to positive hedgehog signaling during mouse limb patterning. *Cell* 118, 505–516. doi: 10.1016/j.cell.2004.07.023

Balemans, W., Ebeling, M., Patel, N., Van Hul, E., Olson, P., Dioszegi, M., et al. (2001). Increased bone density in sclerosteosis is due to the deficiency of a novel secreted protein (SOST). *Hum. Mol. Genet.* 10, 537–543. doi: 10.1093/hmg/10.5.537

Chavarry, N. G., Vettore, M. V., Sansone, C., and Sheiham, A. (2009). The relationship between diabetes mellitus and destructive periodontal disease: a meta-analysis. *Oral Health Prev. Dent.* 7, 107–127. doi: 10.3290/j.ohpd.a15518

Chen, G., Deng, C., and Li, Y. P. (2012). TGF-beta and BMP signaling in osteoblast differentiation and bone formation. *Int. J. Biol. Sci.* 8, 272–288. doi: 10.7150/ijbs.2929

Corps, K., Stanwick, M., Rectenwald, J., Kruggel, A., and Peters, S. B. (2021). Skeletal deformities in Osterix-Cre;Tgfbr2f/f mice may cause postnatal death. *Genes (Basel)* 12:975. doi: 10.3390/genes12070975

Douglass, C. W., and Fox, C. H. (1993). Cross-sectional studies in periodontal disease: current status and implications for dental practice. *Adv. Dent. Res.* 7, 25–31. doi: 10.1177/08959374930070010301

Feng, J., Jing, J., Li, J., Zhao, H., Punj, V., Zhang, T., et al. (2017). BMP signaling orchestrates a transcriptional network to control the fate of mesenchymal stem cells in mice. *Development* 144, 2560–2569. doi: 10.1242/dev.150136

Fox, C. H. (1992). New considerations in the prevalence of periodontal disease. *Curr. Opin. Dent.* 2, 5–11.

Fox, C. H., Jette, A. M., McGuire, S. M., Feldman, H. A., and Douglass, C. W. (1994). Periodontal disease among New England elders. *J. Periodontol.* 65, 676–684. doi: 10.1902/jop.1994.65.7.676

Hallmon, W. W., and Mealey, B. L. (1992). Implications of diabetes mellitus and periodontal disease. *Diabetes Educ.* 18, 310–315. doi: 10.1177/014572179201800409

Hinton, R. J., Jing, J., and Feng, J. Q. (2015). Genetic influences on temporomandibular joint development and growth. *Curr.*

Top. Dev. Biol. 115, 85–109. doi: 10.1016/bs.ctdb.2015.07.008

Hinton, R. J., Jing, Y., Jing, J., and Feng, J. Q. (2017). Roles of chondrocytes in endochondral bone formation and fracture repair. *J. Dent. Res.* 96, 23–30. doi: 10.1177/0022034516668321

Hosoya, A., Shalehin, N., Takebe, H., Fujii, S., Seki, Y., Mizoguchi, T., et al. (2020). Stem cell properties of Gli1-positive cells in the periodontal ligament. *J. Oral Biosci.* 62, 299–305. doi: 10.1016/j.job.2020.08.002

Jing, Y., Zhou, X., Han, X., Jing, J., von der Mark, K., Wang, J., et al. (2015). Chondrocytes directly transform into bone cells in mandibular condyle growth. *J. Dent. Res.* 94, 1668–1675. doi: 10.1177/0022034515598135

Khader, Y. S., Dauod, A. S., El-Qaderi, S. S., Alkafajei, A., and Batayha, W. Q. (2006). Periodontal status of diabetics compared with nondiabetics: a meta-analysis. *J. Diabetes Complicat.* 20, 59–68. doi: 10.1016/j.jdiacomp.2005.05.006

Kim, T. H., Bae, C. H., Lee, J. Y., Lee, J. C., Ko, S. O., Chai, Y., et al. (2015). Temporo-spatial requirement of Smad4 in dentin formation. *Biochem. Biophys. Res. Commun.* 459, 706–712. doi: 10.1016/j.bbrc.2015.03.014

Kitaura, Y., Hojo, H., Komiyama, Y., Takato, T., Chung, U. I., and Ohba, S. (2014). Gli1 haploinsufficiency leads to decreased bone mass with an uncoupling of bone metabolism in adult mice. *PLoS ONE* 9:e109597. doi: 10.1371/journal.pone.0109597

Liu, A. Q., Zhang, L. S., Chen, J., Sui, B. D., Liu, J., Zhai, Q. M., et al. (2020). Mechanosensing by Gli1(+) cells contributes to the orthodontic force-induced bone remodelling. *Cell Prolif.* 53:e12810. doi: 10.1111/cpr.12810

Long, F. (2011). Building strong bones: molecular regulation of the osteoblast lineage. *Nat. Rev. Mol. Cell Biol.* 13, 27–38. doi: 10.1038/nrm3254

Mealey, B. L., and Ocampo, G. L. (2007). Diabetes mellitus and periodontal disease. *Periodontol* 44, 127–153. doi: 10.1111/j.1600-0757.2006.00193.x

Men, Y., Wang, Y., Yi, Y., Jing, D., Luo, W., Shen, B., et al. (2020). Gli1+ periodontium stem cells are regulated by osteocytes and occlusal force. *Dev. Cell* 54, 639–654. doi: 10.1016/j.devcel.2020.06.006

Meng, X., Vander Ark, A., Daft, P., Woodford, E., Wang, J., Madaj, Z., et al. (2018). Loss of TGF-beta signaling in osteoblasts increases basic-FGF and promotes prostate cancer bone metastasis. *Cancer Lett.* 418, 109–118. doi: 10.1016/j.canlet.2018.01.018

Oka, K., Oka, S., Sasaki, T., Ito, Y., Bringas, P. Jr., Nonaka, K., et al. (2007). The role of TGF-beta signaling in regulating chondrogenesis and osteogenesis during mandibular development. *Dev. Biol.* 303, 391–404. doi: 10.1016/j.ydbio.2006.11.025

Peters, S. B., Wang, Y., and Serra, R. (2017). Tgfbr2 is required in osterix expressing cells for postnatal skeletal development. *Bone* 97, 54–64. doi: 10.1016/j.bone.2016.12.017

Pihlstrom, B. L., Michalowicz, B. S., and Johnson, N. W. (2005). Periodontal diseases. *Lancet* 366, 1809–1820. doi: 10.1016/S0140-6736(05)67728-8

Preshaw, P. M., Alba, A. L., Herrera, D., Jepsen, S., Konstantinidis, A., Makrilakis, K., et al. (2012). Periodontitis and diabetes: a two-way relationship. *Diabetologia* 55, 21–31. doi: 10.1007/s00125-011-2342-y

Qin, X., Jiang, Q., Miyazaki, T., and Komori, T. (2019). Runx2 regulates cranial suture closure by inducing hedgehog, Fgf, Wnt and Pthlh signaling pathway gene expressions in suture mesenchymal cells. *Hum. Mol. Genet.* 28, 896–911. doi: 10.1093/hmg/ddy386

Qiu, T., Wu, X., Zhang, F., Clemens, T. L., Wan, M., and Cao, X. (2010). TGF-beta type II receptor phosphorylates PTH receptor to integrate bone remodelling signalling. *Nat. Cell Biol.* 12, 224–234. doi: 10.1038/ncb2022

Ren, Y., Han, X., Ho, S. P., Harris, S. E., Cao, Z., Economides, A. N., et al. (2015). Removal of SOST or blocking its product sclerostin rescues defects in the periodontitis mouse model. *FASEB J.* 29, 2702–2711. doi: 10.1096/fj.14-265496

Rios, H., Koushik, S. V., Wang, H., Wang, J., Zhou, H. M., Lindsley, A., et al. (2005). Periostin null mice exhibit dwarfism, incisor enamel defects, and an early-onset periodontal disease-like phenotype. *Mol. Cell. Biol.* 25, 11131–11144. doi: 10.1128/MCB.25.24.11131-11144.2005

Rios, H. F., Ma, D., Xie, Y., Giannobile, W. V., Bonewald, L. F., Conway, S. J., et al. (2008). Periostin is essential for the integrity and function of the periodontal ligament during occlusal loading in mice. *J Periodontol.* 79, 1480–1490. doi: 10.1902/jop.2008.070624

Rossert, J., Eberspaecher, H., and de Crombrugghe, B. (1995). Separate cis-acting DNA elements of the mouse pro-alpha 1(I) collagen promoter direct expression of reporter genes to different type I collagen-producing cells in transgenic mice. *J. Cell Biol.* 129, 1421–1432. doi: 10.1083/jcb.129.5.1421

Salvi, G. E., Carollo-Bittel, B., and Lang, N. P. (2008). Effects of diabetes mellitus on periodontal and peri-implant conditions: update on associations and risks. *J. Clin. Periodontol.* 35, 398–409. doi: 10.1111/j.1600-051X.2008.01282.x

Sasaki, T., Ito, Y., Bringas, P. Jr., Chou, S., Urata, M. M., Slavkin, H., et al. (2006). TGFbeta-mediated FGF signaling is crucial for regulating cranial neural crest cell proliferation during frontal bone development. *Development* 133, 371–381. doi: 10.1242/dev.02200

Seo, H. S., and Serra, R. (2007). Deletion of Tgfbr2 in Prx1-cre expressing mesenchyme results in defects in development of the long bones and joints. *Dev. Biol.* 310, 304–316. doi: 10.1016/j.ydbio.2007.07.040

Seo, H. S., and Serra, R. (2009). Tgfbr2 is required for development of the skull vault. *Dev. Biol.* 334, 481–490. doi: 10.1016/j.ydbio.2009.08.015

Shi, Y., He, G., Lee, W. C., McKenzie, J. A., Silva, M. J., and Long, F. (2017). Gli1 identifies osteogenic progenitors for bone formation and fracture repair. *Nat. Commun.* 8:2043. doi: 10.1038/s41467-017-02171-2

Tang, S. Y., and Alliston, T. (2013). Regulation of postnatal bone homeostasis by TGFbeta. *Bonekey Rep.* 2:255. doi: 10.1038/bonekey.2012.255

Wang, C. J., and McCauley, L. K. (2016). Osteoporosis and periodontitis. *Curr. Osteoporos. Rep.* 14, 284–291. doi: 10.1007/s11914-016-0330-3

Wang, F., Flanagan, J., Su, N., Wang, L. C., Bui, S., Nielson, A., et al. (2012). RNAscope: a novel *in situ* RNA analysis platform for formalin-fixed, paraffin-embedded tissues. *J. Mol. Diagn.* 14, 22–29. doi: 10.1016/j.jmoldx.2011.08.002

Wang, J., Jiang, Y., Xie, X., Zhang, S., Xu, C., Zhou, Y., et al. (2020). The identification of critical time windows of postnatal root elongation in response to Wnt/beta-catenin signaling. *Oral Dis. [Preprint].* 1–10 doi: 10.1111/ODI.13753/v2/response1

Wang, J., Massoudi, D., Ren, Y., Muir, A. M., Harris, S. E., Greenspan, D. S., et al. (2017). BMP1 and TLL1 are required for maintaining periodontal homeostasis. *J. Dent. Res.* 96, 578–585. doi: 10.1177/0022034516686558

Wang, Y., Cox, M. K., Coricor, G., MacDougall, M., and Serra, R. (2013). Inactivation of Tgfbr2 in Osterix-Cre expressing dental mesenchyme disrupts molar root formation. *Dev. Biol.* 382, 27–37. doi: 10.1016/j.ydbio.2013.08.003

Wu, M., Chen, G., and Li, Y. P. (2016). TGF-beta and BMP signaling in osteoblast, skeletal development, and bone formation, homeostasis and disease. *Bone Res.* 4:16009. doi: 10.1038/boneres.2016.9

Xia, C., Ge, Q., Fang, L., Yu, H., Zou, Z., Zhang, P., et al. (2020). TGF-beta/Smad2 signalling regulates enchondral bone formation of Gli1(+) periosteal cells during fracture healing. *Cell Prolif.* 53:e12904. doi: 10.1111/cpr.12904

Xie, X., Wang, J., Wang, K., Li, C., Zhang, S., Jing, D., et al. (2019). Axin2(+)-mesenchymal PDL cells, instead of K14(+) epithelial cells, play a key role in rapid cementum growth. *J. Dent. Res.* 98, 1262–1270. doi: 10.1177/0022034519871021

Yi, Y., Stenberg, W., Luo, W., Feng, J. Q., and Zhao, H. (2021). Alveolar bone marrow Gli1+ stem cells support implant osseointegration. *J. Dent. Res. [Preprint].* doi: 10.1177/00220345211013722 (accessed September 4, 2021)

Zhou, X., Zhang, Z., Feng, J. Q., Dusevich, V. M., Sinha, K., Zhang, H., et al. (2010). Multiple functions of Osterix are required for bone growth and homeostasis in postnatal mice. *Proc. Natl. Acad. Sci. U. S. A.* 107, 12919–12924. doi: 10.1073/pnas.0912855107

Conflict of Interest: The authors declare that the research was conducted in the absence of any commercial or financial relationships that could be construed as a potential conflict of interest.

Publisher's Note: All claims expressed in this article are solely those of the authors and do not necessarily represent those of their affiliated organizations, or those of the publisher, the editors and the reviewers. Any product that may be evaluated in this article, or claim that may be made by its manufacturer, is not guaranteed or endorsed by the publisher.

frontiers in Physiology

ORIGINAL RESEARCH
published: 30 September 2021
doi: 10.3389/fphys.2021.731549

Discovering Myeloid Cell Heterogeneity in Mandibular Bone – Cell by Cell Analysis

*Kyu Hwan Kwack[1], Natalie A. Lamb[2], Jonathan E. Bard[2,3], Elliot D. Kramer[4,5], Lixia Zhang[1], Scott I. Abrams[5] and Keith L. Kirkwood[1,6]**

[1] Department of Oral Biology, University at Buffalo, The State University of New York, Buffalo, NY, United States, [2] Genomics and Bioinformatics Core, New York State Center of Excellence in Bioinformatics and Life Sciences, University at Buffalo, The State University of New York, Buffalo, NY, United States, [3] Department of Biochemistry, Jacobs School of Medicine and Biomedical Sciences, University at Buffalo, Buffalo, NY, United States, [4] Department of Medicine, University at Buffalo, Buffalo, NY, United States, [5] Department of Immunology, Roswell Park Comprehensive Cancer Center, Buffalo, NY, United States, [6] Department of Head and Neck, Plastic and Reconstructive Surgery, Roswell Park Comprehensive Cancer Center, Buffalo, NY, United States

The myeloid-derived bone marrow progenitor populations from different anatomical locations are known to have diverse osteoclastogenesis potential. Specifically, myeloid progenitors from the tibia and femur have increased osteoclast differentiation potential compared to myeloid progenitors from the alveolar process. In this study, we explored the differences in the myeloid lineage progenitor cell populations in alveolar (mandibular) bone versus long (femur) bone using flow cytometry and high-throughput single cell RNA sequencing (scRNA-seq) to provide a comprehensive transcriptional landscape. Results indicate that mandibular bone marrow-derived cells exhibit consistent deficits in myeloid differentiation, including significantly fewer myeloid-derived suppressor cell (MDSC)-like populations ($CD11b^+Ly6C^+$, $CD11b^+Ly6G^+$), as well as macrophages ($CD11b^+F4/80^+$). Although significantly fewer in number, MDSCs from mandibular bone exhibited increased immunosuppressive activity compared to MDSCs isolated from long bone. Using flow cytometry panels specific for bone marrow progenitors, analysis of hematopoietic stem cells showed no defects in mandibular bone marrow in LSK ($Lin^-Sca1^+cKit^+$) cell and LK ($Lin^-Sca1^-cKit^+$) cell populations. While there was no significant difference in granulocyte progenitors, the granulocyte-monocyte progenitors and monocyte progenitor population were significantly decreased in the mandibular bone marrow. T-lymphocyte subsets were not significantly different between mandibular and femoral bone, except for $CD4^+CD25^+Foxp3^+$ regulatory T lymphocytes, which were significantly increased in the mandible. In addition, B lymphocytes were significantly increased in mandible. Single cell RNA sequencing from mandible and femur BM revealed distinct differences in transcriptomic profiles in myeloid populations establishing previously unappreciated aspects of mandibular bone marrow populations. These analyses reveal site-specific differences in the myeloid progenitor cellular composition and transcriptional programs providing a deeper appreciation of the complex differences in myeloid cell heterogeneity from different anatomical bone marrow sites.

Keywords: hematopoietic progenitor cell (HPCs), myeloid cell, transcriptome, bone marrow, cellular microenvironment, mandible

OPEN ACCESS

Edited by:
Frédéric Lézot, Institut National de la Santé et de la Recherche Médicale (INSERM), France

Reviewed by:
James Cray, The Ohio State University, United States
Marta Nardini, University of Genoa, Italy

****Correspondence:***
Keith L. Kirkwood
klkirk@buffalo.edu

Specialty section:
This article was submitted to Craniofacial Biology and Dental Research, a section of the journal Frontiers in Physiology

Received: *27 June 2021*
Accepted: *06 September 2021*
Published: *30 September 2021*

Citation:
Kwack KH, Lamb NA, Bard JE, Kramer ED, Zhang L, Abrams SI and Kirkwood KL (2021) Discovering Myeloid Cell Heterogeneity in Mandibular Bone – Cell by Cell Analysis. Front. Physiol. 12:731549. doi: 10.3389/fphys.2021.731549

INTRODUCTION

Bone mass and shape is continuously adapting to variations in load caused by physical activity, mechanical force, hormones, nutrients, and several additional osteotropic signaling molecules. The adult skeleton is a highly specialized and dynamic organ that undergoes a constant and cyclic bone remodeling process where old bone is removed by bone resorption followed by new bone formation – a process essential for skeleton health maintenance. This sequential process requires bone-forming osteoblasts and bone-resorbing osteoclasts, which in the case of osteoclasts demand a constant pool of progenitor populations. Currently, it has been appreciated that these the bone marrow progenitor cells not only differ depending on anatomic location, but also these progenitor cells respond differently to biological signals (Faloni et al., 2011). Thus, understanding bone marrow progenitor cellular populations may provide new insights into their site-specific function.

Alveolar bone differs morphologically and functionally from another skeletal bones. The adult alveolar bone remodels more rapidly than any other skeletal bones (Huja et al., 2006). This bone turnover distinction is most likely due to the fact that the alveolar bone arises from the neural crest cells of the neuroectoderm germ layer, not from the mesoderm (Chai and Maxson, 2006). Moreover, bone ossification is different in the alveolar process compared to other bones, which proceeds by intramembranous rather than endochondral ossification (Karaplis, 2002). In addition, occlusal stress stimulation and tooth-derived inflammatory responses, which exist only in the alveolar bone, affects metabolism as well as remodeling (Huja et al., 2006; Gruber, 2019; Lerner et al., 2019; Connizzo et al., 2021). The clinical significance of these differences can be appreciated from skeletal diseases that have a greater predilection for the alveolar bone, including hyperparathyroid jaw tumor syndrome, cherubism and osteonecrosis associated with anti-resorptive therapeutics, including bisphosphonates (Ueki et al., 2001; Simonds et al., 2002; Ruggiero et al., 2004). Likewise, there are conditions in which the skeletal bone is affected more than the alveolar process. In the case of malnutrition and ovariectomy, mandibular bone decreases bone mineral density in the trabecular compartment at a lower rate than what is observed in the tibia (Mavropoulos et al., 2007). Additional differences have been observed osteogenic potential where alveolar-derived bone marrow stromal cells or mesenchymal stem cells show exhibit higher osteogenic potential compared to other skeletal bones (Matsubara et al., 2005; Akintoye et al., 2006; Aghaloo et al., 2010; Damek-Poprawa et al., 2010; Yamaza et al., 2011). Thus, fundamental differences exist between mandibular bone and other long bones leading to different physiological and pathological responses and clinical presentations. Consequently, due to the specificity of the mandibular bone and the ease of access cells from long bone versus mandibular bone, there is a relative paucity of data focused on cellular differences between mandibular/oral and long bone.

The bone marrow derived cellular populations that play a major role in bone remodeling are osteoblasts that help generate a mineralized matrix and osteoclasts that resorb this matrix (Crockett et al., 2011). The osteoclastogenic populations are derived with the hematopoietic progenitor stem cell lineage. However, the myeloid progenitor cells are osteoclastogenic precursors that differentiate into highly diverse populations. Mononuclear myeloid cells include monocytes as well as macrophages, dendritic cells (DC) and osteoclasts that terminally differentiate in tissues under physiologic and inflammatory conditions alike. Granulocytic myeloid cells contain populations of eosinophils, basophils, polymorphic nuclear neutrophils, and mast cells. The proliferation and differentiation of myeloid progenitor cells in the bone marrow is strictly controlled according to the physiological and pathological conditions. Hematopoietic stem cells (HSCs) reside in the bone marrow, maintaining a pool of pluripotent stem cells through self-renewal, or progenitor cellular populations capable of differentiation into committed lineages (Seita and Weissman, 2010). The HSC population can be identified based on expression of cell surface markers. Accordingly, HSC/progenitor cells are negative for mature hematopoietic markers (Lineage markers) and positive for the stem cell markers Sca-1 and c-Kit (Lineage$^-$Sca-1$^+$c-Kit$^+$; LSK) (Challen et al., 2009). The myeloid progenitor population downstream of HSC, can be identified as a Sca-1 negative subset of the lineage negative and c-Kit positive population (Lineage$^-$Sca-1$^-$c-Kit$^+$; LK). This fraction is called hematopoietic progenitor cells (HPCs) and can be further divided into subtypes of common myeloid progenitors (CMPs), megakaryocyte-erythroid progenitors (MEPs), and granulocyte-macrophage progenitors (GMPs). Myeloid-derived suppressor cells (MDSCs) are a heterogenous population of myeloid-cell lineage consisting of precursors of myeloid cells and myeloid-cell progenitors. MDSCs include two relatively well characterized subtypes of monocytic (M)-MDSCs and granulocytic (PMN)-MDSCs. In mice, M-MDSC can be defined as CD11b$^+$Ly6G$^-$Ly6C^{high} and PMN-MDSC as CD11b$^+$Ly6G$^+$Ly6C^{low}. These cells have the ability to modulate the innate and adaptive immune response. Under pathologic conditions, the immature myeloid cells (IMCs) generated in the bone marrow are partially blocked from differentiation into mature myeloid cells, resulting in the expansion of the IMC population. And the prolonged and marked expansion of the IMCs lead to the expansion of MDSC population (Gabrilovich and Nagaraj, 2009). Several reports support MDSC plasticity as osteoclast progenitors under various pathological conditions associated with bone destruction (Sawant et al., 2013; Zhang et al., 2015; Kirkwood et al., 2018). Therefore, to study whether the specificity of mandibular bone is due to the heterogeneity of bone marrow cells, it is necessary to explore not only the populations of lineage committed bone marrow cells but also their progenitors.

Single cell RNA sequencing (scRNA-seq) provides a comprehensive transcriptional environment for analyzing tissue heterogeneity at the individual cell level and exploring the contribution of various cell subtypes to physiological function. To date, there are no studies directly comparing the transcriptomic landscape between mandibular and long bone marrow. In this study, we analyzed the heterogeneity of myeloid cells in the mandibular bone and the femur by performing

flow cytometry and scRNA-seq. We have found that not only these progenitor cells, but also myeloid cells have distinct transcriptomic profiles.

MATERIALS AND METHODS

Animals

Animal maintenance and experimental protocols were conducted under an approved Institutional Animal Care and Use Committee protocol from the University at Buffalo using ARRIVE guidelines. Male C57BL/6J mice were purchased from The Jackson Laboratory (Bar Harbor, ME, United States) at 12 weeks of age. All animals were housed in an environment-controlled conditions of 22 ± 2°C, 40–70% humidity with a light/dark cycle of 12 h.

Bone Marrow Cell Isolation

Soft tissue was dissected from 3-month-old C57BL/6 mouse femurs and mandibles. Long-bone BM cells were flushed from the femurs with RPMI 1640 (Corning Inc., Corning, NY, United States) medium. To obtain the bone marrow cells from mandible, cut the anterior bone along the mental foramen at the mesial of the first molar. Mandibular ramus, including the angular, condylar and coronoid process, was removed along the distal edge of the third molar on the distal side to expose the bone marrow cavity. Bones were then placed in 1.5 ml microfuge tubes supported by 0.5 ml microfuge tube inserts with a lower hole, and centrifuge at 8,000 rpm for 10 min. The bone marrow pellet was resuspended 5 ml of RPMI 1640 culture medium. A single cell suspension was obtained by passing 18-, 21-, and 25-gauge needles in sequence.

Flow Cytometry Analysis

The isolated bone marrow cells were depleted of red blood cells using RBC lysis buffer (Gibco, Invitrogen, United States) and filtered through 70 μm nylon membrane (BD) to make a single cell suspension. Cells were suspended in staining buffer (dPBS + 0.5% BSA + 2 mM EDTA) and treated with Mouse Fc block (BD Biosciences). To characterize the phenotype of bone marrow cells, we stained for various anti-mouse: anti-Ly6C FITC (REA 796), anti-Ly6G PE (REA 526), anti-F4/80 PE-Vio770 (REA 126), anti-CD11b APC (M1/70 15.11.5), anti-CD4-Vioblue (REA 604), anti-CD8-APC-Vio770 (REA 601), anti-CD25-PE-Vio770 (7D4), anti-Foxp3-PE (REA 788), anti-CD19-FITC (6D5), anti-NK1.1-PE (PK136), anti-CD11c-APC (REA 754). Intracellular staining for Foxp3 was performed using Fixation/Permeabilization Solution Kit (BD Biosciences). Stained cells were collected on MACSQuant System (Miltenyi Biotec) and analyzed with FlowJo software (version 10.6).

For the analysis of bone marrow progenitor cells, the following directly conjugated Abs were used for staining: anti-CD16/32 PerCP-Cy5.5 (clone 93), anti-cKit APC/Fire 750 (2B8), anti-CD150 BV605 (TC15-12F12.2), anti-Ly6C Ax700 (HK1.4), anti-Sca1 PECy7 (D7), anti-Flit3 PE (A2F10), anti-CD115 APC (AFS98), anti-Lineage Cocktail Pacific Blue (17A2; RB69C5; RA36B2; Ter119; M1/70), anti-CD105 PeCy5 (MJ7/18). Stained samples were then treated with DAPI (Thermo Fisher Scientific) for dead cell exclusion. Samples were acquired on the LSR II flow cytometer (BD Biosciences) via FACSDiva version 6.1.3 software. Data analysis was performed using FCS Express 7.0 following the bone marrow progenitor markers described in Netherby et al. (2017).

T Cell Proliferation Assay

Monocytic-Myeloid-derived suppressor cells were isolated from the femur/mandible bone marrow using the Myeloid-Derived Suppressor Cell Isolation Kit (Miltenyi Biotec) according to the manufacturer's instruction. Total T cells were separated from the spleen using the CD3ε MicroBead Kit (Miltenyi Biotec) accordance of the manufacturer's protocol. Isolated T cells were labeled with CTV (Invitrogen) and plated in a round-bottom 96-well plate at the density of 2×10^5 cells/well. The plated T cells were activated by CD3/CD28 (Thermo Fisher Scientific), and co-cultured with the isolated M-MDSCs. After 3 days, the cells were collected, treated with Fc block and stained with antibodies as follows: CD3-APC (REA641, Miltenyi), CD4-pE-cy7 (GK1.5, eBioscience), and CD8-APC-cy7 (REA601, Miltenyi). Data were collected on MACSQuant System (Miltenyi Biotec) and analyzed with FlowJo 10.6 software.

Single-Cell RNA Sequencing

For detailed scRNA-seq characterization, bone marrow cells isolated from the femur and mandible of the same mouse were obtained and used in these analyses. Cell suspensions were sequenced on the 10x genomics chromium platform. Following library preparation according to manufacturer protocol, libraries were loaded on an Illumina NextSeq in high-output mode, with a general target of 30,000 reads per cell to provide for sufficient depth and transcriptomic saturation. Post sequencing, the data was demultiplexed and provided as input into the 10X Genomics Cell Ranger pipeline (version 5), which quantified the transcriptomic profile of each cell against a reference genome. Sequence saturation, barcodes detected per cell, percent of transcripts in cell, and general alignment statistics were evaluated for quality. Cell Ranger matrix files were then used as input into the R Bioconductor package Seurat version 4 (Stuart et al., 2019).

Mapping rates to the mouse reference genome were above 95% for both samples. Approximately 16,140 cells from the femur and 14,338 cells from the mandible were sequenced. Cells with outlier-status, abnormal gene detection rates (<200 and >6,000), and high mitochondrial transcript load (>15%), which is an indicator of cellular stress, were filtered from the analysis (**Supplementary Figure 1**). After filtering, the data underwent Seurat normalization, followed by principal component analysis (PCA) and Uniform Manifold Approximation and Projection (UMAP) dimensionality reduction, and the construction of a Shared Nearest Neighbor (SNN) graph to cluster cells with similar transcriptomic profiles.

Cluster Generation and Labeling

Both samples (femur and mandible) were integrated and run through the Seurat pipeline for guided clustering, identifying 19 distinct clusters. Clusters were first annotated through an

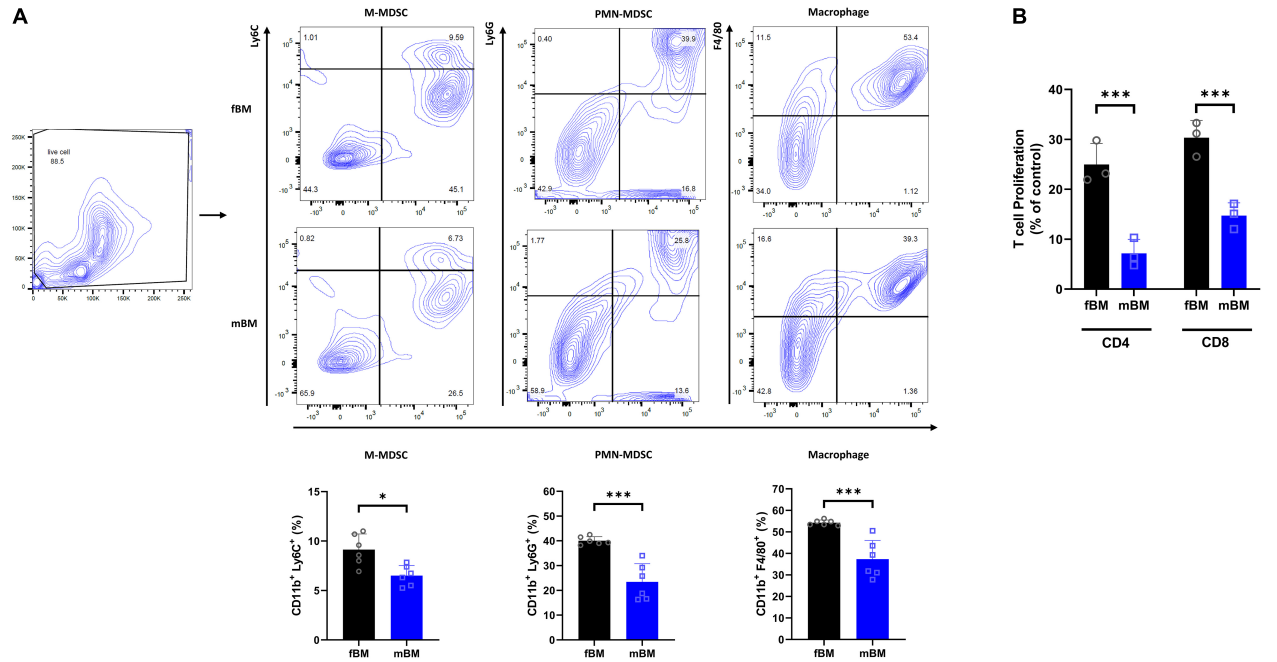

FIGURE 1 | Myeloid population of mBM exhibits consistent deficits compared to fBM. **(A)** Gating strategy (Top) and calculated frequencies (Bottom) of immune cell population from fBM and mBM by flow cytometry. **(B)** T cell proliferation assay of MDSCs isolated from fBM and mBM. The graph of the statistical analyses is presented. Unpaired *t* test; data are presented as mean ± SEM of value from four independent experiments from fBM and mBM, $^{*}P < 0.05$, $^{***}P < 0.001$.

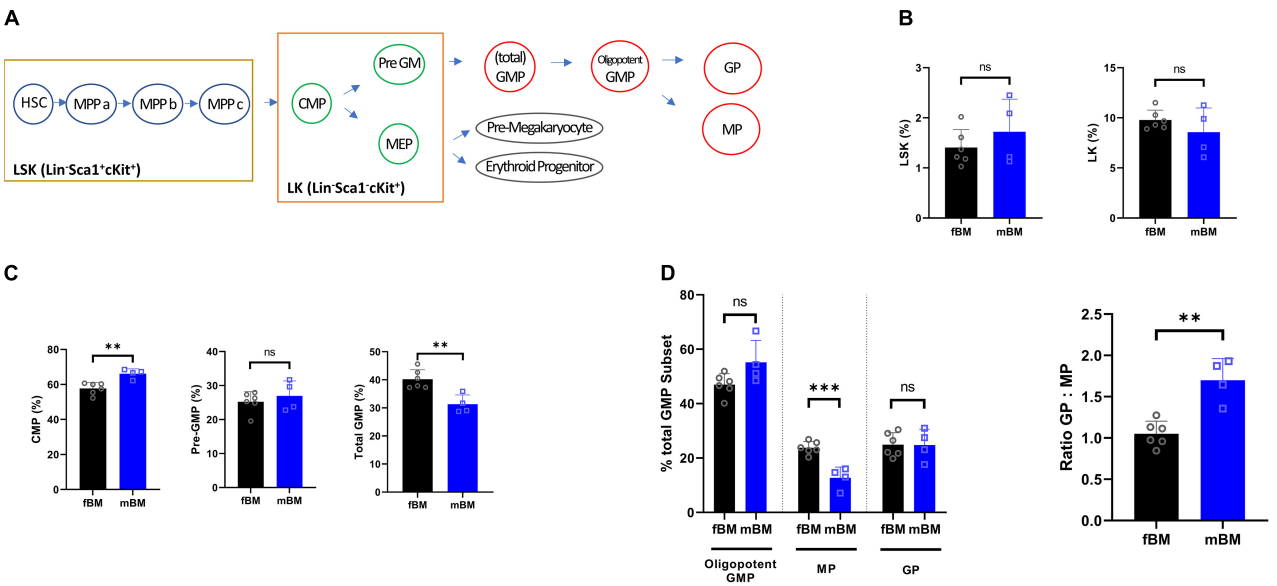

FIGURE 2 | Myeloid progenitors show a decrease in the total GMP population in mandibular bone. **(A)** Schematic view for mouse HSC hierarchy. **(B)** Percentages of LSK ($Lin^{-}Sca1^{+}cKit^{+}$) or LK fractions ($Lin^{-}Sca1^{-}cKit^{+}$) from the bone marrow of same subject-matched fBM and mBM. **(C)** Calculated frequencies of CMPs, Pre-GMPs, and total GMPs from bone marrow of same subject-matched fBM and mBM. **(D)** Percentage of GPs, MPs and oligopotent GMPs within the total GMP population (Left). Ratio of GP to MP in fBM and mBM (Right). Unpaired *t* test; data are presented as mean ± SEM of value from four independent experiments from fBM and mBM, $^{**}P < 0.01$, $^{***}P < 0.001$.

automated platform for identifying cell types called scCATCH (Shao et al., 2020). scCATCH provided a foundation for identifying cell types, followed by manual review of marker gene on each individual cluster. To identify cell-types of interest that exist as smaller populations within the total bone marrow, individual clusters were isolated, and subjected to further sub clustering. Two initial myeloid populations were identified, which through manual review of expressed markers, were annotated into the populations of GMPs, CMPs, MEPs, and mesenchymal stem cells in total bone marrow.

M-MDSC and PMN-MDSC Composite Score Analysis

Due to the low frequency of MDSCs in bone marrow, particularly under wildtype conditions, a composite gene scoring approach was utilized to define both M-MDSCs and PMN-MDSCs. Gene panels from M-MDSC and PMN-MDSC transcriptomic signatures previously determined through scRNA-seq were used to define these cell types (Alshetaiwi et al., 2020). To identify M-MDSCs, which are even more scarce in total bone marrow. The M-MDSC population was defined as the monocytic cluster with the highest expression of the M-MDSC gene panel (*Cxcr2, S100a9, S100a8, Ifitm1, Lrg1, Stfa2l1, Retnlg, Il1b, BC100530*, and *Gm5483*). PMN-MDSCs show similar gene expression profiles to neutrophils and thus the two cell types are grouped together in UMAP (Alshetaiwi et al., 2020). To identify PMN-MDSCs, the neutrophil cluster was subset and new clusters were then called. The PMN-MDSC cluster was identified based on expression of the PMN-MDSC gene panel (*Cd84, Ctsd, Arg2, Pla2g7, Il1b, Clec4e, Il1f9, Junb, Wfdc17, Clec4d, BC100530, Ifitm1, Dusp1, Socs3, Ccl6, Srgn*, and *Cxcr2*).

Statistical Analysis

Flow cytometry experiments were analyzed using GraphPad Prism 8.4 (GraphPad Software Inc., La Jolla, CA, United States) with two-tailed unpaired Student's *t* test. For scRNA-Seq, per-cell gene expression measurements were log normalized using a scale factor of 10,000 using the Seurat function NormalizeData. Cluster-to-cluster differential expression testing was preformed using the Wilcoxon Rank Sum test, using Seurat's FindMarkers and FindAllMarkers functions requiring at least a 0.25 log2 fold change and minimum cluster participation of 10%. Heatmap and DotPlot visualization utilized Seurat's data scaling function, centering mean gene expression values to 0 per-cell and scaling the expression of each gene per-cell to equal variance of 1.

RESULTS

Mandibular Bone Marrow-Derived Cells Exhibit Consistent Deficits in Myeloid Differentiation

To determine whether the mandibular bone marrow-derived cells (mBM) differ from the femoral bone marrow-derived cells (fBM), we first confirmed the myeloid population in each bone marrow cell by flow cytometry (**Figure 1A**). The frequency of M-MDSC ($CD11b^+Ly6G^-Ly6C^{high}$), PMN-MDSC ($CD11b^+Ly6G^+Ly6C^{low}$), and macrophage ($CD11b^+F4/80^+$) were consistently lower in mandibular bone marrow-derived cells (**Figure 1A**). Next, we performed a T cell proliferation assay to confirm MDSC functional phenotype (Bronte et al., 2016). As shown in **Figure 1B**, both MDSCs isolated from fBM and mBM showed the ability to inhibit T cell proliferation, confirming that they were genuine MDSCs. Unexpectedly, although the percentage of MDSC in mBM was lower than that of fBM, MDSCs from the mandible exhibited a much greater capacity to inhibit both $CD4^+$ and $CD8^+$ T cellular proliferation (**Figure 1B**).

Monocyte Progenitors Are Significantly Reduced in Mandibular Bone Marrow

Next, flow cytometry was employed using an antibody panels specific to bone marrow progenitor populations to determine the difference in the composition of the direct antecedents to differentiated myeloid cell populations. A schematic diagram of the mouse HSC hierarchy is shown to facilitate data presentation (**Figure 2A**). The LSK ($Lin^-Sca1^+cKit^+$) and LK ($Lin^-Sca1^-cKit^+$) populations showed no overall significant difference between fBM and mBM (**Figure 2B**). The total GMP subset of LK cells contains both the lineage committed granulocyte and monocyte progenitors, as well as their still oligopotent-GMP parent population (Yanez et al., 2015). This oligopotent-GMP is the bifurcation point between granulocytic and monocytic differentiation. Although there was no significant difference in the LK population as a whole, there was a significant decrease in total GMPs and an increase in CMP in the mBM compared to the fBM (**Figure 2C**). To further explore the difference in total GMPs, we next checked the relative frequencies of the distinct populations downstream of the total GMP. As shown in **Figure 2D**, MPs significantly decreased in mBM while GPs and oligopotent GMPs were unaffected. Thus, the decrease in MPs seen in mBM appears to account for most of the observed reduction in the classically defined total GMP population. To reflect further on how the total GMP response to the monocytic lineage was skewed in mBM, the ratio of GPs to MPs was calculated, which significantly increased in mBM compared to fBM (**Figure 2D**). Collectively, these data indicate that the decrease in total GMPs was mainly due to the reduction of the MP subsets, revealing an early instance of myelopoietic deregulation within the mBM monocytic lineage.

Regulatory T Cells and B Cells Appear Significantly More in Mandibular Bone Marrow-Derived Cells

We next investigated the lymphocytic and dendritic population (**Figure 3**). There was no significant difference in $CD4^+$ T cells and $CD8^+$ T cells, while there was a significant elevation of regulatory T cells in mBM (**Figure 3A**). In addition, there were no defects in dendritic cells ($CD11c^+CD19^-$) and natural killer

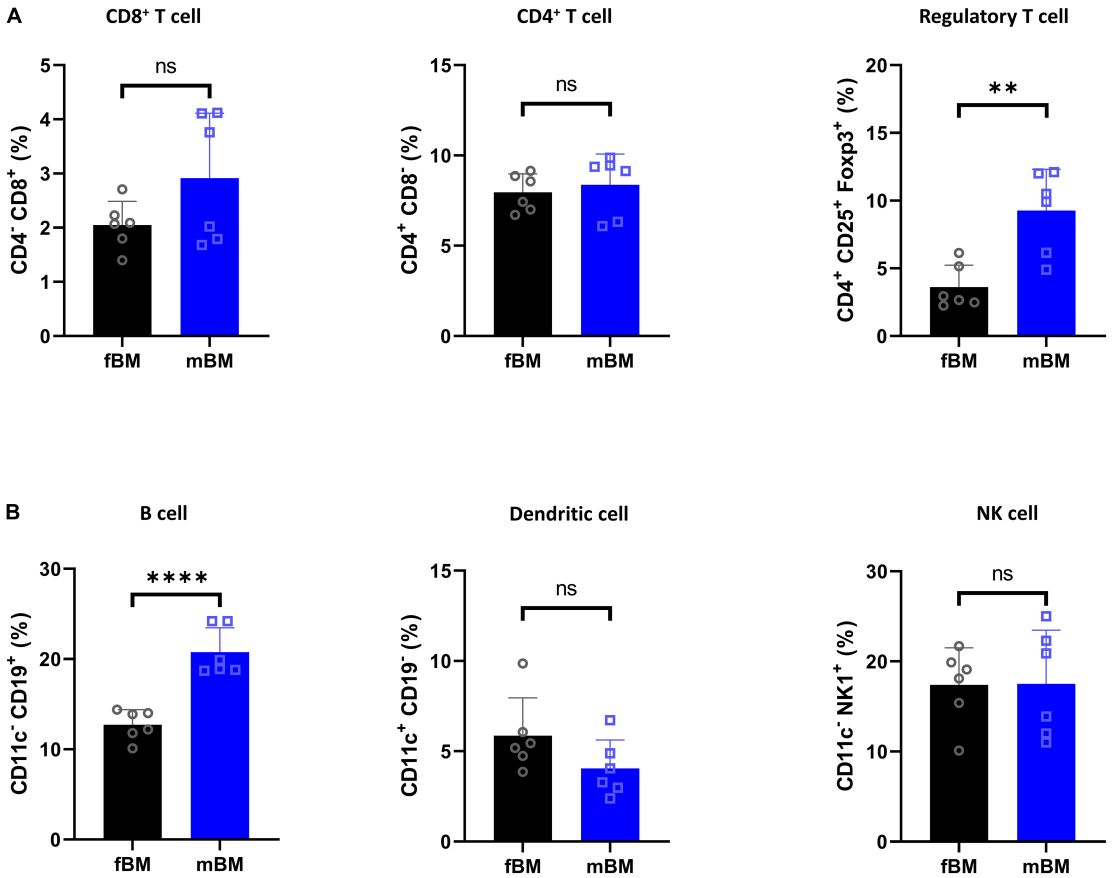

FIGURE 3 | Regulatory T cell and B cells are present in higher proportions in mandibular bone. **(A)** Flow cytometry of T cell subpopulation from fBM and mBM. **(B)** Percentage of B cell, dendritic cell and NK cell from fBM and mBM. Unpaired *t* test; data are presented as mean ± SEM of value from four independent experiments consisting fBM and mBM, $^{**}P < 0.01$, $^{****}P < 0.0001$.

(NK) cells ($CD11c^{-}NK1.1^{+}$), but B cells ($CD11c^{-}CD19^{+}$) were significantly increased in mBM compared to fBM (**Figure 3B**).

Characteristics of Bone Marrow Single Cell Atlas

We performed scRNA-seq to identify cell populations and their transcriptomic signatures in both fBM and mBM. Through manual marker gene analysis, paired with the automated annotation via scCATCH, 19 distinct cell subpopulations were identified in total bone marrow (**Figure 4A**). Two initial clusters were merged into one monocytic population, based on *Ccr2* expression, in addition to other marker genes (**Figure 4B**). Cell cycle analysis also informed monocyte cluster annotation (**Supplementary Figure 2**), as this group contained cells in all three phases of the cell cycle. With this approach, erythroblasts based on *Hba-a2* expression (**Figure 4C**) and neutrophils based in *Ly6g* expression (**Figure 4D**) were defined. Myeloid progenitor populations were initially identified by *Mpo* expression (**Figure 4E**) and then further divided into MEPs, CMPs, and GMPs based on their transcriptomic signature (Paul et al., 2016), paired with scCATCH. Additional markers were used to define and annotate the remaining clusters within the UMAP (**Supplementary Figure 3**).

Comparisons at the Single-Cell Level of Femoral Bone Marrow-Derived Cells and Mandibular Bone Marrow-Derived Cells

To investigate heterogeneity between fBM and mBM at the level of individual cells, in an unbiased manner, we analyzed both cell population and transcriptomic differences between the two samples. There are notable differences between the distribution of femoral and mandibular bone marrow as seen in UMAP (**Figure 5A**). To accurately compare the differences seen in UMAP, the percentage of each cell population in the fBM and mBM sample were determined (**Figure 5B**). As shown by flow cytometry, B cells were increased in the mBM, while monocytes and neutrophils were decreased in the mBM (**Figure 5B**). However, contrary to the flow cytometry results, the total number of CMP populations reduced in the mouse mBM compared to the fBM (**Figure 5B**). To examine the CMP and GMP population in more detail, transcriptomic differences were examined (**Figure 6**). As a result of flow cytometry

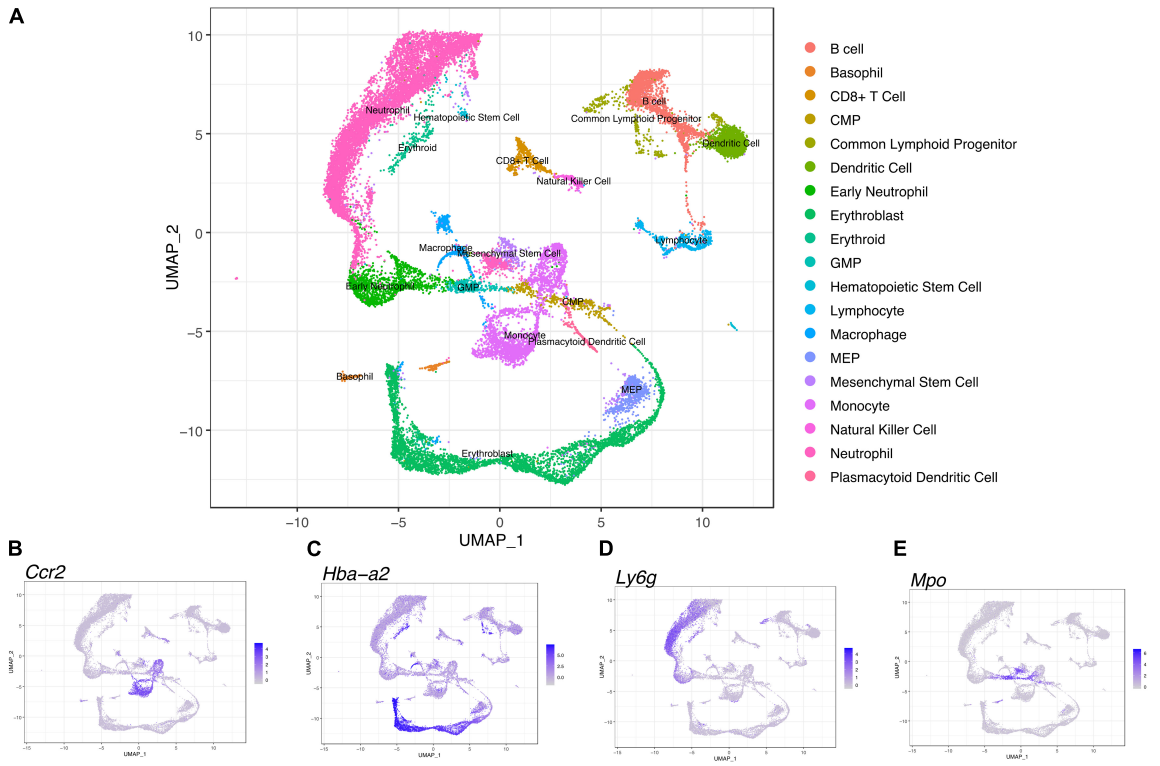

FIGURE 4 | Transcriptional profiling of bone marrow-derived cells reveals a differentiation landscape with 19 distinct cell subpopulations. **(A)** Integrated Seurat analysis of femur and mandible samples from total mouse bone marrow displayed in UMAP. Clusters were annotated based on known marker genes. Feature plots of **(B)** *Ccr2*, **(C)** *Hba-a2*, **(D)** of *Ly6g*, and **(E)** *Mpo* expression shown as representative markers of monocytes, erythroblasts, neutrophils, and myeloid progenitor populations, respectively.

analysis showed differences in the distribution of CMP and GMP populations, CMP and GMP populations also revealed nuanced transcriptomic differences at the single cell level (**Figure 6**).

Comparative Analysis of Heterogeneity Between Mandible and Femur Myeloid-Derived Suppressor Cells

Although we have provided an overall atlas of the immune cell, there may be limitations in detailing the sub-clusters of each immune cell. To further identify M-MDSCs, we first selected and displayed *Ccr2*-expressing monocyte clusters in UMAP (**Figure 7A**). The monocyte population was then further divided into nine distinct sub-clusters (**Figure 7B**) and cluster 7 was identified as the M-MDSC population based on expression of an M-MDSC specific gene panel (**Figure 7C**). There are notable differences in the M-MDSC population which also correspond to differences in transcriptomic profiles between the femur and the mandible (**Figures 7D,E**).

To further identify PMN-MDSCs, we selected and displayed the neutrophil cluster expressing *Ly6g* gene in UMAP (**Figure 8A**). 12 different clusters were identified within the neutrophil population (**Figure 8B**). PMN-MDSCs were identified in cluster 1 based on the expression of the PMN-MDSC gene panel described in the materials and methods (**Figure 8C**). In the feature map, in both fBM and mBM, the gene expression of PMN-MDSC was most enriched in cluster 1 (**Figures 8B,C**). Consistent with the flow cytometry results in **Figure 1A**, the expression of PMN-MDSCs in mBM appeared to be lower (**Figure 8C**). We identified genes highly expressed in the PMN-MDSC cluster (**Figure 8D**), including *Fth1*, *Fgl2*, *Sirpb1c*, and *Mpeg1*, which were not included in our PMN-MDSC gene panel. This analysis also allowed us to pick up nuanced differences in gene expression within the PMN-MDSC sub-cluster between the femur and the mandible (**Figure 8E**).

DISCUSSION

Alveolar bone is the only osseous tissue continuously exposed to a complex array of microbial oral flora found within dental plaque biofilms. Indeed, periodontal homeostasis is maintained by a balanced host immune response to polymicrobial oral biofilms (Hathaway-Schrader and Novince, 2021). However, during disease states periodontal pathogenic microorganisms can penetrate the periodontal barrier to the reside in intimate contact with alveolar bone (Lamont et al., 2018). Therefore, the immune homeostasis of alveolar bone is more likely to be directly affected by microorganisms than any other osseous tissue. To highlight the need for alveolar bone to

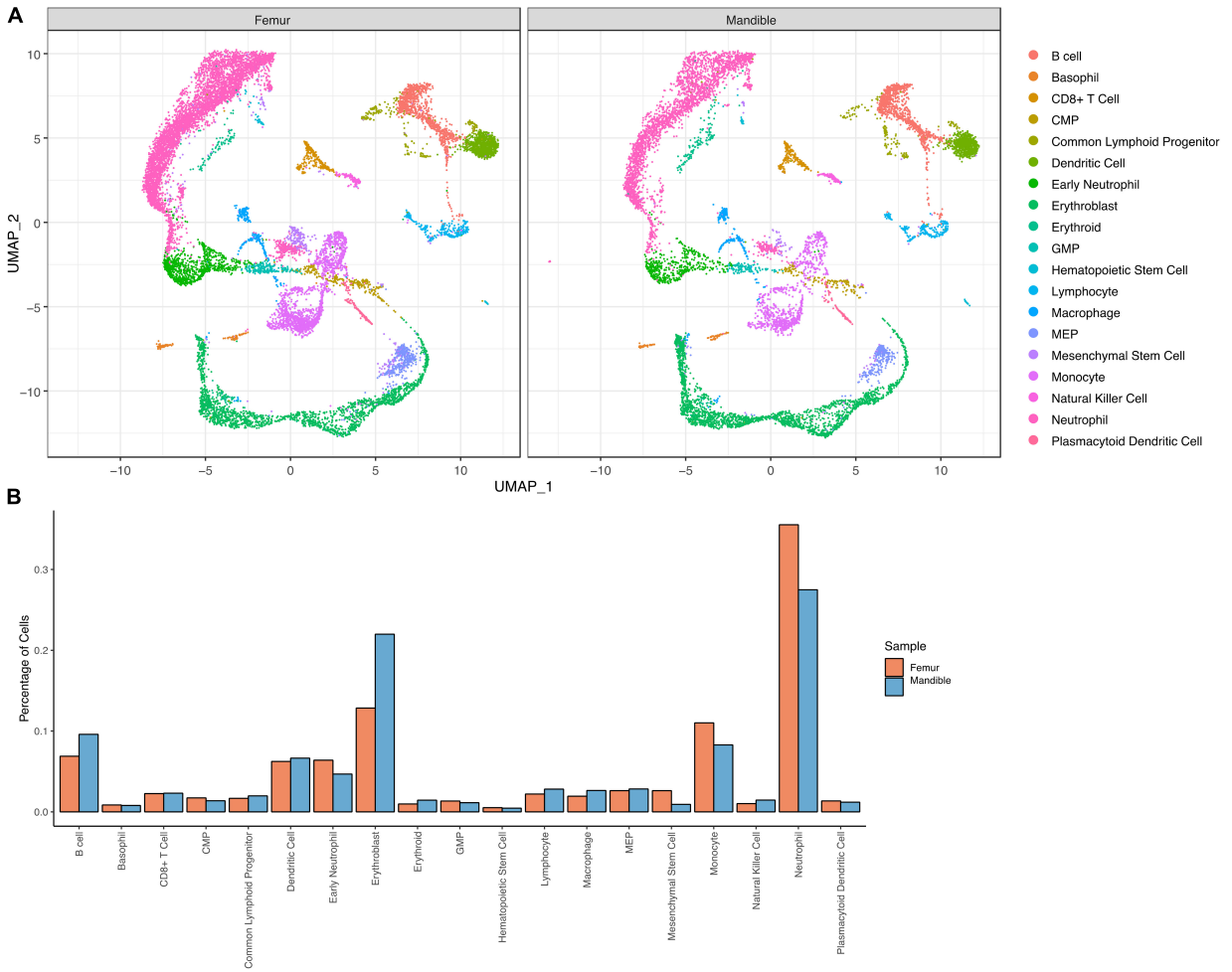

FIGURE 5 | Transcriptional profiling of bone marrow-derived cells reveals slightly distinct differentiation landscapes in fBM and mBM. **(A)** UMAP of femur and mandible samples displayed individually. **(B)** The percentage of cells in each annotated cluster for both the femur (orange) and mandible (blue), plotted as a percentage of total cells sequenced in each sample.

maintain homeostasis in this microbial laden microenvironment, stem/progenitor cells in the craniofacial region found in the mesenchymal compartment including dental pulp, periodontal ligament and alveolar bone have a higher osteoblastic capacity (Li et al., 2012). While other studies have suggested that neural crest-derived HSC harbor in the mandible (Jiang et al., 2016), in-depth studies of HSC have been lacking to better comprehend alveolar bone homeostasis in addition to understanding HSC in pathological conditions, including osteonecrosis and oral infection. The BM cell population may vary depending on the difference in developmental origin as well as the environmental niche. The differentiation and maturation of steady-state HPSCs is tightly regulated by intrinsic/extrinsic signals from a microenvironment called the niche. In this study, we found that immune cells in the mouse mandibular microenvironment have distinctive myeloid cell population differences with clearly different transcriptomic landscapes compared to femoral bone.

We observed that myeloid populations from murine mandibular bone marrow exhibit were consistently lower percentage of the total bone marrow population compared to long bone marrow myeloid cell populations. These data are consistent with published data indicating that monocytes ($CD31^{-}/Ly6C^{high}$) and myeloid blasts ($CD31^{+}/Ly6C^{+}$) were reduced in mBM (Faloni et al., 2011). Using flow cytometry to compare mandibular bone marrow and femur, we found that not only macrophage, but also M-MDSC populations, which are osteoclastic progenitors, are reduced in the mandibular bone. From scRNA-seq analyses, monocytes and neutrophils also showed lower percentages in mBM compared to fBM. The heterogeneity of myeloid cells between femur and mandible was additionally supported by detailed flow cytometry analysis of myeloid cell progenitor populations. Total GMP, a precursor of monoblast and myeloblast, was found in reduced percentage in mBM compared to fBM. Further analysis of macrophage progenitor (MP) populations indicated that

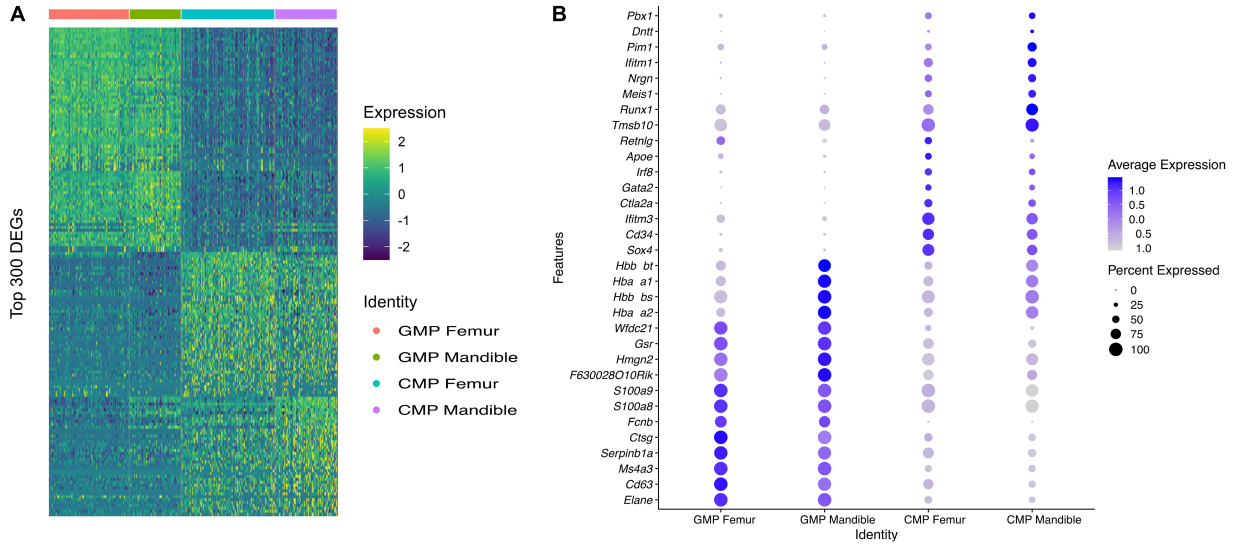

FIGURE 6 | CMP and GMP populations show transcriptomic differences in fBM and mBM. **(A)** Heatmap of the topmost differentially expressed genes in both CMP and GMP populations, as well as between fBM and mBM. **(B)** DotPlot showing the top genes that are differentially expressed between the femur and the mandible in both CMP and GMP populations.

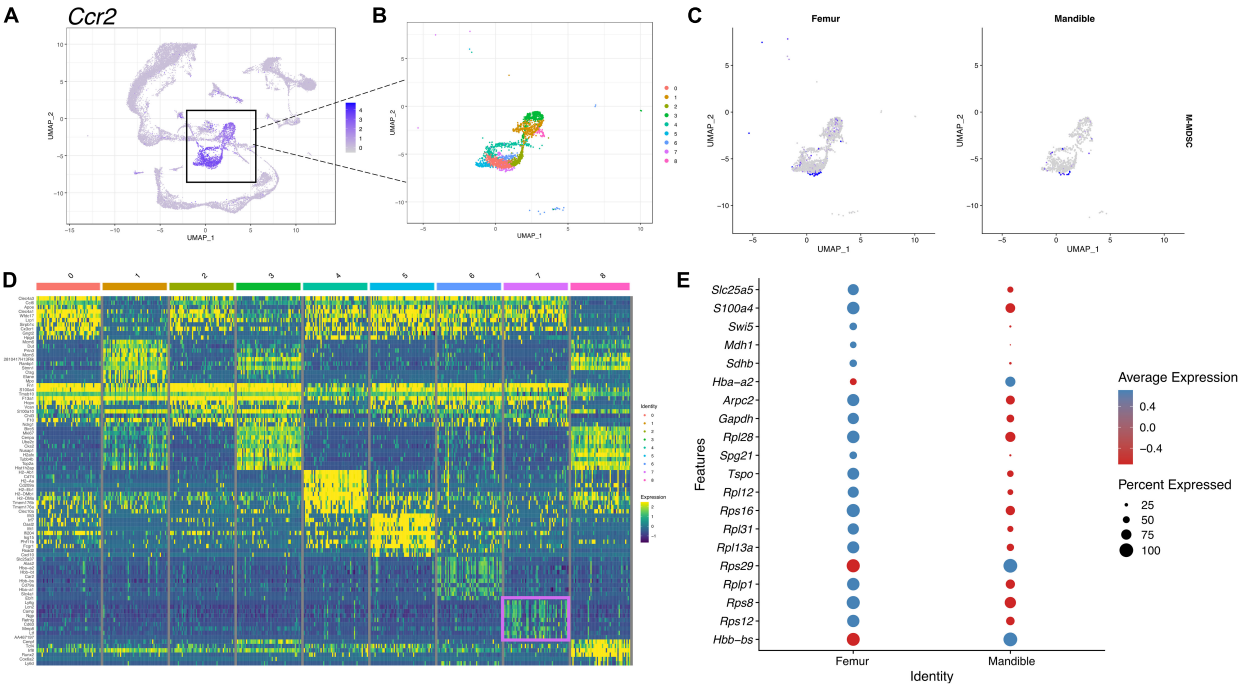

FIGURE 7 | scRNA-seq of M-MDSCs in mBM reveals a transcriptional profile distinct from M-MDSCs in fBM. **(A)** M-MDSCs were identified as a subpopulation of the monocyte cluster marked by *Ccr2* expression. **(B)** The monocytic population was broken into nine distinct clusters. **(C)** Feature plots showing the M-MDSC composite score in femur and mandible. **(D)** The top ten most highly expressed genes in each cluster displayed in a heatmap showing expression on a log scale. The M-MDSC cluster seven genes are boxed in pink. **(E)** The top 20 differentially expressed genes in cluster 7 comparing the femur and mandible displayed in a dotplot, showing M-MDSC transcriptomic differences between the two anatomical locations.

this population was significantly reduced in the mandible compared to femur, indicating that the overall myeloid cell was deficient in mBM.

In this study, results between flow cytometry and scRNA-seq analyses were largely consistent except for observations made in the CMP population. Discrepancies in flow cytometry and

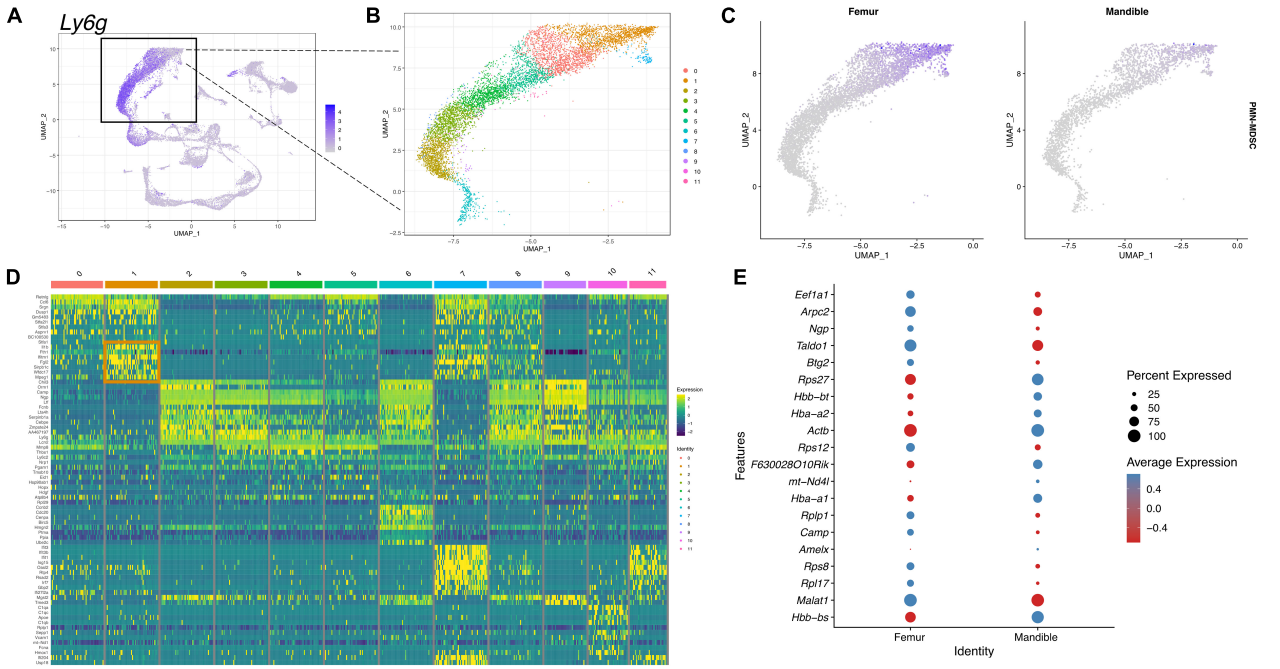

FIGURE 8 | scRNA-seq of PMN-MDSCs in mBM reveals transcriptional profile distinct from PMN-MDSCs in fBM. **(A)** To identify PMN-MDSCs, the neutrophil cluster marked by *Ly6g* expression **(B)** was divided into 12 clusters. **(C)** A feature map of the PMN-MDSC composite genes show cluster 1 is enriched for PMN-MDSC genes. **(D)** Heatmap of the top 10 most highly expressed genes in each cluster. PMN-MDSC genes from cluster 1 are boxed in orange. **(E)** The top 20 differentially expressed genes in cluster 1 between femur and mandible displayed in a dotplot, showing PMN-MDSC specific transcriptomic differences.

scRNA-seq results have also been reported in previous study using bone marrow cells from healthy individuals (Oetjen et al., 2018). We suspect that the reason for these inconsistent results may be due to the small number within the CMP populations and the low number of distinct genes with overlapping transcriptional programs. This phenomenon is particularly likely to occur in cells from healthy mice that would not have expanded bone marrow populations due to infectious disease or tumor burden. Thus, fewer activated cells in this homeostatic system may limit the data set with fewer distinct differentiated cellular populations. Although most of the results were consistent, opportunities for further refinement should be highlighted as the use of single-cell technology expands.

Unexpectedly, we observed that M-MDSC isolated from the mandible had stronger immunosuppressive capacity than M-MDSC isolated from femur despite having fewer cellular percentage of this myeloid cell population. From a functional perspective, MDSCs isolated from normal healthy individuals have much lower immunosuppressive properties than those with pathological activation (Cheng et al., 2008; Huang et al., 2014; Heine et al., 2017). Although the mandibular bone is not a pathological condition *per se*, it is closer to a pathological condition than the femoral bone since the oral cavity is frequently exposed to foreign substances. As alveolar bone is bearing mechanical loads, whose force is two times higher than that of long bones (Ehrlich and Lanyon, 2002), coupled with a recent data indicating that mechanical stimulation promotes activation of myeloid-derived monocytes (Lin et al., 2021), implies that occlusal forces might lead to the difference of the immune microenvironment between alveolar bone and long bone. Thus, it is likely that M-MDSCs from mandibular bone are more activated and participating in immune surveillance, which may explain why M-MDSCs from mandible shows higher immunosuppressive capabilities than M-MDSCs from long bone. These data support an new and perhaps underappreciated function of MDSCs in the maintenance of alveolar bone homeostasis.

Myeloid-derived suppressor cells, as potent immunosuppressive cell populations, inhibit immune responses through complex mechanisms (Gabrilovich and Nagaraj, 2009; Ma et al., 2018; Consonni et al., 2019; Groth et al., 2019). The most widely accepted mechanism for MDSCs' immunosuppressive ability by TGF-β, an immunosuppressive molecule, which can induce *Foxp3* expression in T cells (Chen et al., 2003; Fantini et al., 2004; Fu et al., 2004). Regulatory T cell also exhibits immunosuppression with various immunosuppressive molecules (Vignali et al., 2008). Based on this information, it is possible to postulate that mandibular M-MDSCs are more activated than in long bone M-MDSCs and induce regulatory T-cells by immunosuppressive molecules such as TGF-β to have stronger immunosuppressive properties. Indeed, we looked at mandibular M-MDSC transcriptomic profiles for *Tgfb* and other genes that would inhibit T-cell proliferation/function in our scRNAseq data set, but cell number and expression profile was too low to draw definitive conclusions (data not presented). This experimental limitation, due to number of mandibular bone M-MDSCs

in healthy mice, necessitates additional studies to determine the immunosuppressive mechanisms within homeostatic mandibular bone.

Several studies have shown that osteoclasts, including the dynamics of osteoclastogenesis, exhibit different characteristics between mandibular and long bone (Aghaloo et al., 2010; Faloni et al., 2011). In experiments to differentiate progenitor cells into osteoclasts, it was reported that progenitor cells within mandibular and long bone undergo distinct differentiation processes. When we examined differentially expressed genes in the two groups for the CMP and GMP clusters, we observed that mandibular bone marrow myeloid progenitor populations have distinct transcriptomic programs. Several differences in gene expression profiling suggest that there could be differences in the transcriptional program of these osteoclastic progenitors in homeostatic mandibular bone. Indeed, early stage osteoclast differentiation in mandibular bone showed more osteoclast-like cells compared to long bone with increased multinucleation with increased number of large osteoclasts having greater than 10 nuclei in alveolar bone, although no differences in resorptive capacity were noted (Faloni et al., 2011).

In summary, we provide reference data sets for cell populations in the mandibular bone compared to long bone by multiple cell analysis approaches. Our study provides the possibility that the nature myeloid directed immune response and cellular fate in both oral health and disease may be due to the myeloid heterogeneity of the mandibular bone. These studies indicate the mandibular bone has a distinct transcriptional landscape compared to femoral bone with MDSCs that exhibit a more immunosuppressive phenotype. This highlights the need to investigate site-specific immune response in mandibular bone marrow populations during both homeostasis as well as pathological conditions, including periodontitis. Through better appreciation of the unique myeloid lineage microenvironment in the mandibular bone, more precise immunomodulatory targets for the treatment of oral-specific diseases are envisioned.

DATA AVAILABILITY STATEMENT

The datasets presented in this study can be found in online repositories. The names of the repository/repositories and accession number(s) can be found below: https://www.ncbi.nlm.nih.gov/geo/query/acc.cgi?acc=GSE179152.

ETHICS STATEMENT

The animal study was reviewed and approved by the Animal Care and Use Committee protocol from the University at Buffalo using ARRIVE guidelines.

AUTHOR CONTRIBUTIONS

KHK performed the experiments and wrote the manuscript. NL, JB, EK, and LZ performed the experiments and edited the manuscript. SA and KLK designed the concept and all of the experiments and edited the manuscript. All authors contributed to the article and approved the submitted version.

FUNDING

This work was supported by the National Institutes of Health (NIH) grants, R01DE028258 and K18DE029526 (to KLK).

SUPPLEMENTARY MATERIAL

The Supplementary Material for this article can be found online at: https://www.frontiersin.org/articles/10.3389/fphys.2021.731549/full#supplementary-material

REFERENCES

Aghaloo, T. L., Chaichanasakul, T., Bezouglaia, O., Kang, B., Franco, R., Dry, S. M., et al. (2010). Osteogenic Potential of Mandibular vs. Long-bone Marrow Stromal Cells. *J. Dent. Res.* 89, 1293–1298. doi: 10.1177/0022034510378427

Akintoye, S. O., Lam, T., Shi, S. T., Brahim, J., Collins, M. T., and Robey, P. G. (2006). Skeletal site-specific characterization of orofacial and iliac crest human bone marrow stromal cells in same individuals. *Bone* 38, 758–768. doi: 10.1016/j.bone.2005.10.027

Alshetaiwi, H., Pervolarakis, N., McIntyre, L. L., Ma, D., Nguyen, Q., Rath, J. A., et al. (2020). Defining the emergence of myeloid-derived suppressor cells in breast cancer using single-cell transcriptomics. *Sci. Immunol.* 5:eaay6017. doi: 10.1126/sciimmunol.aay6017

Bronte, V., Brandau, S., Chen, S. H., Colombo, M. P., Frey, A. B., Greten, T. F., et al. (2016). Recommendations for myeloid-derived suppressor cell nomenclature and characterization standards. *Nat. Commun.* 7:12150. doi: 10.1038/ncomms12150

Chai, Y., and Maxson, R. E. (2006). Recent advances in craniofacial morphogenesis. *Dev. Dyn.* 235, 2353–2375. doi: 10.1002/dvdy.20833

Challen, G. A., Boles, N., Lin, K. K. Y., and Goodell, M. A. (2009). Mouse Hematopoietic Stem Cell Identification and Analysis. *Cytometry A* 75, 14–24. doi: 10.1002/cyto.a.20674

Chen, W., Jin, W., Hardegen, N., Lei, K. J., Li, L., Marinos, N., et al. (2003). Conversion of peripheral CD4+CD25- naive T cells to CD4+CD25+ regulatory T cells by TGF-beta induction of transcription factor Foxp3. *J. Exp. Med.* 198, 1875–1886. doi: 10.1084/jem.20030152

Cheng, P., Corzo, C. A., Luetteke, N., Yu, B., Nagaraj, S., Bui, M. M., et al. (2008). Inhibition of dendritic cell differentiation and accumulation of myeloid-derived suppressor cells in cancer is regulated by S100A9 protein. *J. Exp. Med.* 205, 2235–2249. doi: 10.1084/jem.20080132

Connizzo, B. K., Sun, L., Lacin, N., Gendelman, A., Solomonov, I., Sagi, I., et al. (2021). Nonuniformity in Periodontal Ligament: mechanics and Matrix Composition. *J. Dent. Res.* 100, 179–186. doi: 10.1177/00220345209624455

Consonni, F. M., Porta, C., Marino, A., Pandolfo, C., Mola, S., Bleve, A., et al. (2019). Myeloid-Derived Suppressor Cells: ductile Targets in Disease. *Front. Immunol.* 10:949. doi: 10.3389/fimmu.2019.00949

Crockett, J. C., Rogers, M. J., Coxon, F. P., Hocking, L. J., and Helfrich, M. H. (2011). Bone remodelling at a glance. *J. Cell Sci.* 124, 991–998. doi: 10.1242/jcs.063032

Damek-Poprawa, M., Stefanik, D., Levin, L. M., and Akintoye, S. O. (2010). Human bone marrow stromal cells display variable anatomic site-dependent response and recovery from irradiation. *Arch. Oral Biol.* 55, 358–364. doi: 10.1016/j.archoralbio.2010.03.010

Ehrlich, P. J., and Lanyon, L. E. (2002). Mechanical strain and bone cell function: a review. *Osteoporos. Int.* 13, 688–700. doi: 10.1007/s001980200095

Faloni, A. P. D., Schoenmaker, T., Azari, A., Katchburian, E., Cerri, P. S., de Vries, T. J., et al. (2011). Jaw and Long Bone Marrows Have a Different Osteoclastogenic Potential. *Calcif. Tissue Int.* 88, 63–74. doi: 10.1007/s00223-010-9418-4

Fantini, M. C., Becker, C., Monteleone, G., Pallone, F., Galle, P. R., and Neurath, M. F. (2004). Cutting edge: tGF-beta induces a regulatory phenotype in CD4+CD25- T cells through Foxp3 induction and down-regulation of Smad7. *J. Immunol.* 172, 5149–5153. doi: 10.4049/jimmunol.172.9.5149

Fu, S., Zhang, N., Yopp, A. C., Chen, D., Mao, M., Chen, D., et al. (2004). TGF-beta induces Foxp3 + T-regulatory cells from CD4 + CD25 - precursors. *Am. J. Transplant.* 4, 1614–1627. doi: 10.1111/j.1600-6143.2004.00566.x

Gabrilovich, D. I., and Nagaraj, S. (2009). Myeloid-derived suppressor cells as regulators of the immune system. *Nat. Rev. Immunol.* 9, 162–174. doi: 10.1038/nri2506

Groth, C., Hu, X., Weber, R., Fleming, V., Altevogt, P., Utikal, J., et al. (2019). Immunosuppression mediated by myeloid-derived suppressor cells (MDSCs) during tumour progression. *Br. J. Cancer* 120, 16–25. doi: 10.1038/s41416-018-0333-1

Gruber, R. (2019). Osteoimmunology: inflammatory osteolysis and regeneration of the alveolar bone. *J. Clin. Periodontol.* 46, 52–69. doi: 10.1111/jcpe.13056

Hathaway-Schrader, J. D., and Novince, C. M. (2021). Maintaining homeostatic control of periodontal bone tissue. *Periodontol* 86, 157–187. doi: 10.1111/prd.12368

Heine, A., Held, S. A. E., Schulte-Schrepping, J., Wolff, J. F. A., Klee, K., Ulas, T., et al. (2017). Generation and functional characterization of MDSC-like cells. *Oncoimmunology* 6:e1295203. doi: 10.1080/2162402X.2017.1295203

Huang, A., Zhang, B., Yan, W., Wang, B., Wei, H., Zhang, F., et al. (2014). Myeloid-derived suppressor cells regulate immune response in patients with chronic hepatitis B virus infection through PD-1-induced IL-10. *J. Immunol.* 193, 5461–5469. doi: 10.4049/jimmunol.1400849

Huja, S. S., Fernandez, S. A., Hill, K. J., and Li, Y. (2006). Remodeling dynamics in the alveolar process in skeletally mature dogs. *Anat. Rec. A Discov. Mol. Cell. Evol. Biol.* 288, 1243–1249. doi: 10.1002/ar.a.20396

Jiang, N., Chen, M., Yang, G., Xiang, L., He, L., Hei, T. K., et al. (2016). Hematopoietic Stem Cells in Neural-crest Derived Bone Marrow. *Sci. Rep.* 6:36411. doi: 10.1038/srep36411

Karaplis, A. (2002). Embryonic development of bone and the molecular regulation of intramembranous and endochondral bone formation. *Principle. Bone Biol.* 2002, 33–58. doi: 10.1016/b978-012098652-1/50105-0

Kirkwood, K. L., Zhang, L., Thiyagarajan, R., Seldeen, K. L., and Troen, B. R. (2018). Myeloid-Derived Suppressor Cells at the Intersection of Inflammaging and Bone Fragility. *Immunol. Invest.* 47, 844–854. doi: 10.1080/08820139.2018.1552360

Lamont, R. J., Koo, H., and Hajishengallis, G. (2018). The oral microbiota: dynamic communities and host interactions. *Nat. Rev. Microbiol.* 16, 745–759. doi: 10.1038/s41579-018-0089-x

Lerner, U. H., Kindstedt, E., and Lundberg, P. (2019). The critical interplay between bone resorbing and bone forming cells. *J. Clin. Periodontol.* 46, 33–51. doi: 10.1111/jcpe.13051

Li, Z., Lan, Y., He, W., Chen, D., Wang, J., Zhou, F., et al. (2012). Mouse embryonic head as a site for hematopoietic stem cell development. *Cell Stem Cell* 11, 663–675. doi: 10.1016/j.stem.2012.07.004

Lin, W., Li, Q., Zhang, D., Zhang, X., Qi, X., Wang, Q., et al. (2021). Mapping the immune microenvironment for mandibular alveolar bone homeostasis at single-cell resolution. *Bone Res.* 9:17. doi: 10.1038/s41413-021-00141-5

Ma, J., Xu, H., and Wang, S. (2018). Immunosuppressive Role of Myeloid-Derived Suppressor Cells and Therapeutic Targeting in Lung Cancer. *J. Immunol. Res.* 2018:6319649. doi: 10.1155/2018/6319649

Matsubara, T., Suardita, K., Ishii, M., Sugiyama, M., Igarashi, A., Oda, R., et al. (2005). Alveolar bone marrow as a cell source for regenerative medicine: differences between alveolar and iliac bone marrow stromal cells. *J. Bone Miner. Res.* 20, 399–409. doi: 10.1359/Jbmr.041117

Mavropoulos, A., Rizzoli, R., and Ammann, P. (2007). Different responsiveness of alveolar and tibial bone to bone loss stimuli. *J. Bone Miner. Res.* 22, 403–410. doi: 10.1359/Jbmr.061208

Netherby, C. S., Messmer, M. N., Burkard-Mandel, L., Colligan, S., Miller, A., Gomez, E. C., et al. (2017). The Granulocyte Progenitor Stage Is a Key Target of IRF8-Mediated Regulation of Myeloid-Derived Suppressor Cell Production. *J. Immunol.* 198, 4129–4139. doi: 10.4049/jimmunol.1601722

Oetjen, K. A., Lindblad, K. E., Goswami, M., Gui, G., Dagur, P. K., Lai, C., et al. (2018). Human bone marrow assessment by single-cell RNA sequencing, mass cytometry, and flow cytometry. *JCI Insight* 3:e124928. doi: 10.1172/jci.insight.124928

Paul, F., Arkin, Y., Giladi, A., Jaitin, D. A., Kenigsberg, E., Keren-Shaul, H., et al. (2016). Transcriptional Heterogeneity and Lineage Commitment in Myeloid Progenitors (vol 163, pg 1663, 2015). *Cell* 164, 325–325. doi: 10.1016/j.cell.2015.12.046

Ruggiero, S. L., Mehrotra, B., Rosenberg, T. J., and Engroff, S. L. (2004). Osteonecrosis of the jaws associated with the use of bisphosphonates: a review of 63 cases. *J. Oral Maxillofac. Surg.* 62, 527–534. doi: 10.1016/j.joms.2004.02.004

Sawant, A., Deshane, J., Jules, J., Lee, C. M., Harris, B. A., Feng, X., et al. (2013). Myeloid-derived suppressor cells function as novel osteoclast progenitors enhancing bone loss in breast cancer. *Cancer Res.* 73, 672–682. doi: 10.1158/0008-5472.CAN-12-2202

Seita, J., and Weissman, I. L. (2010). Hematopoietic stem cell: self-renewal versus differentiation. *Wiley Int. Rev. Syst. Biol. Med.* 2, 640–653. doi: 10.1002/wsbm.86

Shao, X., Liao, J., Lu, X. Y., Xue, R., Ai, N., and Fan, X. H. (2020). scCATCH: automatic Annotation on Cell Types of Clusters from Single-Cell RNA Sequencing Data. *Iscience* 23:100882. doi: 10.1016/j.isci.2020.100882

Simonds, W. F., James-Newton, L. A., Agarwal, S. K., Yang, B., Skarulis, M. C., Hendy, G. N., et al. (2002). Familial isolated hyperparathyroidism - Clinical and genetic characteristics of 36 kindreds. *Medicine* 81, 1–26. doi: 10.1097/00005792-200201000-00001

Stuart, T., Butler, A., Hoffman, P., Hafemeister, C., Papalexi, E., Mauck, W. M., et al. (2019). Comprehensive Integration of Single-Cell Data. *Cell* 177:1888. doi: 10.1016/j.cell.2019.05.031

Ueki, Y., Tiziani, V., Santanna, C., Fukai, N., Maulik, C., Garfinkle, J., et al. (2001). Mutations in the gene encoding c-Abl-binding protein SH3BP2 cause cherubism. *Nat. Genet.* 28, 125–126. doi: 10.1038/88832

Vignali, D. A., Collison, L. W., and Workman, C. J. (2008). How regulatory T cells work. *Nat. Rev. Immunol.* 8, 523–532. doi: 10.1038/nri2343

Yamaza, T., Ren, G., Akiyama, K., Chen, C., Shi, Y., and Shi, S. (2011). Mouse Mandible Contains Distinctive Mesenchymal Stem Cells. *J. Dent. Res.* 90, 317–324. doi: 10.1177/0022034510387796

Yanez, A., Ng, M. Y., Hassanzadeh-Kiabi, N., and Goodridge, H. S. (2015). IRF8 acts in lineage-committed rather than oligopotent progenitors to control neutrophil vs monocyte production. *Blood* 125, 1452–1459. doi: 10.1182/blood-2014-09-600833

Zhang, H., Huang, Y., Wang, S., Fu, R., Guo, C., Wang, H., et al. (2015). Myeloid-derived suppressor cells contribute to bone erosion in collagen-induced arthritis by differentiating to osteoclasts. *J. Autoimmun.* 65, 82–89. doi: 10.1016/j.jaut.2015.08.010

Conflict of Interest: The authors declare that the research was conducted in the absence of any commercial or financial relationships that could be construed as a potential conflict of interest.

Publisher's Note: All claims expressed in this article are solely those of the authors and do not necessarily represent those of their affiliated organizations, or those of the publisher, the editors and the reviewers. Any product that may be evaluated in this article, or claim that may be made by its manufacturer, is not guaranteed or endorsed by the publisher.

frontiers in Physiology

ORIGINAL RESEARCH
published: 04 October 2021
doi: 10.3389/fphys.2021.708905

Methylsulfonylmethane Increases the Alveolar Bone Density of Mandibles in Aging Female Mice

*Hanan Aljohani[1,2], Linda T. Senbanjo[1], Mohammed Al Qranei[1,3], Joseph P. Stains[4] and Meenakshi A. Chellaiah[1]**

[1] Department of Oncology and Diagnostic Sciences, School of Dentistry, University of Maryland, Baltimore, Baltimore, MD, United States, [2] Department of Oral Medicine and Diagnostics Sciences, School of Dentistry, King Saud University, Riyadh, Saudi Arabia, [3] Department of Preventive Dental Sciences, School of Dentistry, Imam Abdulrahman Bin Faisal University, Dammam, Saudi Arabia, [4] Department of Orthopedics, University of Maryland School of Medicine, Baltimore, MD, United States

OPEN ACCESS

Edited by:
Frédéric Lézot, Institut National de la Santé et de la Recherche Médicale (INSERM), France

Reviewed by:
Victor E. Arana-Chavez, University of São Paulo, Brazil
Francesco De Francesco, Azienda Ospedaliero Universitaria Ospedali Riuniti, Italy

***Correspondence:**
Meenakshi A. Chellaiah
mchellaiah@umaryland.edu

Specialty section:
This article was submitted to Craniofacial Biology and Dental Research, a section of the journal Frontiers in Physiology

Received: *12 May 2021*
Accepted: *06 September 2021*
Published: *04 October 2021*

Citation:
Aljohani H, Senbanjo LT, Al Qranei M, Stains JP and Chellaiah MA (2021) Methylsulfonylmethane Increases the Alveolar Bone Density of Mandibles in Aging Female Mice. Front. Physiol. 12:708905. doi: 10.3389/fphys.2021.708905

Methylsulfonylmethane (MSM) is a naturally occurring anti-inflammatory compound that effectively treats multiple degenerative diseases such as osteoarthritis and acute pancreatitis. Our previous studies have demonstrated the ability of MSM to differentiate stem cells from human exfoliated deciduous (SHED) teeth into osteoblast-like cells. This study examined the systemic effect of MSM in 36-week-old aging C57BL/6 female mice *in vivo* by injecting MSM for 13 weeks. Serum analyses showed an increase in expression levels of bone formation markers [osteocalcin (OCN) and procollagen type 1 intact N-terminal propeptide (P1NP)] and a reduction in bone resorption markers [tartrate-resistant acid phosphatase (TRAP) and C-terminal telopeptide of type I collag (CTX-I)] in MSM-injected animals. Micro-computed tomographic images demonstrated an increase in trabecular bone density in mandibles. The trabecular bone density tended to be higher in the femur, although the increase was not significantly different between the MSM- and phosphate-buffered saline (PBS)-injected mice. In mandibles, an increase in bone density with a corresponding decrease in the marrow cavity was observed in the MSM-injected mice. Furthermore, immunohistochemical analyses of the mandibles for the osteoblast-specific marker – OCN, and the mesenchymal stem cell-specific marker – CD105 showed a significant increase and decrease in OCN and CD105 positive cells, respectively. Areas of bone loss were observed in the inter-radicular region of mandibles in control mice. However, this loss was considerably decreased due to stimulation of bone formation in response to MSM injection. In conclusion, our study has demonstrated the ability of MSM to induce osteoblast formation and function *in vivo*, resulting in increased bone formation in the mandible. Hence, the application of MSM and stem cells of interest may be the right combination in alveolar bone regeneration under periodontal or other related diseases that demonstrate bone loss.

Keywords: osteoblasts, aging mice, bone formation, osteoclasts, methylsulfonylmethane

INTRODUCTION

Bone loss associated with osteoporosis represents a significant health care problem, and it is related to increased activation of osteoclast bone resorption function (Mundy, 2007; Khosla et al., 2012; Soysa and Alles, 2016; Cai et al., 2017). Many contributing factors can cause osteoporosis, and one such aspect is aging (Demontiero et al., 2012). Increased pro-inflammatory markers in older adults represent aging-related osteoporosis (Weitzmann and Pacifici, 2006; Pacifici, 2008). Increased inflammation in aged mammals is correlated with higher circulating pro-inflammatory cytokines than young adults (Abdelmagid et al., 2015). The reason is that increased circulating pro-inflammatory mediators could induce molecular changes in the periodontal tissue and exaggerate bone loss in older adults (Liang et al., 2010). In addition, tooth loss in older adults is linked with periodontal disease (Koduganti et al., 2009).

Experiments with animals and studies with humans have implicated pro-inflammatory cytokines (e.g., interleukin-1, tumor necrosis factor-alpha, and interleukin-6) as primary mediators of physiologic and pathological bone remodeling (Goldring, 2003). Chronic inflammation in aging is specified by increased inflammatory mediators, osteoclast activation, and bone loss. Furthermore, aging leads to underlying modifications in the differentiation of mesenchymal stem cells (MSCs) and therefore impaired osteoblast differentiation and bone formation (Abdelmagid et al., 2015). The deregulation of the balance between bone formation and bone resorption causes age-related osteoporosis. The deregulation is related to increase osteoclast formation and bone resorption and decrease osteoblast differentiation and bone formation. Appropriate alteration of the inflammatory condition is required for typical bone remodeling. Therefore, it is essential to identify a new anti-inflammatory agent to increase osteoblast function and bone formation.

Methylsulfonylmethane (MSM) is a naturally occurring organosulfur compound with several health benefits. It is a potent anti-inflammatory compound, which reduces chronic inflammation and relieves pain. It is used as a dietary supplement with glucosamine and chondroitin sulfate to treat arthritis (Usha and Naidu, 2004; Kim et al., 2006; Gregory et al., 2008; Lubis et al., 2017). An increase in pro-inflammatory cytokines (e.g., IL-6 and TNF-α) has been observed due to activation of the transcriptional factor NF-κB. It is worth noting that MSM reduced the expression of these cytokines by inhibiting NF-κB activity (Kim et al., 2009; Ahn et al., 2015). Moreover, MSM is a selective inhibitor of the NLRP3 inflammasome activation in human macrophages *in vitro*; analyses in mice corroborated this observation *in vivo* (Ahn et al., 2015).

Studies by others and we elucidated MSM's effect on bone formation using stem cells such as MSCs, human periodontal ligament stem cells (hPDLSCs), and stem cells from human exfoliated deciduous teeth (SHED) (Joung et al., 2012; Aljohani et al., 2019; Ha and Choung, 2020). MSM induces osteoblast differentiation *via* activating the JAK2/STAT5b pathway in MSCs (Joung et al., 2012). We found that MSM significantly increases transglutaminase-2 (TG-2) activity and its interaction with extracellular matrix (ECM) proteins such as collagen type 1 and osteopontin (Aljohani et al., 2019). An increase in the expression of osteogenic markers and mineralization by MSM in PDLSCs and SHED suggests that MSM is suitable not only for the inhibition of inflammatory-related events (Kim et al., 2009; Ahn et al., 2015) and diseases but also for increasing bone formation (Joung et al., 2012; Aljohani et al., 2019; Ha and Choung, 2020). *In vivo* analysis with hPDLSCs in calvarial defect and transplantation models indicate that MSM could be used with stem cells for bone regeneration *in vivo* (Ha and Choung, 2020). Mice naturally develop accelerated periodontal bone loss as a function of age (Liang et al., 2010). In addition, aging can cause bone loss in trabecular bone microarchitecture, leading to bone fracture and tooth loss (Huttner et al., 2009; Koduganti et al., 2009; Willinghamm et al., 2010; Eastell et al., 2016). Thus, we believed that the aging mouse model represents a genuinely chronic model to study possible periodontal tissue loss and restoration or remodeling mechanisms. Therefore, we proceeded to identify the effect of MSM on bone formation by osteoblasts in the aging mouse model. Here, we aim to relate the influence of MSM on the trabecular bone density of the femoral head to the mandible. Female C57BL/6 mice at 36 weeks of age were used for aging-related studies (Jilka, 2013). Histological and immunohistochemical analyses demonstrated that MSM could be an applicable osteogenic element in treating bone loss under inflammation, including aging and post-menopausal osteoporosis conditions.

MATERIALS AND METHODS

Osteoblast Studies

Cell Culture

MC3T3-E1 (mouse mesenchyme stem cells) and UMR-106 (rat osteoblast-like cells) were obtained from American Type Culture Collection (ATCC, Manassas, VA, United States). SHED were a kind gift from Dr. Jacques Nör (University of Michigan, Ann Arbor, MI, United States). Briefly, SHED were collected from exfoliated deciduous incisors of 7- to 8-year-old children. Guidelines set and approved by the National Institutes of Health Office of Human Subjects Research were followed during the isolation procedure (Bento et al., 2013). Briefly, the pulp from a remnant crown was digested in a solution containing 3 mg/ml collagenase type I and 4 mg/ml dispase (Worthington Biochem, Freehold, NJ, United States and Roche Molecular Biochemicals, Pleasanton, CA, United States, respectively) for 1 h at 37°C. After digestion, the solution was passed through a 70-μm strainer (Falcon) to obtain a single-cell suspension as described (Gronthos et al., 2000).

UMR-106 cells were cultured in DMEM media containing 10% FBS, 1% penicillin/streptomycin, and 0.05% Gentamicin. In contrast, MC3T3-E1 cells and SHED were maintained in α-minimal essential medium (MEM) with 10% fetal bovine serum and 1% penicillin/streptomycin. All cells were maintained at 37°C in 5% CO_2, and the media was changed every 3 days. For osteogenic differentiation, cells were incubated

with osteogenic medium (OM), consisting of osteogenic factors, such as 50 μM ascorbic acid, 5 mM β-glycerophosphate, and 0.05% Gentamicin. In addition, some cultures were treated with MSM in the basal medium (BM) with no osteogenic factors.

Alkaline Phosphatase Activity Analysis

Alkaline phosphatase (ALP) activity was measured using the colorimetric assay (Aljohani et al., 2019). Cells were seeded in a six-well plate in MSM (20 mM) presence or absence for 7 days, and lysates were made as described (Aljohani et al., 2019). An equal amount of protein was used in triplicates in a 96-well plate to measure the activity. The absorbance was measured (405 nm) in a microplate reader (Cytation3 image) with integrated imaging software (Gen5 version 2.09) after the addition of *p*-nitrophenyl phosphate (10 μl; Sigma, St. Louis, MO, United States) to each well.

Alizarin Red S Staining and Von Kossa Staining

UMR-106 cells seeded and incubated for 7 days in a six-well plate in the presence and absence of MSM (20 mM) were used to determine the effect of MSM on matrix mineralization. Cells without any MSM but grown in the OM were used as controls. Alizarin red S (ARS) is used to stain cells after washing with phosphate-buffered saline (PBS) three times. Absolute ethanol was used to fix the cells for 30 min at room temperature. After ethanol aspiration, 2% ARS solution was added to each well and processed as described previously (Aljohani et al., 2019). For Von Kossa staining, cells were washed with PBS three times and fixed with 10% paraformaldehyde for 10 min at room temperature. After the aspiration of fixative and washing with PBS, a 5% silver nitrate solution was used as described previously (Aljohani et al., 2019). Scanning the culture plates stained for ARS and Von Kossa was done in the scanner (EPSON Perfection V200). Nikon Eclipse TE 2000-inverted light microscope were used to obtain magnified images (10× objective).

Animals and Experimental Procedures

Thirty-six-week-old female C57BL6 mice weighing an average of 30 g were obtained from Charles River (MD, United States). Mice were maintained in the animal facility at the University of Maryland, Baltimore (School of Dentistry) animal care facility at room temperature (21 ± 1°C), with a 12 h light/12 h dark cycle. Pelleted mouse diet was fed *ad libitum*, and the mouse had free access to water. IACUC of the University of Maryland, Baltimore reviewed and approved the experimental procedures (approval number #417006, MD, United States). All experiments were performed under the relevant guidelines and regulations.

The mice were kept in the facility for a week for acclimatization before the injection. Mice were divided at random into two groups: a control group, injected with PBS (n = 6) as Group-1, and MSM injected mice (n = 6) as Group-2. Methylsulfonylmethane (PHR1346-1G, Sigma, St. Louis, MO, United States) was dissolved in PBS and injected subcutaneously (100 mg/kg) in a final volume of 100 μl. The injections were administered three times (i.e., alternate days) per week for 13 weeks. The animal weight was recorded every 4 weeks at the initial phase for 8 weeks and then after 3 and 2 weeks until the sacrifice time at 13 weeks. The mice were 49 weeks old at the time of sacrifice. Soft organs such as the heart, kidney, and liver have been isolated, and histological sections were prepared to assess any abnormalities caused by injections in these organs. Histological sections of these organs were stained with hematoxylin and eosin (H&E). Aperio ScanScope CS System (Vista, CA, United States) was used to scan the histological sections (bone and other tissues) (Aljohani et al., 2021). The assessment was performed blindly by a pathologist.

Bone Histology and Histomorphometry Analysis

Bone histomorphometry analysis was performed as described previously (Chellaiah et al., 2003; Aljohani et al., 2021). The tibia and mandibles were stained with H&E and tartrate-resistant acid phosphatase (TRAP) staining according to the manufacturer's protocols (Sigma, St. Louis, MO, United States). Stained sections were scanned and analyzed using the Aperio Scanscope CS instrument (Aperio Scanscope CS system, Vista, CA, United States). The number of TRAP-positive osteoclasts and cuboidal osteoblasts adherent to the bone surface were counted using the Fiji (ImageJ) software.

Immunohistochemistry Analyses in Bone Sections

Immunohistochemistry was performed as described (Gupta et al., 2012). After blocking the sections with the blocking solution (2.5% BSA or horse serum in PBS) for 60 min, at 4°C, the slides were incubated overnight at 4°C with the primary antibody (Abcam, Cambridge, MA, United States) of interest [e.g., OCN (rabbit polyclonal), or CD105 (Mouse monoclonal)] which was diluted (1:100) in blocking solution. After washing with PBS, the sections were then incubated with the corresponding secondary antibodies for 60 min. The slides were then washed and developed as previously described (Gupta et al., 2012). Finally, immunostained sections were scanned using an Aperio Scanscope CS instrument (Aperio Scanscope CS system, Vista, CA, United States).

Microcomputed Tomography Analysis

The femurs and mandibles were dissected from mice, and the soft tissues from the bones were removed. Bones were fixed in 4% paraformaldehyde for 2 days and then washed with PBS. Subsequently, bones were wrapped with gauze soaked in PBS and kept at 4°C. Three-dimensional microcomputed tomography (micro-CT) was performed on the femurs and mandibles (n = 6) using a Bruker Skyscan 1172 micro-CT scanner (Carteret, NJ, United States). Specimens were scanned with a 20 K resolution, 10 μm voxel size, 0.5 Al filter at 55 kV, and 167 μA, as described previously (Moorer et al., 2017). Bone morphology and microarchitecture were assessed at the distal femoral metaphysis in a region of interest (ROI) chosen for a range of 0.2–2.0 mm proximal to the

distal femoral growth plate. For the mandibles, the ROI was selected in the inter-radicular area of the first molar. The skeletal parameters assessed by micro-CT followed published nomenclature guidelines (Dempster et al., 2013).

Enzyme-Linked Immunosorbent Assay

Serum was separated from blood samples and frozen at −80°C until use. Serum markers of bone resorption (TRAP); (C-terminal telopeptide of type I collag, CTX-I) and of bone formation (osteocalcin, OCN); (procollagen type 1 intact N-terminal propeptide, P1NP), were measured in duplicate using enzyme-linked immunosorbent assay (ELISA) kits (Immunodiagnostics Systems, and LS-Bio Systems) according to the manufacturer's instructions. In addition, serum calcium levels were also measured using a calcium detection kit (Biovision, Inc., Milpitas, CA, United States).

Osteoclast Studies

Differentiation of Osteoclasts From RAW 264.7 Macrophage-Like Cell Line

Recombinant GST-RANKL was purified as described previously (Ma et al., 2010). Osteoclasts were generated from RAW 264.7 (ATCC® TIB-71™) cells as described (AlQranei et al., 2020). Mature multinucleated osteoclasts were observed from day three onward and used for various analyses.

Tartrate-Resistant Acid Phosphatase-Staining

For TRAP staining, undifferentiated macrophages were gently removed with a cell stripper solution, and multinucleated osteoclasts attached to the culture plates were used for staining as described previously (AlQranei et al., 2020). In brief, osteoclasts were fixed with 4% paraformaldehyde and washed three times with PBS. TRAP staining was done using the Leukocyte Acid Phosphatase Kit as described in the manufacturer's protocol (Sigma, St. Louis, MO, United States; 387-A). Stained cells were photographed, and the number of mature osteoclasts was measured using Cytation5 image reader with software (Gen5 version 2.09).

Dentine Resorption Assay

Dentine slices were processed as described previously (Chellaiah et al., 2000). After processing, dentine slices were incubated overnight at 37°C in a serum-free α-MEM medium. The next day, an osteoclast suspension containing 2×10^4 cells was gently added to the dentine slices. After adherence for 2 h, the culture media were replaced with serum-containing α-MEM containing RANKL with or without MSM at different concentrations (20 and 40 mM). After incubation for 48 h, dentine slices were processed and stained with acid hematoxylin (Sigma, St. Louis, MO, United States) for 6 min and washed well with water. Images of resorption pits were captured using a Nikon Eclipse TE 2000 inverted light microscope using a 20× and 40× objective (24).

Statistical Analysis

All data are presented as mean ± SEM. Student's *t*-test or Mann–Whitney *U* test was used to determine the statistical significance (Graph Pad Software, Graph Pad Inc., San Diego, CA, United States). The p-value < 0.05 is considered statistically significant.

RESULTS

Analysis of the Effect of Methylsulfonylmethane on Bone Mineralization *in vitro*

To demonstrate the effect of MSM on ALP activity, we used MC3T3-E1 and UMR-106 osteoblastic cell lines. Consistent with the observation shown in SHED (Aljohani et al., 2019), MSM increased ALP activity in these cells in the basal growth medium (BM) *in vitro*. This increase was equivalent to an OM containing osteogenic factors (**Supplementary Figure 1**).

Effects of Subcutaneous Injection of Methylsulfonylmethane on Body Weight Measurements and Soft Organs

We subsequently sought to determine the effect of MSM on bone formation *in vivo* using an aging mouse model. The injection was performed for 13 weeks, as described in section "Materials and Methods." During the injection period, the mice looked healthy and exhibited normal behavior. Some mice exhibited hair loss when they first arrived at our facility. However, after 6 weeks of injection with MSM, these mice displayed hair growth compared to the PBS-injected control group. At the end of the injection period of 13 weeks, the mice injected with PBS demonstrated hair loss patches (**Supplementary Figure 2A**, white arrows) compared to the MSM group. The hair loss was reduced, and hair growth was observed in MSM injected group (**Supplementary Figure 2A**). No severe abnormalities were observed in the mice injected with PBS or MSM at the end of the injection period. It was also observed that MSM did not affect body weight changes compared to the PBS-injected mice (**Supplementary Figure 2B**). In histological sections, all soft organs (heart, kidney, and liver) showed normal histology with no signs of damage, inflammation, or defects (**Supplementary Figure 3**).

Depiction of the Region of Interest Chosen for Microcomputed Tomography Analyses in Femoral and Mandibular Bones

A two-dimensional (2D) model of the bones dissected from the injected mice was performed using the micro-CT. The ROI used in the femur and mandible is shown in **Figure 1**. In the femur, the chosen ROI for the trabecular bone lies below the growth plate region (i.e., in the metaphyseal area), where the cancellous or trabecular bones are present. In the mandible, the ROI was chosen in the inter-radicular area between the first molar roots. As depicted in **Figure 1A**, blue brackets in the femur and squares inside the sagittal (**Figure 1B**) and coronal (**Figure 1C**) sections indicate the ROI for scanning in micro-CT.

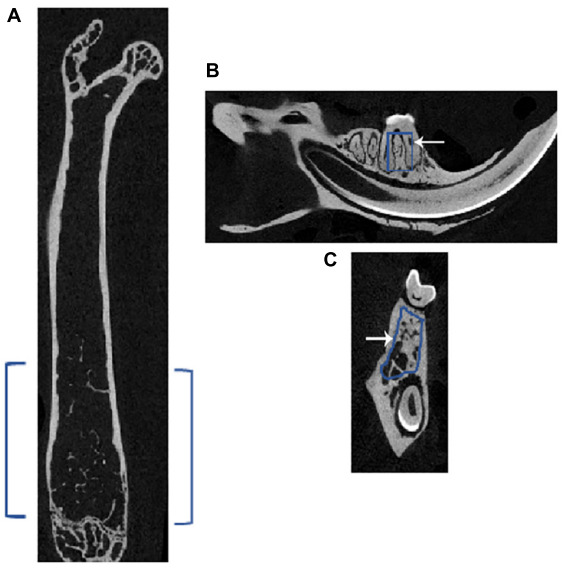

FIGURE 1 | Representative micro-CT image of a femur and mandible of a mouse showing the region of interest (ROI) for subsequent analyses. Micro-CT of **(A)** femur in the axial plane showing the selected ROI in blue brackets, and mandible shows the chosen ROI, outlined in blue in the **(B)** sagittal and **(C)** coronal sections; white arrow points to the outline. In the femur, the ROI for the trabecular bone lies just below the growth plate region, which is called the metaphyseal area, where cancellous or trabecular bones are present. In the mandible, the ROI was chosen in the inter-radicular area between the roots of the first molar.

Microcomputed Tomography Analyses in the Right Femurs of Mice Injected With Phosphate-Buffered Saline and Methylsulfonylmethane

Microcomputed tomography images partially reveal the trabecular bone microarchitecture and cortical bone morphology (**Figures 2A,B**). The 3D reconstruction of the bone (**Figure 2C**) provides the visualization of trabecular bone density in the ROI chosen for scanning (**Figure 1A**). Although trabecular bone density appeared to be more in MSM-injected mice (**Figure 2C**; right panel) than PBS-injected controls, statistical analyses showed no significant changes in the trabecular number (Tb. N) (**Figure 2E**). Bone volume to tissue volume (BV/TV) tended to be higher in the MSM-treated mice than the control mice (**Figures 2D–G**), but the difference was not statistically significant. There also were no significant changes in the Tb. N, trabecular thickness (Tb. Th), and trabecular separation or spacing (Tb. S) in mice injected with MSM compared with PBS controls (**Figures 2D–G**).

Microcomputed Tomography Analyses in the Mandible From Mice Injected With Phosphate-Buffered Saline and Methylsulfonylmethane

Microcomputed tomography scanning analyses of the alveolar bone of the mandibles showed a considerable increase in BV/TV, Tb. N, and Tb. Th accompanied by a decrease in the Tb. S in MSM-injected mice (**Figure 3**) compared with the PBS control mice. The ROI of the inter-radicular bone is projected with a blue rectangle in **Figure 1C**. Inter-radicular bones or septa are thin plates of bones that separate the roots of multi-rooted teeth. The 3D construction of inter-radicular bone is shown in **Figures 3C″,D″**. As can be seen, the bone density is higher in MSM-injected mice (**Figure 3D″**) compared to the control group. An increase was also observed in the inter-radicular bone of the mandible. These observations suggest that MSM can systematically induce bone formation, but its effect is more prominent in the bones in the mandibular region than in the long bones.

Morphometric Analysis of the Tibial and Mandibular Bone Sections

Methylsulfonylmethane injection appears to have increased the Tb. N in MSM-injected mice (**Figures 4B,B′,B″**) compared with PBS injected mice (**Figures 4A,A′,A″**). As detected by the micro-CT morphometry analyses, static histomorphometric measurements exhibited no significant femoral Tb. N or density changes in mice injected with MSM (**Figure 2**) compared to the control mice. Although no significant differences were noted in the number of the trabecular bone or its density, a considerable increase in the number of osteoblasts with no changes in the number of osteoclasts was observed between the two groups (**Figures 4C,D**).

As seen in the micro-CT analyses (**Figure 3D″**), TRAP-stained mandibular bone sections of MSM-injected mice also exhibited an increase in bone density and a decrease in the marrow cavity (**Figure 5B′**, arrow) as compared with PBS-injected mice. Although the marrow cavity is wider in PBS-injected mice (**Figure 5A′**, arrow), the osteoclast number is not significantly different in mice injected with PBS or MSM (**Figure 5C**). Thus, an increase in the marrow cavity in PBS-injected mice may result from increased osteoclast activity and decreased or normal osteoblast function. While these findings support the prominent effect of MSM in bone formation, further studies are needed to confirm the exact mechanism by which MSM exerts its osteoinductive effects. Furthermore, *in vitro* experiments with osteoclasts derived from RAW cells demonstrated that MSM did not affect osteoclast differentiation or function *in vitro* (**Supplementary Figure 4**).

Immunohistochemistry Analyses With Osteocalcin and CD105 Antibody

We then used the mandible sections for immunohistochemistry analyses with OCN, a biomarker for osteoblast activity, and CD105, a stem cell marker. Immunostained sections demonstrated an increase in bone density in the inter-radicular bone region of the mandible with a significant rise in OCN-positive bone cells and a decline in CD105 positive stem cells in MSM injected mice (**Figures 6,B,B′,C,D**). In addition, as compared with PBS-injected mice (**Figures 6A,A′**), the inter-radicular bone width (IRB) is more in MSM injected mice (**Figures 6B,B′**). Thus, these observations indicate that MSM

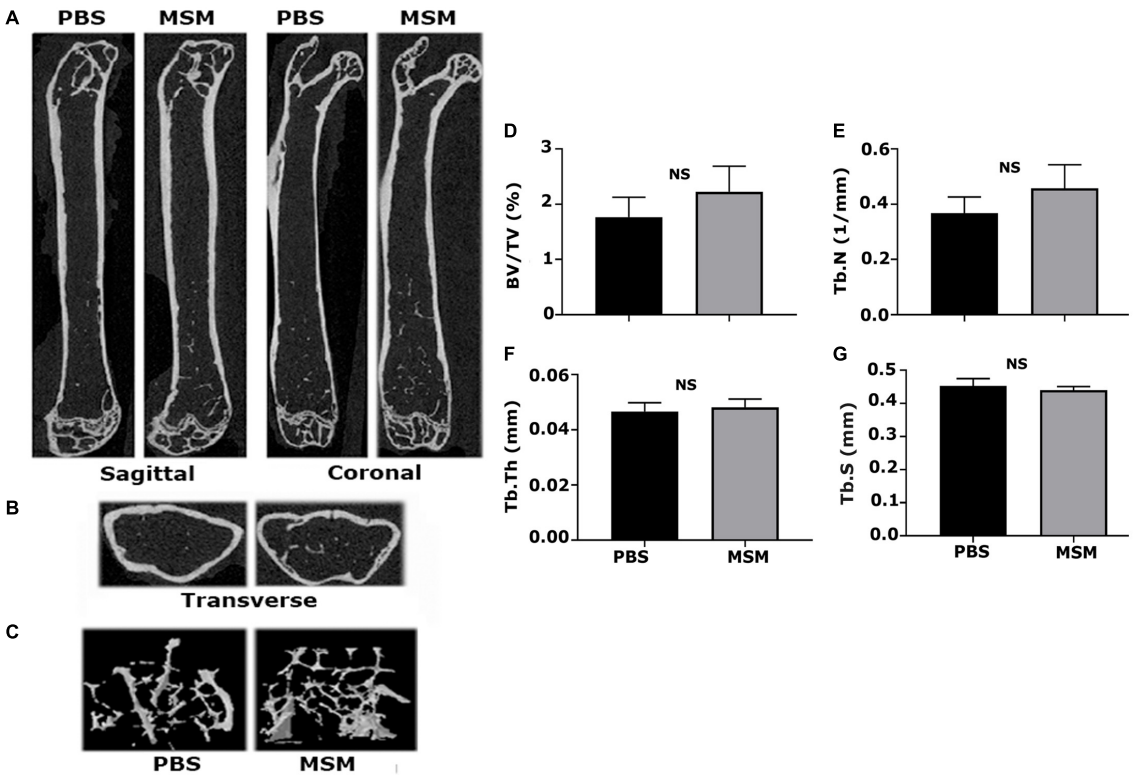

FIGURE 2 | Microcomputed tomography analysis of trabecular and cortical bone isolated from mice femurs injected with PBS and MSM. **(A)** Representative longitudinal sections of the femur are shown in two different planes, i.e., the sagittal and coronal, **(B)** The ROI indicated in **Figure 1** was used for transverse plane scanning, and **(C)** For three-dimensional (3D) construction. The micro-CT parameters were compared in six mice femurs injected with PBS and MSM. Statistical analyses were performed using the Mann–Whitney *U* test for morphometric parameters, including **(D)** bone volume to tissue volume (BV/TV), **(E)** trabecular number (Tb. N) and **(F)** trabecular thickness (Tb. Th), and **(G)** trabecular spacing (Tb. S), all shown as bar graphs. Data are shown as the mean ± SEM; NS, not statistically significant.

increases bone formation and the differentiation of CD105 positive stem cells into OCN-positive osteoblast-like cells.

Analysis of Serum Biomarkers for Bone Formation and Resorption by Enzyme-Linked Immunosorbent Assay

Serum was analyzed by ELISA for bone resorption (TRAP and CTX-I) and bone formation (OCN, P1NP) markers (**Figure 7**). An increase in osteoblast markers such as OCN and P1NP was observed in mice injected with MSM compared to PBS-injected mice (**Figures 7B,D**). Interestingly, we also detected a notable decrease in the levels of TRAP and CTX-I in the MSM-injected mice group as compared to the control group, which suggests that osteoclast activity may be reduced by MSM (**Figures 7A,C**) even though the osteoclast number was not significantly different between PBS- and MSM-injected mice (**Figure 5C**).

DISCUSSION

Our previous studies have shown that MSM influences the differentiation of SHED into osteoblast-like cells and their osteogenic potential. In SHED, TG-2 enzyme is involved in the cross-linking of ECM proteins (collagen and osteopontin) and the mineralization process *in vitro* in the presence of MSM (Aljohani et al., 2019). MC3T3 and UMR-106 cells are commonly used for *in vitro* studies. Validating the results of our earlier studies in SHED (Aljohani et al., 2019), here we showed that MSM increased ALP activity and mineralization in UMR-106 cells. Furthermore, besides MC3T3, SHED, and UMR-106 cells, MSM also increased the expression levels of osteogenic specific markers (ALP, osteopontin, OCN, RUNX2, and osterix) in hPDLSCs (Ha and Choung, 2020). We experimented with aging mice to comprehend whether *in vitro* findings of increased bone formation by MSM *in vitro* are also relevant *in vivo*. We performed a series of observations in aging mice, especially in the mandibular bone area, to elucidate whether MSM is an attractive therapeutic compound for the treatment of bone loss.

Bone loss occurs under conditions of periodontitis and osteoporosis, and both progress with increasing age (Jonasson and Rythen, 2016). Most clinical studies on the effects of human aging on periodontal tissues suggest a significant correlation between the aging and incidence of periodontal disease (Papapanou et al., 1989; Ismail et al., 1990; Haffajee et al., 1991; Huttner et al., 2009). MSM is commonly used as a supplement to treat arthritis and other inflammatory conditions

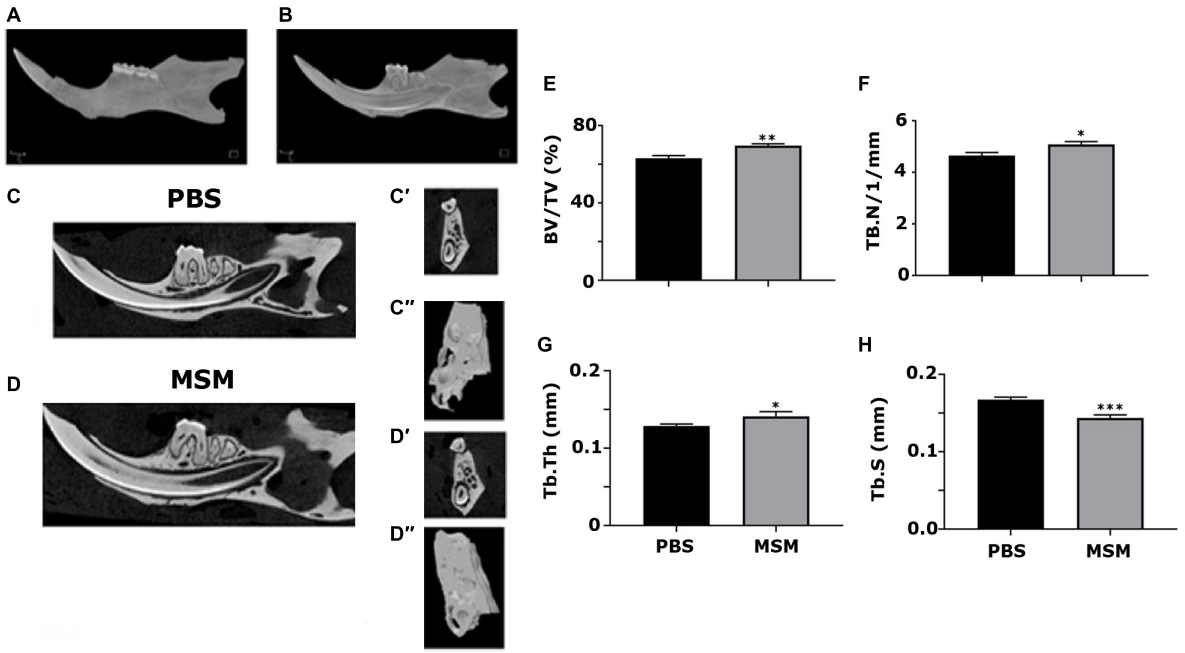

FIGURE 3 | Microcomputed tomography analysis of mandibular bone in mice injected with PBS and MSM. **(A,B)** A 3D construction of the **(A)** whole mandible and a sagittal section displaying the **(B)** teeth inside their respective sockets are shown. Representative sagittal **(C,D)** and coronal **(C′,D′)** planes of mandibles isolated from mice injected with **(C)** PBS and **(D)** MSM are shown. For the micro-CT scanning of the panels **(C′,D′,C″**, and **D″)**, the ROI outlined (blue) in the **(B)** sagittal and **(C)** coronal planes are shown in **Figure 1** were used. The micro-CT parameters were compared in six mice per group, and statistical analyses were performed using the Mann–Whitney *U* test for the indicated morphometric parameters **(E–H)**. The data are shown as mean ± SEM; $*p < 0.05$, $**p < 0.01$, $***p < 0.001$, vs. PBS-injected mice (BV/TV, bone volume-to-tissue volume; Tb. N, trabecular number; Tb, Th, trabecular thickness; Tb. S, trabecular spacing, or separation).

(Butawan et al., 2017). Aging itself has been considered a chronic inflammatory state (Gibon et al., 2017). Periodontal tissues of aged mice have increased inflammation and elevated alveolar bone loss compared to young mice (Liang et al., 2010). Therefore, we used the aging mice model to identify the effect of MSM on bone cells. Mice were injected with MSM subcutaneously for 13 weeks. Our study demonstrated more bone loss in control mice which is diminished in MSM injected mice in the mandibular region.

We then did a series of studies in aging mice and analyzed the bone by micro-CT and histomorphometry analyses. We determined the quantitative differences in PBS- and MSM-injected mice by measuring BV/TV, Tb. Th, trabecular spacing, and Tb. N. Although bone loss was observed in both long bones and mandibular bones due to aging in PBS-injected mice, bone formation by MSM was more significant in the mandibular bones than in long bones. Since MSM is an anti-inflammatory compound, injection of MSM may have reduced the inflammatory events in the mandibular area and improved bone density. Clark et al. reported depletion of macrophages in old mice resulted in decreased inflammatory cytokines within the gingiva and reduced bone loss (Clark et al., 2021).

Furthermore, as suggested by others, it may be due to the unique characteristics of collagen in the mandible compared to the long bones (Matsuura et al., 2014). The uniqueness may include a more significant amount of collagen with a smaller amount of mature cross-links and a lower extent of Lysine hydroxylation. These structures support the mandibular matrix's distinct interactions with bone remodeling cells, including osteoblasts, osteoclasts, and precursors (Matsuura et al., 2014). Moreover, the differentiation of osteoblasts occurs in optimal collagen cross-linking (Turecek et al., 2008). Studies have also shown that proteinases used for bone resorption in mandible displayed different properties from long bones (Azari et al., 2011; de Souza Faloni et al., 2011; Vermeer et al., 2013). Furthermore, the bone formation rate decreases with age in femoral bones, whereas it remains elevated in the jawbones (Huja and Beck, 2008). Nevertheless, irrespective of the mechanism, it is possible that the arrangement of collagen in mandibular bone may assist in bone remodeling *via* their interaction with bone remodeling cells. Therefore, the collagen matrix structure and its interaction with bone cells in the mandible may provide a notable difference in the remodeling process compared with long bones.

Studies have shown that inter-radicular bone loss is associated with the progression of bone loss in multirooted teeth in patients with chronic periodontitis (Desai and Shinde, 2012). Inter-radicular alveolar bone is exposed to occlusal stimuli and is often used for alveolar bone histomorphometry. Here, in the TRAP-stained mandibular bone sections, we have shown a significant bone loss in the inter-radicular bone region of PBS-injected mice (**Figures 5A,A′**); however, although the osteoclast number remains the same in both PBS- and MSM-injected mice, a considerable decrease in the bone loss was observed in MSM-injected mice (**Figures 5B,B′**). *In vitro* experiments with

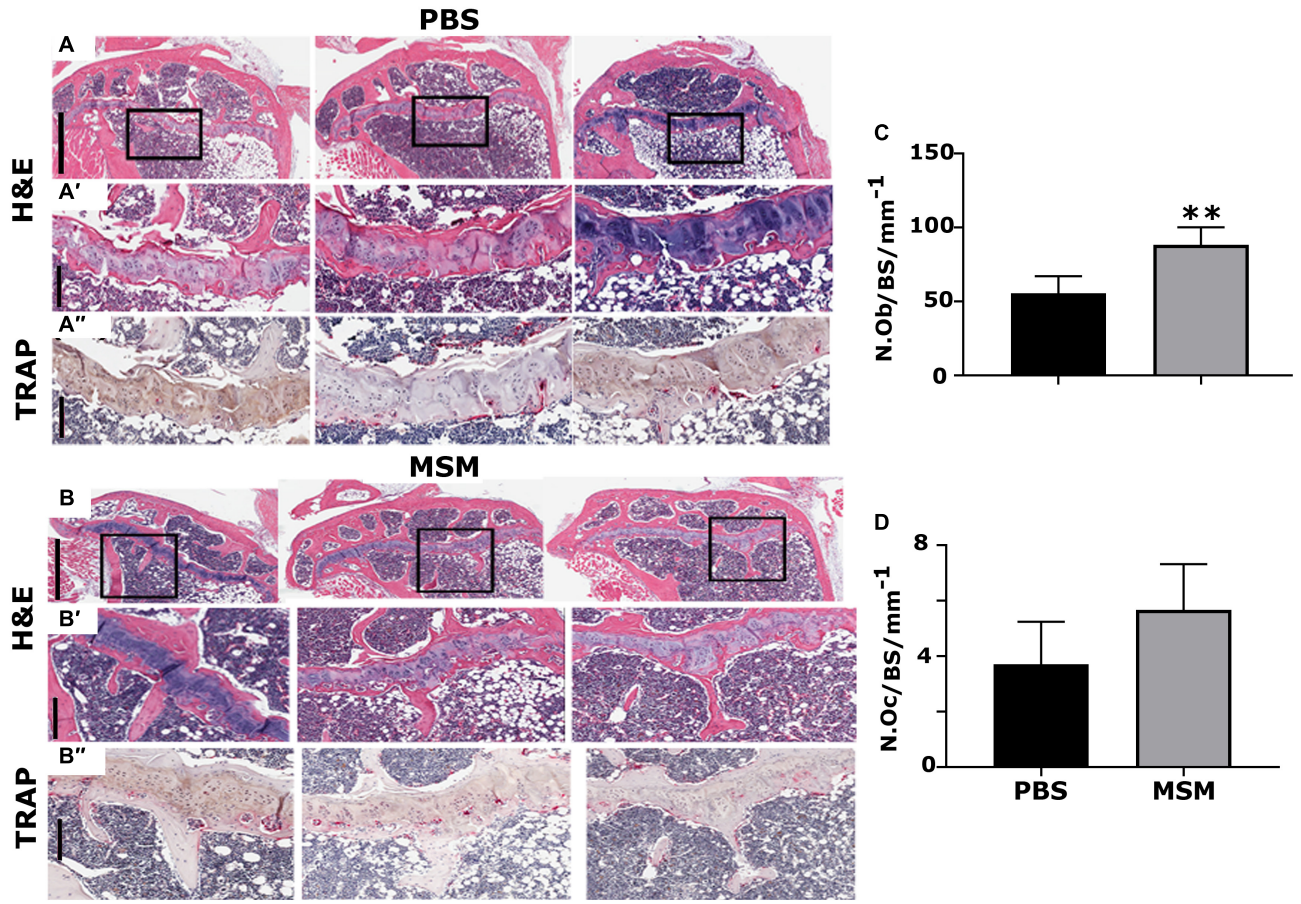

FIGURE 4 | Histological assessment of the proximal right tibial bone sections in mice injected with PBS **(A)** and MSM **(B)** for 13 weeks. **(A,A′,B,B′)** Hematoxylin and Eosin (H&E) stained and **(A″,B″)** TRAP-stained proximal right tibial sections are shown in triplicate for each injection. Black squares in panels **(A,B)** indicate the region enlarged in panels **(A′,B′)**. The same area of the magnified bone section stained for TRAP is shown in panels **(A″,B″)**. Dark purple-stained cells seen attached to the bone surface are TRAP-positive osteoclasts [panels in **(A″,B″)**]. Scale bars represent 800 μm in panels **(A,B)**; 200 μm in the magnified H&E **(A′,B′)** and TRAP- **(A′,B′)** stained panels. Quantification of the number of osteoblasts (N. Ob) and osteoclasts (N. Oc) was performed in the tibial metaphyseal bone surface (BS) region. Quantification was performed using the Fiji (ImageJ) software, and the results are shown as the mean ± SEM of six mice per injection. A standard Student's *t*-test was used to analyze *p*-values. $^{**}p < 0.01$.

osteoclasts also demonstrated no changes in osteoclast number in MSM untreated or treated osteoclasts. We then raised the question, Is this related to an increase in bone formation?

To further determine that MSM stimulated bone formation, we analyzed the serum for bone resorption (TRAP and CTX-1) and formation (OCN and P1NP) markers. Although MSM did not affect the bone resorption of osteoclasts from RAW cells *in vitro*, a significant decrease in the bone resorption markers was observed in the serum of mice injected with MSM compared with PBS-injected mice. The levels of TRAP and CTX1 represent the measurement of enzymes and peptides released during bone resorption. As indicated by others (Milne et al., 2009), serum phosphatase levels (TRAP) can be used as an alternative measure to validate osteoclast activity. We found that MSM can reduce bone resorption. The measurement of serum levels of P1NP is precisely comparative to the amount of new collagen produced by osteoblasts. Osteocalcin level is a valid marker of bone formation and represents osteoid formation rather than mineralized bone formation. Both P1NP and OCN are currently the best and widely used indicators of bone formation (Melkko et al., 1996; Huja and Beck, 2008; Chavassieux et al., 2015). In addition to reducing bone resorption by osteoclasts, an increase in bone formation by osteoblasts may have contributed to the rise in bone density in the inter-radicular bone region of the bone.

Consistent with an increase in serum levels of OCN, immunohistochemistry analyses also displayed more OCN-positive cells in the mandibular area. The intriguing observation in the immunohistochemistry analyses is a decrease in CD105 positive cells and a corresponding increase in OCN-positive cells in the mandibular bone sections of MSM-injected mice. Several types of stem cells (DPSCs, SHED, PDLSCs, SCAPs, and DFPCs) are present in the dental tissue (Gronthos et al., 2000; Sonoyama et al., 2006, 2008; Morsczeck et al., 2009; Morsczeck and Schmalz, 2010; Morsczeck, 2015), and these stem cells can provide novel therapies in dentistry and support bone formation *in vitro* and *in vivo*. The expression of CD105 (aka endoglin)

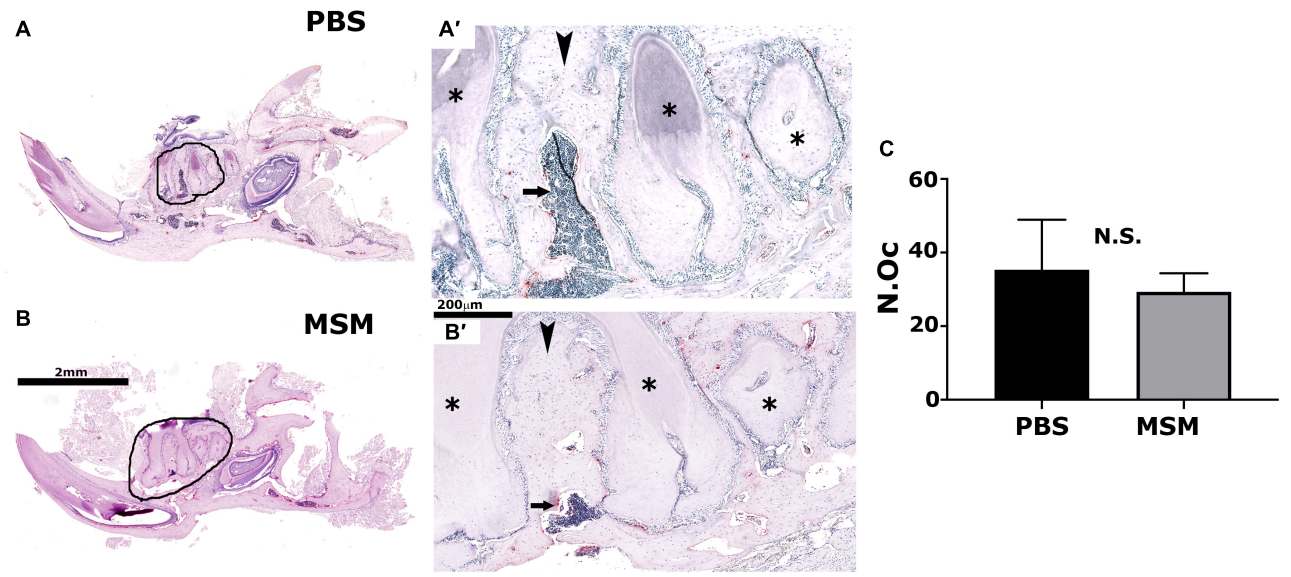

FIGURE 5 | Tartrate-resistant acid phosphatase-stained mandible bone sections in mice injected with PBS **(A)** and MSM **(B)**. Representative TRAP-stained mandible sections for each injection are shown. Black circles in panels **(A,B)** indicate an enlarged view of the bone section in panels **(A′,B′)**. Arrowheads and arrows point to the inter-radicular bone and the bone marrow cavity, respectively, in PBS- and MSM-injected mice. Asterisks (*) denote the dentine of adjacent teeth roots. Scale bars: 2 mm in panels **(A,B)** and 200 μm in panels **(A′,B′)**. Quantification of the number of osteoclasts (N.Oc) **(C)** was performed in six mice per group using Fiji software (ImageJ). A standard Student's *t*-test was used to analyze the data. The number of osteoclasts was not significantly (NS) different between the experimental groups tested.

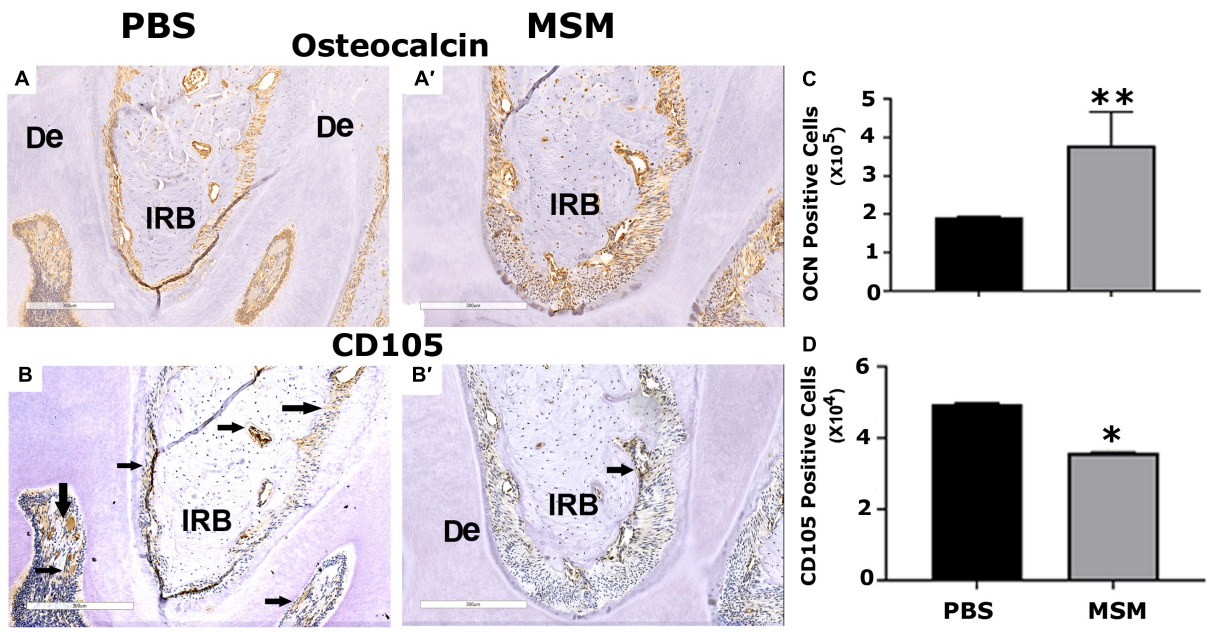

FIGURE 6 | Immunohistochemistry analysis in mandible sections. Bone sections were stained with an antibody against **(A,B)** OCN or **(A′,B′)** CD105. Inter-radicular bone and dentine are abbreviated as IRB and De; arrows point to cells stained for CD105 **(A′,B′)**. Quantification of **(C)** OCN- and **(D)** CD105-positive cells was performed using Fiji (ImageJ) software, and the results are shown as the mean ± SEM of six mice per injection. A standard Student's *t*-test was used to analyze *p*-values. $^{**}p < 0.01$ and $^{*}p < 0.05$. Scale bar: 300 μm.

in MSC is necessary for self-renewal. These cells are shown to form bone *in vivo* and are a promising tool for bone regeneration (Aslan et al., 2006). A decrease in CD105 positive cells and a corresponding increase in OCN-positive osteoblast-like cells in MSM-injected mice strongly suggest that MSM can induce osteogenic differentiation of stem cells *in vivo*. Future studies will

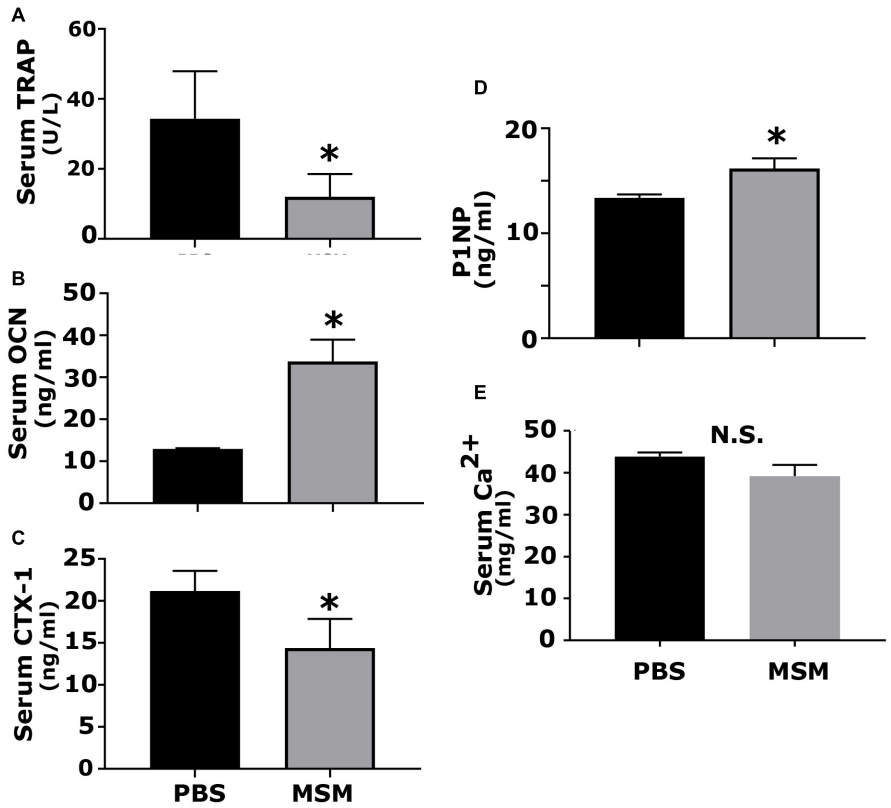

FIGURE 7 | Analysis of the serum levels of indicated biomarkers of bone formation and resorption in mice injected with PBS and MSM. The serum levels of **(A)** TRAP, **(B)** OCN, **(C)** CTX-I, **(D)** P1NP, and **(E)** calcium were measured using ELISA kits. Serum from six mice per injection was used for the analyses, and each analysis was performed in triplicates. The results are presented as mean ± SEM; standard Student's *t*-test was used to analyze the *p*-value; $*p < 0.05$; N.S., not statistically significant.

evaluate the mechanism and potential of CD105 positive cells to differentiate into osteoblast-like cells in the presence of MSM.

We showed in this study the initial characterization of the effects of MSM on bone formation in aging mice. Yet, we recognize that this study has limitations, and our future studies will address these limitations. More specifically, our further investigation includes analyzing the effects of MSM on: (1) bone formation using dynamic histomorphometry as shown previously (Jilka et al., 1996; Weinstein et al., 1997; Chellaiah et al., 2000) and (2) the differentiation of CD105 positive cells into OCN-positive osteoclast-like cells *in vitro* and *in vivo*. *In vitro* analysis will also focus on the molecular mechanisms by which MSM induces the osteogenic differentiation of stem cells (SHED) and increases bone formation. For example, is there any role for the Wnt pathway to stimulate the differentiation of SHED into osteoblast-like cells and bone formation?

CONCLUSION

Based on histomorphometry, micro-CT, biochemical, and immunohistochemistry analyses, we have found that MSM increases bone formation in the inter-radicular region of the mandible of the aging mice. Furthermore, OCN-positive osteoblast-like cells were more in the inter-radicular areas of bone, where more bone density was observed. A decrease in CD105 positive stem cells with a concomitant increase in osteoblast-like cells suggests that MSM can induce the differentiation process *in vivo* based on the needs. Although these findings additionally support the bone remodeling effect of MSM, more studies are necessary to identify the molecular mechanisms involved in this differentiation process *in vitro* and *in vivo*. We suggest that the therapeutic effect of MSM on bone loss could go beyond alveolar bone loss that occurs in periodontitis Studies have shown that estrogen loss promotes continual inflammation, which supports post-menopausal osteoporosis (PMO). Pro-inflammatory cytokines (e.g., TNF-alpha and IL-17A) contribute to osteoclast activation and bone loss in PMO. Thus, the potent anti-inflammatory MSM can be used as a therapeutic agent to improve bone loss-associated diseases, including periodontitis, PMO, and rheumatoid arthritis.

DATA AVAILABILITY STATEMENT

The original contributions presented in the study are included in the article/**Supplementary Material**, further inquiries can be directed to the corresponding author.

ETHICS STATEMENT

The experimental procedures were reviewed and approved by the Institutional Animal Care and Use Committee of the University of Maryland, Baltimore (approval number #417006, MD, United States). All experiments were performed under the relevant guidelines and regulations.

AUTHOR CONTRIBUTIONS

MC and HA were involved in the conceptualization, data curation, and formal analyses. HA performed the injections and maintained the animals. She also collected the tissues (blood, liver, heart, kidney, and bones) for various studies and serum to analyze biomarkers for bone resorption and bone formation by ELISA. LS and MA performed IHC staining and osteoclast studies, respectively. HA and JS conducted micro-CT scanning, data analyses, and computations. MC also completed funding acquisition, project administration, resources, supervision, validation, and writing the original draft. All authors contributed to the article and approved the submitted version.

FUNDING

The National Institutes of Health supported the research reported in this publication (NIH) grants under Award Number R01 AR066044 to MC.

ACKNOWLEDGMENTS

We thank Crystal Idleburg (Research Specialist, Washington University School of Medicine, Orthopedic Surgery Research, St. Louis, MO, United States) for assistance with the decalcification, sectioning, and staining (H&E and TRAP) of long bones and mandibles. In addition, we would like to thank Editage (http://www.editage.com) for editing and reviewing this manuscript for the English language.

SUPPLEMENTARY MATERIAL

The Supplementary Material for this article can be found online at: https://www.frontiersin.org/articles/10.3389/fphys.2021.708905/full#supplementary-material

REFERENCES

Abdelmagid, S. M., Barbe, M. F., and Safadi, F. F. (2015). Role of inflammation in the aging bones. *Life Sci.* 123, 25–34. doi: 10.1016/j.lfs.2014.11.011

Ahn, H., Kim, J., Lee, M. J., Kim, Y. J., Cho, Y. W., and Lee, G. S. (2015). Methylsulfonylmethane inhibits NLRP3 inflammasome activation. *Cytokine* 71, 223–231. doi: 10.1016/j.cyto.2014.11.001

Aljohani, H., Senbanjo, L. T., and Chellaiah, M. A. (2019). Methylsulfonylmethane increases osteogenesis and regulates the mineralization of the matrix by transglutaminase 2 in SHED cells. *PLoS One* 14:e0225598. doi: 10.1371/journal.pone.0225598

Aljohani, H., Stains, J. P., Majumdar, S., Srinivasan, D., Senbanjo, L., and Chellaiah, M. A. (2021). Peptidomimetic inhibitor of L-plastin reduces osteoclastic bone resorption in aging female mice. *Bone Res.* 9:22. doi: 10.1038/s41413-020-00135-9

AlQranei, M. S., Aljohani, H., Majumdar, S., Senbanjo, L. T., and Chellaiah, M. A. (2020). C-phycocyanin attenuates RANKL-induced osteoclastogenesis and bone resorption in vitro through inhibiting ROS levels, NFATc1 and NF-kappaB activation. *Sci. Rep.* 10:2513. doi: 10.1038/s41598-020-59363-y

Aslan, H., Zilberman, Y., Kandel, L., Liebergall, M., Oskouian, R. J., Gazit, D., et al. (2006). Osteogenic differentiation of noncultured immunoisolated bone Marrow-Derived CD105+ cells. *Stem Cells* 24, 1728–1737. doi: 10.1634/stemcells.2005-0546

Azari, A., Schoenmaker, T., de Souza Faloni, A. P., Everts, V., and de Vries, T. J. (2011). Jaw and long bone marrow-derived osteoclasts differ in shape and their response to bone and dentin. *Biochem. Biophys. Res. Commun.* 409, 205–210. doi: 10.1016/j.bbrc.2011.04.120

Bento, L. W., Zhang, Z., Imai, A., Nor, F., Dong, Z., Shi, S., et al. (2013). Endothelial differentiation of SHED requires MEK1/ERK signaling. *J. Dent. Res.* 92, 51–57. doi: 10.1177/0022034512466263

Butawan, M., Benjamin, R. L., and Bloomer, R. J. (2017). Methylsulfonylmethane: applications and safety of a novel dietary supplement. *Nutrients* 9:290. doi: 10.3390/nu9030290

Cai, M., Yang, L., Zhang, S., Liu, J., Sun, Y., and Wang, X. (2017). A bone-resorption surface-targeting nanoparticle to deliver anti-miR214 for osteoporosis therapy. *Int. J. Nanomed.* 12, 7469–7482. doi: 10.2147/IJN.S139775

Chavassieux, P., Portero-Muzy, N., Roux, J. P., Garnero, P., and Chapurlat, R. (2015). Are biochemical markers of bone turnover representative of bone histomorphometry in 370 postmenopausal women? *J. Clin. Endocrinol. Metab.* 100, 4662–4668. doi: 10.1210/jc.2015-2957

Chellaiah, M., Kizer, N., Silva, M., Alvarez, U., Kwiatkowski, D., and Hruska, K. A. (2000). Gelsolin deficiency blocks podosome assembly and produces increased bone mass and strength. *J. Cell Biol.* 148, 665–678.

Chellaiah, M. A., Kizer, N., Biswas, R., Alvarez, U., Strauss-Schoenberger, J., Rifas, L., et al. (2003). Osteopontin deficiency produces osteoclast dysfunction due to reduced CD44 surface expression. *Mol. Biol. Cell* 14, 173–189.

Clark, D., Halpern, B., Miclau, T., Nakamura, M., Kapila, Y., and Marcucio, R. (2021). The contribution of macrophages in old mice to periodontal disease. *J. Dent. Res. [Online ahead of print]* 220345211009463. doi: 10.1177/00220345211009463

de Souza Faloni, A. P., Schoenmaker, T., Azari, A., Katchburian, E., Cerri, P. S., de Vries, T. J., et al. (2011). Jaw and long bone marrows have a different osteoclastogenic potential. *Calcif Tissue Int.* 88, 63–74. doi: 10.1007/s00223-010-9418-4

Demontiero, O., Vidal, C., and Duque, G. (2012). Aging and bone loss: new insights for the clinician. *Ther. Adv. Musculoskelet. Dis* 4, 61–76. doi: 10.1177/1759720X11430858

Dempster, D. W., Compston, J. E., Drezner, M. K., Glorieux, F. H., Kanis, J. A., Malluche, H., et al. (2013). Standardized nomenclature, symbols, and units for bone histomorphometry: a 2012 update of the report of the ASBMR Histomorphometry Nomenclature Committee. *J. Bone Miner. Res.* 28, 2–17. doi: 10.1002/jbmr.1805

Desai, S., and Shinde, H. (2012). Correlation of interdental and interradicular bone loss in patients with chronic periodontitis: a clinical and radiographic study. *Nigerian J. Clin. Practice* 15, 125–131. doi: 10.4103/1119-3077.97280

Eastell, R., O'Neill, T. W., Hofbauer, L. C., Langdahl, B., Reid, I. R., Gold, D. T., et al. (2016). Post-menopausal osteoporosis. *Nat. Rev. Dis. Primers* 2:16069. doi: 10.1038/nrdp.2016.69

Gibon, E., Lu, L. Y., Nathan, K., and Goodman, S. B. (2017). Inflammation, ageing, and bone regeneration. *J. Orthop. Translat.* 10, 28–35. doi: 10.1016/j.jot.2017.04.002

Goldring, S. R. (2003). Inflammatory mediators as essential elements in bone remodeling. *Calcif Tissue Int.* 73, 97–100. doi: 10.1007/s00223-002-1049-y

Gregory, P. J., Sperry, M., and Wilson, A. F. (2008). Dietary supplements for osteoarthritis. *Am. Fam. Physician* 77, 177–184.

Gronthos, S., Mankani, M., Brahim, J., Robey, P. G., and Shi, S. (2000). Postnatal human dental pulp stem cells (DPSCs) in vitro and in vivo. *Proc. Natl. Acad. Sci. U.S.A.* 97, 13625–13630. doi: 10.1073/pnas.240309797

Gupta, A., Cao, W., and Chellaiah, M. A. (2012). Integrin avb3 and CD44 pathways in metastatic prostate cancer cells support osteoclastogenesis via RUNX2/Smad5/RANKL signaling axis. *Mol. Cancer* 11:66. doi: 10.1186/1476-4598-11-66

Ha, S. H., and Choung, P. H. (2020). MSM promotes human periodontal ligament stem cells differentiation to osteoblast and bone regeneration. *Biochem. Biophys. Res. Commun.* 528, 160–167. doi: 10.1016/j.bbrc.2020.05.097

Haffajee, A. D., Socransky, S. S., Lindhe, J., Kent, R. L., Okamoto, H., and Yoneyama, T. (1991). Clinical risk indicators for periodontal attachment loss. *J. Clin. Periodontol.* 18, 117–125. doi: 10.1111/j.1600-051x.1991.tb01700.x

Huja, S. S., and Beck, F. M. (2008). Bone remodeling in maxilla, mandible, and femur of young dogs. *Anat Rec. (Hoboken)* 291, 1–5. doi: 10.1002/ar.20619

Huttner, E. A., Machado, D. C., Oliveira, R. B., Antunes, A. G. F., and Hebling, E. (2009). Effects of human aging on periodontal tissues. *Spec. Care Dent.* 29, 149–155.

Ismail, A. I., Morrison, E. C., Burt, B. A., Caffesse, R. G., and Kavanagh, M. T. (1990). Natural history of periodontal disease in adults: findings from the Tecumseh Periodontal Disease Study, 1959-87. *J. Dent. Res.* 69, 430–435. doi: 10.1177/00220345900690020201

Jilka, R. L. (2013). The relevance of mouse models for investigating age-related bone loss in humans. *J. Gerontol. A Biol. Sci. Med. Sci.* 68, 1209–1217. doi: 10.1093/gerona/glt046

Jilka, R. L., Weinstein, R. S., Takahashi, K., Parfitt, A. M., and Manolagas, S. C. (1996). Linkage of decreased bone mass with impaired osteoblastogenesis in a murine model of accelerated senescence. *J. Clin. Invest* 97, 1732–1740.

Jonasson, G., and Rythen, M. (2016). Alveolar bone loss in osteoporosis: a loaded and cellular affair? *Clin. Cosmet Investig. Dent.* 8, 95–103. doi: 10.2147/CCIDE.S92774

Joung, Y. H., Lim, E. J., Darvin, P., Chung, S. C., Jang, J. W., Do, P. K., et al. (2012). MSM enhances GH signaling via the Jak2/STAT5b pathway in osteoblast-like cells and osteoblast differentiation through the activation of STAT5b in MSCs. *PLoS. One* 7:e47477. doi: 10.1371/journal.pone.0047477

Khosla, S., Oursler, M. J., and Monroe, D. G. (2012). Estrogen and the skeleton. *Trends Endocrinol. Metab.* 23, 576–581. doi: 10.1016/j.tem.2012.03.008

Kim, L. S., Axelrod, L. J., Howard, P., Buratovich, N., and Waters, R. F. (2006). Efficacy of methylsulfonylmethane (MSM) in osteoarthritis pain of the knee: a pilot clinical trial. *Osteoarthritis Cartilage* 14, 286–294. doi: 10.1016/j.joca.2005.10.003

Kim, Y. H., Kim, D. H., Lim, H., Baek, D. Y., Shin, H. K., and Kim, J. K. (2009). The anti-inflammatory effects of methylsulfonylmethane on lipopolysaccharide-induced inflammatory responses in murine macrophages. *Biol. Pharm. Bull.* 32, 651–656. doi: 10.1248/bpb.32.651

Koduganti, R. R., Gorthi, C., Reddy, P. V., and Sandeep, N. (2009). Osteoporosis: "A risk factor for periodontitis". *J. Ind. Soc. Periodontol.* 13, 90–96.

Liang, S., Hosur, K. B., Domon, H., and Hajishengallis, G. (2010). Periodontal inflammation and bone loss in aged mice. *J. Periodontal. Res.* 45, 574–578. doi: 10.1111/j.1600-0765.2009.01245.x

Lubis, A. M. T., Siagian, C., Wonggokusuma, E., Marsetyo, A. F., and Setyohadi, B. (2017). Comparison of glucosamine-chondroitin sulfate with and without methylsulfonylmethane in grade I-II knee osteoarthritis: a double blind randomized controlled trial. *Acta Med. Indones* 49, 105–111.

Ma, T., Sadashivaiah, K., and Chellaiah, M. A. (2010). Regulation of sealing ring formation by L-plastin and cortactin in osteoclasts. *J. Biol. Chem* 285, 29911–29924.

Matsuura, T., Tokutomi, K., Sasaki, M., Katafuchi, M., Mizumachi, E., and Sato, H. (2014). Distinct characteristics of mandibular bone collagen relative to long bone collagen: relevance to clinical dentistry. *BioMed. Res. Int.* 2014:769414. doi: 10.1155/2014/769414

Melkko, J., Kauppila, S., Niemi, S., Risteli, L., Haukipuro, K., Jukkola, A., et al. (1996). Immunoassay for intact amino-terminal propeptide of human type I procollagen. *Clin. Chem.* 42(Pt 1), 947–954.

Milne, T. J., Ichim, I., Patel, B., McNaughton, A., and Meikle, M. C. (2009). Induction of osteopenia during experimental tooth movement in the rat: alveolar bone remodelling and the mechanostat theory. *Eur. J. Orthod.* 31, 221–231. doi: 10.1093/ejo/cjp032

Moorer, M. C., Hebert, C., Tomlinson, R. E., Iyer, S. R., Chason, M., and Stains, J. P. (2017). Defective signaling, osteoblastogenesis and bone remodeling in a mouse model of connexin 43 C-terminal truncation. *J. Cell Sci.* 130, 531–540. doi: 10.1242/jcs.197285

Morsczeck, C. (2015). Molecular mechanisms in dental follicle precursor cells during the osteogenic differentiation. *Histol. Histopathol.* 30, 1161–1169. doi: 10.14670/HH-11-634

Morsczeck, C., Frerich, B., and Driemel, O. (2009). Dental stem cell patents. *Recent Pat. DNA Gene Seq.* 3, 39–43. doi: 10.2174/187221509787236200

Morsczeck, C., and Schmalz, G. (2010). Transcriptomes and proteomes of dental follicle cells. *J. Dent. Res.* 89, 445–456. doi: 10.1177/0022034510366899

Mundy, G. R. (2007). Osteoporosis and inflammation. *Nutr. Rev.* 65(Pt 2), S147–S151.

Pacifici, R. (2008). Estrogen deficiency, T cells and bone loss. *Cell Immunol* 252, 68–80.

Papapanou, P. N., Wennstrom, J. L., and Grondahl, K. (1989). A 10-year retrospective study of periodontal disease progression. *J. Clin. Periodontol.* 16, 403–411. doi: 10.1111/j.1600-051x.1989.tb01668.x

Sonoyama, W., Liu, Y., Fang, D., Yamaza, T., Seo, B. M., Zhang, C., et al. (2006). Mesenchymal stem cell-mediated functional tooth regeneration in swine. *PLoS One* 1:e79. doi: 10.1371/journal.pone.0000079

Sonoyama, W., Liu, Y., Yamaza, T., Tuan, R. S., Wang, S., Shi, S., et al. (2008). Characterization of the apical papilla and its residing stem cells from human immature permanent teeth: a pilot study. *J. Endod.* 34, 166–171. doi: 10.1016/j.joen.2007.11.021

Soysa, N. S., and Alles, N. (2016). Osteoclast function and bone-resorbing activity: an overview. *Biochem. Biophys. Res. Commun* 476, 115–120. doi: 10.1016/j.bbrc.2016.05.019

Turecek, C., Fratzl-Zelman, N., Rumpler, M., Buchinger, B., Spitzer, S., Zoehrer, R., et al. (2008). Collagen cross-linking influences osteoblastic differentiation. *Calcif Tissue Int.* 82, 392–400. doi: 10.1007/s00223-008-9136-3

Usha, P. R., and Naidu, M. U. (2004). Randomised, double-blind, parallel, placebo-controlled study of oral glucosamine, methylsulfonylmethane and their combination in osteoarthritis. *Clin. Drug Investig.* 24, 353–363. doi: 10.2165/00044011-200424060-00005

Vermeer, J. A., Jansen, I. D., Marthi, M., Coxon, F. P., McKenna, C. E., Sun, S., et al. (2013). Jaw bone marrow-derived osteoclast precursors internalize more bisphosphonate than long-bone marrow precursors. *Bone* 57, 242–251. doi: 10.1016/j.bone.2013.08.007

Weinstein, R. S., Jilka, R. L., Parfitt, A. M., and Manolagas, S. C. (1997). The effects of androgen deficiency on murine bone remodeling and bone mineral density are mediated via cells of the osteoblastic lineage. *Endocrinology* 138, 4013–4021.

Weitzmann, M. N., and Pacifici, R. (2006). Estrogen deficiency and bone loss: an inflammatory tale. *J. Clin. Invest.* 116, 1186–1194.

Willinghamm, M. D., Brodt, M. D., Lee, K. L., Stephens, A. L., Ye, J., and Silva, M. J. (2010). Age-related changes in bone structure and strength in female and male BALB/c mice. *Calcif. Tissue Int.* 86, 470–483. doi: 10.1007/s00223-010-9359-y

Author Disclaimer: Solely the authors' responsibility and does not necessarily represent the official views of National Institutes of Health.

Conflict of Interest: The authors declare that the research was conducted in the absence of any commercial or financial relationships that could be construed as a potential conflict of interest.

Publisher's Note: All claims expressed in this article are solely those of the authors and do not necessarily represent those of their affiliated organizations, or those of the publisher, the editors and the reviewers. Any product that may be evaluated in this article, or claim that may be made by its manufacturer, is not guaranteed or endorsed by the publisher.

frontiers in Physiology

ORIGINAL RESEARCH
published: 11 October 2021
doi: 10.3389/fphys.2021.735234

Epithelial Cell Rests of Malassez Provide a Favorable Microenvironment for Ameliorating the Impaired Osteogenic Potential of Human Periodontal Ligament Stem Cells

Yanjiao Li[1†], Anqi Liu[1,2†], Liqiang Zhang[3,4], Zhiwei Wang[1], Nana Hui[1], Qiming Zhai[1,3,4], Lishu Zhang[1,3,4], Zuolin Jin[1] and Fang Jin[1,4*]*

[1] State Key Laboratory of Military Stomatology & National Clinical Research Center for Oral Diseases & Shaanxi Clinical Research Center for Oral Diseases, Department of Orthodontic, School of Stomatology, The Fourth Military Medical University, Xi'an, China, [2] Department of Stomatology, The 985 Hospital of PLA, Taiyuan, China, [3] Xi'an Institute of Tissue Engineering and Regenerative Medicine, Xi'an, China, [4] State Key Laboratory of Military Stomatology & National Clinical Research Center for Oral Diseases & Shaanxi International Joint Research Center for Oral Diseases, Center for Tissue Engineering, School of Stomatology, The Fourth Military Medical University, Xi'an, China

Human periodontal ligament stromal/stem cells (PDLSCs) are ideal candidates for periodontal regeneration and are of significant importance in clinical practice. However, PDLSCs derived from diseased microenvironments exert impaired behavior, which leads to the failure of periodontal regeneration. The epithelial cell rests of Malassez (ERM), which are involved in periodontal homeostasis, are residual cells from Hertwig's epithelial root sheath (HERS). However, the function of ERM remains largely unknown. Therefore, the aim of this study was to evaluate the effect of ERM on the osteogenic potential of PDLSCs from an impaired microenvironment. PDLSCs from healthy donors (H-PDLSCs), periodontitis donors (P-PDLSCs) and human ERM were harvested. Osteogenic evaluation showed a lower osteogenic potential of P-PDLSCs compared to that of H-PDLSCs. Then, we co-cultured ERM with P-PDLSCs, and the data showed that ERM promoted the expression of osteogenic genes and proteins in P-PDLSCs. In addition, we collected the PDLSCs from aged donors (A-PDLSCs) and analyzed the osteogenesis capacity of the A-PDLSCs and A-PDLSCs + ERM groups, which displayed similar results to P-PDLSCs. Finally, we evaluated the Wnt pathway, which is associated with osteogenic differentiation of stromal/stem cells, in A-PDLSCs + ERM and P-PDLSCs + ERM groups, which indicated that suppression of the Wnt pathway may result in an increase in the osteogenic properties of A-PDLSCs + ERM and P-PDLSCs + ERM groups. Taken together, the above findings shed new light on the function of ERM and provide a novel therapeutic for optimizing PDLSCs-based periodontal regeneration.

Keywords: periodontal ligament stromal/stem cells, epithelial cell rests of Malassez, osteogenesis, co-culture, Wnt pathway

OPEN ACCESS

Edited by:
Petros Papagerakis, University of Saskatchewan, Canada

Reviewed by:
Javier Catón, Universidad Complutense de Madrid, Spain
Francesca Diomede, University of Studies G. d'Annunzio Chieti and Pescara, Italy
Thanaphum Osathanon, Faculty of Dentistry, Chulalongkorn University, Thailand

***Correspondence:**
Fang Jin
fangjin191@163.com
Zuolin Jin
zuolinj@163.com

[†]These authors have contributed equally to this work and share first authorship

Specialty section:
This article was submitted to Craniofacial Biology and Dental Research, a section of the journal Frontiers in Physiology

Received: *02 July 2021*
Accepted: *14 September 2021*
Published: *11 October 2021*

Citation:
Li Y, Liu A, Zhang L, Wang Z, Hui N, Zhai Q, Zhang L, Jin Z and Jin F (2021) Epithelial Cell Rests of Malassez Provide a Favorable Microenvironment for Ameliorating the Impaired Osteogenic Potential of Human Periodontal Ligament Stem Cells. Front. Physiol. 12:735234. doi: 10.3389/fphys.2021.735234

INTRODUCTION

Periodontal regeneration has always been widely investigated in periodontal field (Liu et al., 2018; Behm et al., 2020; Wang et al., 2020). Due to the complex periodontal ligament structure and oral environment, satisfactory periodontal regeneration still has not achieved (Li et al., 2020; Nibali et al., 2021; Shang et al., 2021a). Human periodontal ligament stromal/stem cells (PDLSCs), which are a kind of mesenchymal stromal/stem cells (MSCs) have been widely used in periodontal tissue regeneration (Liu et al., 2018). However, studies have recognized that purely applying PDLSCs barely regenerates ideal periodontal tissue. Therefore, numerous studies have focused on facilitating the capacities of PDLSCs to improve the effect of periodontal regeneration (Shang et al., 2017, 2021b; Abdelaziz et al., 2021).

The periodontal ligament is a complex tissue that maintains various cell types such as PDLSCs, fibroblasts and epithelial cell rests of Malassez (ERM) (LeBlanc et al., 2020). Among them, ERM are the remaining epithelial cells of Hertwig's epithelial root sheath (HERS), which play important roles in maintaining the homeostasis of periodontal tissue (Yang et al., 2015) and preventing root resorption (Tsunematsu et al., 2016). However, it remains unclear how ERM impacts PDLSCs. The microenvironment is involved in regulating the biological behavior of stromal/stem cells (Sui et al., 2019). For instance, the osteogenic capacity of PDLSCs derived from the inflammatory microenvironment is lower than that of PDLSCs from a healthy microenvironment (Tang et al., 2016). Thus, the alleviation of the impaired microenvironment would be helpful for enhancing the results of periodontal regeneration.

In this study, we established a co-culture system to observe the effect of ERM on the osteogenesis of PDLSCs derived from an impaired microenvironment., thereby providing a theoretical basis for further optimization of periodontal regeneration.

MATERIALS AND METHODS

Cell Isolation and Culture

Healthy PDLSCs (H-PDLSCs) were obtained by culturing explants of healthy periodontal tissues from patients (24–35 years of age) whose premolar or third molar was extracted for orthodontic reasons. Periodontitis PDLSCs (P-PDLSCs) were obtained from patients (24–35 years of age) diagnosed with periodontitis who exhibited 2/3 alveolar bone loss and more than one pocket with a depth $\geq$5 mm. Aged PDLSCs (A-PDLSCs) were collected from patients aged 52–65 years. Periodontal tissues were gently separated from the root surface. After washing in sterile phosphate-buffered solution (PBS), the tissues were digested with type I collagenase (0.66 mg/mL; Sigma, USA) for 20 min. Single cell suspensions were generated and cultured in culture medium containing α-minimum essential medium (α-MEM; Gibco, USA) supplemented with 10% fetal bovine serum (FBS; Thermo Electron, USA), 0.292 mg/mL glutamine (*Invitrogen*, USA), 100 U/mL penicillin, 100 mg/mL streptomycin (Gibco, USA) at 37°C in a humidified atmosphere of 5% CO_2 and 95% air.

To obtain human ERM, 15 systemically healthy donors aged between 11 and 30 years were recruited. Healthy premolars or third molars were extracted for orthodontic reasons. The first third of the tooth which proximately to the crown was removed. After thoroughly scraping the periodontal tissue of upper 1/3 of root to remove the gingival tissue, the tooth was washed in sterile PBS and totally digested with type I collagenase (0.66 mg/mL; Sigma, USA) for 2 h at 37°C in a humidified atmosphere of 5% CO_2 and 95% air. Single cell suspensions were generated by filtration using a 70 μm strainer, then washed and re-suspended in α-MEM (Gibco, USA) supplemented with 15% FBS (Thermo Electron, USA), 0.292 mg/mL glutamine (*Invitrogen*, USA), 100 U/mL penicillin, and 100 mg/mL streptomycin (Gibco, USA). The culture medium was changed every 3 days. The explants were maintained in 6-well culture dishes for 2 weeks until cell clusters were formed. After digestion, cells were seeded and cultured with epithelial cell medium consisting of α-MEM (Gibco, USA), 2% FBS (Thermo Electron, USA), 1% epithelial cell growth supplement (Gibco, USA), and 1% penicillin/streptomycin (Gibco, USA) for 7 days. Then, differential digestion was performed using trypsin-EDTA (9:1) for 10 min to detach the fibroblast-like-cells.

All samples were collected at the School of Stomatology, The Fourth Military Medical University. Written informed consent was provided by all participants, and the study was approved by the hospital's ethics committee.

Osteogenic Differentiation Assay

The induction of osteogenic differentiation was performed as previously described (Li et al., 2016). Briefly, PDLSCs in passage 3–4 were used for osteogenic differentiation assay. 2×10^5 cells per well were maintained in 6-well plates with culture medium. When the cells reached ∼90% confluence, the culture medium was changed to osteoinductive medium which supplemented with 100 nM dexamethasone, 50 mg/ml ascorbic acid, and 5 mM b-glycerophosphate (Sigma, USA).

After 7 days of osteogenic induction, cells were fixed in 4% paraformaldehyde for 30 min. Subsequently, alkaline phosphatase (ALP) staining was performed using the BCIP/NBT Alkaline Phosphatase Kit (Beyotime, China). In addition, total RNA and protein were extracted and analyzed for the expression of osteogenic genes (ALP and RUNX2) and proteins (ALP and RUNX2).

Immunofluorescence Staining

ERM were fixed in 4% paraformaldehyde and incubated in 0.1% Triton X-100 for 15 min. Next, the cells were incubated overnight with a rabbit anti-human CK14 primary antibody (Abcam, 1:200) at 4°C and then the secondary antibody (Jackson, 1:200) was applied to react with the primary antibody. The cell nuclei were stained with DAPI (Sigma, 1:200) and observed under fluorescence microscope.

Co-culture System

The coculture system was established as previously described (Liu et al., 2014a). Cell coculture assay was assessed using 12-well inserts with 0.4-μm pores (Corning, China) according to the

manufacturer's protocol. Briefly, ERM were loaded into the upper chamber (5.5×10^3), while P-PDLSCs or A-PDLSCs were loaded into the lower chamber (4.0×10^4) in osteoinductive medium.

Quantitative Real-Time PCR (qRT-PCR)

To compare gene expression, qRT-PCR was used according to protocol. After 7 days of osteogenic induction, cells were washed with PBS and total RNA was extracted. Synthesis of cDNA was performed using SYBR1 Premix Ex Taq II (Perfect Real Time kit; TaKaRa, Japan). The primers are listed below:

GAPDH: Forward *5′- TCT GCA TCA TCC AGG AGC TTA TT−3′*, Reverse *5′- TGA TAC AGA AGG CAG GTT CAC AA−3′; ALP:* Forward *5′- AGC TTT CGA AGA ACA ACG GA−3′*, Reverse *5′- TCT TGA AAT GCT TTG GGT CC-3′; RUNX2:* Forward *5′- CCC GTG GCC TTC AAG GT−3′*, Reverse *5′- CGT TAC CCG CCA AGA CAG TA-3′*.

Western Blot Analysis

After 7 days of osteogenic induction, cells were washed with PBS and total protein was obtained by RIPA lysis buffer (Beyotime, China). Quantitative analysis was performed using BCA (Sigma, USA). Next, proteins were isolated on NuPAGE 10–12% polyacrylamide gel and transferred to a PVDF membrane (Millipore, USA). The membrane was blocked with 5% milk for 2 h and then incubated with primary antibodies overnight. The following primary antibodies were used: ALP (Abcam, 1:400), RUNX2 (Abcam, 1:400), total-β-catenin (Abcam, 1:1000), active-β-catenin (Cell Signaling, 1:500), GSK-3β (Abcam, 1:1000), p-GSK-3β (Santa Cruz, 1:500) and GAPDH (Cwbiotech, 1:500). The secondary antibody (Corning, 1:5000) was incubated according to the source of primary antibody, and the chemiluminescence ECL kit (Sigma, USA) was used for protein detection. ImageJ was used to analyze the corresponding spectral band intensity of scanned images.

Statistical Analysis

Statistical analysis was performed using GraphPad Prism 8.0. The results are expressed as the mean ± SD from at least three independent experiments and analyzed by two-tailed unpaired Student's *t*-test. A value of $P < 0.05$ was considered statistically significant.

RESULTS

PDLSCs From the Inflammatory Microenvironment Display Impaired Osteogenic Potential

First, to identify the MSCs properties of PDLSCs, we analyzed the surface markers of PDLSCs from healthy (H-PDLSCs) and inflammatory (P-PDLSCs) microenvironments. Flow cytometry evaluation showed that H-PDLSCs and P-PDLSCs were both positive for the MSCs surface markers CD105, CD90 and CD29, but were negative for the hematopoietic marker CD45 (**Supplementary Figure S1A**). In addition, they both possessed colony-formation capacity (**Supplementary Figure S1B**), positive for ALP activity staining (**Supplementary Figure S1C**) and formed osteogenic nodules, as shown through Alizarin red S staining (**Supplementary Figure S1D**).

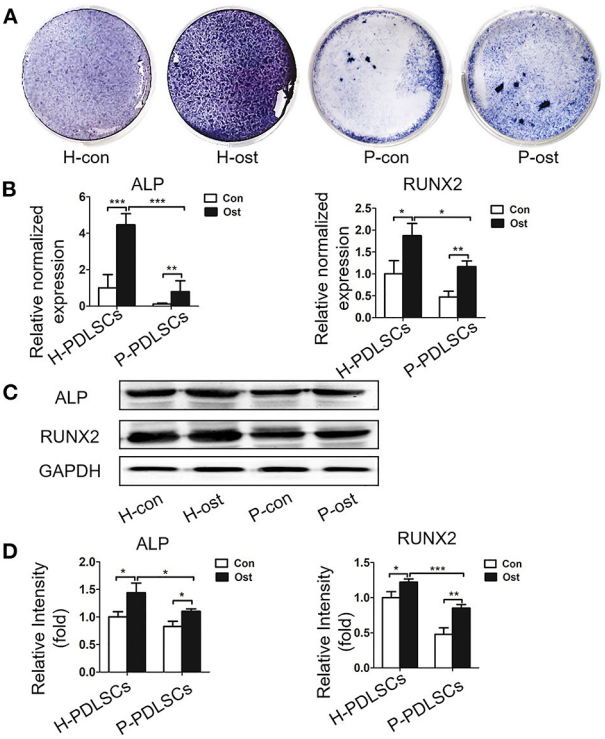

FIGURE 1 | PDLSCs from the inflammatory microenvironment display impaired osteogenic potential. **(A)** ALP staining shows that ALP positive staining reduced in P-PDLSCs, comparing to H-PDLSCs, after 7 days of osteogenic induction ($n = 3$). **(B)** The qRT-PCR results display higher expression levels of the osteogenic genes ALP and RUNX2 after osteogenic induction in both P-PDLSCs and H-PDLSCs than in PDLSCs without osteogenic induction, while the expression of ALP and RUNX2 decrease in P-PDLSCs after 7 days of osteogenic induction ($n = 3$). **(C)** Expression of ALP and RUNX2 are examined by Western blot analysis. **(D)** The quantitative evaluation of Western blot demonstrates that compare to H-PDLSCs, the expression levels of ALP and RUNX2 reduce in P-PDLSCs ($n = 3$). $^*P < 0.05$, $^{**}P < 0.01$, $^{***}P < 0.001$.

Next, the osteogenic capacity of H-PDLSCs and P-PDLSCs was compared after 7 days of osteogenic induction. There were four groups: H-PDSLCs with (H-ost) or without osteogenic induction (H-con) and P-PDSLCs with (P-ost) or without osteogenic induction (P-con). ALP staining showed that the expression level of ALP increased after osteogenic induction in both H-PDLSCs and P-PDLSCs. The ALP expression level was obviously decreased in the P-ost group compared with the H-ost group (**Figure 1A**). Additionally, mRNA expression of the osteogenic genes ALP and RUNX2, which are classical markers of osteogenesis, was determined by qRT-PCR, and their protein expression levels were assessed by Western blot. The results showed that osteogenic induction enhanced the ALP and RUNX2 gene expression of PDLSCs and that the P-PDLSCs exhibited lower gene expression levels than H-PDLSCs after osteogenic induction ($P < 0.001$; **Figure 1B**), which is consistent with the Western blot results ($^*P < 0.05$, $^{***}P < 0.001$; **Figures 1C,D**).

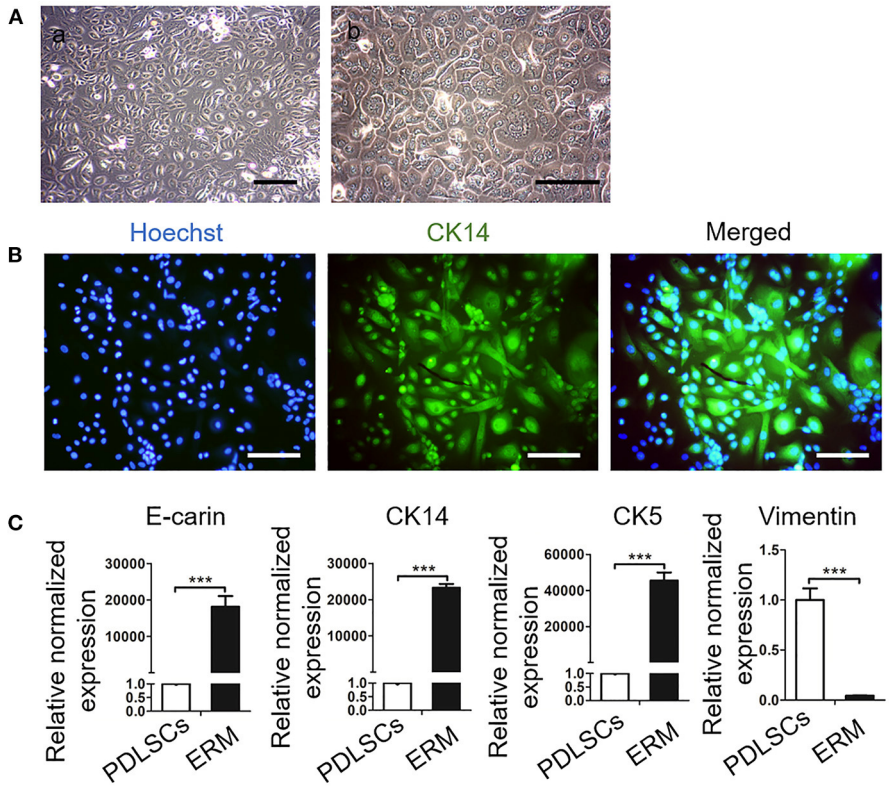

FIGURE 2 | Culture and Identification of epithelial rests of Malassez (ERM). **(A)** Representative morphologies of ERM. (a) Low magnification of ERM. Scale bar, 200 mm; (b) High magnification of ERM; Scale bar, 20 mm. **(B)** Immunofluorescence staining shows that the cells are positive for the epithelial specific marker CK14. Scale bar, 50 mm. **(C)** qRT-PCR reveals that ERM cells express epithelial specific markers CK14, CK5 and E-cadrin, but barely express PDLSCs specific marker vimentin ($n = 3$). $^{***}P < 0.001$.

The findings revealed that the P-PDLSCs showed impaired osteogenic ability, which was consistent with previous results (Sun et al., 2017), thereby indicating that the inflammatory microenvironment impairs the osteogenic capacity of PDLSCs.

ERM Promote the Osteogenic Potential of PDLSCs From Inflammatory Microenvironment

It has been reported that ERM express extracellular matrix proteins that regulate the function of PDLSCs and maintain PDL homeostasis (Keinan and Cohen, 2013; Xiong et al., 2013). In this study, ERM were successfully isolated and purified from periodontal tissues and displayed a "paving stone" shape (**Figure 2A**). Immunofluorescence showed ERM were positive for the epithelial marker cytokeratin 14 (CK14) (**Figure 2B**). qRT-PCR showed high expression levels of the epithelial markers amelogenin, CK14, cytokeratin 5 E-cadherin in ERM, but these were poorly detected in PDLSCs. Additionally, ERM barely expressed in MSCs marker vimentin which was highly expressed in PDLSCs ($P < 0.001$; **Figure 2C**). The findings showed that the ERM we cultured possessed the characteristics of epithelial cells which can be applied for further studies.

To assess the effect of ERM on P-PDLSCs, we established an osteogenic co-culture system. ALP staining showed that higher ALP expression in the P-PDLSCs and ERM co-culture group (P-PDLSCs + ERM) than P-PDLSCs group (**Figure 3A**). The mRNA expression of ALP and RUNX2, which are associated with osteogenesis, increased in P-PDLSCs + ERM group ($^{**}P < 0.01$, $^{***}P < 0.001$; **Figure 3B**). However, the fold change of RUNX2 is lower than that of ALP after statistical analysis which we will confirm in future studies. The Western blot findings also displayed increased expression levels of ALP and RUNX2 in the P-PDLSCs + ERM group, consisting with qRT-PCR findings ($^{*}P < 0.05$, $^{**}P < 0.01$; **Figures 3C,D**). The data above first determined that ERM co-cultured with P-PDLSCs enhanced the osteogenic capacity of P-PDLSCs, implying that ERM may create a favorable microenvironment to rescue the impaired osteogenic properties of P-PDLSCs.

ERM Enhance the Osteogenic Ability of PDLSCs From Aged Microenvironment

Given that cells from unfavorable microenvironment exhibited impaired biological characteristics (Sui et al., 2019), we further analyzed osteogenic capacity of PDLSCs from aged microenvironment (A-PDLSCs). Flow cytometry analysis showed that A-PDLSCs were positive for the MSCs surface markers CD105, CD90 and CD29, but were negative for the hematopoietic marker CD45

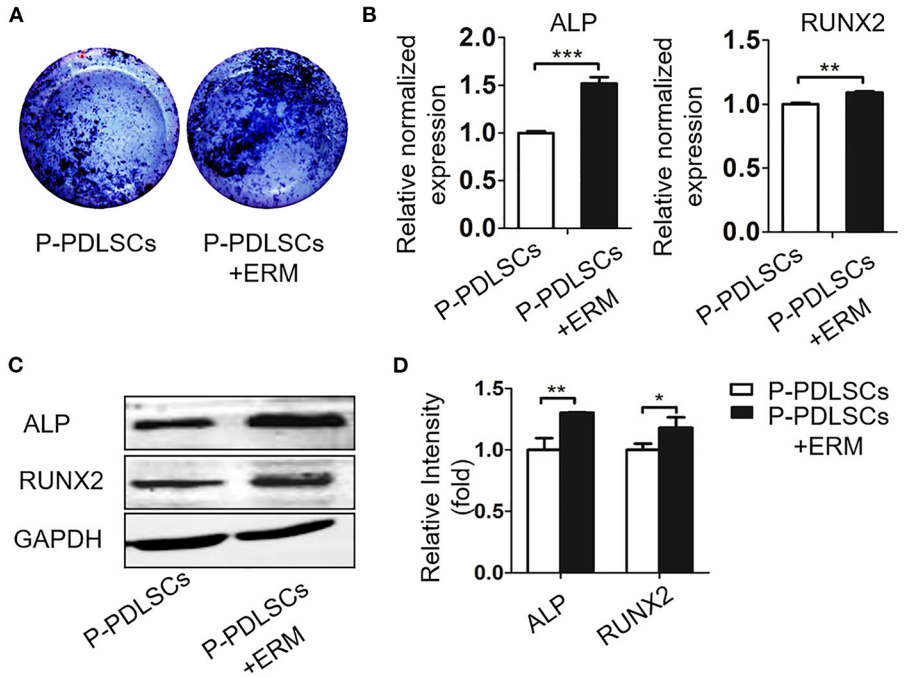

FIGURE 3 | ERM promote the osteogenic potential of PDLSCs from inflammatory microenvironment. **(A)** ALP staining exhibits that co-cultured with ERM elevates the ALP expression of P-PDLSCs after osteogenic induction. **(B)** qRT-PCR analysis shows P-PDLSCs + ERM group expresses higher levels of osteogenic genes ALP and RUNX2 than P-PDLSCs group ($n = 3$). **(C)** Protein expression levels of ALP and RUNX2 also increase in P-PDLSCs + ERM group. **(D)** The quantitative evaluation of Western blot ($n = 3$). $^{*}P < 0.05$, $^{**}P < 0.01$, $^{***}P < 0.001$.

(**Supplementary Figure S2A**). Besides, A-PDLSCs possessed colony-formation (**Supplementary Figure S2B**), ALP positive staining (**Supplementary Figure S2C**), and osteogenic nodule formation potential (**Supplementary Figure S2D**). After seven days of osteogenic induction, the ALP staining showed the reduced expression of ALP in A-PDLSCs compared to H-PDLSCs (**Figure 4A**). The gene and protein expression of ALP and RUNX2, which are classical markers of osteogenesis, were both decreased in A-PDLSCs ($^{*}P < 0.05$, $^{**}P < 0.01$; **Figures 4B-D**). The data determined that PDLSCs from aged microenvironment exhibit impaired osteogenic potential, consistent with previous findings.

Since ERM co-cultured with P-PDLSCs alleviated the reduced osteogenic property of P-PDLSCs, we next analyzed the osteogenesis capacity of A-PDLSCs + ERM. ALP staining displayed an increase in ALP expression in the A-PDLSCs + ERM group after 7 days of osteogenic induction (**Figure 5A**). Comparing to A-PDLSCs group, the gene and protein expression levels of ALP and RUNX2 also increased in A-PDLSCs + ERM group ($^{*}P < 0.05$, $^{**}P < 0.01$; **Figures 5B-D**). The results first showed that ERM promote the osteogenic ability of PDLSCs from aged microenvironment, indicating that ERM may provide a beneficial microenvironment for PDLSCs to elevate their impaired properties.

ERM Alleviate the Osteogenic Property of PDLSCs From Impaired Microenvironment via Suppressing the Wnt Pathway

Recent studies have demonstrated that the Wnt signaling pathway plays an important role in the osteogenic differentiation of PDLSCs (Liu et al., 2011a). However, it is still elusive whether ERM alleviate the impaired osteogenic ability of PDLSCs which were from unfavorable microenvironment via Wnt signaling. In this study, we evaluated β-catenin and GSK-3β, which are key proteins in the Wnt pathway. The findings showed that the GSK-3β and total-β-catenin expression levels were essentially unchanged, while P-GSK-3β and active-β-catenin protein expression levels in the P-PDLSCs + ERM group were lower than those in the P-PDLSCs group ($P < 0.05$; **Figures 6A,B**). Furthermore, the Wnt pathway in A-PDLSCs + ERM and A-PDLSCs group was also analyzed. The results displayed that there was no significant difference in GSK-3β and total-β-catenin expression levels, but that P-GSK-3β and active-β-catenin protein expression levels decreased in the A-PDLSCs + ERM group ($P < 0.05$; **Figures 6C,D**). The results revealed that the Wnt pathway was inhibited in PDLSCs from impaired microenvironment when they were co-cultured with ERM, which may be associated with their enhanced osteogenic properties. However, further studies are needed to confirm the findings.

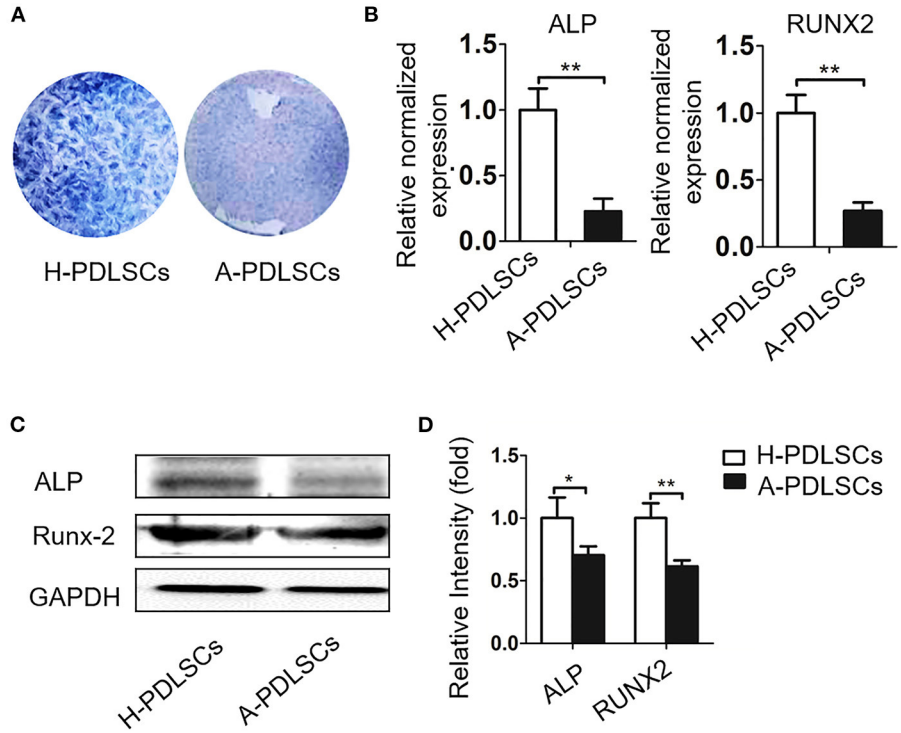

FIGURE 4 | The PDLSCs from aged microenvironment exhibit impaired osteogenic capacity. **(A)** ALP staining shows that after osteogenic induction, ALP positive staining reduced in A-PDLSCs, comparing to H-PDLSCs ($n = 3$). **(B)** qRT-PCR demonstrates lower expression of osteogenic genes ALP and RUNX2 in A-PDLSCs than H-PDLSCs ($n = 3$). **(C)** Expression of the ALP and RUNX2 are examined by Western blot analysis. **(D)** The quantitative evaluation of Western blot shows that P-PDLSCs express lower level of ALP and RUNX2 than H-PDLSCs ($n = 3$). $^{*}P < 0.05$, $^{**}P < 0.01$.

DISCUSSION

A favorable microenvironment promotes the biological properties of PDLSCs, which leads to better outcomes of periodontal regeneration (Liu et al., 2018; Zhou et al., 2021). Our results first found that ERM enhance the osteogenic capacity of PDLSCs from inflammatory and aging microenvironments, providing a novel role of ERM and a new thought for optimizing periodontal regeneration.

The extracellular microenvironment tightly regulates the biological behavior of resident stem cells (Sui et al., 2019). For instance, the efficacy of periodontal regeneration declines in diabetes compared with healthy animals (Kim et al., 2020; Nguyen et al., 2020). Furthermore, PDLSCs from aged microenvironment exhibited reduced colony-forming ability, proliferative, migratory and osteogenic potential than PDLSCs from healthy PDL (Zheng et al., 2009; Wu et al., 2015; Aung et al., 2020). For PDLSCs isolated from periodontitis, our team previously found that the proliferative capacity of them increased but the osteogenic potential of them was significantly lower than that of PDLSCs isolated from healthy PDL (Liu et al., 2011; Tang et al., 2016; Sun et al., 2017). In this study, flow cytometry analysis and colony-forming assays showed the PDLSCs we cultured from different origins expressed MSCs surface markers and owed self-renew potential, suggesting the PDLSCs we collected displayed MSCs properties (**Supplementary Figures S1, S2**). Then, we analyzed the osteogenic potential of PDLSCs derived from periodontitis and older donors. The findings demonstrated dysfunctional osteogenic potential, which was consistent with previous studies (**Figures 1**, **3A–D**) (Tang et al., 2016; Sun et al., 2017).

ERM, as the descendant of HERS which are crucial in root formation, play an important role in cementum repair and periodontal homeostasis (Keinan and Cohen, 2013; Nam et al., 2014; Yang et al., 2020). During root dentine formation, HERS cells dislocate and disintegrate from the root, which allows the attachment of cementum-forming cells to the newly formed root dentin surface (Duan et al., 2020). The remaining epithelial cells are further removed from the root surface and retained in the developing periodontal membrane, which are known as ERM. Through HERS act as a transient structure, their epithelial residue ERM exist throughout life with a fish net structure surrounded the root surface (Ohshima et al., 2008). Compared with HERS, ERM cells derive from a wider variety of sources, which are ideal cells to investigate the biological function of epithelial cells in periodontal ligament (Nam et al., 2014; Athanassiou-Papaefthymiou et al., 2015). Since there are only a small amount of the ERM cells in PDL, it is difficult to obtain and culture human ERM cells. While several studies have cultured the human ERM cells *in vitro* and evaluated

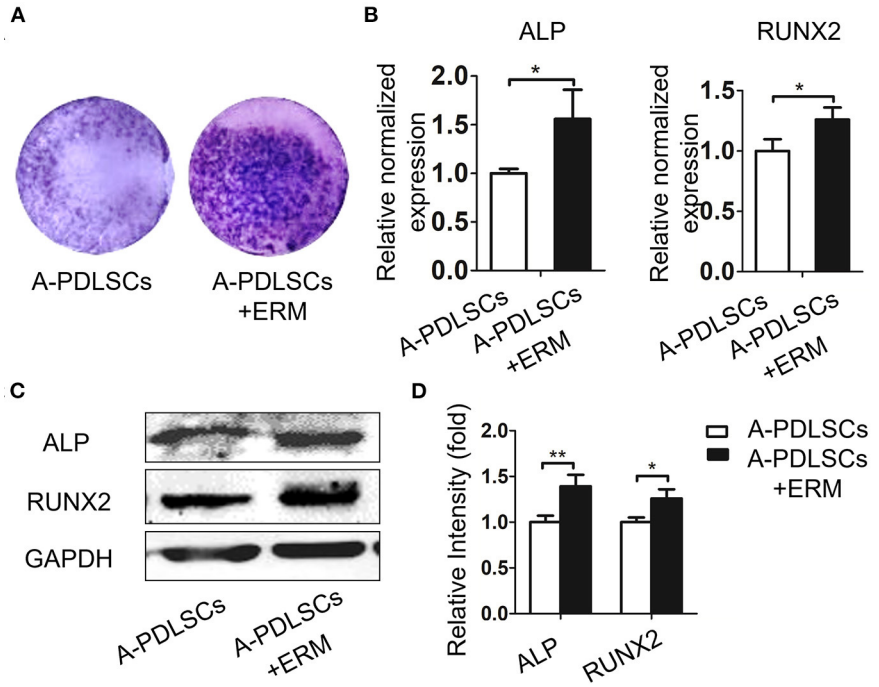

FIGURE 5 | ERM enhance the osteogenic ability of PDLSCs from aged microenvironment. **(A)** ALP staining exhibits that co-cultured with ERM elevates the ALP expression of A-PDLSCs after osteogenic induction. **(B)** qRT-PCR analysis shows that the A-PDLSCs + ERM group expresses higher levels of ALP and RUNX2 than the A-PDLSCs group ($n = 3$). **(C)** Protein expression levels of ALP and RUNX2 also increase in the A-PDLSCs + ERM group. **(D)** The quantitative evaluation of Western blot ($n = 3$). $^{*}P < 0.05$, $^{**}P < 0.01$.

their characteristics (Nam et al., 2011; Lee et al., 2012; Kitajima et al., 2019). As the ERM coexist with PDL cells and close to gingival cells, the improvement of purification of the ERM is a matter of considerable interest in order to clarify the function of this subpopulation (Athanassiou-Papaefthymiou et al., 2015). Summarizing the methods of others, we mechanically scraping the periodontal tissue of upper 1/3 of root to avoid the effects of gingival epithelial cells. Additionally, enzymatic digestion of the explants culture, which contains PDL cells and ERM, allows the less-adherent periodontal ligament fibroblasts to be released and separated from the more-adherent ERM (Nam et al., 2014; Kitajima et al., 2019). However, eliminating any residual other cells from the remaining adherent ERM remains difficult which needs advanced technology such as flow cytometry sorting. Given that heterogeneity of cell types exists throughout the evolution in every functional entity (Krivanek et al., 2017), the heterogeneity in the ERM population we isolated still exists. For example, some cell tracing studies have uncovered the critical role of biomarkers such as $Sox2^{+}$ dental epithelial stem cells in renewal of continuously growing mouse incisor (Juuri et al., 2012). Our team found that $Gli1^{+}$ cells in PDL can sense mechanical forces and participated in periodontal remodeling (Liu et al., 2020). In the future, we will further investigate the specific biomarkers in ERM and their function. In this study, based on the experimental methods of others, we successfully obtained high purity ERM through expression of $CK14^{+}$ cells and gene expression of epithelial markers. Our results showed that high purity ERM were obtained from human periodontal tissues which can be applied for further studies (**Figure 2**).

A co-culture system provides an ideal model to mimic the microenvironment *in vivo*, facilitating cell communication (Liu et al., 2014a). Several previous *in vitro* studies have demonstrated that ERM are capable of expressing extracellular matrix proteins that are involved in regulating mineralization such as osteopontin, bone sialoprotein and osteoprotegerin (Xiong et al., 2013; Yang et al., 2015). Furthermore, the osteogenic ability of PDLSCs can be enhanced by co-culture with HERS (Sonoyama et al., 2007). However, whether ERM inherit HERS function and how ERM impact PDLSCs remain largely unknown. In this study, we examined ALP and RUNX-2 as classical osteogenic markers. Although ALP and RUNX-2 are considered as early osteogenic markers, studies have showed that in the process of new bone formation, the expression of oteocalcin (OCN) which is considered as late osteogenic marker parallels with the expression of ALP. They both increase with the bone formation process and decrease with the maturation process (Diemar et al., 2021). Even so, further examination of the osteogenic markers such as OCN and osterix (OSX) are needed to confirm the influence of ERM in osteogenic differentiation of PDLSCs and the ALP activity also needs analysis. Besides,

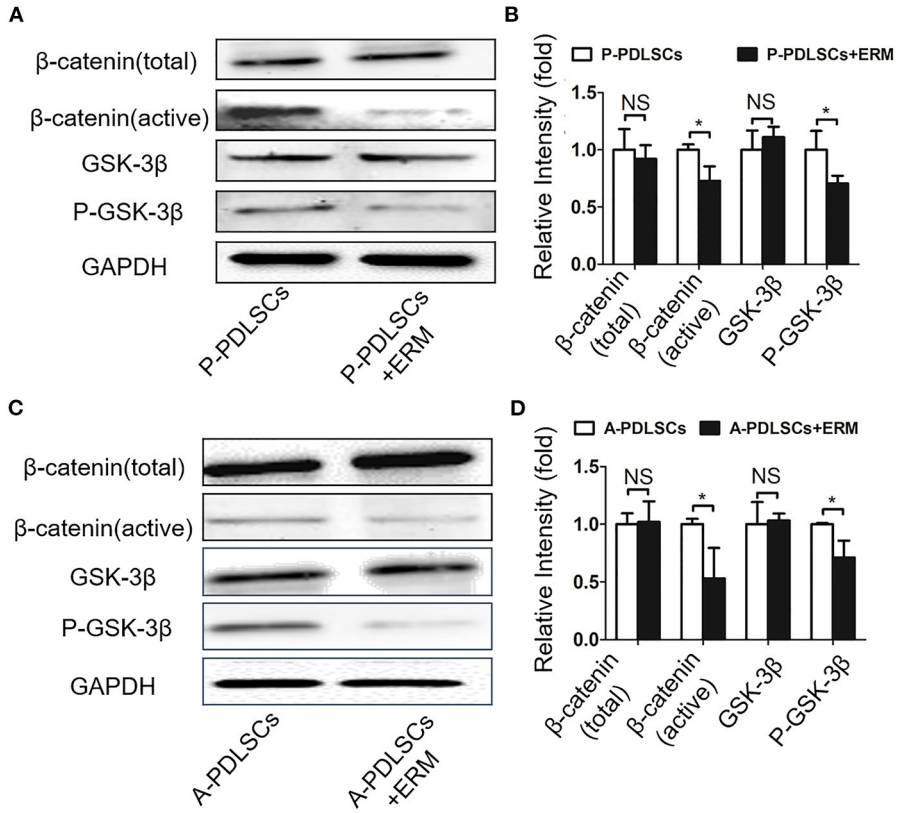

FIGURE 6 | ERM alleviate the osteogenic property of PDLSCs from impaired microenvironment via suppressing the Wnt pathway. **(A)** Western blot analysis exhibits that the expression levels of active-β-catenin and P-GSK-3β decrease in P-PDLSCs + ERM group. **(B)** Quantitative evaluation of Western blot ($n = 3$). **(C)** Western blot analysis shows that the expression levels of active-β-catenin and P-GSK-3β also decrease in the A-PDLSCs + ERM group. **(D)** Quantitative evaluation of Western blot ($n = 3$). $^*P < 0.05$.

functional experiments *in vitro* and *in vivo* such as Aizarin red S staining and ectopic osteogenesis assay are also needed in future investigation.

In this study, we established a co-culture system of ERM and PDLSCs derived from different microenvironment. The data first showed that both P-PDLSCs and A-PDLSCs possessed a higher expression of ALP and RUNX-2 after co-cultured with ERM, which suggests that ERM may create a beneficial microenvironment for ameliorating the impaired osteogenic capacity of PDLSCs from an unfavorable microenvironment (**Figures 3**, **5**). However, since the experiments were lack of the H-PDLSC control, the findings only implied that ERM could increase the impaired osteogenic capacity of PDLSCs, whether ERM improved osteogenic capacity of H-PDLSC needs further investigation.

Wnt signaling is putatively involved in various developmental processes such as skeletal development and tooth formation (Hu et al., 2019; Wang et al., 2019). It has been shown in various report that canonical Wnt signaling is activated during osteogenic differentiation in human bone marrow mesenchymal stem cells (BMMSCs) (Matsushita et al., 2020; Xiang et al., 2020). Our group has observed that a diverse regulation of the BMMSCs and PDLSCs via canonical Wnt pathway modulation (Liu et al., 2014a,b). The osteogenic differentiation process of BMMSCs activated the canonical Wnt signaling with increased level of active β-catenin and P-GSK-3β. While the osteogenic differentiation process of PDLSCs inhibited the canonical Wnt signaling with decreased level of active β-catenin and P-GSK-3β (Liu et al., 2011b; Li et al., 2016, 2018). It has been reported that the microenvironment influents the Wnt pathway (Liu et al., 2011a). For example, PDLSCs treated with the inflammatory factor TNF-α under osteogenic induction conditions exhibit the upregulation of Wnt signaling (Fang et al., 2020). Our team also detected that the application of the Wnt signaling antagonist DKK1 led to an increase in osteogenic differentiation in PDLSCs derived from the inflammatory microenvironment (Sun et al., 2017). Earlier studies have found that aging is also a chronic inflammatory process (Zhang et al., 2012; Aung et al., 2020), which implicates similar trends of cells from donors with periodontitis and aged donors. In this study, the results showed that P-GSK-3β and active-β-catenin decreased in the co-culture system, while GSK-3β and total-β-catenin remained unmodified, suggesting the suppression of the Wnt pathway in PDLSCs from an impaired microenvironment after co-cultured with ERM (**Figure 6**). Whereas more in-depth mechanism exploration is needed such as wheather ERM release factors to effect PDLSCs proliferation or differentiation.

In conclusion, we first found that ERM alleviated the osteogenic potential of PDLSCs from inflammatory and aged microenvironments, providing a novel function of ERM and a novel therapeutic to optimize PDLSCs derived from unfavorable microenvironments for better periodontal regenerative outcomes.

DATA AVAILABILITY STATEMENT

The raw data supporting the conclusions of this article will be made available by the authors, without undue reservation.

ETHICS STATEMENT

The studies involving human participants were reviewed and approved by Ethics Board of School of Stomatology, the Fourth Military Medical University. The patients/participants provided their written informed consent to participate in this study.

AUTHOR CONTRIBUTIONS

YL and AL conceptualized and performed the experiments and wrote the manuscript. LiqZ, ZW, and NH analyzed the data. QZ and LisZ contributed to the *in vitro* experiments. ZJ and FJ conceptualized the experiments, interpreted results, and provide critical revisions of the manuscript. All authors approved the final version of the manuscript.

FUNDING

This study was supported by the National Natural Science Foundation of China (Project No. 81870796).

SUPPLEMENTARY MATERIAL

The Supplementary Material for this article can be found online at: https://www.frontiersin.org/articles/10.3389/fphys.2021.735234/full#supplementary-material

REFERENCES

Abdelaziz, D., Hefnawy, A., Al-Wakeel, E., El-Fallal, A., and El-Sherbiny, I. (2021). New biodegradable nanoparticles-in-nanofibers based membranes for guided periodontal tissue and bone regeneration with enhanced antibacterial activity. *J. Adv. Res.* 28, 51–62. doi: 10.1016/j.jare.2020.06.014

Athanassiou-Papaefthymiou, M., Papagerakis, P., and Papagerakis, S. J. J. o. d. r. (2015). Isolation and characterization of human adult epithelial stem cells from the periodontal ligament. *J. Dent. Res.* 94, 1591–1600. doi: 10.1177/0022034515606401

Aung, K., Akiyama, K., Kunitomo, M., Mun, A., Tosa, I., Nguyen, H., et al. (2020). Aging-affected MSC functions and severity of periodontal tissue destruction in a ligature-induced mouse periodontitis model. *Int. J. Mol. Sci.* 21:8103. doi: 10.3390/ijms21218103

Behm, C., Blufstein, A., Gahn, J., Kubin, B., Moritz, A., Rausch-Fan, X., et al. (2020). Continuing effect of cytokines and toll-like receptor agonists on indoleamine-2,3-dioxygenase-1 in human periodontal ligament stem/stromal cells. *Cells* 9:2696. doi: 10.3390/cells9122696

Diemar, S., Lylloff, L., Rønne, M., Møllehave, L., Heidemann, M., Thuesen, B., et al. (2021). Reference intervals in Danish children and adolescents for bone turnover markers carboxy-terminal cross-linked telopeptide of type I collagen (β-CTX), pro-collagen type I N-terminal propeptide (PINP), osteocalcin (OC) and bone-specific alkaline phosphatase (bone ALP). *Bone* 146:115879. doi: 10.1016/j.bone.2021.115879

Duan, Y., Li, X., Zhang, S., Wang, S., Wang, T., Chen, H., et al. (2020). Therapeutic potential of HERS spheroids in tooth regeneration. *Theranostics* 10, 7409–7421. doi: 10.7150/thno.44782

Fang, H., Yang, K., Tang, P., Zhao, N., Ma, R., Luo, X., et al. (2020). Glycosylation end products mediate damage and apoptosis of periodontal ligament stem cells induced by the JNK-mitochondrial pathway. *Aging* 12, 12850–12868. doi: 10.18632/aging.103304

Hu, Y., Wang, C., Ha, S., Zhu, N., Cao, Z., and Song, Y. (2019). Peroxisome proliferator activated receptor γ promotes mineralization and differentiation in cementoblasts via inhibiting Wnt/β-catenin signaling pathway. *J. Cell. Biochem.* doi: 10.1002/jcb.29509. [Epub ahead of print].

Juuri, E., Saito, K., Ahtiainen, L., Seidel, K., Tummers, M., Hochedlinger, K., et al. (2012). Sox2+ stem cells contribute to all epithelial lineages of the tooth via Sfrp5+ progenitors. *Dev. Cell.* 23, 317–328. doi: 10.1016/j.devcel.2012.05.012

Keinan, D., and Cohen, R. (2013). The significance of epithelial rests of Malassez in the periodontal ligament. *J. Endod.* 39, 582–587. doi: 10.1016/j.joen.2013.01.004

Kim, H., Park, H., Kim, H., and Lee, Y. (2020). Association between the severity of periodontitis and osteoarthritis in middle-aged and older patients with type 2 diabetes: a nationwide population-based study. *Arthritis. Care. Res.* doi: 10.1002/acr.24484. [Epub ahead of print].

Kitajima, K., Das, R., Liang, X., Neppelberg, E., Johannessen, A., Costea, D., et al. (2019). Isolation and characterization of cells derived from human epithelial rests of Malassez. *Odontology* 107, 291–300. doi: 10.1007/s10266-018-0397-7

Krivanek, J., Adameyko, I., and Fried, K. (2017). Heterogeneity and developmental connections between cell types inhabiting teeth. *Front. Physiol.* 8:376. doi: 10.3389/fphys.2017.00376

LeBlanc, A., Paparella, I., Lamoureux, D., Doschak, M., and Caldwell, M. (2020). Tooth attachment and pleurodont implantation in lizards: histology, development, and evolution. *J. Anat.* 238, 1156–1178. doi: 10.1111/joa.13371

Lee, J., Lee, D., Nam, H., Lee, G., Seo, B., Cho, Y., et al. (2012). Dental follicle cells and cementoblasts induce apoptosis of ameloblast-lineage and Hertwig's epithelial root sheath/epithelial rests of Malassez cells through the Fas-Fas ligand pathway. *Eur. J. Oral. Sci.* 120, 29–37. doi: 10.1111/j.1600-0722.2011.00895.x

Li, B., Sun, J., Dong, Z., Xue, P., He, X., Liao, L., et al. (2016). GCN5 modulates osteogenic differentiation of periodontal ligament stem cells through DKK1 acetylation in inflammatory microenvironment. *Sci. Rep.* 6:26542. doi: 10.1038/srep26542

Li, L., Liu, W., Wang, H., Yang, Q., Zhang, L., Jin, F., et al. (2018). Mutual inhibition between HDAC9 and miR-17 regulates osteogenesis of human periodontal ligament stem cells in inflammatory conditions. *Cell. Death. Dis.* 9:480. doi: 10.1038/s41419-018-0480-6

Li, Q., Yang, G., Li, J., Ding, M., Zhou, N., Dong, H., et al. (2020). Stem cell therapies for periodontal tissue regeneration: a network meta-analysis of preclinical studies. *Stem. Cell. Res. Ther.* 11:427. doi: 10.1186/s13287-020-01938-7

Liu, A., Zhang, L., Chen, J., Sui, B., Liu, J., Zhai, Q., et al. (2020). Mechanosensing by Gli1 cells contributes to the orthodontic force-induced bone remodelling. *Cell. Prolif.* 53:e12810. doi: 10.1111/cpr.12810

Liu, A. Q., Hu, C. H., Jin, F., Zhang, L. S., and Xuan, K. (2018). Contributions of bioactive molecules in stem cell-based periodontal regeneration. *Int. J. Mol. Sci.* 19:1016. doi: 10.3390/ijms19041016

Liu, J., Wang, L., Liu, W., Li, Q., Jin, Z., and Jin, Y. (2014a). Dental follicle cells rescue the regenerative capacity of periodontal ligament stem cells in an inflammatory microenvironment. *PLoS ONE* 9:e108752. doi: 10.1371/journal.pone.0108752

Liu, N., Shi, S., Deng, M., Tang, L., Zhang, G., Liu, N., et al. (2011a). High levels of β-catenin signaling reduce osteogenic differentiation of stem cells in

inflammatory microenvironments through inhibition of the noncanonical Wnt pathway. *J. Bone. Miner. Res.* 26, 2082–2095. doi: 10.1002/jbmr.440

Liu, W., Konermann, A., Guo, T., Jäger, A., Zhang, L., and Jin, Y. (2014b). Canonical Wnt signaling differently modulates osteogenic differentiation of mesenchymal stem cells derived from bone marrow and from periodontal ligament under inflammatory conditions. *Biochim. Biophys. Acta.* 1840, 1125–1134. doi: 10.1016/j.bbagen.2013.11.003

Liu, Y., Liu, W., Hu, C., Xue, Z., Wang, G., Ding, B., et al. (2011b). MiR-17 modulates osteogenic differentiation through a coherent feed-forward loop in mesenchymal stem cells isolated from periodontal ligaments of patients with periodontitis. *J. Bone. Miner. Res.* 29, 1804–1816. doi: 10.1002/stem.728

Matsushita, Y., Nagata, M., Kozloff, K., Welch, J., Mizuhashi, K., Tokavanich, N., et al. (2020). A Wnt-mediated transformation of the bone marrow stromal cell identity orchestrates skeletal regeneration. *Nat. Commun.* 11:332. doi: 10.1038/s41467-019-14029-w

Nam, H., Kim, J., Kim, J., Seo, B., Park, J., Kim, J., et al. (2014). Establishment of Hertwig's epithelial root sheath/epithelial rests of Malassez cell line from human periodontium. *Molecules* 37, 562–567. doi: 10.14348/molcells.2014.0161

Nam, H., Kim, J., Park, J., Park, J., Kim, J., Seo, B., et al. (2011). Expression profile of the stem cell markers in human Hertwig's epithelial root sheath/Epithelial rests of Malassez cells. *Mol. Cells.* 31, 355–360. doi: 10.1007/s10059-011-0045-3

Nguyen, A., Akhter, R., Garde, S., Scott, C., Twigg, S., Colagiuri, S., et al. (2020). The association of periodontal disease with the complications of diabetes mellitus. A systematic review. *Diabetes. Res. Clin. Pract.* 165:108244. doi: 10.1016/j.diabres.2020.108244

Nibali, L., Sultan, D., Arena, C., Pelekos, G., Lin, G., and Tonetti, M. (2021). Periodontal infrabony defects: systematic review of healing by defect morphology following regenerative surgery. *J. Clin. Periodontol.* 48, 100–113. doi: 10.1111/jcpe.13381

Ohshima, M., Yamaguchi, Y., Micke, P., Abiko, Y., and Otsuka, K. (2008). *In vitro* characterization of the cytokine profile of the epithelial cell rests of Malassez. *J. Periodontol.* 79, 912–919. doi: 10.1902/jop.2008.070553

Shang, F., Liu, S., Ming, L., Tian, R., Jin, F., Ding, Y., et al. (2017). Human umbilical cord MSCs as new cell sources for promoting periodontal regeneration in inflammatory periodontal defect. *Theranostics* 7, 4370–4382. doi: 10.7150/thno.19888

Shang, F., Yu, Y., Liu, S., Ming, L., Zhang, Y., Zhou, Z., et al. (2021a). Advancing application of mesenchymal stem cell-based bone tissue regeneration. *Bioact. Mater.* 6, 666–683. doi: 10.1016/j.bioactmat.2020.08.014

Shang, L., Liu, Z., Ma, B., Shao, J., Wang, B., Ma, C., et al. (2021b). Dimethyloxallyl glycine/nanosilicates-loaded osteogenic/angiogenic difunctional fibrous structure for functional periodontal tissue regeneration. *Bioact. Mater.* 6, 1175–1188. doi: 10.1016/j.bioactmat.2020.10.010

Sonoyama, W., Seo, B., Yamaza, T., and Shi, S. (2007). Human Hertwig's epithelial root sheath cells play crucial roles in cementum formation. *J. Dent. Res.* 86, 594–599. doi: 10.1177/154405910708600703

Sui, B. D., Hu, C. H., Liu, A. Q., Zheng, C. X., Xuan, K., and Jin, Y. (2019). Stem cell-based bone regeneration in diseased microenvironments: challenges and solutions. *Biomaterials* 196, 18–30. doi: 10.1016/j.biomaterials.2017.10.046

Sun, J., Dong, Z., Zhang, Y., He, X., Fei, D., Jin, F., et al. (2017). Osthole improves function of periodontitis periodontal ligament stem cells via epigenetic modification in cell sheets engineering. *Sci. Rep.* 7:5254. doi: 10.1038/s41598-017-05762-7

Tang, H.-N., Xia, Y., Yu, Y., Wu, R.-X., Gao, L.-N., and Chen, F.-M. (2016). Stem cells derived from "inflamed" and healthy periodontal ligament tissues and their sheet functionalities: a patient-matched comparison. *J. Clin. Periodontol.* 43, 72–84. doi: 10.1111/jcpe.12501

Tsunematsu, T., Fujiwara, N., Yoshida, M., Takayama, Y., Kujiraoka, S., Qi, G., et al. (2016). Human odontogenic epithelial cells derived from epithelial rests of Malassez possess stem cell properties. *Lab. Invest.* 96, 1063–1075. doi: 10.1038/labinvest.2016.85

Wang, F., Tarkkonen, K., Nieminen-Pihala, V., Nagano, K., Majidi, R. A., Puolakkainen, T., et al. (2019). Mesenchymal cell-derived Juxtacrine Wnt1 signaling regulates osteoblast activity and osteoclast differentiation. *J. Bone. Miner. Res.* 364:e3680. doi: 10.1002/jbmr.3680

Wang, Y., Song, W., Cui, Y., Zhang, Y., Mei, S., and Wang, Q. (2020). Calcium-siRNA nanocomplexes optimized by bovine serum albumin coating can achieve convenient and efficient siRNA delivery for periodontitis therapy. *Int. J. Nanomed.* 15, 9241–9253. doi: 10.2147/IJN.S278103

Wu, R., Bi, C., Yu, Y., Zhang, L., and Chen, F. (2015). Age-related decline in the matrix contents and functional properties of human periodontal ligament stem cell sheets. *Acta. Biomater.* 22, 70–82. doi: 10.1016/j.actbio.2015.04.024

Xiang, L., Zheng, J., Zhang, M., Ai, T., and Cai, B. (2020). FOXQ1 promotes the osteogenic differentiation of bone mesenchymal stem cells via Wnt/β-catenin signaling by binding with ANXA2. *Stem. Cell. Res. Ther.* 11:403. doi: 10.1186/s13287-020-01928-9

Xiong, J., Gronthos, S., and Bartold, P. (2013). Role of the epithelial cell rests of Malassez in the development, maintenance and regeneration of periodontal ligament tissues. *Periodontol. 2000* 63, 217–233. doi: 10.1111/prd.12023

Yang, S., Choi, H., Kim, T., Jeong, J., Liu, Y., Harada, H., et al. (2020). Cell dynamics in Hertwig's epithelial root sheath are regulated by β-catenin activity during tooth root development. *J. Cell. Physiol.* 236, 5387–5398. doi: 10.1002/jcp.30243

Yang, Z., Li, Y., Ma, X., Shen, L., Zhao, Z., and Jin, F. (2015). Role of the epithelial cell rests of Malassez in periodontal homeostasis and regeneration - A review. *Curr. Stem. Cell. Res. Ther.* 10, 398–404. doi: 10.2174/1574888X10666150312100957

Zhang, J., An, Y., Gao, L., Zhang, Y., Jin, Y., and Chen, F. (2012). The effect of aging on the pluripotential capacity and regenerative potential of human periodontal ligament stem cells. *Biomaterials* 33, 6974–6986. doi: 10.1016/j.biomaterials.2012.06.032

Zheng, W., Wang, S., Ma, D., Tang, L., Duan, Y., and Jin, Y. (2009). Loss of proliferation and differentiation capacity of aged human periodontal ligament stem cells and rejuvenation by exposure to the young extrinsic environment. *Tissue. Eng. Part A.* 15, 2363–2371. doi: 10.1089/ten.tea.2008.0562

Zhou, M., Gao, S., Zhang, X., Zhang, T., Zhang, T., Tian, T., et al. (2021). The protective effect of tetrahedral framework nucleic acids on periodontium under inflammatory conditions. *Bioact. Mater.* 6, 1676–1688. doi: 10.1016/j.bioactmat.2020.11.018

Conflict of Interest: The authors declare that the research was conducted in the absence of any commercial or financial relationships that could be construed as a potential conflict of interest.

Publisher's Note: All claims expressed in this article are solely those of the authors and do not necessarily represent those of their affiliated organizations, or those of the publisher, the editors and the reviewers. Any product that may be evaluated in this article, or claim that may be made by its manufacturer, is not guaranteed or endorsed by the publisher.

frontiers in Physiology

ORIGINAL RESEARCH
published: 18 November 2021
doi: 10.3389/fphys.2021.689807

Impact of High-Altitude Hypoxia on Early Osseointegration With Bioactive Titanium

Yarong Wang[1], Zekun Gan[1], Haibin Lu[2], Ziyi Liu[1], Peng Shang[3], Jian Zhang[3], Wuwei Yin[1], Hongxing Chu[1], Renlei Yuan[4], Yingxin Ye[1], Pei Chen[1] and Mingdeng Rong[1]**

[1]Department of Periodontology and Implantology, Stomatological Hospital, Southern Medical University, Guangzhou, China, [2]Department of Implantology, Stomatological Hospital, Southern Medical University, Guangzhou, China, [3]College of Animal Science, Tibet Agriculture and Animal Husbandry University, Linzhi, China, [4]Linzhi People's Hospital, Linzhi, China

Nowadays, the bone osseointegration in different environments is comparable, but the mechanism is unclear. This study aimed to investigate the osseointegration of different bioactive titanium surfaces under normoxic or high-altitude hypoxic environments. Titanium implants were subjected to one of two surface treatments: (1) sanding, blasting, and acid etching to obtain a rough surface, or (2) extensive polishing to obtain a smooth surface. Changes in the morphology, proliferation, and protein expression of osteoblasts on the rough and smooth surfaces were examined, and bone formation was studied through western blotting and animal-based experiments. Our findings found that a hypoxic environment and rough titanium implant surface promoted the osteogenic differentiation of osteoblasts and activated the JAK1/STAT1/HIF-1α pathway *in vitro*. The animal study revealed that following implant insertion in tibia of rabbit, bone repair at high altitudes was slower than that at low altitudes (i.e., in plains) after 2 weeks; however, bone formation did not differ significantly after 4 weeks. The results of our study showed that: (1) The altitude hypoxia environment would affect the early osseointegration of titanium implants while titanium implants with rough surfaces can mitigate the effects of this hypoxic environment on osseointegration, (2) the mechanism may be related to the activation of JAK1/STAT1/HIF-1α pathway, and (3) our results suggest the osteogenesis of titanium implants, such as oral implants, is closely related to the oxygen environment. Clinical doctors, especially dentists, should pay attention to the influence of hypoxia on early osseointegration in patients with high altitude. For example, it is better to choose an implant system with rough implant surface in the oral cavity of patients with tooth loss at high altitude.

Keywords: osseointegration, bioactive titanium, hypoxia, normoxia, osteoblast

OPEN ACCESS

Edited by:
Petros Papagerakis, University of Saskatchewan, Canada

Reviewed by:
Victor E. Arana-Chavez, University of São Paulo, Brazil
Marta Nardini, University of Genoa, Italy

***Correspondence:**
Mingdeng Rong
rmdeng@smu.edu.cn
Pei Chen
cpei3057@126.com

Specialty section:
This article was submitted to Craniofacial Biology and Dental Research, a section of the journal Frontiers in Physiology

Received: *01 April 2021*
Accepted: *22 October 2021*
Published: *18 November 2021*

Citation:
Wang Y, Gan Z, Lu H, Liu Z, Shang P, Zhang J, Yin W, Chu H, Yuan R, Ye Y, Chen P and Rong M (2021) Impact of High-Altitude Hypoxia on Early Osseointegration With Bioactive Titanium. Front. Physiol. 12:689807. doi: 10.3389/fphys.2021.689807

INTRODUCTION

The theory of "osseointegration" has existed for more than 50 years (Lee and Bance, 2019). Several basic and clinical studies have confirmed that formation of the osseointegration interface of dental implants is the basis for successful implant restoration (Chen et al., 2019; Lee and Bance, 2019). Although the current success rate of implant restoration in

plains and flatlands is relatively high, approximately 1–2% of patients experience implant failure due to the lack of binding at the initial stage of implant insertion (Guglielmotti et al., 2019). Meanwhile, the hypoxic atmosphere characteristic of high-altitude environments in plateau regions is associated with a higher risk of osteoporosis and a longer healing time of bone fractures in the elderly population compared to those from regions of low altitudes, such as plains (Bernardi et al., 2020; Feng et al., 2020). This suggests that oxygen concentration is an important factor for bone defect repair. However, to date, the success rate of oral planting and relevant clinical guidelines in plateaus remains unreported. Thus, the only available clinical guidelines related to planting are specific to plains regions with constant oxygen (Guglielmotti et al., 2019). In this study, the osteogenesis of implants in different environment was evaluated in Xizang, China (highland zone, altitude near 3,000 m, severe cold; Liu et al., 2021) and Guangzhou, China (plain zone, altitude near 1,000 m, Warm and rainy; Liu et al., 2020a).

Bone defect repair is a complex and multifactorial interactive process (Mavrogenis et al., 2009; Dashnyam et al., 2019). Bone trauma and bone defects lead to local vascular rupture followed by bleeding, which leads to tissue ischemia, hypoxia, and acidosis (Ma et al., 2020; Wu et al., 2020a). This pathological process is not conducive to the growth and repair of bone tissue; thus, the application of tissue engineering to repair and restore bone defects has become a popular and important research topic (Wu et al., 2020b). Current research is focused on establishing a suitable microenvironment for the growth and proliferation of osteoblasts in bone defects and promoting the growth and differentiation of new bone to ultimately form a normal structure with normal function (Bernardi et al., 2020; Feng et al., 2020; Wen and Lv, 2020).

Autogenous bone grafts are typically the first choice of material for use on large bone defects; however, their application is restricted due to limited sources, the risk of infection, and adverse immune responses (Gonzaga et al., 2019; Brunello et al., 2020). Titanium and titanium alloys are widely used in the medical field, particularly in orthopedics due to their stable chemical properties, accessibility, and excellent resistance to corrosion (Lee et al., 2017; Talley et al., 2018). Meanwhile, physical, chemical, and biological surface modification methods can improve the roughness of titanium mesh and promote the adhesion and proliferation of osteoblasts (Lee et al., 2017; Talley et al., 2018). However, research on the effects of modified materials under high-altitude hypoxia is still in the exploratory stages.

In the present study, the microenvironment of bone defects was simulated by establishing a hypoxia model and bone defect model of the rabbit tibial plateau. We aimed to observe and compare osteoblasts cultured on titanium disks with different surfaces under normoxic or hypoxic conditions. The effect of these conditions on the morphology, proliferation, and repair of bone defects has the potential to provide a theoretical basis for the clinical application of titanium plate modification in the treatment of bone defects under normoxic or hypoxic conditions.

MATERIALS AND METHODS

Titanium Plate Preparation

Pure industrial TA2 titanium disks (TA2, Baoji, Shanxi Province, China) were customized (10 mm diameter and 2 mm thickness) and divided into two groups based on their altered surface (smooth and rough) for evaluation. To obtain a smooth surface, the disks were gradually polished using 600#, 800#, 1,200#, and 1,500# metallographic sandpaper and washed in an ultrasonic bath. To obtain a rough surface, the disks were sandblasted using alumina particles (90–250 μm in diameter, at 4.5 kPa and 90°C for 30 s) and treated with a mixture of 18% hydrochloric acid and 49% sulfuric acid at 60°C for 40 min to complete the acid etching process.

Cell Culture and Establishment of the Hypoxia Model

MG-63 cells (Sigma, United States) were cultured in minimum Eagle's medium (MEM, Gibco, NY, United States) supplemented with 10% high-quality fetal bovine serum (FBS, Gibco, United States) and 1% penicillin-streptomycin antibiotic solution (Beyotime, Beijing, China). The culture medium was replaced every 2–3 days. Once the cells reached 80% confluence, they were passaged at a ratio of 1:3 and incubated with 5% CO2 at 37°C in a saturated humidity incubator (Sanyo, Toshima-ku, Japan). The MG-63 cell suspension was collected and its concentration adjusted to 1×10^5 cells/ml. A titanium plate was placed in a 48-well plate (Corning, NY, United States), and 100 μl of cell suspension was added to the surface of each disk. The plate was then incubated for 3 h, and cell adherence to titanium was confirmed by scanning electron microscopy (SEM). Following cell adherence, 400 μl of culture medium was added to each well. The 48-well plate was then transferred into a portable hypoxia cell culture device (Billups-Rothenberg, NY, United States) and continuously supplied with mixed gas (90% N_2, 5% CO_2, and 5% O_2). The hypoxia device was placed in an incubator at 37°C to maintain saturated humidity levels. In osteogenic condition, the osteogenic induction medium was added (MEM with 10% FBS, 10 mmol/L, β-glycerophosphate, 10 nmol/L dexamethasone, and 50 μg/mL ascorbic acid).

Cell Proliferation Assay

MG-63 cell proliferation was determined using the Cell Counting Kit-8 (CCK-8, Sigma, MO, United States) and EdU assay (Sigma). For the CCK-8 assay, the MG-63 cell suspension was adjusted to 1×10^5 cells/ml and 100 μl was seeded on a titanium plate in a 48-well plate. Following adherence, the cells were cultured under normoxia and hypoxia conditions for 24 and 48 h. When the hypoxia treatment reached the corresponding time point, the CCK-8 assay was carried out according to the manufacturer's protocol. Briefly, the CCK-8 solution was added to each well and incubated for 3 h. Absorbance was measured at 450 nm using a microplate reader.

An EdU assay was performed by treating 5×10^3 MG-63 cells with 50 mM EdU at 37°C for 6 h. The cells were stilled attached to the titanium in this assay. After fixation in 4%

paraformaldehyde, MG-63 cells were treated with glycine for 10 min and 0.5% Triton X-100 for 10 min. The cells were then mixed with 4,6-diamidino-2-phenylindole (DAPI) in the dark for 30 min, and images were captured by fluorescence microscopy.

Morphological Assessment of the Different Bioactive Titanium Surfaces

Scanning electron microscopy was employed to observe the titanium disk morphologies. MG-63 cells were inoculated on both smooth and rough disks and cultured for 24 h, followed by fixing with pre-cooled 3% glutaraldehyde overnight at 4°C. Next, each sample was fixed with pre-cooled 1% acetic acid at 4°C for 1 h. The samples were then dehydrated for 10 min using acetone/isoamyl acetate (1:1) and dehydrated for 30 min with isoamyl acetate. Each dehydrated sample was immersed first in a 520% acetonitrile solution, followed by 15-min immersions in 70, 80, 90, 95, and 100% acetonitrile solutions, and a final transfer to a solution of 100% acetonitrile. The samples were then vacuum-dried for 30 min and coated with carbon and gold particles for observation under SEM.

TABLE 1 | Gene sequences.

Gene	Sequence (5′–3′)
BMP2	ACCCGCTGTCTTCTAGCGTTTTCAGGCCGAACATGCTGAG
COL1	GAGGGCCAAGACGAAGACATCCAGATCACGTCATCGCACAAC
RUNX2	TGGTTACTGTCATGGCGGGTATCTCAGATCGTTGAACCTTGCTA
GAPDH	GGAGCGAGATCCCTCCAAAATGGCTGTTGTCATACTTCTCATGG

Western Blot Analysis

MG-63 cells cultured on the different bioactive titanium disks under normoxia and hypoxia were collected and fully lysed using RIPA Lysis Buffer (Beyotime, China). Protein content was quantified using a bicinchoninic acid kit (Beyotime, China). After adjusting the sample concentrations, SDS-polyacrylamide gel electrophoresis (Amresco, OH, United States) was carried out using 30 μg of protein per sample. The separated protein bands were then transferred to a nitrocellulose membrane and incubated in a blocking buffer solution containing 5% skimmed milk powder (Sangon Biotech, China) overnight at 4°C. Next, the membrane was washed with TBST, incubated with goat anti-human p-JAK1, p-STAT1, JAK1, STAT1, HIF-1α, BMP2, COL-1, and RUNX2 antibodies (Abcam, 1:1000, United States), and visualized using ECL reagent (Pierce, IL, United States). Membranes were cleared with a clearing buffer and re-incubated

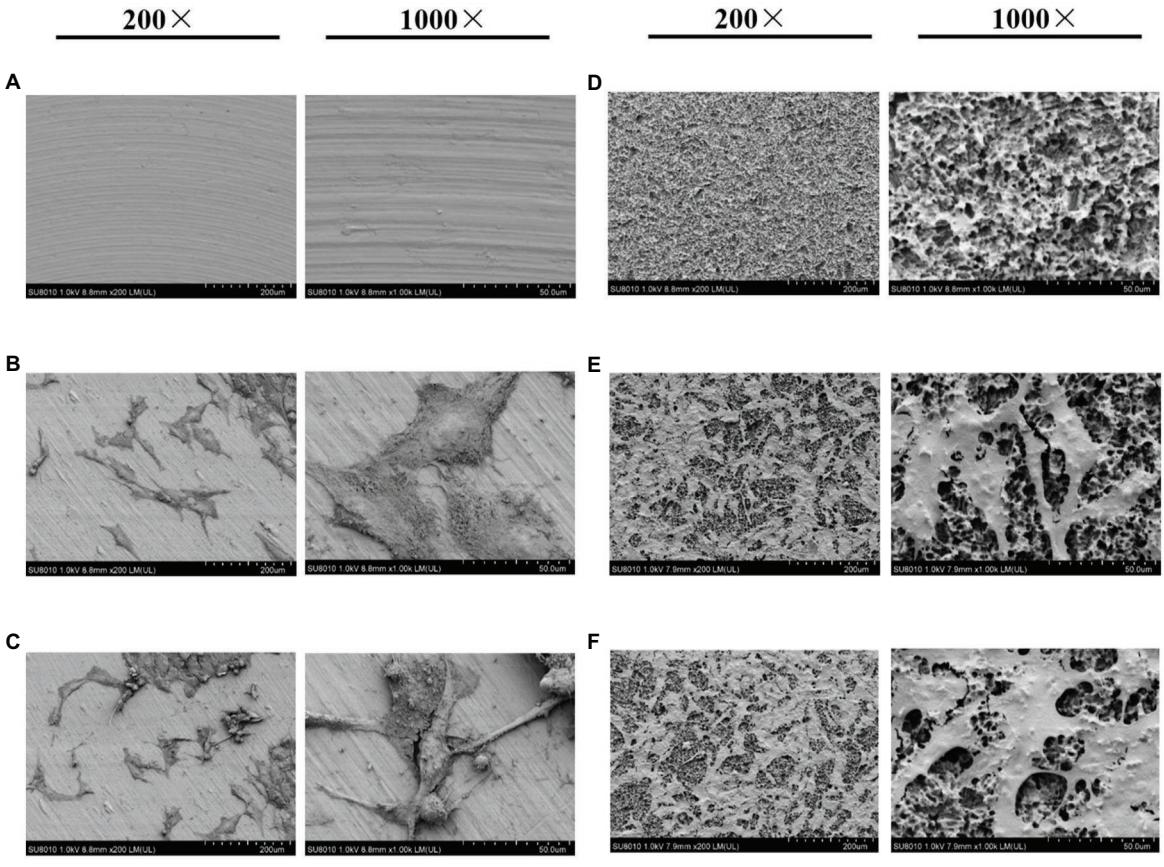

FIGURE 1 | Scanning electron microscopy (SEM) images of titanium plates and osteoblasts. **(A)** Smooth titanium plate, **(B)** MG-63 cells on a smooth surface under normoxic conditions, **(C)** MG-63 cells on a smooth surface under hypoxic conditions, **(D)** Rough titanium plate, **(E)** MG-63 cells on a rough surface under normoxic conditions, and **(F)** MG-63 cells on a rough surface under hypoxic conditions.

with GAPDH (Abcam, 1:5,000, United States) for visualization as an internal reference. The results were analyzed using the Chemi-Genius gel imaging system for the expression of the target protein.

RT-qPCR

RNA was extracted using TRIzol and reverse-transcribed into cDNA using a reverse transcription kit (Tiangen, China) according to the manufacturer's instructions. Next, the RNA content was detected using fluorescence (Bio-Rad, United States). The sequences of the RT-PCR primers used are listed in **Table 1**. The reaction cycle was carried out at 95°C for 20 s, annealing at 60°C for 30 s, and extension at 72°C for 30 s. The results were calculated using the $2^{-\Delta\Delta CT}$ method.

Animal Experiments

The protocol for our animal experiments was approved by the Ethics Committee of Long Gui Xing Ke Animal Farm, Baiyun District, Guangzhou. Titanium implants from different groups (3.45 mm × 10 mm) were implanted into four adult male New Zealand white rabbits (aged 20 weeks and weighing approximately 3.0 kg). Animal experiments were performed in a plain zone (Guangzhou, China) and a highland zone (Xizang, China). Before experiments, all animals were lived in the correspondent place at least 6 months in the SPF environment. Animals were anesthetized using Sumian Xin (Animal Husbandry Research Institute, Jilin, China) at 0.15 ml/kg body weight. Preoperatively, 0.6 ml of Primacaine (Merignac Cedex, France; 0.2 ml/kg of body weight) was locally injected into the surgical site of the tibia. The titanium plates were implanted approximately 7 mm–12 mm beneath the joint, and a similar operation was performed on the other side of the tibia. The rough plate was placed in one side, and the smooth plate was placed in other side. After the operation, all animals were injected with 0.3 mg (Pharmaceutical Company, Sichuan, China) and allowed to move freely. At either 2 or 4 weeks post-surgery ($n = 5$ at each time point), the animals were sacrificed by excessive anesthetic (1.5 ml/kg) and samples were collected for histological analysis. Bone grafts and soft tissues were collected and fixed in 10% neutral-buffered formalin (Cohen et al., 2020).

Bone-to-Implant Contact Evaluation

Tissue specimens were dehydrated in a gradient dilution of ethanol, immersed in 100% resin, and embedded in methyl methacrylate. They were then cut in the buccolingual direction and parallel to the axis of the implants using a low-speed diamond saw (SP1600, Leica Biosystems, Germany). The section containing the implant was ground until its thickness reached 60–80 µm. It was then stained with methylene blue-acid fuchsin. Each specimen was observed under an optical microscope (Olympus BX41, Olympus Co., Japan) and analyzed using the OsteoMeasure™ software. Bone-to-implant contact (BIC) was quantitatively measured as follows: BIC (%) = (sum of the length of BIC)/(circumference of the implant chamber region) × 100. BIC was defined as the interface where the bone tissue was located within 20 µm of the implant surface without any intervention of the soft tissue.

Statistical Analysis

Each measurement was repeated in triplicate and averaged. Data were collected and reported as the mean ± SD. One-way ANOVA was carried out between the compared groups, followed by the Student-Newman-Keuls method. All analyses were conducted using SPSS Statistics 17, and the significance level was set at 0.05.

RESULTS

Morphological Characteristics of the Different Titanium Surfaces

Scanning electron microscopy analysis showed that mechanical polishing resulted in a smooth, "mirror-like" titanium surface (**Figure 1A**), whereas the sandblasted and acid-etched surface was rough and displayed a "honeycomb" structure with different porosities (**Figure 1D**). MG-63 cells were inoculated on the two titanium surfaces. Under normoxic or hypoxic conditions, titanium disks with a smooth surface contained numerous cells connected by cell matrix that grew in a single layer and with a flat appearance (**Figures 1B,C**). Conversely, under normoxic and hypoxic conditions, disks with a rough surface were covered with multiple cell layers connected by the matrix, with fractures at multiple sites, unclear boundaries, and unevenness (**Figures 1D–F**).

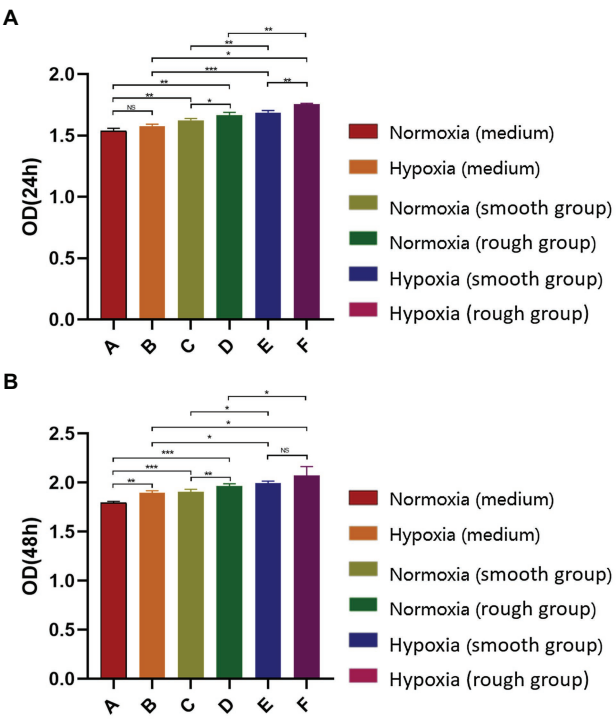

FIGURE 2 | Detection of MG-63 cell proliferation rate using a CCK-8 kit. **(A)** MG-63 cell proliferation rate at 24 h and **(B)** MG-63 cell proliferation rate at 48 h. NS, no significance; $^{*}p < 0.05$, $^{**}p < 0.01$, and $^{***}p < 0.001$.

Titanium Plates Promote Cell Proliferation Under Hypoxia

At both 24 and 48 h, the hypoxic condition was better than the normoxic one in term of proliferation ($p < 0.05$; **Figures 2A,B**). After 48 h, the EdU assay showed that cell proliferation was significantly higher under hypoxia than normoxia. Moreover, cell viability was higher on titanium disks with a rough surface than on those with a smooth surface (**Figure 3**). Our findings suggest that hypoxic conditions might benefit cell proliferation. Additionally, the two surface treatments improved cell proliferation, with a particularly significant affect induced by the rough surface.

A Rough Surface Enhances Osteogenic Differentiation Under Hypoxia

To evaluate the osteogenic differentiation of MG-63 cells in environments with different oxygen levels and on different surfaces, the expression of osteogenic-related proteins was detected 14 days after culture. The results showed that the expression of osteogenic-related proteins was promoted under

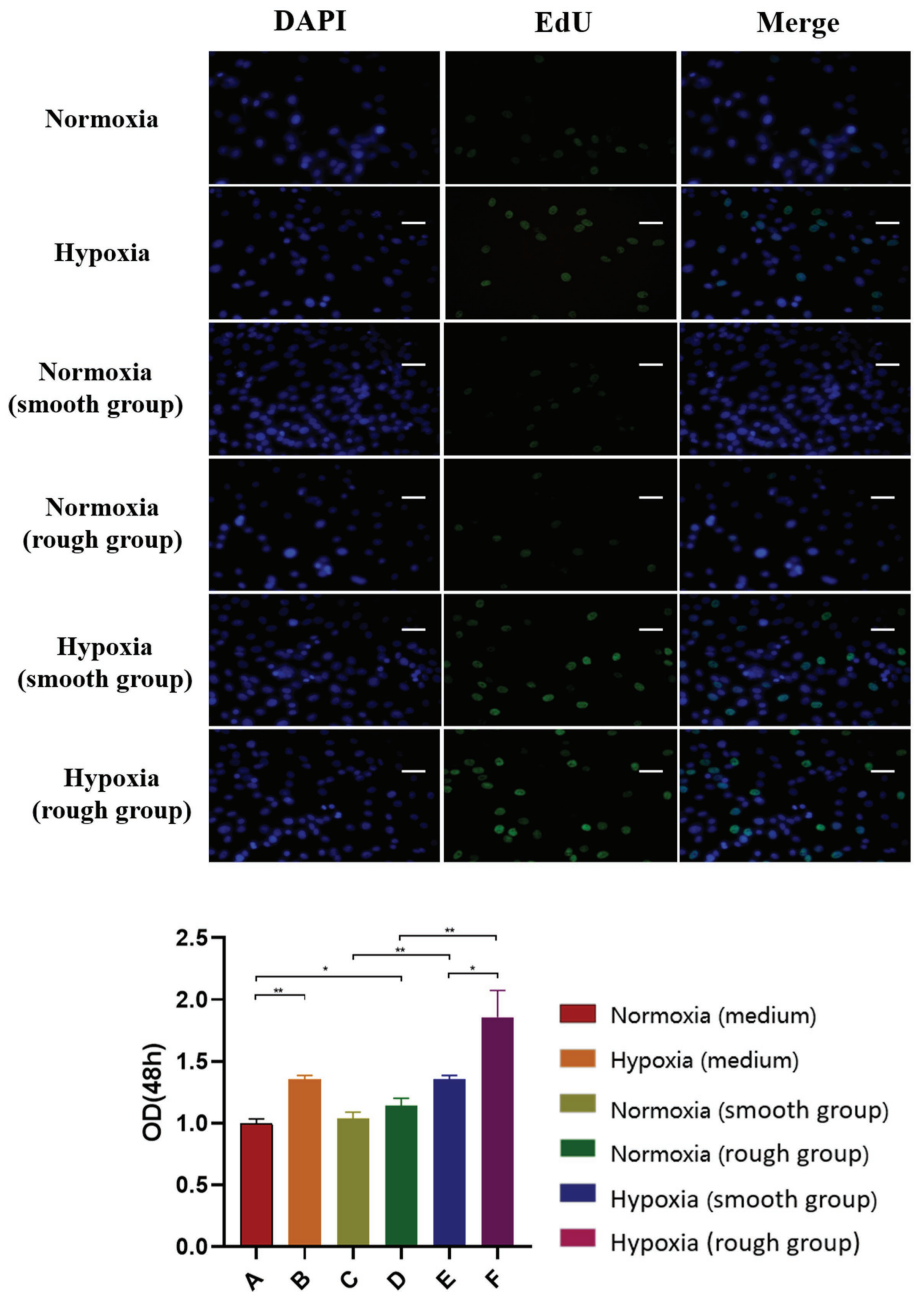

FIGURE 3 | EdU staining results for the different groups. The EdU staining results and quantification of different groups under different environment [Blue: 4,6-diamidino-2-phenylindole (DAPI), Green: EdU]. Scale bar = 200 μm. *$p < 0.05$, **$p < 0.01$.

hypoxic conditions and further enhanced by the rough surface (**Figure 4A**; BMP2, $p < 0.05$; COL-1 $p < 0.05$; RUNX2, $p < 0.01$). These results were confirmed by the RT-qPCR findings with the rough surface found to increase the expression of genes associated with osteogenesis in MG-63 cells (**Figure 4B**).

JAK1/STAT1/HIF-1α Pathway Activation Under Different Conditions

From the western blot analysis of MG-63 cells, we determined that the JAK1/STAT1/HIF-1α pathway displayed a reduced expression (p-JAK1/JAK1, p-STAT1/STAT1, and HIF-1α/GADPH) under normoxic conditions, but was activated under hypoxic conditions (**Figures 5A,B**). Although the rough surface promoted activation of the JAK1/STAT1/HIF-1α pathway (p-JAK1/JAK1, p-STAT1/STAT1, and HIF-1α/GADPH) under normoxic conditions, no significant differences were observed in the activation of this pathway between the smooth surface and rough surface groups under hypoxia (**Figures 5A,B**).

Histological Analysis

Data collected from our animal-based experiments showed that no implant loss occurred at 2 and 4 weeks post-operation. In the high-altitude hypoxic environment, new bone formation was detected on all of the implants, and osseointegration was observed. Compared to implants with a smooth surface, those with a rough surface showed more bone regeneration at 2 weeks post-operation. Intimate bone contact with the implant surface was observed in the healing cavity around the implants; only a small amount of new bone tissue was found on implants with a smooth surface. At 4 weeks in both high-altitude and plain area, new bone covered most of the implants with rough surfaces, whereas relatively few covered areas were detected on implants with smooth surfaces (**Figure 6A**). By comparing the BIC (%) of each group, we noted that at week 2, implants

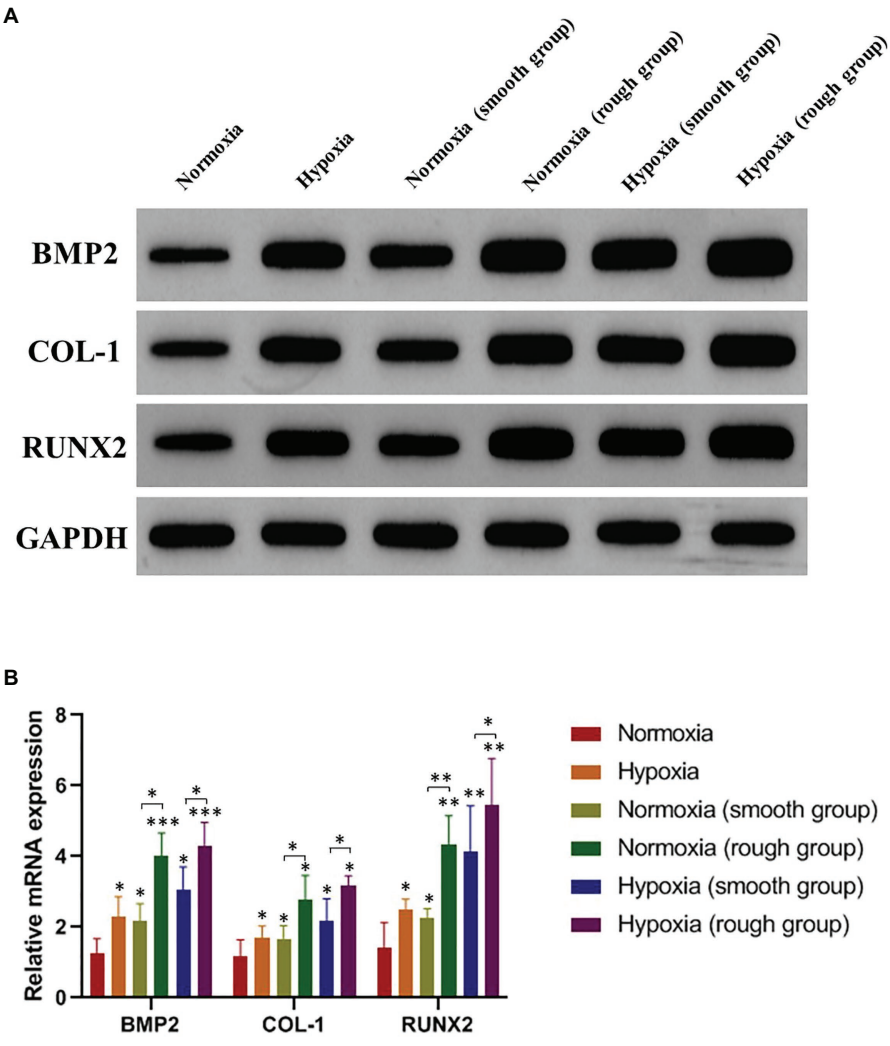

FIGURE 4 | Osteogenic-related proteins and mRNA (BMP2, COL-1, and RUNX2) expression of MG-63 cells in different groups. **(A)** Western blotting and **(B)** RT-qPCR. $^{*}p < 0.05$, $^{**}p < 0.01$, and $^{***}p < 0.001$, *compared with the corresponding group maintained under normoxic conditions.

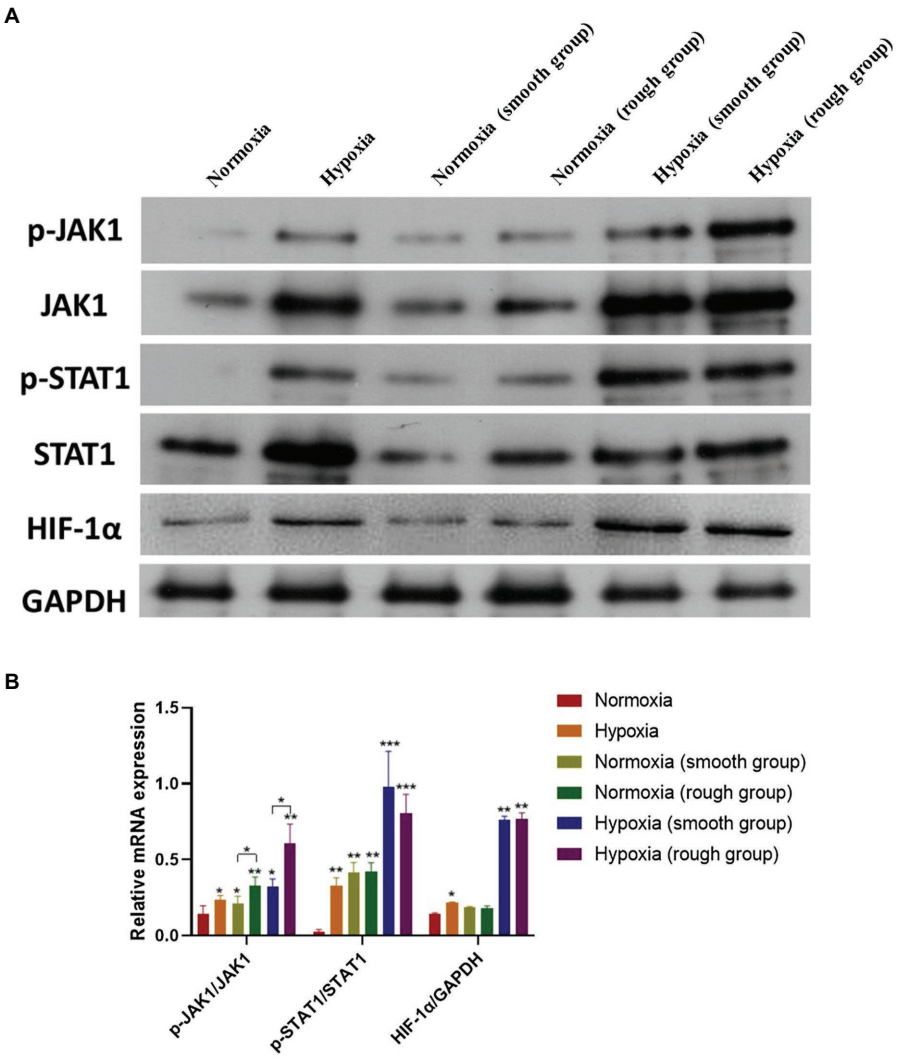

FIGURE 5 | The JAK1/STAT1/HIF-1α pathway activation in different groups. **(A)** Protein expression of p-JAK1, JAK1, p-STAT1, STAT1, HIF-1α, and GAPDH; **(B)** Relative protein expression of p-JAK1/JAK1, p-STAT1/STAT1, and HIF-1α/GAPDH. *$p < 0.05$, **$p < 0.01$, and ***$p < 0.001$, *compared with the corresponding group maintained under normoxic conditions.

with a rough surface showed superior bone formation and osseointegration capacity compared to those with a smooth surface, under both normoxic and hypoxic conditions (**Figure 6B**). At week 4, significant differences were detected between smooth and rough surface both in plain and highland. Titanium plates with a rough surface had significantly better osteogenesis to the hypoxic microenvironment compared to those with a smooth surface and were able to regenerate and bind bone in a hypoxic environment.

DISCUSSION

Titanium and its alloys are metal materials commonly used in the field of biomedicine (He et al., 2020; Tan et al., 2020), more specifically in the treatment of bone defects, as implant devices to replace damaged or defective tissues. Recent research on titanium surface modifications has focused primarily on slurry spray coating, hydroxyapatite coating, micro-arc oxidation, laser irradiation, and anodic oxidation (Liu et al., 2017; He et al., 2019; Pippenger et al., 2019). Moreover, studies have reported that surface treatment of uncoated grafts is superior to that of coated grafts, for example, in terms of outstanding biocompatibility and osteoconductive properties (Horvathy et al., 2016; Wu et al., 2018a). However, bone formation is not only affected by bone materials, but also by O2 concentration. Indeed, hypoxic environments can promote bone formation and bone healing (Xue et al., 2020; Yu et al., 2020). Therefore, in the present study, we explored the activities of osteoblasts on the surface of different bioactive titanium implants under normoxic and hypoxic conditions.

Currently, sandblasting and acid etching (SLA) is one of the most widely used non-coating surface treatment methods (Corvino et al., 2020; Lu et al., 2020). SLA combines the

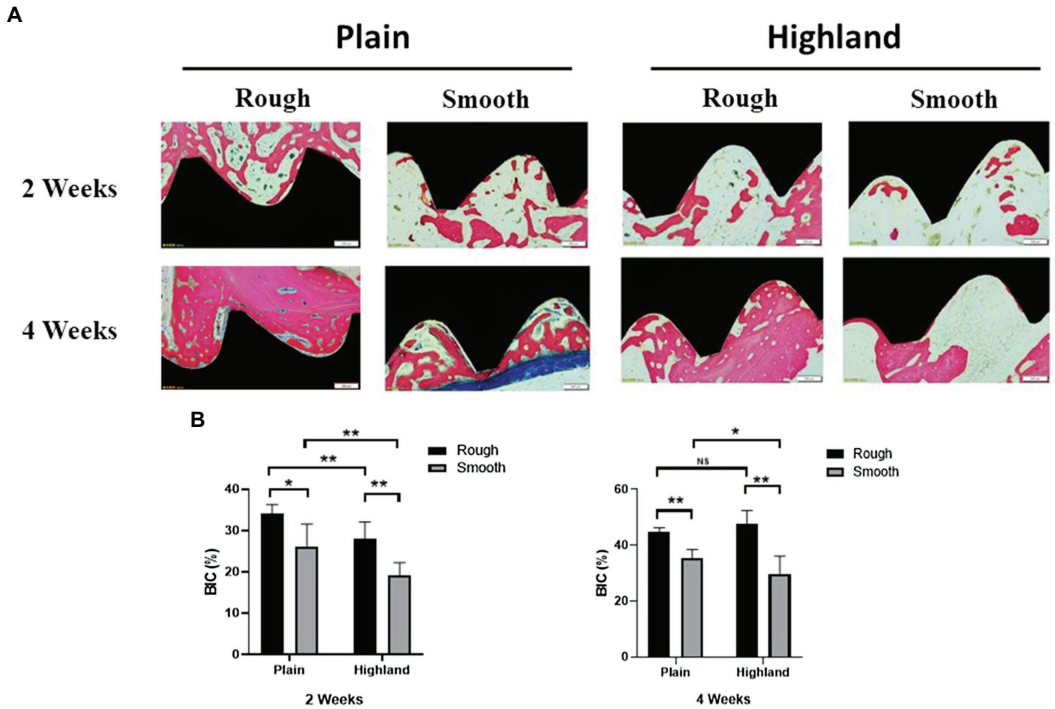

FIGURE 6 | Histological observation of implants and the surrounding tissues [methylene blue-acid fuchsin **(A)**]; comparison of Bone-to-Implant Contact (BIC; %) at week 2 and 4 **(B)**. NS, no significance; $^{*}p<0.05$, $^{**}p<0.01$.

advantages of physical and chemical etching, while also offering an inexpensive and simple platform (Lu et al., 2020). In our study, irregular honeycomb-shaped holes were formed on the surface of the titanium plate following SLA. Considering that cell adhesion is a prerequisite for the proliferation and differentiation of bone cells, the surface morphology of biomaterials directly affects early adhesion (Kim et al., 2019). Studies have confirmed that SLA not only effectively increases the contact area of osteoblasts, but also enhances their adhesive and proliferative capacity (Bayram et al., 2012; Ding et al., 2015). The results of the CCK-8 and EdU analyses in the current study support that rough surface promotes cell proliferation under hypoxia. Moreover, at 2 weeks, the expression of osteogenic-related proteins and genes (BMP2, COL-1, and RUNX2) was promoted under hypoxic conditions (**Figure 4**). The rough surface further enhanced osteogenic differentiation and hypoxia enhanced the expression of JAK1 and STAT1.

The JAK1/STAT1 pathway plays an integral role in the transmission of hypoxia signals and mediates the effects of hypoxia (Yang et al., 2017; Wu et al., 2018b; Liu et al., 2020b). Moreover, mesenchymal stem cells ameliorate hypoxia and reoxygenation injury in renal tubular epithelial cells through the JAK/STAT signaling pathway (Zhang et al., 2017). In addition, activation of the JAK1/STAT1 pathway can promote HIF-1α expression in hypoxic environments (Yang et al., 2017). Similarly, in our study, activation of the JAK1/STAT1 pathway stimulated HIF-1α expression by western blotting. Overexpression of HIF-1α can upregulate the vascular endothelial growth factor, induce neovascularization, and accelerate bone formation (Du et al., 2018; Liu et al., 2019). Therefore, hypoxia can enhance osteogenic differentiation *via* the JAK1/STAT1/HIF-1α pathway.

Our animal model revealed that bone formation under high-altitude hypoxic conditions was significantly slower than that under normoxia; this result was consistent with previous studies (Lezon et al., 2016; Suresh et al., 2019). In highland environments, the extent of osteogenesis on both rough and smooth surfaces was lower than that observed in plains at 2 weeks. However, no significant difference was observed in the BIC for the rough surface between the two conditions at 4 weeks. Moreover, the roughness of the implant surface was positively associated with the amount of newly generated bone. Studies have reported that high-altitude hypoxic environments delay the healing of bone tissue and produce a relatively insufficient mass of new bone, while also affecting the osseointegration efficiency of the implant (Shan et al., 2017; Uhl, 2018). In contrast, hypoxic conditions promote osteogenic differentiation *in vitro*. This difference may be the result of a complex *in vivo* environment. For example, in addition to hypoxic conditions, low-pressure conditions also play an important role in osteogenesis *in vivo* (Wang et al., 2006; Torigoe et al., 2007). In fact, a low-pressure system has been shown to facilitate the perfusion of a larger number of mesenchymal stem cells into the porous scaffold, enhancing bone formation within the composites (Torigoe et al., 2007). The difference of *in vitro* and *in vivo* condition caused the discrepancy of osteogenesis results under normoxia and hypoxia

environment. To further assess these effects, our future work will include constructing a low-pressure model and determining how different titanium surfaces affect osseointegration.

Collectively, the findings of this study indicate that rough surfaces more effectively promote bone formation in the plains and highlands compared to smooth surfaces. Moreover, under hypoxic conditions, implants with a rough surface enhanced the efficiency of bone binding at an early stage, that is, both at 2 and 4 weeks. However, no significant difference was detected between the two conditions in implants with a rough surface at 4 weeks, suggesting that implant loading should be performed after 4 weeks in highland environments.

CONCLUSION

Compared to a smooth surface, a rough surface was more conducive to the proliferation of osteogenesis and implant osseointegration. The early enhanced osteogenic differentiation detected on tibial implants under hypoxic conditions appears to be associated with upregulation of the JAK1/STAT1/HIF-1α pathway. Meanwhile, long-term observation showed that hypoxia inhibited bone formation and osseointegration.

DATA AVAILABILITY STATEMENT

The raw data supporting the conclusions of this article will be made available by the authors, without undue reservation.

ETHICS STATEMENT

The animal study was reviewed and approved by Ethics Committee of Long Guixingke Animal Farm, Baiyun District, Guangzhou.

AUTHOR CONTRIBUTIONS

MR, YW, and PC conceived and designed the study. YW, ZG, HL, ZL, PS, JZ, WY, HC, RY, and YY performed the experiments and analyzed the data. YW wrote the manuscript. YW, ZG, PC, and MR revised the manuscript. All authors contributed to the article and approved the submitted version.

FUNDING

This study was funded by the Natural Science Foundation of Guangdong Province (grant number 2016A030310240), the Guangdong Science and Technology Innovation Strategy Special Fund Project (grant number 2018KJY2014), the Medical Research Foundation of Guangdong Province (grant number B2019117), the Guangdong Provincial Administration of Traditional Chinese Medicine, Chinese Medicine Research Project (grant number 20202129), the Natural Science Foundation of Tibet Autonomous Region (grant number XZ2017ZR-ZYZ37), and the National Natural Science Foundation of China for Youth (grant number 81600900).

REFERENCES

Bayram, C., Demirbilek, M., Caliskan, N., Demirbilek, M. E., and Denkbas, E. B. (2012). Osteoblast activity on anodized titania nanotubes: effect of simulated body fluid soaking time. *J. Biomed. Nanotechnol.* 8, 482–490. doi: 10.1166/jbn.2012.1391

Bernardi, S., Re, F., Bosio, K., Dey, K., Almici, C., Malagola, M., et al. (2020). Chitosan-hydrogel polymeric scaffold acts as an independent primary inducer of osteogenic differentiation in human mesenchymal stromal cells. *Materials* 13:3546. doi: 10.3390/ma13163546

Brunello, G., Panda, S., Schiavon, L., Sivolella, S., Biasetto, L., and Del Fabbro, M. (2020). The impact of bioceramic scaffolds on bone regeneration in preclinical in vivo studies: a systematic review. *Mater. Aust.* 13:1500. doi: 10.3390/ma13071500

Chen, Y., Han, P., Vandi, L. J., Dehghan-Manshadi, A., Humphry, J., Kent, D., et al. (2019). A biocompatible thermoset polymer binder for direct ink writing of porous titanium scaffolds for bone tissue engineering. *Mater. Sci. Eng. C Mater. Biol. Appl.* 95, 160–165. doi: 10.1016/j.msec.2018.10.033

Cohen, D. J., Scott, K. M., Kulkarni, A. N., Wayne, J. S., Boyan, B. D., and Schwartz, Z. (2020). Acellular mineralized allogenic block bone graft does not remodel during the 10 weeks following concurrent implant placement in a rabbit femoral model. *Clin. Oral Implants Res.* 31, 37–48. doi: 10.1111/clr.13544

Corvino, E., Pesce, P., Mura, R., Marcano, E., and Canullo, L. (2020). Influence of modified titanium abutment surface on peri-implant soft tissue behavior: a systematic review of in vitro studies. *Int. J. Oral Maxillofac. Implants* 35, 503–519. doi: 10.11607/jomi.8110

Dashnyam, K., Buitrago, J. O., Bold, T., Mandakhbayar, N., Perez, R. A., Knowles, J. C., et al. (2019). Angiogenesis- promoted bone repair with silicate-shelled hydrogel fiber scaffolds. *Biomater. Sci.* 7, 5221–5231. doi: 10.1039/c9bm01103j

Ding, X., Zhou, L., Wang, J., Zhao, Q., Lin, X., Gao, Y., et al. (2015). The effects of hierarchical micro/nanosurfaces decorated with TiO2 nanotubes on the bioactivity of titanium implants in vitro and in vivo. *Int. J. Nanomedicine* 10, 6955–6973. doi: 10.2147/IJN.S87347

Du, Y., Ge, Y., Xu, Z., Aa, N., Gu, X., Meng, H., et al. (2018). Hypoxia-inducible factor 1 alpha (HIF- 1alpha)/vascular endothelial growth factor (VEGF) pathway participates in angiogenesis of myocardial infarction in Muscone-treated mice: preliminary study. *Med. Sci. Monit.* 24, 8870–8877. doi: 10.12659/MSM.912051

Feng, H., Xing, W., Han, Y., Sun, J., Kong, M., Gao, B., et al. (2020). Tendon-derived cathepsin K-expressing progenitor cells activate hedgehog signaling to drive heterotopic ossification. *J. Clin. Invest.* 130, 6354–6365. doi: 10.1172/JCI132518

Gonzaga, M. G., Dos, S. K. B., de Figueiredo, F., Feldman, S., Ervolino, E., Dos Santos, M. C. G., et al. (2019). Effectiveness of rhBMP-2 association to autogenous, allogeneic, and heterologous bone grafts. *Microsc. Res. Tech.* 82, 689–695. doi: 10.1002/jemt.23215

Guglielmotti, M. B., Olmedo, D. G., and Cabrini, R. L. (2019). Research on implants and osseointegration. *Periodontol.* 2000, 178–189. doi: 10.1111/prd.12254

He, W., Yin, X., Xie, L., Liu, Z., Li, J., Zau, S., et al. (2019). Enhancing osseointegration of titanium implants through large-grit sandblasting combined with micro-arc oxidation surface modification. *J. Mater. Sci. Mater. Med.* 30:73. doi: 10.1007/s10856-019-6276-0

He, W., Zhang, H., and Qiu, J. (2020). Osteogenic effects of bioabsorbable magnesium implant in rat mandibles and in vitro. *J. Periodontol.* 92, 1181–1191. doi: 10.1002/JPER.20-0162

Horvathy, D. B., Vacz, G., Szabo, T., Szigyarto, I. C., Toro, I., Vámos, B., et al. (2016). Serum albumin coating of demineralized bone matrix results in stronger new bone formation. *J. Biomed. Mater. Res. B Appl. Biomater.* 104, 126–132. doi: 10.1002/jbm.b.33359

Kim, S., Choi, J. Y., Jung, S. Y., Kang, H. K., Min, B. M., Yeo, I. L., et al. (2019). A laminin-derived functional peptide, PPFEGCIWN, promotes bone formation on sandblasted, large-grit, acid-etched titanium implant surfaces. *Int. J. Oral Maxillofac. Implants* 34, 836–844. doi: 10.11607/jomi.7178

Lee, J., and Bance, M. L. (2019). Physiology of osseointegration. *Otolaryngol. Clin. N. Am.* 52, 231–242. doi: 10.1016/j.otc.2018.11.004

Lee, S. H., Moon, J. H., Jeong, C. M., Bae, E. B., Park, C. E., Jeon, G. R., et al. (2017). The mechanical properties and biometrical effect of 3D preformed titanium membrane for guided bone regeneration on alveolar bone defect. *Biomed. Res. Int.* 2017:7102123. doi: 10.1155/2017/7102123

Lezon, C., Bozzini, C., Aguero, R. A., Pinto, P., Champin, G., Alippi, R. M., et al. (2016). Effect of chronic undernutrition on body mass and mechanical bone quality under normoxic and altitude hypoxic conditions. *Br. J. Nutr.* 115, 1687–1695. doi: 10.1017/S000711451600060X

Liu, S., Chow, I., Lu, L., Ren, Y. M., Yang, H. L., Jian, S. Y., et al. (2020a). Comparison of sleep disturbances Between older nursing home residents in high- and low-altitude areas. *J. Geriatr. Psychiatry Neurol.* 33, 370–376. doi: 10.1177/0891988719892335

Liu, P., Hao, Y., Zhao, Y., Yuan, Z., Ding, Y., and Cai, K. (2017). Surface modification of titanium substrates for enhanced osteogenetic and antibacterial properties. Colloids surf. *Colloids Surf. B Biointerfaces* 160, 110–116. doi: 10.1016/j.colsurfb.2017.08.044

Liu, Y., Huang, X., Yu, H., Yang, J., Li, Y., Yuan, X., et al. (2019). HIF-1alpha-TWIST pathway restrains cyclic mechanical stretch-induced osteogenic differentiation of bone marrow mesenchymal stem cells. *Connect. Tissue Res.* 60, 544–554. doi: 10.1080/03008207.2019.1601185

Liu, J., Kang, Y., Yin, S., Chen, A., Wu, J., Liang, H., et al. (2020b). Key role of microtubule and its acetylation in a zinc oxide nanoparticle-mediated lysosome-autophagy system. *Small* 16:e2001857. doi: 10.1002/smll.202001857

Liu, F., Liang, T., Zhang, Z., Liu, L., Li, J., Dong, W., et al. (2021). Effects of altitude on human oral microbes. *AMB Express* 11:41. doi: 10.1186/s13568-021-01200-0

Lu, X., Xiong, S., Chen, Y., Zhao, F., Hu, Y., Guo, Y., et al. (2020). Effects of statherin on the biological properties of titanium metals subjected to different surface modification. *Colloids Surf. B Biointerfaces* 188:110783. doi: 10.1016/j.colsurfb.2020.110783

Ma, D., Zheng, B., Liu, H. L., Zhao, Y. B., Liu, X., Zhang, X. H., et al. (2020). Klf5 down-regulation induces vascular senescence through eIF5a depletion and mitochondrial fission. *PLoS Biol.* 18:e3000808. doi: 10.1371/journal.pbio.3000808

Mavrogenis, A. F., Dimitriou, R., Parvizi, J., and Babis, G. C. (2009). Biology of implant osseointegration. *J. Musculoskelet. Neuronal Interact.* 9, 61–71.

Pippenger, B. E., Rottmar, M., Kopf, B. S., Stubinger, S., Dalla, T. F., Berner, S., et al. (2019). Surface modification of ultrafine-grained titanium: influence on mechanical properties, cytocompatibility, and osseointegration potential. *Clin. Oral Implants Res.* 30, 99–110. doi: 10.1111/clr.13396

Shan, Z., Luo, Z. P., Shen, X., and Chen, L. (2017). Promotion of fracture healing by conjugated linoleic acid in rats. *J. Orthop. Surg.* 25:613379198. doi: 10.1177/2309499017718910

Suresh, S., Rajvanshi, P. K., and Noguchi, C. T. (2019). The many facets of erythropoietin physiologic and metabolic response. *Front. Physiol.* 10:1534. doi: 10.3389/fphys.2019.01534

Talley, A. D., Boller, L. A., Kalpakci, K. N., Shimko, D. A., Cochran, D. L., and Guelcher, S. A. (2018). Injectable, compression-resistant polymer/ceramic composite bone grafts promote lateral ridge augmentation without protective mesh in a canine model. *Clin. Oral Implants Res.* 29, 592–602. doi: 10.1111/clr.13257

Tan, J., Liu, Z., Wang, D., Zhang, X., Qian, S., and Liu, X. (2020). A facile and universal strategy to endow implant materials with antibacterial ability via alkalinity disturbing bacterial respiration. *Biomater. Sci.* 8, 1815–1829. doi: 10.1039/c9bm01793c

Torigoe, I., Sotome, S., Tsuchiya, A., Yoshii, T., Takahashi, M., Kawabata, S., et al. (2007). Novel cell seeding system into a porous scaffold using a modified low-pressure method to enhance cell seeding efficiency and bone formation. *Cell Transplant.* 16, 729–739. doi: 10.3727/000000007783465109

Uhl, E. W. (2018). The pathology of vitamin D deficiency in domesticated animals: An evolutionary and comparative overview. *Int. J. Paleopathol.* 23, 100–109. doi: 10.1016/j.ijpp.2018.03.001

Wang, J., Asou, Y., Sekiya, I., Sotome, S., Orii, H., and Shinomiya, K. (2006). Enhancement of tissue engineered bone formation by a low pressure system improving cell seeding and medium perfusion into a porous scaffold. *Biomaterials* 27, 2738–2746. doi: 10.1016/j.biomaterials.2005.12.005

Wen, D. D., and Lv, Y. L. (2020). Effect of different doses of aspirin on the early osseointegration of titanium alloy implants in rats. *J. Dent. Prevent. Treat.* 28, 285–291. doi: 10.12016/j.issn.2096-1456.2020.05.003

Wu, J., Lai, X., Cui, G., Chen, Q., Liu, J., Kang, Y., et al. (2020a). Dual effects of JNK activation in blood-milk barrier damage induced by zinc oxide nanoparticles. *J. Hazard. Mater.* 399:122809. doi: 10.1016/j.jhazmat.2020.122809

Wu, T., Li, B., Wang, W., Chen, L., Li, Z., Wang, M., et al. (2020b). Strontium-substituted hydroxyapatite grown on graphene oxide nanosheet-reinforced chitosan scaffold to promote bone regeneration. *Biomater. Sci.* 8, 4603–4615. doi: 10.1039/d0bm00523a

Wu, X., Liu, S., Hu, Z., Zhu, G., Zheng, G., and Wang, G. (2018a). Enriched housing promotes post-stroke neurogenesis through calpain 1-STAT3/HIF-1alpha/VEGF signaling. *Brain Res. Bull.* 139, 133–143. doi: 10.1016/j.brainresbull.2018.02.018

Wu, S., Zhang, A., Li, S., Chatterjee, S., Qi, R., Segura-Ibarra, V., et al. (2018b). Polymer functionalization of isolated mitochondria for cellular transplantation and metabolic phenotype alteration. *Adv. Sci.* 5:1700530. doi: 10.1002/advs.201700530

Xue, Y., Li, Z., Wang, Y., Zhu, X., Hu, R., and Xu, W. (2020). Role of the HIF1alpha/SDF1/CXCR4 signaling axis in accelerated fracture healing after craniocerebral injury. *Mol. Med. Rep.* 22, 2767–2774. doi: 10.3892/mmr.2020.11361

Yang, M., Wang, L., Wang, X., Wang, X., Yang, Z., Li, J., et al. (2017). IL-6 promotes FSH-induced VEGF expression through JAK/STAT3 signaling pathway in bovine granulosa cells. *Cell. Physiol. Biochem.* 44, 293–302. doi: 10.1159/000484885

Yu, Y., Ma, L., Zhang, H., Sun, W., Zheng, L., Liu, C., et al. (2020). EPO could be regulated by HIF-1 and promote osteogenesis and accelerate bone repair. *Artif. Cells Nanomed. Biotechnol.* 48, 206–217. doi: 10.1080/21691401.2019.1699827

Zhang, L., Wang, Y., Ma, J., Lai, X., Fang, J., Li, G., et al. (2017). Exogenous MSCs ameliorate hypoxia/reoxygenation injury in renal tubular epithelial cells through JAK/STAT signaling pathway- mediated regulation of HMGB1. *Am. J. Transl. Res.* 9, 2412–2420.

Conflict of Interest: The authors declare that the research was conducted in the absence of any commercial or financial relationships that could be construed as a potential conflict of interest.

Publisher's Note: All claims expressed in this article are solely those of the authors and do not necessarily represent those of their affiliated organizations, or those of the publisher, the editors and the reviewers. Any product that may be evaluated in this article, or claim that may be made by its manufacturer, is not guaranteed or endorsed by the publisher.

frontiers in Physiology

MINI REVIEW
published: 05 January 2022
doi: 10.3389/fphys.2021.798682

Salivary Exosomes: From Waste to Promising Periodontitis Treatment

*Nik Nur Syazana Nik Mohamed Kamal and Wan Nazatul Shima Shahidan**

School of Dental Sciences, Universiti Sains Malaysia, Health Campus, Kota Bharu, Malaysia

Periodontitis is a chronic inflammatory condition that causes tooth loss by destroying the supporting components of the teeth. In most cases, it is difficult to diagnose early and results in severe phases of the disease. Given their endogenous origins, exosomes, which are rich in peptides, lipids, and nucleic acids, have emerged as a cell-free therapeutic approach with low immunogenicity and increased safety. Because the constituents of exosomes can be reprogrammed depending on disease states, exosomes are increasingly being evaluated to act as potential diagnostic biomarkers for dental disease, including periodontitis. Exosomes also have been demonstrated to be involved in inflammatory signal transmission and periodontitis progression *in vitro*, indicating that they could be used as therapeutic targets for periodontal regeneration. Nevertheless, a review on the involvement of salivary exosomes in periodontitis in impacting the successful diagnosis and treatment of periodontitis is still lacking in the literature. Thus, this review is intended to scrutinize recent advancements of salivary exosomes in periodontitis treatment. We summarize recent research reports on the emerging roles and characteristics of salivary exosomes, emphasizing the different expressions and changed biological roles of exosomes in periodontitis.

Keywords: saliva, exosome, periodontitis, waste, promising

OPEN ACCESS

Edited by:
Frédéric Lézot, Institut National de la Santé et de la Recherche Médicale (INSERM), France

Reviewed by:
Alexander E. Berezin, Zaporizhia State Medical University, Ukraine
Guya Diletta Marconi, University of Studies G. d'Annunzio Chieti and Pescara, Italy

***Correspondence:**
Wan Nazatul Shima Shahidan
shima@usm.my

Specialty section:
This article was submitted to Craniofacial Biology and Dental Research, a section of the journal Frontiers in Physiology

Received: *20 October 2021*
Accepted: *30 November 2021*
Published: *05 January 2022*

Citation:
Nik Mohamed Kamal NNS and Shahidan WNS (2022) Salivary Exosomes: From Waste to Promising Periodontitis Treatment. Front. Physiol. 12:798682. doi: 10.3389/fphys.2021.798682

METHODOLOGY AND DELIMITATION

A PubMed database search on July 27, 2021 with the keywords "exosome AND periodontitis" resulted in a total of 86 articles. Only 81 articles remained after applying the "full-text" parameter. A total of 45 articles remained when a second parameter, "free full-text," was added. Afterward, the articles were manually divided into two groups: original articles and "others" (not related to the topic, reviews, reports, editorials, commentaries, etc.). Here, we are focusing on original articles addressing salivary exosomes and periodontitis. Only six of the original articles on salivary exosomes and periodontitis were selected.

INTRODUCTION

Periodontitis is a major public health concern with a high global prevalence (Papapanou et al., 2018). It is the most frequent osteolytic inflammatory severe disease, and it has been shown to have a detrimental effect on disease states like atherosclerosis, rheumatoid arthritis, and diabetes. The pathology is of an osteoimmune disorder defined by periodontal inflammation and subsequent destruction of the tooth-supporting tissue as alveolar bone, which is a leading cause of tooth loss in adults. Periodontitis is initiated by the accumulation of periodontal bacteria-associated biofilm, but it is not fully adequate to cause the disease since the host immune response is required

for its development and progression (Yuki et al., 2021). The creation of high-impact diagnostic biomarkers that have a significant impact on clinical decision-making, patient outcomes, and healthcare providers is one of the goals of periodontology research (Ghallab, 2018). This could be accomplished by utilizing protein-containing exosomes.

Saliva has a variety of functions in the human body, including those that are crucial not only for the oral system and other bodily systems. Several research articles have been published in the last few years describing various salivary components and their distribution, confirming the biochemical composition and physiology of the proteins found in salivary fluids (Schenkels et al., 1995; Marotz et al., 2021). Many researchers have shown that exosomes may be found in human saliva and that they can be used to diagnose and investigate many diseases (Imai et al., 2021).

Exosomes are small vesicles (30–120 nm) that are secreted by all types of cultured cells and found in abundance in body fluids such as blood (Damanti et al., 2021), urine (Blijdorp et al., 2021), ascites (Cai et al., 2021), amniotic fluid (Bellio et al., 2020), and cultured medium of cell cultures (Ivica et al., 2020) including reticulocytes (Jiaqi et al., 2017); cytotoxic T lymphocytes (Chen et al., 2019); B lymphocytes (Calvo and Izquierdo, 2020); dendritic cells (Hosseini et al., 2021) and neoplastic intestinal epithelial cells (Scavo et al., 2020). These tiny vesicles play a key role in intercellular communication, both locally and systemically, allowing proteins, cytokines, and miRNA to be transferred between cells (Hergenreider et al., 2012). A review article comparing whether non-exosomal or exosomal miRNAs are more valid as biomarkers was recently published. Exosomes were chosen as the best origin for miRNAs used in biomarker studies (Nik Mohamed Kamal and Shahidan, 2020). Recently, exosomes have gained interest as a tool in regenerative medicine. They have been shown to be involved in the transmission of inflammatory signals and the development of periodontitis *in vitro*, indicating that they could be utilized as therapeutic targets for periodontal regeneration (Wang et al., 2020; Xin et al., 2020). Exosomes generated from dental pulp stem cells (DPSCs) have been found to minimize edema and enhance angiogenesis while suppressing inflammation (Pivoraite et al., 2015). Exosome-mediated dental pulp regeneration has only been demonstrated *in vitro* in the studies mentioned above. On the other hand, exosomes' effects on the regeneration of dental pulp *in situ,* are little explored.

We evaluated over a decade of experience with salivary exosome, with an emphasis on the study of periodontitis. We compiled and updated the uses of salivary exosome as it relates to periodontitis from the literature and considered their physiological and clinical significance. We also examine their disease associations and potential clinical applications.

ORIGIN, COMPOSITION, AND POTENTIAL USE OF EXTRACELLULAR VESICLES

Exosomes, microvesicles, and apoptotic bodies are three types of vesicles secreted by cells, surrounded by lipid bilayer, and collectively known as extracellular vesicles (EVs) (Skotland et al., 2020). The vesicles can be distinguished by their sizes, biogenesis, and mechanism of release (Nik Mohamed Kamal and Shahidan, 2020). The diameter of the vesicles is recorded in the range of either 30–150 nm (exosomes), 100–1000 nm (microvesicles), or 1–5 μm (apoptotic bodies) (Rilla et al., 2019). The classical pathway for biogenesis of exosomes starts from the generation of endosomes from endocytoic activity of parent cells, leading to invagination of endosomal limiting membranes and formation of intraluminal vesicles (ILVs) that then mature into multivesicular bodies (MVBs). MVBs that are directed to plasma membranes are released into the extracellular environment as exosomes (**Figure 1**). Biogenesis of microvesicles is much simpler, where, upon stimulation, the outward parent cells' membrane blebs. The blebs are then detached from parent cells as microvesicles. Biogenesis of apoptotic bodies starts from parent cells that are undergoing apoptosis (Skotland et al., 2020), leading to cell shrinkage and blebbing. The detached blebs are called apoptotic bodies (Rilla et al., 2019). Previous literature reported the detection of EVs from a variety of body fluids, e.g., bile (Nakashiki et al., 2021), saliva (Comfort et al., 2021), semen, blood (Vojtech et al., 2019), breast milk (Jiang et al., 2021), synovial fluid (Mustonen et al., 2021), urine (Blijdorp et al., 2021), and ascites (Bortot et al., 2021). Generally, these EVs are composed of nucleic acids [e.g., microRNAs (Nakashiki et al., 2021)], proteins (Bortot et al., 2021), lipids (Skotland et al., 2020), and signaling molecules (Vojtech et al., 2019). The contents can vary, depending on the parent cells, as well as the type of vesicles. For example, the existence of proteins in EVs could be influenced by the biogenesis of that particular EV, e.g., exosomes derived from the classical pathway might be enriched with protein associated with the endosomal pathway (e.g., Alix and TSG101) (Bruno et al., 2019). Up till now, many works of literature have been published describing EVs' potential as biomarkers for diseases [e.g., asthma (Comfort et al., 2021), periodontitis (Kamal et al., 2020)], cargo for drug delivery [e.g., in treating wound healing, tissue repair, and regeneration (Rilla et al., 2019; Cao et al., 2021)], tools in understanding the membranes structure and mechanism for vesicular trafficking (Skotland et al., 2020), parts that function in the immune response system (e.g., source of self-antigens/forming immune complexes/autoantigen presentation) and as well as vesicles that contribute to the coagulation process (Turpin et al., 2016).

In other studies, the use of mesenchymal stromal cells (MSCs)-derived EV to treat chronic skin ulcers has offered a range of advantages, including accelerating healing and minimizing scar formation. This is the fact that the EV has immunosuppressive and immunomodulatory effects. They can also stimulate angiogenesis, proliferation, migration, and differentiation of the various cell types involved in skin regeneration (Casado-Díaz et al., 2020). In the case of using EVs as cargo for drug delivery systems, Villa et al. (2019) have described three different ways in their review paper. First, using tumor-derived EVs for targeting specific organs where EVs should be delivered to. By using tumor-derived EVs, the tumor-specific integrin expression pattern can be manipulated, which guarantees efficient organotropism (Sun et al., 2010; Hoshino et al., 2015). Secondly, using MSCs' EVs

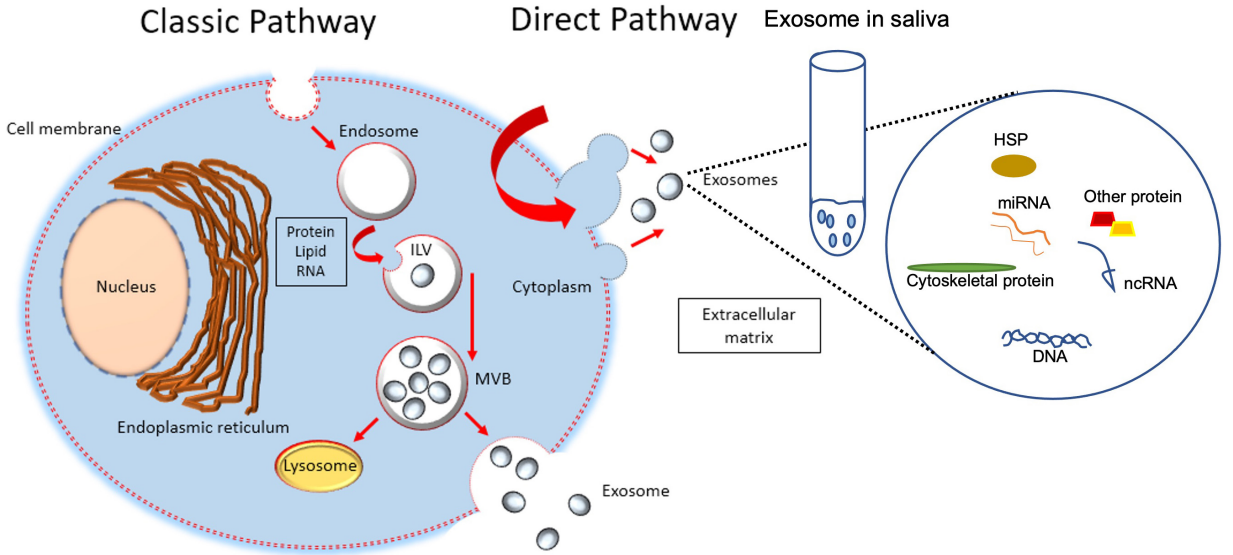

FIGURE 1 | Formation of intraluminal vesicles (ILVs) within MVBs. Exosomes are derived from the multivesicular bodies (MVBs) which are known as late endosomes. MVBs are formed during the maturation of early endosomes into late endosomes with the accumulation of intraluminal vesicles. Upon maturation, MVBs are either destined for fusion with lysosomes where their contents will undergo lysosomal degradation, or with the plasma membrane where their contents are released into the extracellular space. The membrane of MVB fuses with the plasma membrane, resulting in the release of ILVs. When secreted, ILVs are called exosomes, release into saliva from submandibular gland cells and play a role in periodontal tissue and cells.

to avoid oncogenic or immunogenic effects (Lai et al., 2019; Melzer et al., 2019). Thirdly, using light-induced hyperthermia to incorporate hollow gold nanoparticles into MSCs' EVs to produce EVs that will be targeting specific cell types (Sancho-Albero et al., 2019). Interestingly, their potential application in the previously reported treatments opens the door for the design of new highly effective therapeutic strategies.

SALIVARY EXOSOME

Although the mechanism of exosome biogenesis is still unclear, currently, there are two known ways of exosomal generation (Van der Pol et al., 2012; Gurung et al., 2021; **Figure 1**). Exosomes were reported to be released into the saliva either from the ductal or acinar cells. The salivary glands have been involved in constitutive-like secretory pathways that are involved in the secretion of vesicles such as exosomes. These secretory vesicles are derived directly from the *trans*-Golgi or involve elements of the endosomal-lysosomal trafficking pathway (Palanisamy et al., 2010). Exosomes can be shuttled from the systemic circulation into the oral cavity (Cheng et al., 2019).

Although the mechanisms of vesicle secretion in the blood are still unknown, findings from Marie-Pierre et al. (2005) gave strong evidence that exosomes can be secreted by all blood cells and retrieved in blood fluids. Since these EVs can cross the epithelial barriers, they may be essential for transporting components from the blood into saliva. Thus, in comparison with the other bodily fluids, salivary exosomes are probably a better and more accessible tool to examine the function of exosomes in the diagnosis and treatment of disease.

SALIVARY EXOSOME IN PERIODONTITIS

Emerging functional and clinical applications of exosomes in human oral disease such as Oral disease, Oral squamous cell carcinoma, Primary Sjögren's syndrome, Oral tissue regeneration, including periodontitis has been reported (Peng et al., 2020). The report discussed the role of exosomes in periodontitis, with increasing evidence that using natural nanostructured exosomes as a new disease treatment strategy is feasible. In early periodontal infection, periodontal ligament fibroblasts (PDLFs) are the predominant cell types that come into contact with pathogenic microbes. Human PDLF-derived exosomes enhance the expression of IL-6 and TNF-α in osteoblasts in response to lipopolysaccharide (LPS) stimuli, while simultaneously inhibiting the expression of osteogenesis-related elements such as collagen-I and osteoprotegerin and lowering alkaline phosphatase activity (Zhao et al., 2019). These findings suggest that LPS-pretreated PDLFs secrete exosomes, which cause inflammation and decrease osteogenic activity in osteoblasts. This is important to suggest that localized periodontal inflammation could influence bone remodeling by releasing exosomes. In the oral mechanical environment, PDLFs also help to maintain periodontal tissue homeostasis. When PDLFs were stimulated by cyclic stretch, they produced exosomes that inhibited the NF-κB signaling pathway, which suppressed IL-1 production in LPS-treated macrophages. PDLF cells in mechanical environments contribute to the maintenance of periodontal immune/inflammatory homeostasis by releasing exosomes (Wang et al., 2019). When they interact with their surrounding inflammatory milieu, periodontal ligament stem cells (PDLSCs) exhibit self-renewal ability and multipotency. Exosomes generated

TABLE 1 | List progression of exosome study in periodontitis.

No.	Progression of exosome study in periodontitis	Source of exosome	Reference
1.	PDLF derived exosome help to maintain periodontal tissue homeostasis.	Culture media of PDLF cell	Wang et al., 2019
2.	PDLF derived exosome enhanced expression of IL-6 and TNF in response to LPS.	Culture media of PDLF cell	Zhao et al., 2019
3.	LPS-stimulated PDLSCs exosome relieve inflammation.	Culture media of PDLSCs cell	Zheng et al., 2019
4.	Exosome PD-L1 mRNA in saliva linked to advanced stage periodontitis.	Saliva	Tobón-Arroyave et al., 2019
5.	miRNAs from salivary exosomes of chronic periodontitis patients were shown to be a possible diagnostic biomarker.	Saliva	Kamal et al., 2020
6.	miRNA from saliva exosome could be reliable candidates for the development of periodontitis biomarker.	Saliva	Kamal et al., 2020
7.	The diagnostic potential of salivary small extracellular-associated miRNAs in periodontal disease is being investigated for the first time in the pilot study.	Saliva	Han et al., 2020
8.	In various periodontal conditions, the pilot study gave important insight into the human global DNA methylation profiles of saliva sEVs and Gram-negative bacterial outer membrane vesicles (OMVs) (healthy, gingivitis and periodontitis).	Saliva	Han et al., 2020
9.	Salivary exosome miRNA correlated with periodontitis progression.	Saliva	Fujimori et al., 2021

from LPS-stimulated PDLSCs contained more miR155 than its downstream target, Sirtuin1, which lowered T17 expression but enhanced Treg expression, relieving inflammation through the T17/Treg/miR1555p/Sirtuin1 regulatory network (Zheng et al., 2019). Periodontitis patients had higher levels of exosomal periodontal ligaments (PD-L1) mRNA in saliva than controls, and high levels of PD-L1 expression were linked to advanced stages of periodontitis. The level of salivary CD9 and CD81 exosomes, on the other hand, was reduced in periodontitis and was adversely linked with the disease state. According to the findings, an assay of exosome-based PD-L1 mRNA in saliva has the capacity to identify periodontitis from the healthy, and its levels correspond with periodontitis severity and stage (Tobón-Arroyave et al., 2019).

Kamal et al. (2020) demonstrated for the first time that miRNAs from plasma and salivary exosomes of chronic periodontitis (CP) patients were shown to be a possible diagnostic biomarker. When compared to prior CP miRNA studies, the profile revealed the most abundant number of miRNAs with a significant differential in expression. hsa-miR-125a-3p [$FC = 2.03$; $AUC = 1$; $r = 0.91$ (p-value = 0.02)] is worth additional investigation using salivary-exosomal samples. Because they were expressed considerably differently, had a good discriminatory value, and strongly correlated with the mean of periodontal pocket depth, these miRNAs can be concluded to be reliable candidates for the development of periodontitis biomarkers (Kamal et al., 2020).

The diagnostic potential of salivary small extracellular-associated (sEV) miRNAs in periodontal disease is being investigated for the first time by Han et al. (2020) in a pilot study. The ultimate goal was to evaluate the diagnostic utility of miRNAs extracted from sEVs to those extracted from total saliva in terms of differentiating between periodontal conditions. Three miRNAs (hsa-miR-140-5p, hsa-miR-146a-5p, and hsa-miR-628-5p) were found to be significantly upregulated (p 0.05) in salivary sEVs from periodontitis patients compared to healthy controls, suggesting that they could be potential periodontitis biomarkers. In microarray analysis of patients with CP, salivary hsa-miR-5571-5p, hsa-let-7f-5p, hsa-miR-99a-5p, hsa-miR-28-5p, and hsa-miR-320d expression was linked to periodontitis development. These salivary miRNAs could be novel biomarkers for periodontitis progression and monitoring them could lead to new periodontal diagnostics and precision therapy (Fujimori et al., 2021).

In various periodontal conditions, the pilot study of Han et al. (2021) gave important insight into the human global DNA methylation profiles of saliva sEVs and Gram-negative bacterial outer membrane vesicles (OMVs) (healthy, gingivitis, and periodontitis). The researchers discovered that periodontitis sEVs have considerably higher levels of LPS + OMVs, global 5mC methylation, and four periodontal pathogen OMVs (*Treponema denticola, Eikenella corrodens, Porphyromonas gingivalis, and Fusabacterium nucleatum*) than healthy sEVs.

SALIVARY EXOSOMES' CURRENT AND FUTURE POTENTIAL IN PERIODONTITIS TREATMENT

The expression of PD-L1 mRNA in exosomes obtained from saliva of periodontitis patients was studied, as well as the clinical significance of salivary exosomes PD-L1 mRNA levels in the disease. The level of salivary exosomes PD-L1 mRNA in periodontitis patients differs significantly from non-periodontitis controls, according to one of the study's key findings. Furthermore, a high amount of salivary exosomes PD-L1 was linked to advanced periodontitis, implying that it can represent disease progression. This is the first study to develop a method for detecting exosomal PD-L1 in saliva, as well as the first salivary exosomal biomarker for periodontitis (Yu et al., 2019). The specimens used in the majority of previous periodontitis biomarker studies have been gingival tissues or gingival crevicular fluids (GCF) (Kebschull et al., 2014). However, sample collection procedures for gingival tissues and GCF are challenging: gingival tissue biopsy requires invasive and limited tissue, while GCF sample collection requires sampling a minute amount of fluid on filter paper strips, which takes much longer.

Our previous study, which involved an easy, non-invasive, and quick collection of salivary specimens, demonstrated that a saliva-based assay overcomes the existing challenges. We also show that salivary exosomes may be used to extract miRNA, confirming the idea that exosome-derived samples protect

miRNA from degradation (Kamal et al., 2020). According to recent studies, MSC-derived exosomes are increasingly being recognized as viable techniques to alleviate tissue injury and stimulate tissue regeneration in dental treatments, such as dental pulp regeneration, oral oncotherapy, and periodontal regeneration (Peng et al., 2020). To summarize, salivary exosomes may promote dental pulp regeneration by increasing the expression of specific proteins, promoting vascularization, modulating the interaction between epithelial and mesenchymal cells, and enhancing the abilities of dental pulp cells, all of which could be useful therapeutic methods in the future. Even though the current review focuses on salivary exosomes, some other study mimics the condition of salivary exosomes *in vitro* by collecting the exosome from the periodontal cell culture (**Table 1**). From **Table 1**, exosome research in periodontitis has only recently progressed, even though studies on exosomes and periodontitis have been ongoing for over a decade. Based on this progress, salivary exosomes showed potential as nano biomaterial that needs attention in the dental field.

CONCLUSION

Even though the role of salivary exosomes in periodontitis is very limited, based on growing evidence, exosomes may play a significant role in the regulation of periodontitis. Exosomes derived from saliva act as essential promoters in periodontal regenerators and periodontitis biomarkers, which have been a research focus all along. Exosomes' effects on oral diseases, such as periodontitis have received increasing attention in recent years, giving us a better understanding of the functions that exosomes play in oral diseases. Furthermore, saliva exosomes are economical, carrying numerous biological components that have a lot of promise for assisting clinical diagnosis and determining prognosis.

AUTHOR CONTRIBUTIONS

NNS wrote the first draft of the manuscript. WNS revised the manuscript. Both authors approved the final version of the manuscript and agreed to be accountable for all aspects of the work.

FUNDING

This review was funded by Research University Individual Grant (RUI), Universiti Sains Malaysia [1001/PPSG/8012280], which enabled the conduct of the research related to this review.

REFERENCES

Bellio, M. A., Abdullah, Z., Steward, D., Khan, A., Xu, X., Shapiro, G. C., et al. (2020). MicroRNA sequencing of amniotic fluid derived exosome cargo reveals a therapeutic potential for the treatment of osteoarthritis. *Cytotherapy* 22:S47. doi: 10.1016/j.jcyt.2020.03.054

Blijdorp, C. J., Tutakhel, O. A., Hartjes, T. A., van den Bosch, T. P., van Heugten, M. H., Rigalli, J. P., et al. (2021). Comparing approaches to normalize, quantify, and characterize urinary extracellular vesicles. *J. Am. Soc. Nephrol.* 32, 1210–1226. doi: 10.1681/ASN.2020081142

Bortot, B., Apollonio, M., Rampazzo, E., Valle, F., Brucale, M., Ridolfi, A., et al. (2021). Malignant-ascites-derived small extracellular vesicles in advanced ovarian cancer patients: insights into the dynamics of the extracellular matrix. *Mole. Oncol.* 6:13110. doi: 10.1002/1878-0261.13110

Bruno, S., Chiabotto, G., Favaro, E., Deregibus, M. C., and Camussi, G. (2019). Role of extracellular vesicles in stem cell biology. *Am. J. Physiol. Cell Physiol.* 317, C303–C313. doi: 10.1152/ajpcell.00129.2019

Cai, J., Gong, L., Li, G., Guo, J., Yi, X., and Wang, Z. (2021). Exosomes in ovarian cancer ascites promote epithelial–mesenchymal transition of ovarian cancer cells by delivery of miR-6780b-5p. *Cell Death Dis.* 12, 1–17. doi: 10.1038/s41419-021-03490-5

Calvo, V., and Izquierdo, M. (2020). Inducible polarized secretion of exosomes in T and B lymphocytes. *Int. J. Mol. Sci.* 21:2631. doi: 10.3390/ijms21072631

Cao, Z., Wu, Y., Yu, L., Zou, L., Yang, L., Lin, S., et al. (2021). Exosomal miR-335 derived from mature dendritic cells enhanced mesenchymal stem cell-mediated bone regeneration of bone defects in athymic rats. *Mole. Med.* 27, 1–13. doi: 10.1186/s10020-021-00268-5

Casado-Díaz, A., Quesada-Gómez, J. M., and Dorado, G. (2020). Extracellular Vesicles Derived From Mesenchymal Stem Cells (MSC) in Regenerative Medicine: Applications in Skin Wound Healing. *Front. Bioeng. Biotechnol.* 8:146. doi: 10.3389/fbioe.2020.00146

Chen, L., Huang, H., Zhang, W., Ding, F., Fan, Z., and Zeng, Z. (2019). Exosomes derived from t regulatory cells suppress CD8+ cytotoxic T lymphocyte proliferation and prolong liver allograft survival. *Med. Sci. Mon.* 25, 4877–4884. doi: 10.12659/MSM.917058

Cheng, J., Nonaka, T., and Wong, D. (2019). Salivary exosomes as nanocarriers for cancer biomarker delivery. *Materials* 12:654. doi: 10.3390/ma12040654

Comfort, N., Bloomquist, T. R., Shephard, A. P., Petty, C. R., Cunningham, A., Hauptman, M., et al. (2021). Isolation and characterization of extracellular vesicles in saliva of children with asthma. *Extracell. Ves. Circul. Nucleic Acids* 2, 29–48. doi: 10.20517/evcna.2020.09

Damanti, C. C., Gaffo, E., Lovisa, F., Garbin, A., Di Battista, P., Gallingani, I., et al. (2021). miR-26a-5p as a reference to normalize microRNA qRT-PCR levels in plasma exosomes of pediatric hematological malignancies. *Cells* 10:101. doi: 10.3390/cells10010101

Fujimori, K., Yoneda, T., Tomofuji, T., Ekuni, D., Azuma, T., Maruyama, T., et al. (2021). Detection of salivary miRNAs that predict chronic periodontitis progression: A Cohort Study. *Int. J. Environ. Res. Public Health* 18:8010. doi: 10.3390/ijerph18158010

Ghallab, N. A. (2018). Diagnostic potential and future directions of biomarkers in gingival crevicular fluid and saliva of periodontal diseases: review of the current evidence. *Arch. Oral. Biol.* 87, 115–124. doi: 10.1016/j.archoralbio.2017.12.022

Gurung, S., Perocheau, D., Touramanidou, L., and Baruteau, J. (2021). The exosome journey: from biogenesis to uptake and intracellular signalling. *Cell Comm. Signal.* 19, 1–19. doi: 10.1186/s12964-021-00730-1

Han, P., Bartold, P. M., Salomon, C., and Ivanovski, S. (2020). Salivary small extracellular vesicles associated miRNAs in periodontal status- A pilot study. *Int. J. Mol. Sci.* 21:2809. doi: 10.3390/ijms21082809

Han, P., Bartold, P. M., Salomon, C., and Ivanovski, S. (2021). Salivary outer membrane vesicles and DNA methylation of small extracellular vesicles as biomarkers for periodontal status: A pilot study. *Int. J. Mol. Sci.* 22:2423. doi: 10.3390/ijms22052423

Hergenreider, E., Heydt, S., Treguer, K., Boettger, T., Horrevoets, A. J., Zeiher, A. M., et al. (2012). Atheroprotective communication between endothelial cells and smooth muscle cells through miRNAs. *Nat. Cell Biol.* 14, 249–256. doi: 10.1038/ncb2441

Hoshino, A., Costa-Silva, B., Shen, T. L., Rodrigues, G., Hashimoto, A., Tesic Mark, M., et al. (2015). Tumour exosome integrins determine organotropic metastasis. *Nature* 527, 329–335. doi: 10.1038/nature15756

Hosseini, R., Asef-Kabiri, L., and Yousefi, H. (2021). The roles of tumor-derived exosomes in altered differentiation, maturation and function of dendritic cells. *Mol. Cancer* 20:83. doi: 10.1186/s12943-021-01376-w

Imai, A., Oka, S., Susuga, M., Tsutsui, N., Haga-Tsujimura, M., and Saitoh, E. (2021). Comprehensive analysis and comparison of proteins in salivary

exosomes of climacteric and adolescent females. *Odontology* 109, 82–102. doi: 10.1007/s10266-020-00538-4

Ivica, A., Ghayor, C., Zehnder, M., Valdec, S., and Weber, F. E. (2020). Pulp-derived exosomes in a fibrin-based regenerative root filling material. *J. Clin. Med.* 9:491. doi: 10.3390/jcm9020491

Jiang, X., You, L., Zhang, Z., Cui, X., Zhong, H., Sun, X., et al. (2021). Biological properties of milk-derived extracellular vesicles and their physiological functions in infant. *Front. Cell Dev. Biol.* 9:1591. doi: 10.3389/fcell.2021.693534

Jiaqi, W., Xuang, S., Zhao, J., Yang, Y., Cai, X., Xu, J., et al. (2017). Exosomes: A Novel Strategy for Treatment and Prevention of Diseases. *Front. Pharm.* 8:300. doi: 10.3389/fphar.2017.00300

Kamal, N. N. S. N. M., Awang, R. A. R., Mohamad, S., and Shahidan, W. N. S. (2020). Plasma-and saliva exosome profile reveals a distinct microRNA signature in chronic periodontitis. *Front. Physiol.* 2020:11. doi: 10.3389/fphys.2020.587381

Kebschull, M., Demmer, R. T., Grün, B., Guarnieri, P., Pavlidis, P., and Papapanou, P. N. (2014). Gingival tissue transcriptomes identify distinct periodontitis phenotypes. *J Dent Res* 93, 459–468. doi: 10.1177/0022034514527288

Lai, P., Weng, J., Guo, L., Chen, X., and Du, X. (2019). Novel insights into MSC-EVs therapy for immune diseases. *Biomark. Res.* 7:6. doi: 10.1186/s40364-019-0156-0

Marie-Pierre, C., Danielle, L., Claude, V. S., Graça, R., and Christian, B. (2005). Exosomal-like vesicles are present in human blood plasma. *Internat. Immunol.* 17, 879–887. doi: 10.1093/intimm/dxh267

Marotz, C., Morton, J. T., Navarro, P., Coker, J., Belda-Ferre, P., Knight, R., et al. (2021). Quantifying live microbial load in human saliva samples over time reveals stable composition and dynamic load. *Msystems* 6, e1182–e1120. doi: 10.1128/mSystems.01182-20

Melzer, C., Rehn, V., Yang, Y., Bähre, H., von, der Ohe, J., et al. (2019). Taxol-loaded MSC-derived exosomes provide a therapeutic vehicle to target metastatic breast cancer and other carcinoma cells. *Cancers* 11:798. doi: 10.3390/cancers11060798

Mustonen, A. M., Capra, J., Rilla, K., Lehenkari, P., Oikari, S., Kaariainen, T., et al. (2021). Characterization of hyaluronan-coated extracellular vesicles in synovial fluid of patients with osteoarthritis and rheumatoid arthritis. *BMC Musculoskel. Dis.* 22:1–11. doi: 10.1186/s12891-021-04115-w

Nakashiki, S., Miuma, S., Mishima, H., Masumoto, H., Hidaka, M., Soyama, A., et al. (2021). Bile extracellular vesicles from end-stage liver disease patients show altered microRNA content. *Hepatol. Internat.* 2021, 1–10. doi: 10.1007/s12072-021-10196-5

Nik Mohamed Kamal, N. N. S. B., and Shahidan, W. N. S. (2020). Non-Exosomal and Exosomal Circulatory MicroRNAs: Which Are More Valid as Biomarkers? *Front. Pharm.* 10:1500. doi: 10.3389/fphar.2019.01500

Palanisamy, V., Sharma, S., Deshpande, A., Zhou, H., Gimzewski, J., and Wong, D. T. (2010). Nanostructural and transcriptomic analyses of human saliva derived exosomes. *PLoS One* 5:e8577. doi: 10.1371/journal.pone.0008577

Papapanou, P. N., Sanz, M., Buduneli, N., Dietrich, T., Feres, M., Fine, D. H., et al. (2018). Periodontitis: Consensus report of workgroup 2 of the 2017 world workshop on the classification of periodontal and peri-Implant diseases and conditions. *J. Period.* 89, S173–S182.

Peng, Q., Yang, J. Y., and Zhou, G. (2020). Emerging functions and clinical applications of exosomes in human oral diseases. *Cell Biosci*. 10:68. doi: 10.1186/s13578-020-00424-0

Pivoraite, U., Jarmalaviciute, A., Tunaitis, V., Ramanauskaite, G., Vaitkuviene, A., and Kaseta, V. (2015). Exosomes from human dental pulp stem cells suppress carrageenan-induced acute inflammation in mice. *Inflammation* 38, 1933–1941. doi: 10.1007/s10753-015-0173-6

Rilla, K., Mustonen, A. M., Arasu, U. T., Härkönen, K., Matilainen, J., and Nieminen, P. (2019). Extracellular vesicles are integral and functional components of the extracellular matrix. *Matrix Biol.* 75, 201–219. doi: 10.1016/j.matbio.2017.10.003

Sancho-Albero, M., Navascués, N., Mendoza, G., Sebastián, V., Arruebo, M., Martín-Duque, P., et al. (2019). Exosome origin determines cell targeting and the transfer of therapeutic nanoparticles towards target cells. *J. Nanobiotechnol.* 17:16. doi: 10.1186/s12951-018-0437-z

Scavo, M. P., Rizzi, F., Depalo, N., Fanizza, E., Ingrosso, C., Curri, M. L., et al. (2020). A possible role of FZD10 delivering exosomes derived from colon cancers cell lines in inducing activation of epithelial–mesenchymal transition in normal colon epithelial cell line. *Internat. J. Mole. Sci.* 21:6705. doi: 10.3390/ijms21186705

Schenkels, L. C. P. M., Veerman, E. C. I., and Amerongen, A. V. N. (1995). Biochemical composition of human saliva in relation to other mucosal fluids. *Crit. Rev. Oral Biol. Med.* 6, 161–175.

Skotland, T., Sagini, K., Sandvig, K., and Lorente, A. (2020). An emerging focus on lipids in extracellular vesicles. *Adv. Drug Del. Rev.* 159, 308–321. doi: 10.1016/j.addr.2020.03.002

Sun, D., Zhuang, X., Xiang, X., Liu, Y., Zhang, S., Liu, C., et al. (2010). A novel nanoparticle drug delivery system: The anti-inflammatory activity of curcumin is enhanced when encapsulated in exosomes. *Mol. Ther.* 18, 1606–1614. doi: 10.1038/mt.2010.105

Tobón-Arroyave, S. I., Celis-Mejía, N., Córdoba-Hidalgo, M. P., and Isaza-Guzmán, D. M. (2019). Decreased salivary concentration of CD9 and CD81 exosomerelated tetraspanins may be associated with the periodontal clinical status. *J. Clin. Periodontol.* 46, 470–480. doi: 10.1111/jcpe.13099

Turpin, D., Truchetet, M. E., Faustin, B., Augusto, J. F., Contin-Bordes, C., Brisson, A., et al. (2016). Role of extracellular vesicles in autoimmune diseases. *Autoimm. Rev.* 15, 174–183.

Van der Pol, E., Böing, A. N., Harrison, P., Sturk, A., and Nieuwland, R. (2012). Classification, functions, and clinical relevance of extracellular vesicles. *Pharmacolog. Rev.* 64, 676–705.

Villa, F., Quarto, R., and Tasso, R. (2019). Extracellular vesicles as natural, safe and efficient drug delivery systems. *Pharmaceutics* 11:557.

Vojtech, L., Zhang, M., Davé, V., Levy, C., Hughes, S. M., Wang, R., et al. (2019). Extracellular vesicles in human semen modulate antigen-presenting cell function and decrease downstream antiviral T cell responses. *PLoS One* 14:e0223901.

Wang, R., Ji, Q., Meng, C., Liu, H., Fan, C., and Lipkind, S. (2020). Role of gingival mesenchymal stem cell exosomes in macrophage polarization under inflammatory conditions. *Int. Immunopharmacol.* 81:106030.

Wang, Z., Maruyama, K., Sakisaka, Y., Suzuki, S., Tada, H., and Suto, M. (2019). Cyclic stretch force induces periodontal ligament cells to secrete exosomes that suppress IL-1β production through the inhibition of the NF-κB signalling pathway in macrophages. *Front. Immunol.* 10:1310.

Xin, X., Shuang, H., Zhi, L., and Zubing, L. (2020). Emerging role of exosomes in craniofacial and dental applications. *Theranostics* 10, 8648–8664.

Yu, J., Lin, Y., Xiong, X., Li, K., Yao, Z., Dong, H., et al. (2019). Detection of exosomal PD-L1 RNA in saliva of patients with periodontitis. *Front. Genet.* 10:202.

Yuki, N., Takao, F., Qunzhou, Z., Terukazu, S., Takanori, S., Xiaoxing, K., et al. (2021). Exosomes from TNF-α-treated human gingiva-derived MSCs enhance M2 macrophage polarization and inhibit periodontal bone loss. *Acta Biomat.* 122, 306–324.

Zhao, M., Dai, W., Wang, H., Xue, C., Feng, J., He, Y., et al. (2019). Periodontal ligament fibroblasts regulate osteoblasts by exosome secretion induced by infammatory stimuli. *Arch. Oral. Biol.* 105, 27–34.

Zheng, Y., Dong, C., Yang, J., Jin, Y., Zheng, W., Zhou, Q., et al. (2019). Exosomal microRNA-155-5p from PDLSCs regulated Th17/Treg balance by targeting sirtuin-1 in chronic periodontitis. *J. Cell. Physiol.* 234:1.

Conflict of Interest: The authors declare that the research was conducted in the absence of any commercial or financial relationships that could be construed as a potential conflict of interest.

Advantages of publishing in Frontiers

OPEN ACCESS
Articles are free to read for greatest visibility and readership

FAST PUBLICATION
Around 90 days from submission to decision

HIGH QUALITY PEER-REVIEW
Rigorous, collaborative, and constructive peer-review

TRANSPARENT PEER-REVIEW
Editors and reviewers acknowledged by name on published articles

Frontiers
Avenue du Tribunal-Fédéral 34
1005 Lausanne | Switzerland

Visit us: www.frontiersin.org
Contact us: frontiersin.org/about/contact

REPRODUCIBILITY OF RESEARCH
Support open data and methods to enhance research reproducibility

DIGITAL PUBLISHING
Articles designed for optimal readership across devices

FOLLOW US
@frontiersin

IMPACT METRICS
Advanced article metrics track visibility across digital media

EXTENSIVE PROMOTION
Marketing and promotion of impactful research

LOOP RESEARCH NETWORK
Our network increases your article's readership